ACADEMIC STUDIES IN ENGINEERING

EDITORS:
PROF. ADNAN HAYALOĞLU, PH.D.
DR. ABDURRAHMAN GÜNDAY

gece kitaplığı

İmtiyaz Sahibi / Publisher • Yaşar Hız
Genel Yayın Yönetmeni / Editor in Chief • Eda Altunel
Editörler / Editors • PROF. ADNAN HAYALOĞLU PH.D
DR. ABDURRAHMAN GÜNDAY
Kapak & İç Tasarım / Cover & Interior Design • Karaf Ajans

Birinci Basım / First Edition • © MART 2020

ISBN • 978-625-7912-16-7

Gece Kitaplığı / Gece Publishing
Türkiye Adres / Turkey Address: Kızılay Mah. Fevzi Çakmak 1. Sokak
Ümit Apt. No: 22/A Çankaya / Ankara / TR
Telefon / Phone: +90 312 384 80 40
web: www.gecekitapligi.com
e-mail: gecekitapligi@gmail.com

Baskı & Cilt / Printing & Volume
Sertifika / Certificate No: 47083

Academic Studies in Engineering

Editors

PROF. ADNAN HAYALOĞLU PH.D

DR. ABDURRAHMAN GÜNDAY

gece kitaplığı

CONTENTS

Chapter 1

FINDING OPTIMUM POINTS IN THE TREATMENT OF LEATHER INDUSTRY WASTEWATER WITH CHEMICAL TREATMENT PROCESS

Ceren Sude BALCI[1], Şefika KAYA[2], Yeliz AŞÇI[3]

1 Eskisehir Osmangazi University, Department of Chemical Engineering, Eskişehir
2 Eskisehir Osmangazi University, Department of Chemical Engineering, Eskişehir
3 Eskisehir Osmangazi University, Department of Chemical Engineering, Eskişehir

1. INTRODUCTION

Leather industry wastewater is the water that occurs during the conversion of animal skins into leather products (Tünay et. al., 2010). While leather products are produced, waters with high levels of biological and chemical pollution occur. These waters contains small pieces of leather, dissolved proteins, hairs, blood, dirt, lime, sodium sulfate, sodium hydroxide, chromium compounds, sodium sulfide, neutral salts, protein-based nitrogen compounds, vegetable debogating agents, sugar, starch decomposition products, surfactants, aliphatic contains acids, glycerins, dyes, pigment etc. (Dursun et. al., 2002). Due to the structure of the leather production process, wastewater with different characteristics is formed in various processes. Therefore, it is not possible to categorize the leather industry according to wastewater character and treatability criteria clearly (Töre et. al., 2004). Compounds in the leather wastewater are difficult to remove by conventional processes. Therefore, they cause direct environmental pollution by being given directly to the environment. Leather wastewater that needs to be treated effectively is usually treated with biological treatment. Although biological treatment is cheap and environmentally friendly for leather wastewater, it is known to be inefficient (Dua et. al., 2020). Therefore, new technologies such as advanced oxidation processes, adsorption and membrane processes have been tried as an integral part of biological treatment in this regard (Lofrano et. al., 2013).

Advanced oxidation processes can be successfully used in the field of wastewater treatment to reduce toxicity, convert toxic pollutants into degradable by-products, provide color removal, and remove organic pollutants (Huang, 2012). Advanced Oxidation Processes (AOPs) are physical-chemical treatment processes for the degradation of the organic medium by the generation of high oxidizing free radicals. One of the most common advanced oxidation methods is the Fenton process, discovered in 1894 by Henry Fenton. In Fenton processes, Fe^{2+} ions act as catalysts and produce hydrogen peroxide (H_2O_2) as the oxidizing agent of the reaction, hydroxyl radical (·OH) in an acid medium (pH between 2.5 and 3.0). The hydroxyl radical decomposes toxic organic substances in solution as a result of a series of reactions (Göde et. al., 2019). These reactions are given from equations (1) to (6).

$$Fe^{2+} + H_2O_2 \longrightarrow Fe^{3+} + \cdot OH + OH^- \quad (1)$$

$$Fe^{3+} + H_2O_2 \longrightarrow Fe-OOH^{2+} + H^+ \quad (2)$$

$$Fe-OOH^{2+} \longrightarrow Fe^{2+} + HO_2^{\cdot} \quad (3)$$

$$Fe^{2+} + HO_2^{\cdot} \longrightarrow Fe^{3+} + HO_2^- \quad (4)$$

$$Fe^{3+} + HO_2^{\cdot} \longrightarrow Fe^{2+} + H^+ + O_2 \quad (5)$$

$$\text{Refractory Organic Pollutant} + \cdot OH \longrightarrow CO_2 + H_2O \quad (6)$$

Fenton process has advantages such as converting organic carbon dissolved at ambient temperature and atmospheric pressure into carbon dioxide, breaking down H_2O_2 into oxygen and water, and providing low toxicity. However, it has disadvantages such as high operating cost, pH and H_2O_2 concentration effect and high amount of sludge production (Göde et. al., 2019). Therefore, heterogeneous Fenton processes have been used for leather industry wastewater. In order to overcome the disadvantages in the traditional Fenton process, heterogeneous Fenton process can be applied with the use of stable heterogeneous catalyst (Niveditha and Gandhimatha, 2020). The catalyst consists of Fe^{2+} and Fe^{3+} ions, which are the source of the ·OH generation different from the homogeneous Fenton process (Nidheesh, 2015). Examples of heterogeneous catalysts are iron materials, goethite (a-FeOOH), Fe_3O_4, a-Fe_2O_3 and the like.

In the heterogeneous process, besides chemical changes, the mass transfer of reagents also depends on the physical steps that occur on the surface of the catalyst in active areas where limited adsorption takes place. At the end of the reaction, the products are desorbed from the active sites, and new reactants can be adsorbed onto the active sites. Therefore, the kinetic ratio, efficiency and stability of the solid catalyst are strongly influenced by its surface properties and pore structure (Soon and Hameed, 2011).

Possible reactions in heterogeneous Fenton processes are given in equations (7) and (8).

$$Fe^{2+}_{surface} + H_2O_2 \longleftrightarrow Fe^{3+}_{surface} + OH^{\cdot} + OH^{-} \quad (7)$$

$$Fe^{3+}_{surface} + H_2O_2 \longleftrightarrow Fe^{2+}_{surface} + HO_2 + H^{+} \quad (8)$$

In this study, heterogeneous Fenton method and adsorption method were applied to treat leather industry wastewater. pH, clay amount, hydrogen peroxide concentration, temperature effects were examined and optimum points were determined for the leather industry wastewater. Clay was used as both an adsorbent and a catalyst. The iron ion concentration of the clay used is high, it can be easily found in nature and it is quite cheap. As a result of the experiments, the adsorption method and the heterogeneous Fenton method were compared. Higher color removal efficiency was obtained in experiments performed with heterogeneous Fenton process.

2. MATERIALS AND METHODS

2.1. Materials

In the experimental study conducted, leather industry wastewater was used. The initial pH of the leather wastewater is 2.58, the maximum wavelength is 595 nanometers, and the color value is 3.834. In the experimental study, clay was used as a catalyst. The wastewater used was obtained from a leather factory serving in Tekirdağ province and the catalyst was obtained from a brick factory in Eskişehir. 30% by weight hydrogen peroxide, sulfuric acid and sodium hydroxide were provided by Sigma Aldrich.

2.2. Heterogeneous Fenton experiments

In heterogeneous Fenton experiments, the wastewater was taken to 250 ml of erlenmayers. The pH value of the wastewater sample was adjusted using 2 M H_2SO_4 and 2M NaOH solutions. The desired amount of clay as a catalyst was added to the wastewater sample. The most recent hydrogen peroxide solution was added to the sample and the experiments were carried out in a constant temperature shaking water bath for a predetermined time. After the experiments were completed, 2M NaOH was added to the sample to form a precipitate. At the end of the precipitation process, a clear solution was taken into the sample containers and the color analysis was performed.

2.3. Adsorption experiments

While conducting adsorption experiments, the wastewater was taken to 250 ml of erlenmayers. The pH of the sample was adjusted using 2M H_2SO_4 and 2M NaOH. The desired amount of clay was added to the wastewater sample as an adsorbent. The experiments were carried out in a shaking water bath for a predetermined time at constant temperature. At the end of the experiment, the clear solution formed by waiting for a while for the precipitation process was taken into the sample containers. Finally, the color analysis was performed.

2.4. Analysis

The wavelength and maximum absorbance value of the wastewater sample for the color analysis were determined using UV spectrophotometer. For leather wastewater, the color removal percentages were calculated by reading the color values at 595 nm wavelength.

3. RESULTS AND DISCUSSIONS

3.1. Effect of the pH

Experiments to determine the pH effect were carried out at a constant amount of clay, constant temperature and reaction time. In addition, H_2O_2 amount was kept constant in heterogeneous Fenton experiments. The pH values were adjusted as 1.5, 2, 3, 4 and 5. The Figure 1 obtained as a result of heterogeneous Fenton and adsorption experiments was given in below.

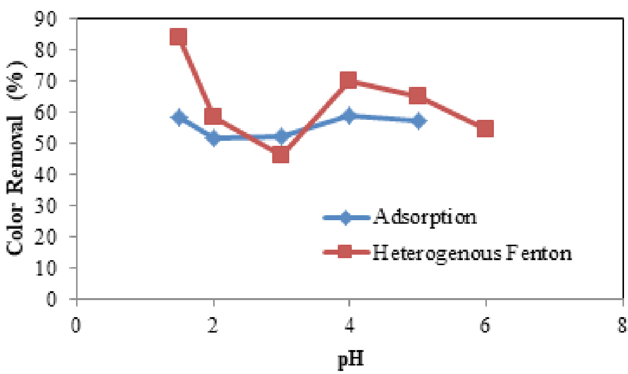

Figure 1. *Effects of the pH on the color removal (for both methods, temperature 30°C, reaction time 2 hour, amount of clay 2 g, for heterogeneous Fenton, H_2O_2 concentration 200ppm).*

The optimum pH value for the adsorption method and the heterogeneous Fenton method is 4. At the optimum point, the color removal in the heterogeneous

Fenton process is 70.24%, while the color removal in the adsorption process is 59.20%. In the heterogeneous Fenton method, the maximum color removal at pH 1.5 was achieved. However, the result obtained at this pH is not very healthy since the environment is very acidic and the total volume increases too much. After the optimum value (pH=4), the color removal decreases. Because the iron ion activity in clay has decreased.

3.2. Effect of the amount of clay

Experiments to determine the effect of clay amount were carried out at optimum pH. The experiments were carried out for two hours at a constant temperature of 30°C, while the amount of clay was set at 0.5, 1, 2, 3, 4, 5 g. The H_2O_2 solution used in the heterogeneous Fenton process is 200 ppm. The results of the adsorption process and heterogeneous Fenton process experiments were given in Figure 2.

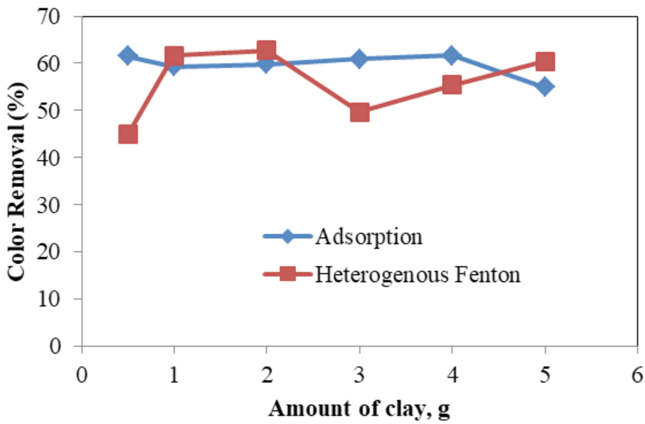

Figure 2. *Effects of the amount of clay on the color removal (for both methods, temperature 30°C, reaction time 2 hour, pH 4, for heterogeneous Fenton, H_2O_2 concentration 200 ppm).*

Looking at the figure, while it performed better in lower amounts of clay in heterogeneous Fenton, it performed better in higher amounts of clay in adsorption. For this reason, 2 grams of optimum clay were selected in heterogeneous Fenton while 4 grams were chosen in adsorption. The maximum color removal for the adsorption process is 61.65% in the amount of 4 gram of clay. In heterogeneous Fenton, the maximum color removal is 62.73% in the amount of 2 gram of clay.

3.3. Effect of the hydrogen peroxide concentration

H_2O_2 solution is used to perform heterogeneous Fenton experiments. In experiments to determine the effect of hydrogen peroxide concentration, hydrogen peroxide concentration is 100, 200, 300, 400, 500 ppm. The experiments were carried out at optimum values for the pH and the amount of clay. The experimental results obtained the hydrogen peroxide effect were given in Figure 3.

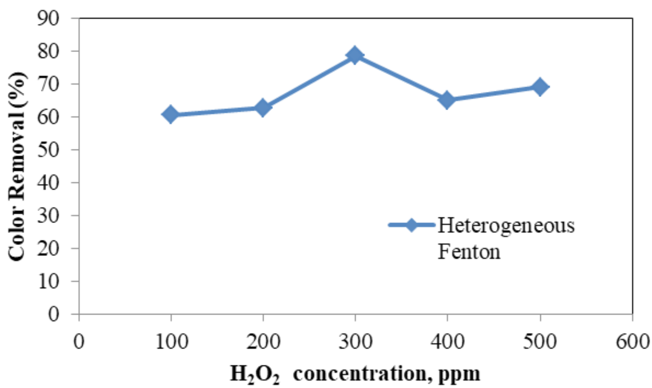

Figure 3. *Effects of the pH on the color removal (temperature 30°C, reaction time 2 hour, pH 4, amount of clay 2 gram).*

When the Figure 3 was examined, the color removal has increased up to 300 ppm. After 300 ppm, the color removal decreased. The color removal at 300 ppm is 78.42%. Therefore, the hydrogen peroxide concentration is 300 ppm optimum for leather industry wastewater. When there is excessive concentration of hydrogen peroxide in the environment, hydrogen peroxide reacts with hydroxyl radicals. Therefore, the color removal efficiency decreases.

3.5. Effect of the temperature

Experiments to determine the temperature effect were carried out at the optimum points for the adsorption process and the heterogeneous Fenton process. Temperature values are 20, 30, 40, 45, 50°C.

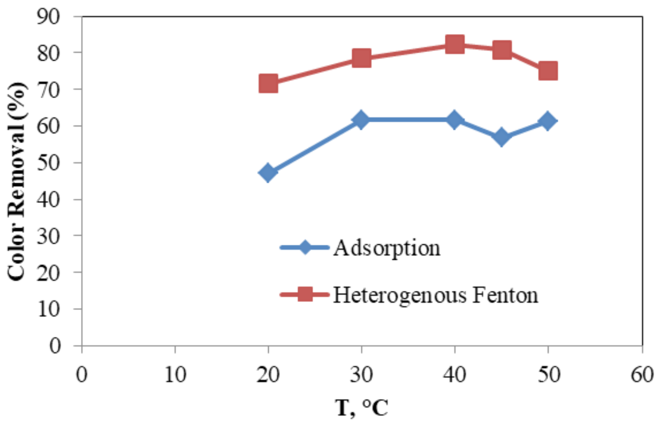

Figure 4. *Effects of the temperature on the color removal (for heterogeneous Fenton, pH 4, amount of clay 2 g, reaction time 2 hour, H_2O_2 concentration 300 ppm, for adsorption, pH 4, amount of clay 4 g, reaction time 2 hour).*

When the temperature effect results were examined, it is seen that the maximum color removal in the adsorption method is 61.66% at 30°C. In heterogeneous Fenton method, the maximum color removal is 82.28% at 40°C. As a result of the literature study, it was observed that the temperature values were at 20-40°C. Therefore, the optimum temperature value is 30°C for adsorption and 40°C in heterogeneous Fenton.

4. CONCLUSION

The heterogeneous Fenton method and adsorption methods have been applied to treat the leather wastewater. The optimum points were determined by comparing the two methods. As a result of the experiments carried out in the adsorption method, the optimum pH value was 4, the amount of clay was 4 grams, and the temperature was 30°C. According to the experiment results carried out at optimum points, the color removal is 62%. In the heterogeneous Fenton method, the optimum pH value is 4, the amount of clay is 2 grams, the hydrogen peroxide concentration is 300 ppm and the temperature is 40°C. The color removal was determined as 82% as a result of the experiment performed at optimum points in the heterogeneous Fenton process. When we look at the color removal, the heterogeneous Fenton method provides more effective treatment than the adsorption method for leather industry wastewater. Because in the heterogeneous Fenton method, unlike the adsorption method, hydrogen peroxide is used. Hydroxyl radicals are formed due to hydrogen peroxide. hydroxyl radicals, by breaking down pollutants, provide a more effective treatment.

REFERENCES

Dursun, Ş., Özdemir, C., Güçlü, D., 2002, Deri Endüstrisi Atıksularının Kimyasal Arıtılabilirliği, Gazi Ünv. Fen Bilimleri Enstitüsü Dergisi, 15 (2), 451 – 456.

Dua, Z., Tiana, W., Qiaoa, K., Zhaoa, J., Wanga, L., Xiea W., Chua, M., Songa, T., 2020, Improved chlorine and chromium ion removal from leather processing wastewater by biocharcoal-based capacitive deionization, Separation and Purification Technology, 233-116024 .

Göde, JN., Souza, DH., Trevisan, V., Skoronski, E., 2019, Application of the Fenton and Fenton-like processes in the landfill leachate tertiary treatment, Journal of Environmental Chemical Engineering, 103352.

Huang W., 2012, Homogeneous and heterogeneous Fenton and photo-Fenton processes : impact of iron complexing agent ethylenediamine-N,N'-disuccinic acid (EDDS). Université Blaise Pascal, D.U. 2241.

Lofrano, G., Meriç, S., Zengin, GE., Orhon, D., 2013, Chemical and biological treatment technologies for leather tannery chemicals and wastewaters: A review, Science of the Total Environment, 461-463, 265-281.

Nidheesh, PV., 2015, Heterogeneous Fenton catalysts for the abatement of organic pollutants from aqueous solution: a review, RSC Advances, 5(51), pp. 40552-40577.

Niveditha, SV., Gandhimatha, R., 2020, Flyash augmented Fe3O4 as a heterogeneous catalyst for degradation of stabilized landfill leachate in Fenton process, Chemosphere, 242-125189.

Soon, A.N. and Hameed, B.H., 2011. Heterogeneous catalysis treatment of synthetic dyes in aqueous media using Fenton and photo-assisted Fenton process. Journal of Desalination, 269 (1-3), pp. 1-16.

Töre, G., Kuru, N., Çokgör, U., Orhon, D., 2004, Çorlu Deri Organize Sanayi Bölgesi Üretim Profili ve Atiksularinin

Biyolojik Aritilabilirlik Esasli Karakterizasyonu, University of Trakya, SKKD 14 (2), 16-22.

Tünay, O., Kabdaşlı I., Arslan I., Ölmez T., 2010, Chemical Oxidation Applications for Industrial Wastewaters, IWA Publishing, p.73.

Chapter 2

EVALUATION OF SEISMIC SITE EFFECT BASED ON MULTICHANNEL ANALYSIS OF SURFACE WAVES METHOD

Murat TÜRKÖZ[1]

1 Eskisehir Osmangazi University, Engineering Faculty, Civil Engineering Department, Eskisehir, Turkey

1. INTRODUCTION

The response of soils to repeated loads has an important effect on the distribution and character of the damage caused by earthquakes. Although the geological structure is important in the formation of the damaging potential of the earthquake, the effect of the local soil properties is much more effective [1, 2, and 3]. Ground conditions such as bedrock depth, groundwater level, properties of soil layers, which can be very different, are among the main factors controlling ground motion characteristics on the surface. The stress-strain properties of the soil layers exposed to repeated stresses of different amplitudes and frequencies may change during earthquakes. In this case, both the behavior of the soil layers and the ground motion characteristics on the surface are affected by the properties of the soil layers. Site-specific ground response analysis is commonly used to assess the effect of local soil conditions.

Different methods have been developed in the field and laboratory to evaluate the soil behavior that is exposed to repeated load. Each of these methods has advantages and limitations for different situations, and most are designed to measure properties at low deformation levels. Seismic experiments based on the formation and propagation of seismic waves is widely used in the field for determining dynamic soil properties for engineering purposes. Geophysical experiments are commonly used in determining dynamic soil properties in the field. By using the shear wave velocity, which is found in geophysical experiments and representing an important feature of the soils, important engineering properties of soils such as soil stratification, soil types, dynamic shear modulus, and soil dominant period can be found.

Surface waves have been described as noise in other seismic methods until recently and have been removed from the data. Then, by the developing technologies and software, the information carried by the surface waves started to be examined. It has been an effective way of calculating the shear wave, which is an indicator of the strength of the ground, and has played an important role in various studies. The Multichannel Analysis of Surface Waves (MASW) method [4, 5] emerged as a non-destructive seismic experiment method to evaluate the shear wave velocity of the soil on the bedrock during geotechnical field investigations and has been used in geotechnical engineering applications [6, 7]. Numerous case studies using the MASW method have been published in recent years [8, 9]. Long and Donahue [7] conducted comparative experiments on Norwegian grounds whose properties are well-defined to evaluate the accuracy, reliability and reproducibility of the data obtained by the MASW method for use in engineering applications. Consistent and reproducible results were obtained with the MASW method, and they gave similar results with the shear wave velocities obtained previously with the Vs profiles obtained in clay, silt and sand layers. Boore and Asten [10] summarized many invasive and non-invasive methods used to obtain underground shear wave velocities using active or passive seismic sources.

In this study, experiments were carried out on the basis of MASW method, which is one of the geophysical methods for the evaluation of shear wave velocity. Studies on the seismic activity of the study area have been carried out by considering the resource zones affecting the region on the basis of probabilistic seismic hazard analysis. Site response analyses were performed in SHAKE 2000 [11] based on shear wave velocity using both synthetic and real earthquake data.

2. Material and Method

2.2. Probabilistic seismic hazard analysis

Since the seismic hazard in a field is defined by the design acceleration spectrum in seismic design specifications, it is necessary to use acceleration records compatible with the design acceleration spectrum in the linear elastic or non-linear elastic earthquake calculations in the time domain of the buildings. Although it is more preferred to use real ground motion records, difficulties may be encountered in the existing strong ground motion databases to find a record compatible with the seismic source and local ground conditions affecting the project site and source-field distance [12]. For this reason, both synthetic records can be produced and real earthquake records can be selected to meet the conditions specified in the regulations and scaled to match the design acceleration spectrum. For this purpose, the seismo-tectonic map presented in Figure 1 has been taken into consideration for use in the seismic hazard analysis of the study area.

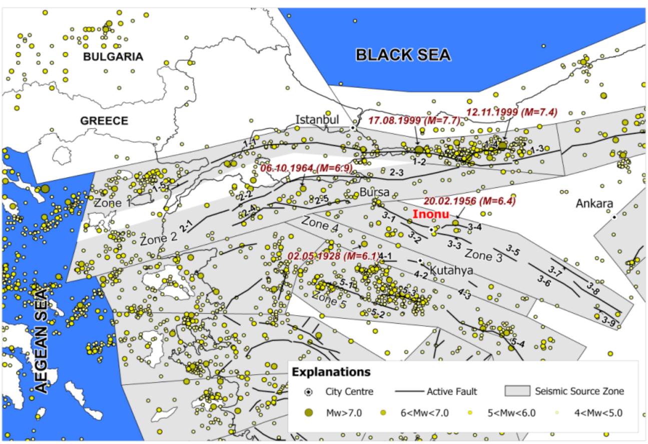

Figure 1. *Resource zones and distribution of earthquakes [13]*

Seismic source zones within the boundary of the 100 km radius study area (İnonu/Eskişehir) were determined and it was observed that it should be evaluated as 5 separate seismic source zones in terms of the influence (Figure 1).

The North Anatolian Fault Zone (NAFZ), which is one of the most moving and important fault zones seismically, is the main sources in the study area. NAFZ, consisting of different fault segments that show strike slip characteristics as a faulting mechanism, has a total length of 1400 km and is divided into two separate branches crossing the north and south in the Marmara Sea Region. In this study, the northern branch of the North Anatolian Fault Zone is shown as Zone 1 and the southern branch as Zone 2. 17 August 1999 Kocaeli (Mw = 7.4) and 12 November 1999 Düzce (Mw = 7.2) earthquakes are important earthquakes within Zone 1. The October 6, 1964 Manyas earthquake (Ms = 6.9) draws attention as the biggest earthquake recorded in the instrumental period in Zone 2. Another source zone that controls the seismic hazard is defined as Zone 3 in this study. It is stated that this fault zone, called İnönü-Eskişehir fault zone, lies between İnegöl and Tuz Gölü and consists of successive segments [14]. The WNW-ESE-orientated Inonu-Eskisehir Fault Zone which separates the Aegean-western Anatolian block from the central Anatolian block is a right lateral strike-slip fault zone with a normal component. The fault zone is characterized by fault segments which trend from E-W to NW-SE in the direction of İnegol-Inönü-Eskişehir-Sivrihisar. The largest earthquake that has occurred on this fault zone is the February 1956 Cukurhisar earthquake with a magnitude of Ms = 6.4). The fault plane solution of the 1956 earthquake and field observations indicate that the Eskisehir fault zone is a trantensional fault zone and plays an important role in the development of Eskisehir and Inonu plains [15]. The Kutahya Fault Zone is situated in the Southwest of İnönü. It is composed of three main fault segments and is identified as Zone 4.

Altınok et al. [16] (2005) stated that paleoseismological and archeoseismological observations indicate that the Kütahya Fault Zone is an active fault zone and has a capable of earthquake potential at least 6.5 magnitude. One of the the most important earthquakes recorded around this fault zone was the 02 Mayıs 1928 Harmancık eartquake (Ms=6.1). Simav is one of the graben systems of Western Anatolia, which is mainly controlled by the extensional neotectonic regime of the Aegean Region of Turkey. Simav fault trends nearly WNW-ESE for 100 km, along the Simav River from Sindirgi at the West to Muratdagi at the East. The fault is not a single fracture; instead it consists of several step faults parallel to the main fracture. In this study Simav fault zone is evaluated as Zone 5.

In determining the maximum seismic magnitude, one of the most important stages of seismic hazard analysis, the surface fracture (L) and earthquake magnitude (Mw) relationship given in Table 1 was used [17]. It should be noted that the L given in Table 1 is in km.

Table 1. *Relationship between moment earthquake magnitude (Mw) and surface rupture length (L) based on Fault type [17].*

Type	Equation
Strike slip Fault	M_w=5.16 + 1.12 log L
Reverse Fault	M_w=5.0 + 1.22 log L
Normal Fault	M_w=4.86 + 1.32 log L
All Faults	M_w=5.08 + 1.16 log L

In a study on world earthquake data, it was stated that between 1/2 and 1/3 of the total length of the fault was broken during the earthquake [18]. In this study, resource zones considered during seismic hazard analyzes and evaluation for each segment was made separately.

Seismic hazard parameters of the relevant zones are given in Table 2.

Table 2. *Seismic sources for the study area*

Zone No	Segment number	Segment name	Segment type	M_{max}
1	S1_1	NAFZ- Marmara	SS	7.2
	S1_2	NAFZ- Marmara	SS	7.2
	S1_3	NAFZ- Marmara	SS	6.6
	S1_4	NAFZ - Duzce	SS	6.7
	S1_5	NA	SS	6.1
2	S2_2	NAFZ Etili-Sarikoy	SS	6.6
	S2_2	NAFZ Etili-Sarikoy	SS	6.6
	S2_3	NAFZ Etili-Sarikoy	SS	7.3
	S2_4	NAFZ Yenice- Gonen- Bursa	SS	6.7
	S2_5	NAFZ Yenice- Gonen- Bursa	SS	6.9
3	S3_1	Inonu-Dodurga Fault	N	6.7
	S3_2	Inonu-Dodurga Fault	N	6.3
	S3_3	Eskisehir Fault	N	6.4
	S3_4	NA	U	6.5
	S3_5	Kaymaz Fault	N	6.2
	S3_6	Eskisehir Sultanhani Fault	N	6.7
	S3_7	Eskisehir Sultanhani Fault	N	6.5
	S3_8	Eskisehir Sultanhani Fault	N	6.7
	S3_9	Eskisehir Sultanhani Fault	N	6.3
4	S4_1	NA	U	6.0
	S4_2	Kutahya Fault	N	6.4
	S4_3	NA	U	5.8
5	S5_1	Simav Fault	N	6.5
	S5_2	Gediz-Dumlupinar Fault	N	6.2
	S5_3	Gediz-Dumlupinar Fault	N	6.4
	S5_4	Sultandagi Fault	N	7.1
	S5_5	Beysehir Lake Fault	N	6.0

SS: strike slip, N: normal, NA: No available, U: unknown, M_{max}: Earthquake magnitude

In the absence of strong ground motion recording in the area for near time interval, it is necessary to use more than one attenuation relation to estimate the ground motion parameters to be created by the design earthquake. Eight separate attenuation equations are used in this study. The most important criterion in the selection of decrease equations is that it has to be compatible with the existing tectonic structure. It should be noted that hazard analyzes are performed for rock environment ($V_{s(30)}$ = 760 m / s). In Table 3, the results of the ground motion level, which is expressed as the maximum design earthquake, which corresponds to the probability of exceeding 10% in 50 years, are presented.

Table 3. *Probabilistic seismic hazard analysis results for the study area.*

Attenuation relationship	Peak ground acceleration (g)
Campbell [19]	0.29
Boore et al. [20]	0.24
Campbell and Bozorgnia [21]	0.39
Ambraseys [22]	0.39
Boore et al. [23]	0.26
Gulkan and Kalkan [24]	0.35
Kalkan and Gulkan [25]	0.34
Ambraseys et al. [26]	0.37
Mean	**0.32**

The average response spectrum in the rock level obtained using the estimation equations developed by Boore et al. [23], Gülkan and Kalkan [24] and Kalkan and Gülkan [25] is presented in Figure 2.

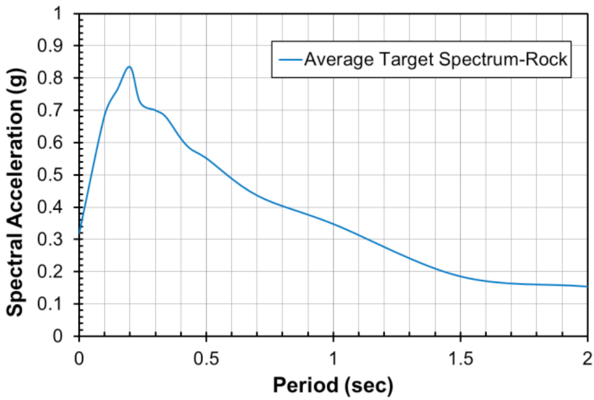

Figure 2. *Average response spectrum in the rock for the study area ($V_{s(30)}$= 760 m/s)*

2.2. MASW studies

MASW is one of the most used techniques in recent years to reveal the shallow seismic velocity characteristics of the ground [4] (Park et al., 1999). Development of surface wave methods, theoretical foundations and its application to engineering problems is summarized by Socco and Strobbia [27]. In the study area, active source MASW studies were conducted to determine the seismic wave velocities on a line. The MASW method is a process that allows the determination of the surface bands, wide bandwidth and the highest signal-to-noise ratio, which are created artificially or naturally occurring in the ground. The surface wave analysis method is carried out in 3 main stages [28]:

i) field stage where surface waves are detected and recorded with receivers,

ii) constructing signal processing and dispersion curves, and

iii) determining the change of Vs velocity with depth from the inverse analysis of the dispersion curve (Figure 3).

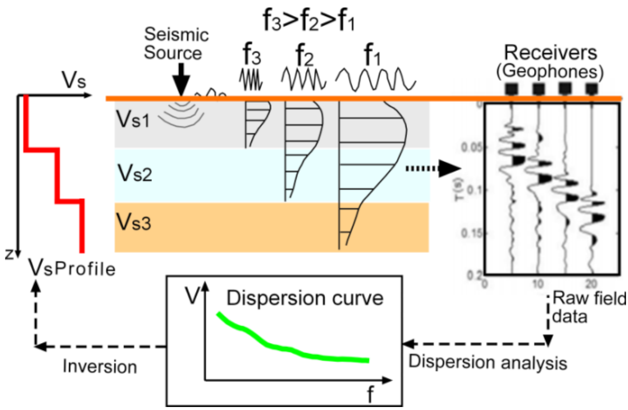

Figure 3. *Schematic representation of MASW data processing stages [28]*

Geotech brand Lakkolit 24M-3 model seismic recorder, 24 channel geophone cable, laptop, 4.5 Hz geophones and 8 kg sledge hammer and gun (blasting technique) were used in the field as presented in Figure 4. The records coming to the geophones, which were arranged at 5-meter intervals along 24 channels, were recorded digitally by laptop. In seismic studies with the Lakkolit 24M-3 device, 8192 samples could be recorded, with the sampling number of the records received 4, and the recording length was 2048 ms.

Figure 4. *MASW application in the field.*

3. Results and Discussion

As a result of the field work with the help of MASW, representative soil and shear wave velocity (Vs) profiles for the two selected locations are presented in Figure 5. In the representative profiles, the average shear wave velocities (V_{s30}) obtained at the top 30 m depth were determined as 210 m/s to be the same although the ground layer properties and thicknesses are different.

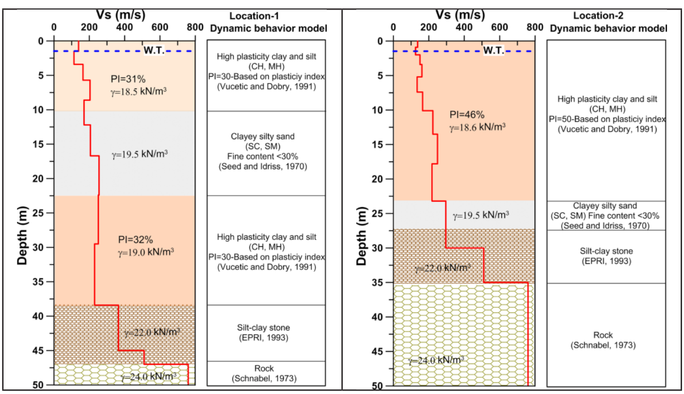

Figure 5. *Representative soil and shear wave velocity (Vs) profiles for selected locations.*

In determining the nonlinear behavior of the soils in the modeled profiles with equivalent linear approaches, the shear modulus and damping ratio should be known depending on the shear deformation. Modulus reduction ratio and damping ratio parameters are often referred to define the equivalent linear material parameters. These two parameters are used directly in defining ground behavior in site response analysis. In site response analysis using the equivalent linear model, the module ratio and damping properties should be determined for different soils. The linearity assumption made in the equivalent linear model allows the use of highly efficient computational models in site response analysis and is therefore widely used. Curves can be selected depending on the soil properties in the literature, since a lot of laboratory experiments are required to define the modulus reduction and damping ratio curves belonging to different soil types. Site response analyses were performed in accordance with the soil profiles defined in the study using one-dimensional site response models defined in the SHAKE 2000 database (Figure 6).

Shear modulus reduction (G/G_{max})-Damping ratio curves are selected depending on the soil type defined in representative profiles: i) for clay soils depending on PI proposed by Vucetic and Dobry [29], ii) for sand soil developed by Seed and Idriss (30], iii) for silt-clay stone layer recommended by EPRI [31] ,and iv) for rock level developed by Schnabel [32].

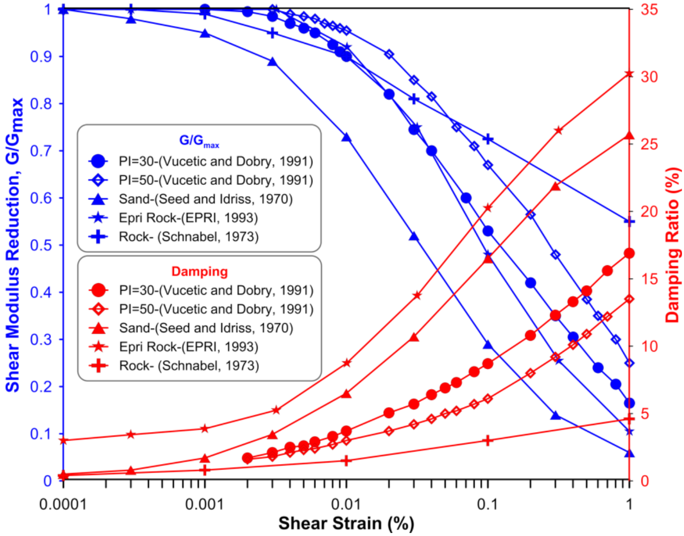

Figure 6. *Shear modulus and damping ratio curves for materials used in the study*

Both simulated and real ground motions for seismic hazard analysis are widely used for site-specific intervention studies [33]. In the dynamic analysis, the synthetic acceleration record obtained from the analysis of the seismic hazard and the real acceleration record measured at the Gebze station of the Kocaeli earthquake on August 17, 1999 were used (Figure 7). Acceleration-time graph is used which is compatible with the hazard spectrum in soil amplification analysis. Figure 7 shows the scaled and non-scaled states of real and artificial acceleration recordings that are harmonized with the average response spectrum.

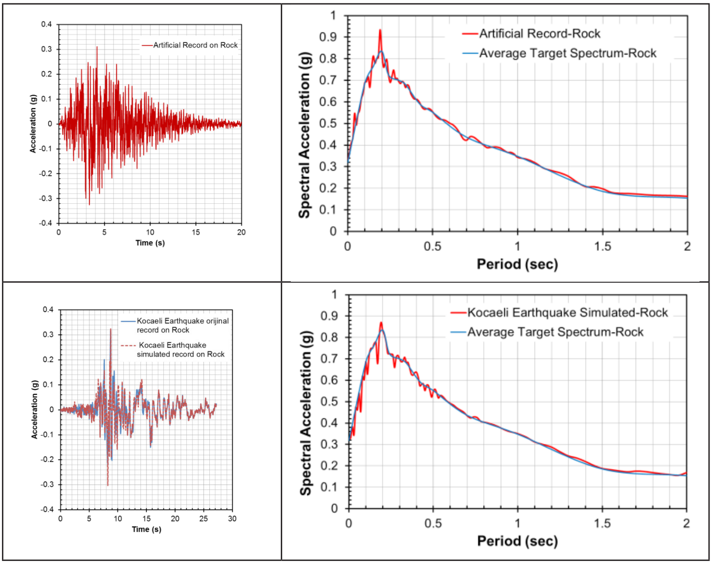

Figure 7. *Acceleration-time records compatible with the hazard spectrum on the bedrock*

Using the bedrock acceleration records shown in Figure 8, the changes in the acceleration-time values obtained on the ground surface as a result of the analyses made in the Shake 2000 program are presented in Figure 8. As seen in the figure, it is seen that it gives greater acceleration values on the surface in location-2 as a result of the analyses made using both artificial and real records. Although they have the same average shear wave velocity in both locations, the surface acceleration values differed due to the difference of the ground layers.

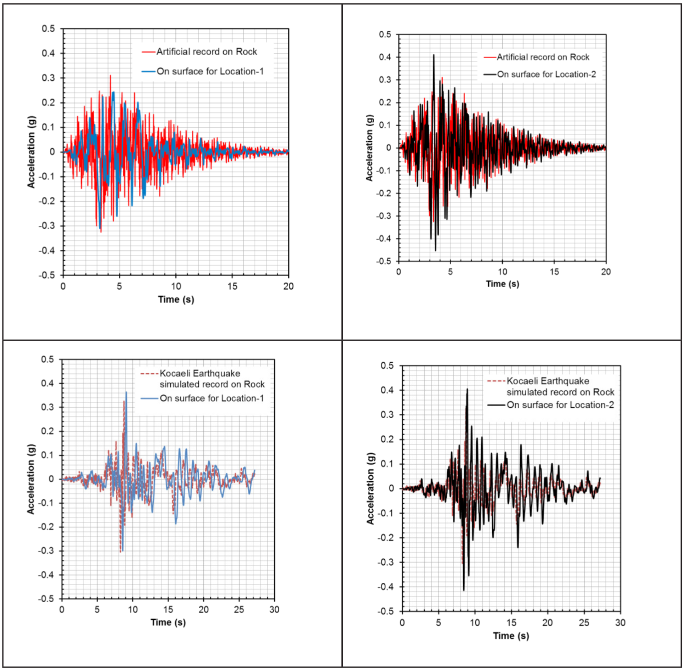

Figure 8. *Acceleration-time records obtained on the surface as a result of analysis*

Examining the acceleration time series on the ground estimated from the equivalent linear analysis of the Location-1, it is obvious that the soil profile amplified the motion (0.364g as the base motion is 0.32 g) for the second case and the peak ground acceleration shifted to the right a little. However, the profile de-amplified the energy (0.244g) through the stratification for the artificial base motion. Although it is the same profile, the frequency content of the base motion is highly effective on the surface behavior.

Regarding the Location-2, both motions were amplified (0.412g for artificial motion and 0.406g for Kocaeli base motion) by the soil layering. The occurrence of the peak ground acceleration was also altered for both case and there is some differences in the frequency characteristics of the ground surface data.

It is very conventional way to assess the seismic behavior with the help of spectrum envelopes. Figure 9 and Figure 10 show the spectrum characteristics of the ground surface for both locations.

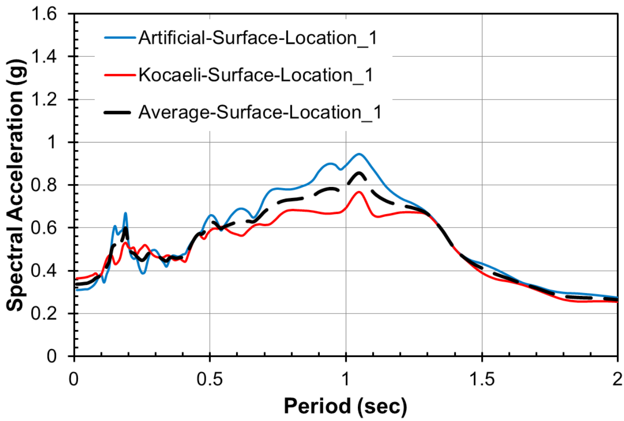

Figure 9. *Variation of the spectral acceleration-time recordings obtained on the soil surface at location-1 (5% damping)*

Although both spectral behaviors fall into the similar path over different periods, there is distinct difference between the important parameters. It is noted that there is almost % 20 changes in peak ground accelerations for location-1. Moreover, the peak spectral accelerations were recorded at around 1.05 s but in different amplitudes (1.25 times larger for artificial compared to Kocaeli earthquake).

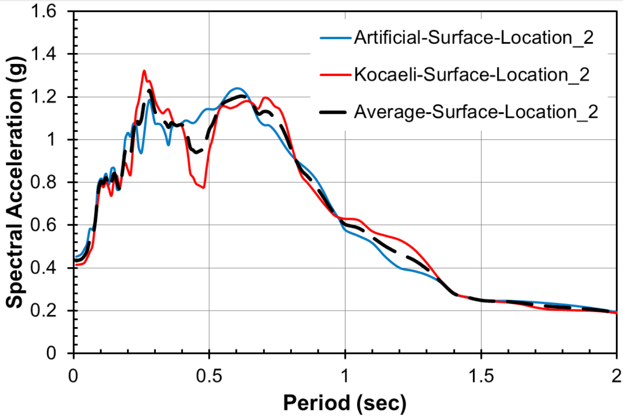

Figure 10. *Variation of the spectral acceleration-time recordings obtained on the soil surface at location-2 (5% damping)*

Comparing to Figure 9, there is a different behavior observed in Figure 10. Both base motions were amplified with the soil profile and gave pretty much similar results. Regarding the peak spectral accelerations, there are two peaks were seen around similar periods however, the magnitudes are totally different for different base motions. The model was shook by the Kocaeli earthquake has the first peak about 1.3g and the second one about 1.2g whereas these values were 1.16g and 1.24g respectively for the analysis done by the artificial motion. Although the peak ground accelerations about the same for both models, the spectral accelerations behavior differ in an interval of 0.2 to 1 seconds.

In order to understand the different at once, the average response spectrum obtained for location-1 and location-2 along with the site specific response offered by the Turkish Building Code (TBC) [34] is presented in Figure 11.

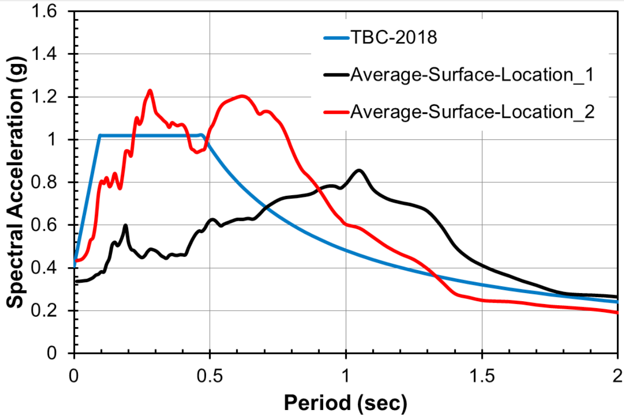

Figure 11. *Variation of the spectral acceleration-time recordings along with the TBC-2018 (5% damping)*

It is clearly seen that response spectra occur different for two locations and they do no match with the spectrum offered by the building code. The main purpose here is not to evaluate the performance of the building code but to see the variation of the data with the reference curve. The average peak ground acceleration and the peak spectral acceleration values vary a lot for the profiles with the exact same average shear velocity values. This underlines the effect of the soil layering over the ground response.

4. Conclusion

Shear wave velocity value is widely used in geotechnical earthquake engineering applications, especially for the design spectra by the building codes. Depending on the average shear wave velocity determined especially at the top 30 m depth; evaluations are made on the responses of the soils exposed to earthquake effects. In this study, from the analysis made in two different locations with the same average shear wave velocity, it was found that the stratification condition of the soil is very important on the ground response of the soil. It does not only affect the peak ground acceleration and the time it happens, it also changes the spectral behavior over the large extend of the period. The soil profile may have different on the characteristics of the motion sometimes as amplification and sometimes as de-amplification. Therefore for the assessment of the seismic behavior of the ground surface, site specific analysis should be run in order to estimate the seismic loads better. In this way, the effects of local ground conditions on earthquake ground motion characteristics and building damages will be taken into consideration in the seismic design.

REFERENCES

1. Seed, H.B., Idriss, I.M. (1969). Influence of Soil Conditions on Ground Motions During Earthquakes. *Journal of the Soil Mechanics and Foundation Division*, ASCE, Vol. 95, SM1, pp.99-137.

2. Seed, H.B., Whitman, R.V., Dezfulian, H., Dobry, R.and Idriss, I.M. (1972). Soil Conditions and Building Damage in Caracas Earthquake. *Journal of the Soil Mechanics and Foundation Division*, ASCE, Vol. 98, SM8.

3. Chang, K.P., and Chang T.S. (1994). *Liquefaction Induced Earth Movements and Mitigation in an Earthquake-Prone area. Developments in Geotechnical Engineering.* Balasubramaniam et al. (eds), Balkana, ISBN 905105224, pp.291-299,

4. Park, C. B., Miller, R. D., and Xia, J. (1999). Multi-channel analysis of surface waves. *Geophysics*, 64(3), 800-808.
5. Xia, J., Miller, R. D. and Park, C. B. (1999). Estimation of near-surface shear-wave velocity by inversion of Rayleigh waves. *Geophysics,* 64(3), 691-700.

6. Penumadu, D. and Park, C. B. (2005). Multi-channel analysis of surface wave method (MASW) for geotechnical site characterization. *American Society of Civil Engineers Geotechnical Special Publication*, Issue 130, 956-967.

7. Long, M., and Donohue, S. (2007). In situ shear wave velocity from multi-channel analysis of surface waves (MASW) tests at eight Norwegian research sites. *Canadian Geotechnical Journal*, 44(5), 533-544.

8. Park, C. B., Xia, J., and Miller, R. D. (1998). Imaging dispersion curves of surface waves on multi-channel record. *Society of Exploration Geophysicists Expanded Abstracts*, 17, 1377-1380.

9. Ivanov, J., Miller, R. D., Lacombe, P., Johnson, C. D., and Lane Jr., J. W. (2006). Delineating a shallow fault zone and dipping bedrock strata using multichannel analysis of surface waves with a land streamer. *Geophysics*, 71(5), A39-A42.

10. Boore, D. M., and Asten, M. W. (2008). Comparisons of shear-wave slowness in the Santa Clara Valley, California, using blind interpretations of data from invasive and non-invasive methods. *Bull. Seism. Soc. Am.*, 98, 1983-2003.

11. SHAKE 2000, A Computer Program for Earthquake Response Analysis of Horizontally Layered Sites; by Schnabel, P. B., Lysmer, J., and Seed, H. B. Report No. UCB/EERC-72/12, Earthquake Engineering Research Center, University of California, Berkeley, December, (1972)., User's Manual, revised by Gustavo A. Ordonez, July 2011.

12. Bommer, J.J., J. Douglas, and F. O. Strasser (2003). Style-of-faulting in ground motion prediction equations. *Bulletin of Earthquake Engineering*, 1 (2), 171–203.

13. Türköz, M., (2019). "The Effect of Soil Type and Different In-situ Test Results on Soil Amplification Analysis", DUJE, Vol. 10, No. 3, pp.1187-1196. DOI: 10.24012/dumf.589196.

14. Bozkurt, E.(2001). Neotectonics of Turkey. *Geodinamica Acta*, 14(1-3):3-30. DOI: 10.1016/S0985-3111(01)01066-X

15. Altunel, E. and Barka, A. (1998). Neotectonic activity of Eskisehir Fault Zone between Inonu and Sultandere. *Geological Bulletin of Turkey*. 41(2), 41–52, (in Turkish).

16. Altinok, S., Karabacak, V., Yalçiner, C.Ç., Bilgen, A.N.,, Altunel, E. , Kiyak, N.G. (2012). Holocene Activity of Kütahya Fault Zone. Türkiye Jeoloji Bülteni *Geological Bulletin of Turkey,* 55(1).

17. Wells, D.L. and Coppersmith, K.J. (1994). New Empirical Relationships Among Magnitude, Rupture Length, Rupture Width, Rupture Area, and Surface Displacement. *Bulletin of the Seismological Society of America*, 84, 4, 9741002.

18. Mark, R.K., (1977). Application of Linear Statistical Models of Earthquake Magnitude Versus Fault Length in Estimating Maximum Expectable Earthquakes. *Geology*, 5, 464– 466.

19. Campbell, K. W. (1981). Near-source attenuation of peak horizontal acceleration. *Bulletin Seism*. Soc. Am., 71, 6, 2039-2070.

20. Boore, D. M., Joyner, W. B.and Fumal, T. E. (1993). *Estimation of Response Spectra and Peak Accelerations from Western North American Earthquakes. An interim repor.* U.S. Geol. Surv. Open-File Rept. 93-509, 72 p.

21. Campbell, K. W. and Bozorgnia, Y. (1994). Near-source Attenuation of Peak Horizontal Acceleration from Worldwide Accelerograms Recorded from 1957 to 1993. Proc. Fifth U.S. National Conference on Earthquake Engineering 3, Chicago, Illinois, July 10-14, 283-292.

22. Ambraseys, N. N. (1995). The Prediction Of Earthquake Peak Ground Acceleration In Europe. *Earthquake Engineering and Structural Dynamics*, 24, 467-490.

23. Boore, D. M., Joyner, W. B. and Fumal, T. E. (1997). Equations For Estimating Horizontal Response Spectra and Peak Acceleration from Western North American Earthquakes: A Summary of Recent Work. *Seismological Research Letters*, 68, 128-153.

24. Gülkan, P. and Kalkan, E.(2002). Attenuation Modeling of Recent Earthquakes in Turkey. *Journal of Seismology*, 6 (3), 397-409.

25. Kalkan, E. and Gülkan, P. (2004). Site-dependent spectra

derived from ground motion records in Turkey. *Earthquake Spectra*, 20(4), 1111-1138.

26. Ambraseys, N.N., Douglas, J., Karma, S.K. and Smit, P.M. (2005). Equations for the estimation of strong ground motions from shallow crustral earthquakes using data from Europe and the Middle East: horizontal peak ground acceleration and spectral acceleration. *Bulletin of Earthquake Engineering*, 3, 1-53.

27. Socco, L.V. and Strobbia, C. (2004). Surface-wave method for near-Surface characterization: a tutorial. Near Surface Geophysics, 2, 165-185.

28. Dikmen Ü., Başokur A. T., Akkaya İ. and Arısoy M. Ö. (2009). Selection of Optimum shot distance in multi-channel analysis of the surface wave method. Yerbilimleri, 31 (1), 23–32.

29. Vucetic M, Dobry R. (1991). Effect of soil plasticity on cyclic response. *Journal of Geotechnical Engineering*, 117(1): 89-107.

30. Seed, H., Idriss, I. (1970). Soil moduli and damping factors for dynamic response analyses. Report No. EERC 70-10, University of California, Berkeley.

31. EPRI (1993) Guidelines for determining design basis ground motion. Palo Alto, CA, Electric Power Research Institute, 1, EPRI TR-102293

32. Schnabel P.B, (1973), Effect of local geology and distance from source on earthquake ground motion. Ph. D. Thesis, University of California, Berkeley, California

33. Ansal A, Tonuk G. (2007). Source and site factors in microzonation. In: KD Pitilakis (eds) Earthq Geotech Eng 73–92.
34. Turkish Building Code (2018) Prime Ministryi Disaster and Emergency Managemenet Authority (AFAD)

Chapter 3

THE ROLE OF PARTICLE SHAPE AND ROUGHNESS IN FLOTATION PROCESS

Can GÜNGÖREN[1]

1 Istanbul University-Cerrahpasa, Engineering Faculty, Mining Engineering Department, 34500, Buyukcekmece, Istanbul, Turkey. can@istanbul.edu.tr

1. INTRODUCTION

The size, shape, and roughness of a particle consist of its morphological characteristics. In mineral processing, particle shape and roughness has a significant effect on the physical and chemical actions occurring on the particle surface during the technological processes. Therefore, it is important to determine the morphology of a particle quantitatively for predicting the behavior of particles in mineral processing operations including flotation (Ahmed, 2010). The size of the particles can be characterized by sieving or laser diffraction particle size analyses. However, the characterization of a particle's shape and roughness is quite complicated which is usually carried out with image analysis.

The first step of image analysis is taking digital images of the individual particles at high magnification rates using different microscopy methods including darkfield, brightfield, polarized light, etc. according to the size, chemical, and physical properties of the particles (Olson, 2011). Then, the measurement of the particle dimensions and calculation of the shape descriptors are generally carried out with the help of automated microscopes and image analyzing software such as Matlab, ImageJ, Olympus, PAXit, etc. (Rishi, 2015).

It is clearly stated in literature that there is no general shape descriptor available, which clearly differentiates between all possible kinds of shapes (Podczeck, 1997). Therefore, various shape descriptors can be used related to the purpose of the study. These shape descriptors are calculated using mathematical procedures. However, it is also seen from literature that the mathematical approaches used for calculating a particle shape descriptor can be varied.

In this context, this study was focused on the calculations of the particle shape and roughness descriptors and the role of them on the flotation process of mineral processing.

2. PARTICLE SHAPE DESCRIPTORS

The simplest method using the classification of particles according to their shapes is a verbal description. The particles can be described using words as spherical, disc, rod, rounded, fibrous, flaky, irregular, etc. However, this description is quite subjective (Singh & Ramakrishnan, 1996). Therefore, more quantitative descriptors are needed in order to describe the shape of a particle. The first procedures developed for describing the shape of particles comprised of the measuring of simple linear parameters including the length, breadth, and width. Then, the ratios of these dimensions were used for describing other shape-dependent properties (Sarkar & Chaudhuri, 1994).

The major particle shape descriptors used in mineral processing and their calculation procedures are given and discussed within this study.

Length (L), Width (W), and Thickness (T): The length (L) and the width (W) (or Breadth, (B)) are the maximum and minimum distances between any two points on the perimeter of the particle. The length is parallel to the major axis while the width is parallel to the minor axis (Olson, 2011).

Yekeler et al. (2004) calculated the length and width, assuming the projection of the particle has an ellipse-like shape. From each particle, five linear lengths and five linear widths were measured and averages of these measurements were taken as length and width (Fig. 1a) (Hicyilmaz et al., 2004; Kursun & Ulusoy, 2006; Ulusoy et al., 2004).

Chan et al. (2002) determined the length and width using a computer software (PC Image, version 2.2.01, Foster Findlay, Newcastle, UK). In their study, the length of a particle was determined as the maximum chord length of the particle regardless of orientation and breadth was the width perpendicular to the length (Fig. 1b).

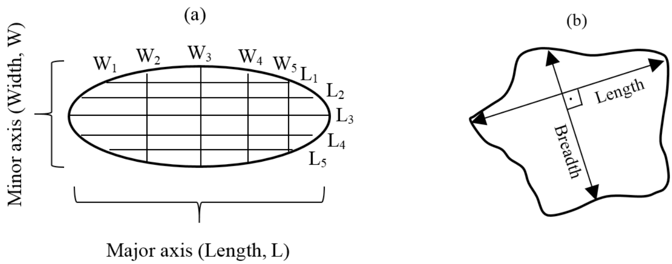

Figure 1. *Measurement of the length and width of a particle according to (a) (Kursun & Ulusoy, 2006) and (b) Chan et al. (2002).*

In three-dimensional conception, it is assumed that the relationship between the Length, Width, and Thickness of a particle is “L>W>T” (Steuer, 2010).

Major and Minor Axes: The major and minor axes pass through the center of mass of the particle and always perpendicular to each other (Fig. 2). The major axis located corresponding to the minimum rotational energy of the shape (Olson, 2011).

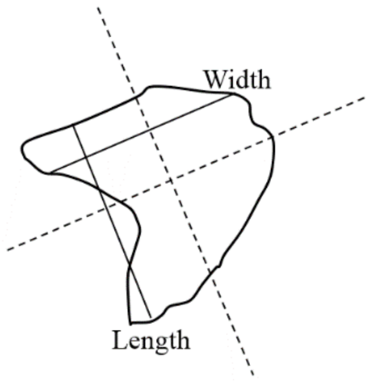

Figure 2. *A particle indicating the major and minor axes (dashed lines), as well as the length and width (Olson, 2011).*

Feret's Diameter: The maximum (X_{max}) and minimum (X_{min}) Feret's diameter is the furthest and shortest distances between any two parallel tangents on the particle, respectively (Fig. 3) (Olson, 2011).

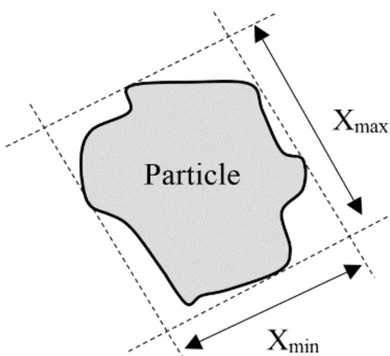

Figure 3. *Feret's diameter for an irregular particle (adapted) (Hogg et al., 2004)).*

Aspect Ratio (AR): Aspect ratio can be described as the ratio of the minimum Feret's diameter to the maximum Feret's diameter as shown in Eq. (1). Therefore, the aspect ratio is always between 0 and 1. The aspect ratio is a useful descriptor for the particles that are not very elongated (Olson, 2011).

$$AR=\frac{X_{F_{min}}}{X_{F_{max}}} \tag{1}$$

Relative Width (RW): The term "relative width" can be widely used instead of aspect ratio and determined by Eq. (2).

$$RW=\frac{W}{L} \tag{2}$$

Elongation Ratio (E): Elongation is the inverse of aspect ratio and calculated with Eq. (3) (Hogg et al., 2004; Olson, 2011).

$$E=\frac{X_{F_{min}}}{X_{F_{max}}}=\frac{L}{W}=1-AR \tag{3}$$

Flatness Ratio: The flatness ratio of a particle was defined by Ahmed (2009) as Eq. (4).

$$\textit{Flatness ratio}=\frac{W}{T} \tag{4}$$

There are other shape descriptors that can be calculated using length, width, and thickness of the particle.

Cubicity: The cubicity of a particle is calculated using Eq. (5) (Unland & Al-Khasawneh, 2009).

$$\text{Cubicity}=\frac{L}{T} \tag{5}$$

Sphericity (ψ): The sphericity of a particle can be calculated with Eq. (6) (Xia, 2017).

$$\text{sphericity} = \frac{\sqrt[3]{T \times W}}{L^2} \tag{6}$$

Corey Shape factor: Corey Shape Factor (also known as Shape Factor) (Allan & Woodcock, 2001; Mora & Kwan, 2000) is defined as Eq. (7) (Xia, 2017).

$$\text{Corey Shape factor} = \frac{T}{\sqrt{W \times L}} \tag{7}$$

Perimeter: The perimeter of a particle is calculated via Eq. (8) (Cauchy-Crofton equation) using the number of intercepts, I, formed by a series of parallel lines, with spacing dL, exploring N directions, from α to π (Olson, 2011).

$$P = \frac{\pi}{N} \sum_{\alpha}^{\pi} I_\alpha d_L \tag{8}$$

Many researchers calculated the perimeter of a particle using Eq. (9) (Dehghani et al., 2013; Hicyilmaz et al., 2004; Kursun & Ulusoy, 2006; Ulusoy et al., 2004; Wang et al., 2018; Yekeler et al., 2004). In some studies, this is stated as the perimeter of the external ellipse as seen in Fig. 4 (Wang et al., 2018; Yin et al., 2019).

$$P \approx \frac{1}{2}\pi \left[\frac{3}{2}(L + W) - (LW)^{1/2}\right] \tag{9}$$

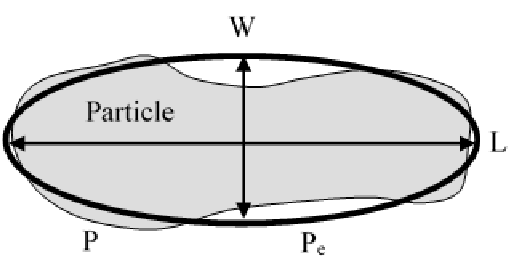

Figure 4. *A schematic representation of the measurement parameters of a particle (adapted from Wang et al. (2018) and Yin et al. (2019)).*

Area (A): The area of a particle can be calculated in the unit of pixels using a digital image as the sum of the areas of each individual pixel (a_p), within the borders of the particle using Eq. (10). Then, the unit is converted to μm^2 by calibrating the software using a micrometer (Olson, 2011).

$$A=\sum a_p \tag{10}$$

Several researchers calculated the area of the particle using Eq. (11) (Dehghani et al., 2013; Hicyilmaz et al., 2004; Kursun & Ulusoy, 2006; Ulusoy et al., 2004; Yekeler et al., 2004).

$$A = \frac{\pi LW}{4} \tag{11}$$

Bilgen et al. (1995) make the particle shape calculations using Eq. (12), assuming that particles have an elliptic shape with a long and short axis of 2a and 2b, respectively.

$$A=\pi ab \tag{12}$$

Circularity (C): Circularity is a measure of how much a particle resembles a circle considering its smoothness and perimeter. The circularity factor decreases as the particle shape moves away from a perfect and smooth circle (Eq. (13)) (Olson, 2011).

$$C = \sqrt{\frac{4\pi A}{P^2}} \tag{13}$$

Xia (2017) calculated circularity with Eq. (14) and high sensitivity circularity with (Eq. (15)), respectively.

$$C = \frac{4\pi A^2}{P^2} \tag{14}$$

$$\text{High Sensitivity Circularity} = \frac{4\pi A}{P^2} \tag{15}$$

Flatness (F) (Angularity): The inverse of circularity is defined as Flatness (Little et al., 2015; Ulusoy & Kursun, 2011) and calculated by Eq. (16). In some studies, this parameter is also called Angularity (Vizcarra et al., 2011).

$$F = \frac{P^2}{4\pi A} \tag{16}$$

Roundness (Ro): In literature, it is seen that roundness is widely used instead of circularity (Bilgen et al., 1995; Dehghani et al., 2013; Guven & Celik, 2016; Hicyilmaz et al., 2004; Kursun & Ulusoy, 2006; Ulusoy et al., 2004; Wang et al., 2018; Wen & Xia, 2017; Yekeler et al., 2004). Meanwhile, ImageJ image analyzing software calculates the roundness of a particle using Eq. (17) (Baecker, 2015).

$$Ro = \frac{4A}{\pi \cdot (major\ axis)^2} \tag{17}$$

Roughness (λ): Roughness is another important parameter that is most likely formed due to the fluctuations around a smooth and sharp interface (Guven et al., 2015b). In Fig 5., while the real surface is XY, AB represents the surface of a hypothetical solid of equal volume with a molecularly smooth surface (Rahimi et al., 2012b).

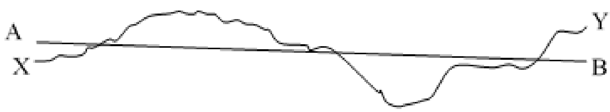

Fig 5. *A profile of a solid surface*

There are various calculations were reported in the literature such as Eq. (18) and Eq. (19).

$$\text{Roughness} = \frac{\text{Area of the real surface XY}}{\text{Area of the surface defined by AB}} \tag{18}$$

$$\text{Roughness} = \frac{P}{P_e} \tag{19}$$

Where, P_e is the perimeter of the external ellipse and P is the perimeter of the particle (Wang et al., 2018; Yin et al., 2019).

Roughness can be also determined directly using some analytical devices such as SEM (Feng & Aldrich, 2000), AFM (Miller et al., 1996), profilometer (Gungoren et al., 2019), and BET (Rezai et al., 2010). When BET is used, the roughness can be calculated using Eq. (20).

$$\text{Roughness} = \frac{\rho D A_{BET}}{6} \tag{20}$$

Where A_{BET} is the BET specific surface area (m^2/g), ρ is the particle density (g/cm^3), D is the average particle diameter (μm), (Rahimi et al., 2012a; Rahimi et al., 2012b).

3. The Relationship Between the Grinding Process and the Particle Shape

Grinding is essential to liberate valuable minerals from their gangue. Several parameters affect the particle shape during the grinding process. The importance of mineral type for the ultimate particle shape after the grinding process was revealed by Tasdemir et al. (2008). The time of the grinding process is another important factor for particle shape. Wang et al. (2018) reported that the roundness of coal particles increased with grinding time.

The choice of the grinding method also influences the particle shape and roughness of the grinding products and therefore the following flotation process. For instance, while dry grinding produces relatively rough particle surfaces, the wet grinding produces smoother surfaces. The dry ground samples exhibited more stable and higher loaded froths as well as faster flotation kinetics (Ahmed, 2009; Ahmed, 2010; Feng & Aldrich, 2000).

Similarly, mill type also has an important role in the shape properties of particles (Rezai et al., 2010). The shape of the particles produced by different mills varies significantly. The work carried out by Bilgen et al. (1995) showed that the barite particles ground by autogenous mill had higher roundness, together with lower surface roughness. On the other hand, the particles that ground in ball mill had higher flatness and elongation ratio with a rougher surface. Hicyilmaz et al. (2004) reported for talc and quartz minerals that the particles ground by rod mill had higher flatness and elongation ratio. The importance of mineral type for the ultimate particle shape after the grinding process was revealed by Ulusoy et al. (2004). According to the results of their study, while the highest elongation ratio and flatness values were obtained by autogenous milling for calcite, the maxima were reached by ball milling for barite particles. Rahimi et al. (2012b) stated that the rod mill products of quartz particles have higher roughness and elongation ratio and lower roundness than the particles of ball mill products. Their results were also showed that the surface roughness for both ball and rod mill products decreases with the reduction of particle size for quartz mineral. For a particular size, the rod mill products have larger surface roughness than the ball mill products. Ulusoy & Igathinathane (2014) investigated the shape analysis of coal particles. The results of their study indicated that the products of ball mill had the highest aspect ratios with the lowest circularity. However, the gyro mill produced particles with the highest circularity along with the lowest aspect ratios. They attribute this relative difference in shape to the difference in grinding action involved in the ball and gyro mills.

4. The Role of Particle Shape and Roughness in Flotation Process

The influence of particle shape on flotation was investigated by many researchers. In most of them, it was revealed that the flotation recovery is decreased with the roundness of the particles. Ulusoy et al. (2004) reported that the calcite and barite particles with higher elongation and flatness were recovered better with flotation, in the opposite of the particles with higher roundness and relative width. Similar results were obtained by Kursun & Ulusoy (2006) for the flotation of talc mineral.

In this context, the flotation kintetic calculations can be used to determine the success of the flotation process quantitatively. For example, Koh et al. (2009) investigated the effect of particle shape on the flotation process using spherical and grounded glass beads. Their results indicated that ground beads generally have higher rates than spherical ones. Xia et al. (2017) reported similar results for the flotation of coal. According to their results, the flotation performance of coarse coal particles with a round corner was worse than that of coal particles with a sharp corner.

Another study carried out with chalcopyrite by Vizcarra et al. (2011). Their results showed that angular particles float faster and more efficiently than comparatively round particles in the absence of a collector. However, the shape factor becomes less important for the particles with high floatability in the presence of a collector (potassium amyl xanthate). The recovery versus time plots of each angularity class is shown in Fig. 6. The plots fitted well to the two-component, first-order batch flotation rate equation (Eq. (21)), and fitted parameters for each angularity class which are shown in Table 1.

$$R = 1 - (m_f \exp(-k_f t) + m_s \exp(-kt)) \quad (21)$$

Where, R is the cumulative fractional recovery at time t, t is time (min), m_s is the fractional mass of slow floating particles, m_f is the fractional mass of fast floating particles=1-m_s, k_s is the first-order rate constant of the slow floating fraction (min^{-1}) and k_f is the first-order rate constant of the fast floating fraction (min^{-1}).

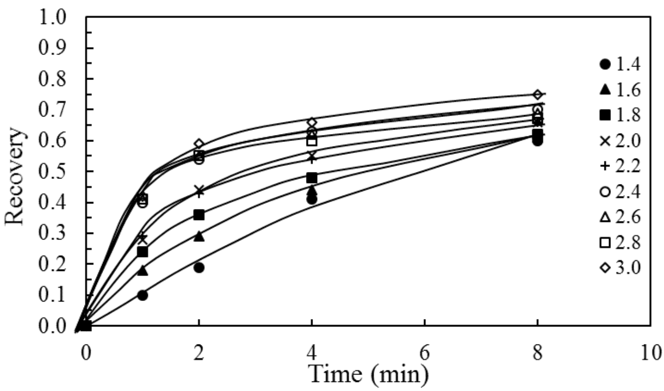

Figure 6. *Recovery of various angularity classes of chalcopyrite floated without a collector with respect to time (Vizcarra et al., 2011).*

Table 1. *Flotation rate equation parameters of concentrates recovered without a collector (Vizcarra et al., 2011).*

Angularity	1.4	1.6	1.8	2.0	2.2	2.4	2.6	2.8	3.0
m_f	0.00	0.32	0.32	0.48	0.42	0.52	0.52	0.51	0.58
m_s	1.00	0.68	0.68	0.52	0.58	0.48	0.48	0.49	0.42
k_s (min^{-1})	0.12	0.07	0.07	0.05	0.06	0.06	0.06	0.05	0.06
k_f (min^{-1})	0.00	0.51	0.86	0.73	0.94	1.22	1.36	1.43	1.15

Likewise, Wen & Xia (2017) reported that the coal particles with lower roundness floated quickly, while the coal particles with higher roundness floated slowly. Another study on coal flotation also revealed that the flotation kinetics constant increased with increasing the aspect ratio, while the particle owning high roundness and circularity value led to smaller flotation kinetics constant (Yin et al., 2019).

The roughness of the particles is another important property for the flotation process. Rahimi et al. (2012) stated that the influence of the surface roughness on the flotation kinetics was greater than that of shape parameters for quartz mineral. Guven et al. (2015b) and Guven et al. (2016) reported that the particles with higher roughness were floated in higher recoveries.

In literature, the effects of particle shape and roughness on the flotation process are attributed to several parameters. The first parameter is the change in the wettability of the minerals. Although Dang-Vu et al. (2006) were reported that surface roughness did not affect the contact angle of glass beads. It has been shown by Miller et al. (1996) that the hydrophobic surfaces can be obtained by appropriate roughening processes with vacuum-deposited polytetrafluoroethylene (PTFE) thin films. In order to measure the contact angle on rough surfaces, Meiron et al. (2004) developed and used a contact angle measurement method. The method consists of vibrating the surface, taking top-view pictures of the drop, monitoring the drop roundness, and calculating the contact angle from the drop diameter and weight. In addition, several other studies on the wettability of various minerals showed that elongation, flatness, and smoothness helped to increase the hydrophobicity, while roundness and roughness caused a decrease in hydrophobicity or floatability of the quartz (Ulusoy et al., 2003), talc (Hicyilmaz et al., 2004), calcite and barite (Ulusoy et al., 2004) minerals.

The second parameter is the change in bubble/ particle interactions. Since the efficiency of flotation process is strongly related to the collision, attachment, and detachment processes between bubbles and particles (Albijanic et al., 2014; Albijanic et al., 2010; Gungoren et al., 2019), it is a popular field of study that if some certain particle shapes have better interaction with bubbles then others, which make them more floatable (Ahmed, 2009; Rahimi et al., 2012b). Since flattened particles settle more slowly in a fluid than cubes of equal mass, they have higher bubble-particle collision probability (Allan & Woodcock, 2001).

In terms of bubble-particle induction time, Verrelli et al. (2014) stated that angular particles exhibiting induction time that was an order of magnitude lower than those of spheres. The elongated and flaky particles have larger contact line and area during the bubble- particle attachment. The angular particles owning sharp corners ruptures the film easily during the attachment process (Wang et al., 2018; Wen & Xia, 2017).

Furthermore, roughness also has a crucial effect on the time of the colliding bubble attachment. Higher roughness of the surface increases the probability of the rupture of the thinning liquid film. In addition, the larger cavities at rough surfaces can hold up a larger amount of gases what leads to faster formation of a long enough perimeter of the three-phase contact (TPC) for the bubble attachment (Krasowska & Malysa, 2007; Krasowska et al., 2009).

The relationship between the roundness, roughness and induction time of low-rank coal particles was studied by Wang et al. (2018). Their induction time measurement results indicated that the particle surface roughness played a significant role in the surface hydrophobicity of low-rank coal particles. The induction times of low-rank coal samples showed an increasing trend after the grinding and abrading processes, which may be attributed to the difficult rupture of the wetting film on the smooth solid surface.

Vaziri Hassas et al. (2016) investigated the effect of particle shape and roughness on the flotation, contact angle, and bubble-particle attachment time using spherical and grounded glass beads without and with acid etching. Their results showed that an increase in the roughness improves the flotation recovery, contact angle, and bubble attachment (Fig. 7). Meanwhile, the shape factor was found to be more predominant in flotation and bubble attachment. This is attributed to the effect of sharp edges of ground particles that triggers the film rupture process and shortens the attachment time.

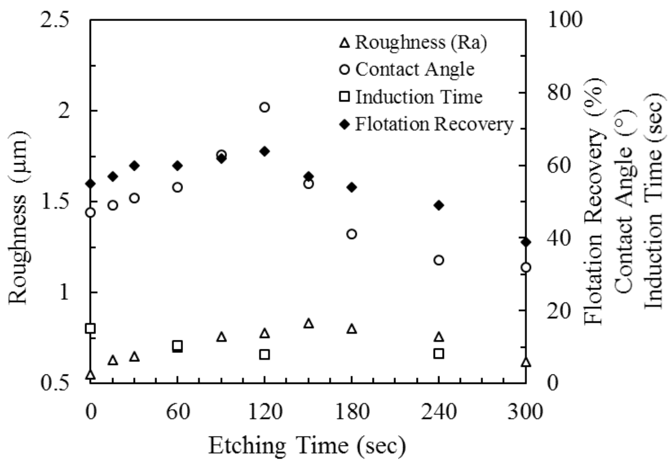

Figure 7. *Change in the roughness, flotation recovery, contact angle, and induction time of the glass beads with respect to etching time (Adapted from Vaziri Hassas et al. (2016)).*

Guven et al. (2015a) reported that the flotation rate constants of roughened particles increased consistently with increasing dimensions of surface asperities. Their theoretical modeling results suggest that the size of nano-sized hydrophobic asperities distributed over spherical microscopic particles dictates the magnitude of the energetic barrier that particles need to overcome in order to attach to bubbles.

Karakas & Vaziri Hassas (2016) studied the effect of roughness on flotation using spherical and etched glass beads. Their results, seen in Fig 8, indicated that the roughness was increased with etching time up to 120 sec and then decreased probably because of the chipping off the sharp corners at longer etching times. The adsorption of the collector (hexadecyltrimethylammonium bromide, HTAB) on to the surface of glass particles was strongly affected by the roughness of particles that affected the interaction forces and governs the flotation efficiency of particles. Therefore, the flotation was improved significantly in the presence of rough particles.

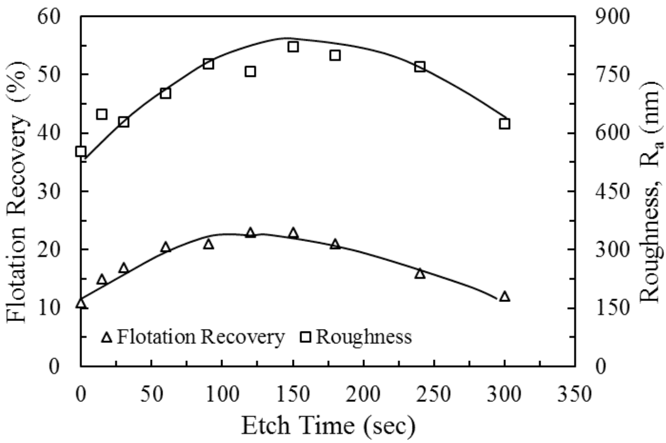

Figure 8. *Micro-flotation recovery (at $1\cdot10^{-6}$ HTAB concentration) and roughness of round glass beads measured by AFM against different etching time (Flotation time was 1 min) (Karakas & Vaziri Hassas, 2016).*

The shape of the particles affects also the detachment process of them from bubbles. Ahmed (2010) stated that the detachment force of angular particles is harder than that of spherical particles.

One other factor responsible for the improved flotation recovery and kinetics is the increased stability and height of the froths in the presence of rough particles owing to the activated particle surfaces. More activated and increased surface area improves the adsorption and activity of the collector used which causes better bubble-particle interactions (Feng & Aldrich, 2000).

Apart from these influences, entrainment is another important process that affects the flotation process. Particles with different shapes in the same size classes have different entrainment properties. Wiese et al. (2015) showed that the entrainment process was increased with an increasing aspect ratio of the particles.

5. Conclusions

The shape and roughness of a particle are important parameters for physical and chemical actions occurring on the particle surface during the mineral processing operations such as flotation. Determining the shape and roughness of a particle quantitatively is a complicated process that requires some elaborate microscopy analyses and specialized image analyzing software.

There are various image descriptors used in the studies on mineral processing with different calculation methods. The most used shape descriptors and calculation methods were reviewed, compiled, and compared within this study.

In the aspect of mineral processing, first, the effect of the grinding process on the particle shape factors was reviewed. It is seen in literature that various parameters have a role in the particle shape during grinding including grinding time and method, mill and mineral type. Although mineral type affects the final particle shape after the grinding process, it can be generally said that the roundness of the particles increased with grinding time. Dry grinding produces rougher surfaces than wet grinding. While autogenous and gyro mills produce rounder particles, the products of the ball and rod mills are more elongated. Meanwhile, the particles that ground by rod mill have rougher surfaces than the products of a ball mill.

The studies on the role of particle morphology in the flotation process indicated that more angular, flaky, and elongated particles have higher flotation efficiencies than rounder particles. The difference in the floatability of the mineral particles with different shapes was attributed to several factors. The floatability of particles is related to the change in the hydrophobicity of particles, the bubble-particle collision probability, the time required for bubble-particle attachment, and other factors such as detachment or entrainment. It can be said that elongation, flatness, and smoothness of the surface increase the hydrophobicity of the particle. Additionally, the adsorption of the collector molecules improves in the presence of a rough surface.

In terms of bubble-particle interactions, since the flaky particles settle slowly, their collision probability with bubbles is higher. In addition, more angular, elongated, and rough particles need less time to attach the bubbles with the help of the sharp corners which ease the rapture of the thinning liquid film. Furthermore, it is hard to detach these particles from the bubbles.

REFERENCES

Ahmed, M. M. (2009). Effect of comminution on particle shape and surface roughness and their relation to flotation process: A review. *Journal of Engineering Sciences Assiut University, 37*(3), 711-741.

Ahmed, M. M. (2010). Effect of comminution on particle shape and surface roughness and their relation to flotation process. *International Journal of Mineral Processing, 94*(3-4), 180-191. doi:10.1016/j.minpro.2010.02.007

Albijanic, B., Ozdemir, O., Hampton, M. A., Nguyen, P. T., Nguyen, A. V., & Bradshaw, D. (2014). Fundamental aspects of bubble–particle attachment mechanism in flotation separation. *Minerals Engineering, 65*, 187-195. doi:10.1016/j.mineng.2014.06.008

Albijanic, B., Ozdemir, O., Nguyen, A. V., & Bradshaw, D. (2010). A review of induction and attachment times of wetting thin films between air bubbles and particles and its relevance in the separation of particles by flotation. *Adv Colloid Interface Sci, 159*(1), 1-21. doi:10.1016/j.cis.2010.04.003

Allan, G. C., & Woodcock, J. T. (2001). A review of the flotation of native gold and electrum. *Minerals Engineering, 14*(9), 931-962.

Baecker, V. (2015). *Workshop: Image Processing and Analysis with ImageJ.*

Bilgen, S., Hicyilmaz, C., Atalay, U., Akdoganb, G., & Ulusoy, U. (1995). *Shape and morphological properties, effect on flotation-barite sample*. Paper presented at the 14th Mining Congress of Turkey.

Chan, L. W., Lee, C. C., & Heng, P. W. S. (2002). Ultrafine Grinding Using a Fluidized Bed Opposed Jet Mill: Effects of Feed Load and Rotational Speed of Classifier Wheel on Particle Shape. *Drug Development and Industrial Pharmacy, 28*(8), 939-947. doi:10.1081/ddc-120006426

Dang-Vu, T., Hupka, J., & Drzymala, J. (2006). Impact of roughness on hydrophobicity of particles measured by the Washburn method. *Physicochemical Problems of Mineral Processing, 40*, 45-52.

Dehghani, F., Rahimi, M., & Rezai, B. (2013). Influence of particle shape on the flotation of magnetite, alone and in the presence of quartz particles. *The Journal of The Southern African Institute of Mining and Metallurgy, 113*, 905-911.

Feng, D., & Aldrich, C. (2000). A comparison of the flotation of ore from the Merensky Reef after wet and dry grinding. *Int. J. Miner. Process., 60*, 115-129.

Gungoren, C., Ozdemir, O., Wang, X., Ozkan, S. G., & Miller, J. D. (2019). Effect of ultrasound on bubble-particle interaction in quartz-amine flotation system. *Ultrason. Sonochem., 52*, 446-454. doi:10.1016/j.ultsonch.2018.12.023

Guven, O., Celik, M. S., & Drelich, J. W. (2015a). Flotation of methylated roughened glass particles and analysis of particle–bubble energy barrier. doi:10.1016/j.mineng.2015.06.003

Guven, O., & Celik, M. S. (2016). Interplay of particle shape and surface roughness to reach maximum flotation efficiencies depending on collector concentration. *Mineral Processing and Extractive Metallurgy Review, 37*(6), 412-417. doi:10.1080/08827508.2016.1218873

Guven, O., Karakas, F., Kodrazi, N., & Celik, M. S. (2016). Dependence of morphology on anionic flotation of alumina. *International Journal of Mineral Processing, 156*, 69-74. doi:10.1016/j.minpro.2016.06.006

Guven, O., Ozdemir, O., Karaagaclioglu, I. E., & Celik, M. S. (2015b). Surface morphologies and floatability of sand-blasted quartz particles. *Minerals Engineering, 70*, 1-7. doi:10.1016/j.mineng.2014.08.007

Hicyilmaz, C., Ulusoy, U., & Yekeler, M. (2004). Effects of the shape properties of talc and quartz particles on the wettability based separation processes. *Applied Surface Science, 233*(1-4), 204-212. doi:10.1016/j.apsusc.2004.03.209

Hogg, R., Turek, M. L., & Kaya, E. (2004). The role of particle shape in size analysis and the evaluation of comminution processes. *Particulate Science and Technology, 22*(4), 355-366. doi:10.1080/02726350490516019

Karakas, F., & Vaziri Hassas, B. (2016). Effect of surface roughness on interaction of particles in flotation. *Physicochem. Probl. Miner. Process., 52*(1), 18-34. doi:10.5277/ppmp160102

Koh, P. T. L., Hao, F. P., Smith, L. K., Chau, T. T., & Bruckard, W. J. (2009). The effect of particle shape and hydrophobicity in flotation. *International Journal of Mineral Processing, 93*(2), 128-134. doi:10.1016/j.minpro.2009.07.007

Krasowska, M., & Malysa, K. (2007). Kinetics of bubble collision and attachment to hydrophobic solids: I. Effect of surface roughness. *International Journal of Mineral Processing, 81*(4), 205-216. doi:10.1016/j.minpro.2006.05.003

Krasowska, M., Zawala, J., & Malysa, K. (2009). Air at hydrophobic surfaces and kinetics of three phase contact formation. *Advances in Colloid and Interface Science, 147-148*, 155-169. doi:10.1016/j.cis.2008.10.003

Kursun, H., & Ulusoy, U. (2006). Influence of shape characteristics of talc mineral on the column flotation behavior. *International Journal of Mineral Processing, 78*(4), 262-268. doi:10.1016/j.minpro.2005.11.003

Little, L., Becker, M., Wiese, J., & Mainza, A. N. (2015). Auto-SEM particle shape characterisation: Investigating fine grinding of UG2 ore. *Minerals Engineering, 82*, 92-100. doi:10.1016/j.mineng.2015.03.021

Meiron, T. S., Marmur, A., & Saguy, I. S. (2004). Contact angle measurement on rough surfaces. *J Colloid Interface Sci, 274*(2), 637-644. doi:10.1016/j.jcis.2004.02.036

Miller, J. D., Veeramasuneni, S., Drelich, J., & Yalamanchili, M. R. (1996). Effect of roughness as determined by atomic force microscopy on the wetting properties of PTFE thin films. *Polymer Engineering and Science, 36*(14), 1849-1855.

Mora, C. F., & Kwan, A. K. H. (2000). Sphericity, shape factor, and convexity measurement of coarse aggregate for concrete using digital image processing. *Cement and Concrete Research, 30*, 351-358.

Olson, E. (2011). Particle shape factors and their use in image analysis–Part 1: Theory. *Journal of GXP Compliance, 15*(3), 85-96.

Podczeck, F. (1997). A shape factor to assess the shape of particles using image analysis. *Powder Technology, 93*, 47-53.

Rahimi, M., Aslani, M. R., & Rezai, B. (2012a). Influence of surface roughness on flotation kinetics of quartz. *Journal of Central South University, 19*(5), 1206-1211. doi:10.1007/s11771-012-1130-2

Rahimi, M., Dehghani, F., Rezai, B., & Aslani, M. R. (2012b). Influence of the roughness and shape of quartz particles on their flotation kinetics. *International Journal of Minerals, Metallurgy and Materials, 19*(4), 284-289.

Rezai, B., Rahimi, M., Aslani, M. R., Eslamian, A., & Dehghani, F. (2010). *Relationship between surface roughness of minerals and their flotation kinetics.* Paper presented at the Proceedings of the XI International Seminar on Mineral Processing Technology (MPT-2010), Jamshedpur, India.

Rishi, N. R. (2015). Particle size and shape analysis using Imagej with customized tools for segmentation of particles. *International Journal of Computer Science and Communication Engineering, 4*(3), 23-28.

Sarkar, N., & Chaudhuri, B. B. (1994). An efficient differential box-counting approach to compute fractal dimension of image. *IEEE Transactions on systems, man, and cybernetics, 24*(1), 115-120.

Singh, P., & Ramakrishnan, P. (1996). Powder Characterization by Particle Shape Assessment. *KONA, 14*.

Steuer, M. (2010). Serial classification. *AT Mineral Processing English Edition, 51*, 2-8.

Tasdemir, A., Oteyaka, B., & Ozdag, H. (2008). Particle Shape Characterization of Chromites Comminuted in Jaw Crusher (in Turkish). *Eng&Arch.Fac. Eskisehir Osmangazi University, 21*(1), 103-123.

Ulusoy, U., Hicyilmaz, C., & Yekeler, M. (2004). Role of shape properties of calcite and barite particles on apparent hydrophobicity. *Chemical Engineering and Processing: Process Intensification, 43*(8), 1047-1053. doi:10.1016/j.cep.2003.10.003

Ulusoy, U., & Igathinathane, C. (2014). Dynamic image based shape analysis of hard and lignite coal particles ground by laboratory ball and gyro mills. *Fuel Processing Technology, 126*, 350-358. doi:10.1016/j.fuproc.2014.05.017

Ulusoy, U., & Kursun, I. (2011). Comparison of different 2D image analysis measurement techniques for the shape of talc particles produced by different media milling. *Minerals Engineering, 24*(2), 91-97. doi:10.1016/j.mineng.2010.05.011

Ulusoy, U., Yekeler, M., & Hicyilmaz, C. (2003). Determination of the shape, morphological and wettability properties of quartz and their correlations. *Minerals Engineering, 16*, 951-964. doi:10.1016/j.mineng.2003.07.002

Unland, G., & Al-Khasawneh, Y. (2009). The influence of particle shape on parameters of impact crushing. *Minerals Engineering, 22*(3), 220-228. doi:10.1016/j.mineng.2008.08.008

Vaziri Hassas, B., Caliskan, H., Guven, O., Karakas, F., Cinar, M., & Celik, M. S. (2016). Effect of roughness and shape factor on flotation characteristics of glass beads. *Colloids* *and Surfaces A: Physicochemical and Engineering Aspects, 492*, 88-99. doi:10.1016/j.colsurfa.2015.12.025

Verrelli, D. I., Bruckard, W. J., Koh, P. T. L., Schwarz, M. P., & Follink, B. (2014). Particle shape effects in flotation. Part 1: Microscale experimental observations. *Minerals Engineering, 58*, 80-89. doi:10.1016/j.mineng.2014.01.004

Vizcarra, T. G., Harmer, S. L., Wightman, E. M., Johnson, N. W., & Manlapig, E. V. (2011). The influence of particle shape properties and associated surface chemistry on the flotation kinetics of chalcopyrite. *Minerals Engineering, 24*, 807–816. doi:10.1016/j.mineng.2011.02.019

Wang, S., Fan, H., He, H., Tang, L., & Tao, X. (2018). Effect of particle shape and roughness on the hydrophobicity of low-rank coal surface. *International Journal of Coal Preparation and Utilization*, 1-16. doi:10.1080/19392699.2017.1423066

Wen, B., & Xia, W. (2017). Effect of particle shape on coal flotation. *Energy Sources, Part A: Recovery, Utilization, and Environmental Effects, 39*(13), 1390-1394. doi:10.1080/15567036.2017.1332697

Wiese, J., Becker, M., Yorath, G., & O'Connor, C. O. (2015). An investigation into the relationship between particle shape and entrainment. *Minerals Engineering, 83*, 211-216. doi:10.1016/j.mineng.2015.09.012

Xia, W. (2017). Role of particle shape in the floatability of mineral particle: An overview of recent advances. *Powder Technology, 317*, 104-116. doi:10.1016/j.powtec.2017.04.050

Xia, W., Niu, C., & Zhang, Z. (2017). Effects of attrition on coarse coal flotation in the absence of collectors. *Powder Technology, 310*, 295-299. doi:10.1016/j.powtec.2017.01.056

Yekeler, M., Ulusoy, U., & Hicyılmaz, C. (2004). Effect of particle shape and roughness of talc mineral ground by different mills on the wettability and floatability.

Powder Technology, 140(1-2), 68-78. doi:10.1016/j.powtec.2003.12.012

Yin, W., Zhu, Z., Yang, B., Fu, Y., & Yao, J. (2019). Contribution of particle shape and surface roughness on the flotation behavior of low-ash coking coal. *Energy Sources, Part A: Recovery, Utilization, and Environmental Effects, 41*(5), 636-644. doi:10.1080/15567036.2018.1520346

Chapter 4

UNDERSTANDING THE EFFECT OF CLAYS IN COAL FLOTATION

Can GÜNGÖREN[1]

1 Istanbul University-Cerrahpasa, Engineering Faculty, Mining Engineering Department, 34500, Buyukcekmece, Istanbul, Turkey. can@istanbul.edu.tr

1. INTRODUCTION

Coal is the most abundant and widely distributed fossil fuel and has an important role in the production of the electricity of the world (Demirbas, 2007; Sivrikaya, 2014; Xia et al., 2020). Coals, especially low-rank coals, have some advantages such as easy access and low mining costs (Yu et al., 2013). However, since they have low calorific value and high ash content, they require cleaning operations before use in industry to protect the environment (Sivrikaya, 2014; Xia et al., 2020).

Flotation, which is a processing technique based on the wettability differences between the coals and minerals is one of the most preferred separation methods for the beneficiation of the coals. In the flotation process, the air is pumped into the suspension in the form of small bubbles. Hydrophobic particles are attached to air bubbles, and rise to the surface of the suspension, while hydrophilic particles remain in the suspension (Gungoren et al., 2019).

Clays are one of the most important and widely present ash forming minerals in the low-rank coals. Clay minerals refer to a group of hydrous aluminum phyllosilicates and they are made up of various combinations of tetrahedral and octahedral sheets stacked on each other and bonded together as seen in Fig. 1 (Chen & Peng, 2018). A tetrahedral sheet is made up of silicon-oxygen tetrahedrons with shared basal oxygen molecules (T layer). An octahedral sheet is made up of aluminum-oxygen octahedrons with shared apical and basal oxygen (O layer). These tetrahedral or octahedral sheets bond together through hydrogen bonding (Farrokhpay et al., 2016; Ndlovu et al., 2013).

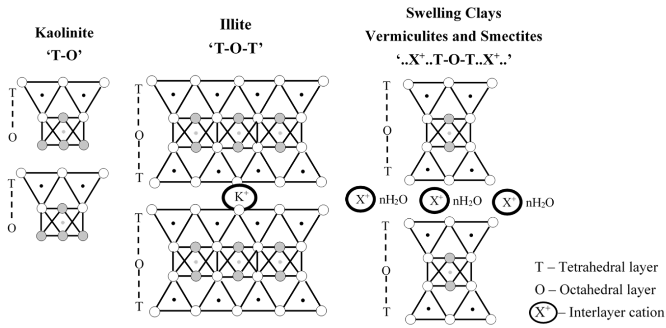

Figure 1. *Classification of phyllosilicate group minerals (adapted from Ndlovu et al. (2013) and Ndlovu et al. (2014)).*

It is seen in previous studies that the presence of clay minerals such as kaolinite, illite, and bentonite generally affects the coal flotation process negatively (Akdemir & Sonmez, 2003) as well as the flotation of many other ores including, copper (Bulatovic et al., 1998; Wang et al., 2015b), gold (Cruz et al., 2013; Cruz et al., 2015; Zhang & Peng, 2015), molybdenum (Bulatovic et al., 1999), chalcopyrite (Forbes et al., 2014), and kimberlite (Boshoff et al., 2007). There is not a very effective way to treat clayey coals. In practice, in order to decrease the clay content, a blend of clayey and non-clayey coals are prepared, and then floatation process is carried out (Wang et al., 2014).

The detrimental effect of clays on the flotation of coal attributed to several parameters related to the clay type. Therefore, slimes should be well characterized for the success of coal flotation (Arnold & Aplan, 1986a). In general, the most commonly occurring clay minerals in ore bodies can be classified into three groups, namely, kaolin, smetite, and illite groups and the mechanism of their detrimental effects on flotation varies significantly related to the network structures formed. While kaolin group clay minerals decrease the concentrate quality with entrainment, smectite group clay minerals increase the pulp viscosity significantly. The effect of illite group clay minerals is relatively lesser compared to other groups (Chen & Peng, 2018). Hussain et al. (1996) investigated the effect of various clay minerals (kaolinite, illite, and chlorite) in coal flotation. Their results showed that illite has the worst effect both on yield and on ash when floated with clean coal while chlorite has an intermediate, and kaolinite has the least effect. Quast et al. (2008) stated that coal depression was stronger in the presence of montmorillonite than kaolinite. According to their results, the effect of clays is stronger in the flotation of moderately floating coal than strongly floating coal. Farrokhpay et al. (2016) reported that kaolinite increases the froth stability and reduces the flotation grade but illite showed the least effect on the flotation performance.

The clays can be also grouped as swelling and non-swelling clays. While, montmorillonite considerably swells when presents in water (up to 1500%), kaolinite shows little or no swelling on hydration. The difference in the swelling characteristics of clays is related to their chemical composition and structure. The swelling clays can affect the flotation process negatively via adsorbing water which changes the rheology and froth stability, reducing both flotation grade and recovery. Meanwhile, non-swelling clays had a lower effect on the rheology (Farrokhpay et al., 2016).

In this study, in line with the purpose of improving the success of coal flotation, the effects and managing methods of clays on the flotation of coal was reviewed in detail.

2. SURFACE COATING EFFECT

The surfaces of coal particles can be coated completely or partially by a layer of hydrophilic fine clay particles (usually less than 10 μm) (Oats et al., 2010).

Electrostatic attraction is one of the theories that explain this coating effect. Based on the electrostatic attraction theory, the clay coating only occurs when the clay mineral and the valuable mineral carry opposite charges (Forbes et al., 2014; Liu & Peng, 2015; Wang et al., 2018). However, different from most minerals, a clay mineral can carry different charges on faces and edges at the same time because of its anisotropic structure and depending on the pH of the medium. The face of clay minerals is always negatively charged. However, the edge can become positively charged at the pH values below its iso-electrical point (IEP) (Forbes et al., 2014). This can be seen in the zeta potential variation of the edges and surfaces of kaolinite, which is the most dominant type of clay presented in fine coal (Dube & Honaker, 2019), with respect to pH (Fig. 2) (Honaker et al., 2005).

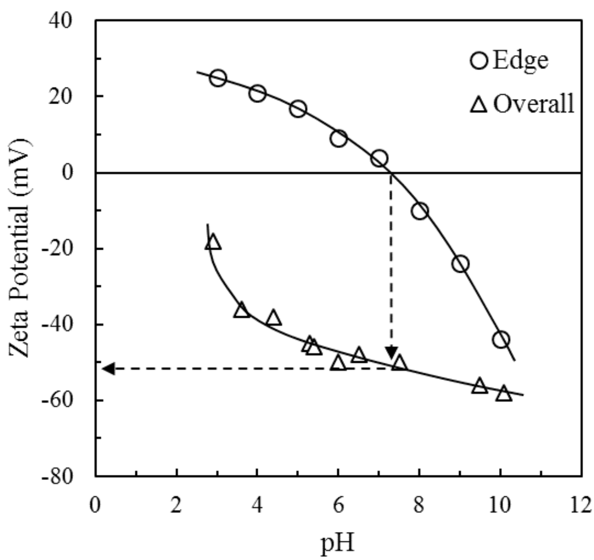

Figure 2. *Overall zeta potentials of kaolinite and calculated zeta potentials of the edge surface. (The dashed lines show the method of identifying the zeta potential (Honaker et al., 2005)).*

Certainly, the type of clay mineral determines the zeta potential on the faces and edges. Hussain et al. (1996) measured the zeta potentials of three clay minerals (kaolinite, illite, and chlorite) between pH 2.5 and 11.0. They found that kaolinite was a more negative clay, compared to chlorite and illite. While chlorite and illite have a point of zero charges (pzc) at pH 3.0 and 2.5, respectively, kaolinite has no pzc (Fig. 3).

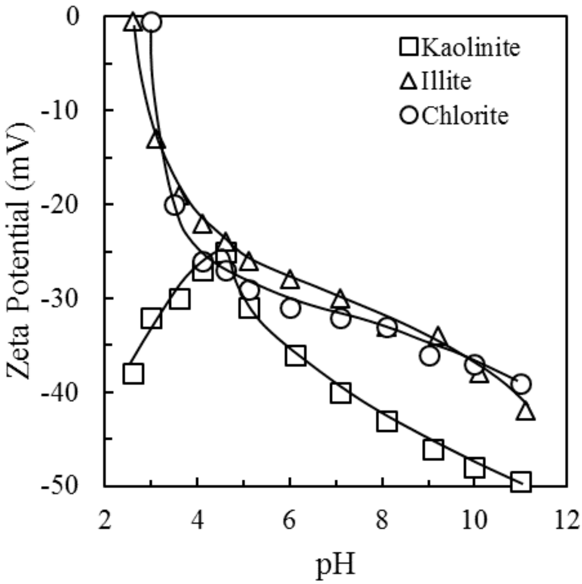

Figure 3. *Zeta potentials of kaolinite, illite, and chlorite clays of Zonguldak, Turkey (Hussain et al., 1996).*

Kelebek et al. (2008) studied the flotation of lignite coal that associated with montmorillonite and kaolinite type clays. They reported that when the pH increases from 5.8 to 9.4 the zeta potentials of the coal and clay fractions become more negative which causes more electrostatic repulsion. An increase in the repulsion forces between coal and clay particles causes the dispersion of clay minerals and therefore provides more effective collector action.

Therewithal, although most of un-oxidized sulfide minerals or coals are negatively charged under normal flotation conditions, the clay coating can still occur through electrostatic attraction between negatively charged mineral/coal particles and positively charged edges of clay particles (Chen & Peng, 2018). Oats et al. (2010) proposed that clay coatings occurred mainly as a result of strong van der Waals attraction, whilst the double-layer interaction played a secondary role. This phenomenon is explained for coal and clay particles by Aplan & Arnold (1991) and Xu et al. (2003). In addition, Xia et al. (2020) attributed the coating of montmorillonite on the coal surface to the combined action of benzene rings and oxygen-containing groups, and van der Waals force.

Clay particles can coat the coal surface and make them equally hydrophilic as clay particles (Xia et al., 2020). Clay coatings on coal surfaces hinder the adsorption of collector molecules on the coal surfaces, reduces their hydrophobicity and therefore caused coal depression (Arnold & Aplan, 1986a; Dube & Honaker, 2019). Arnold & Aplan (1986b) reported that coal depression is much greater with bentonite than with kaolinite or illite clays. Xing et al. (2019) investigated the effect of kaolinite and montmorillonite on the floatability of coal. The effect of kaolinite and montmorillonite on coal floatability and flotation recovery is shown in Fig 4. It is clearly seen in Fig. 4 that flotation recovery was well correlated with the induction time and the maximum bubble-particle attachment angle (BPAA). They stated that the hydrophilic montmorillonite coating on coal surfaces prevented the thinning and rupture of the water film between the bubble and coal particles, thus decreasing floatability and recovery (Xing et al., 2019).

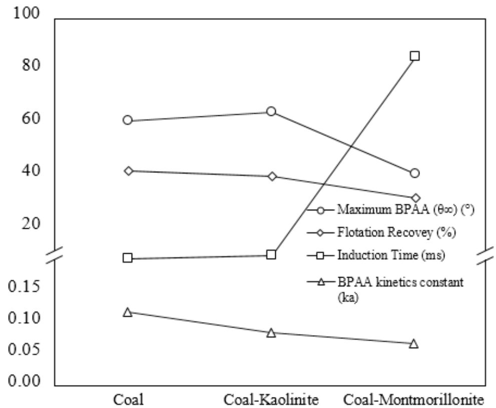

Figure 4. *Effect of kaolinite and montmorillonite in coal floatability and flotation recovery (Xing et al., 2019).*

Similarly, the results of the bubble–particle attachment tests of Oats et al. (2010) showed that the attachment time between the bubble and the coal particles increased in the presence of clay particles because of the surface covering effect (Fig. 5). This phenomenon decreased the bubble–coal attachment probability and therefore decreased the success of the coal flotation.

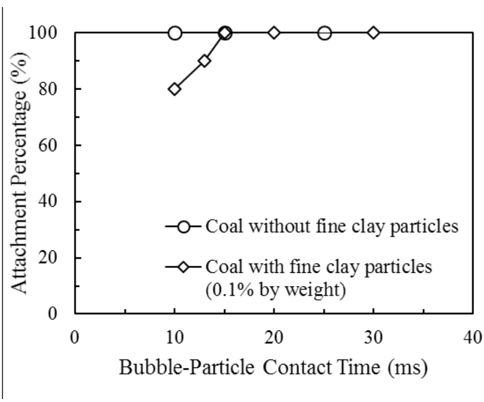

Figure 5. *Bubble-particle attachment with respect to contact time for coal particles in the absence and presence of fine clay particles (Oats et al., 2010).*

Wang et al. (2018) investigated the effect of kaolinite and montmorillonite on the flotation of coal with Extended Derjaguin–Landau–Verwey–Overbeek (EDLVO) analyses. Their results, seen in Fig. 6(a), indicated that the EDLVO energy (E_T^{ED}) between the coal particle and the kaolinite and montmorillonite particles behaved as repulsive potential energy, and it increased with the decrease in particle distance (H). Based on this analysis, it is clearly seen that montmorillonite-coal presented a smaller energy barrier indicating that the energy barrier between montmorillonite and coal was easily broken by the external energy to form montmorillonite coating on the coal surface. In line with these findings, it was also found that while the coal-kaolinite cumulative yield was close to that of coal only, the coal-montmorillonite curve was considerably lower (Fig. 6(a)).

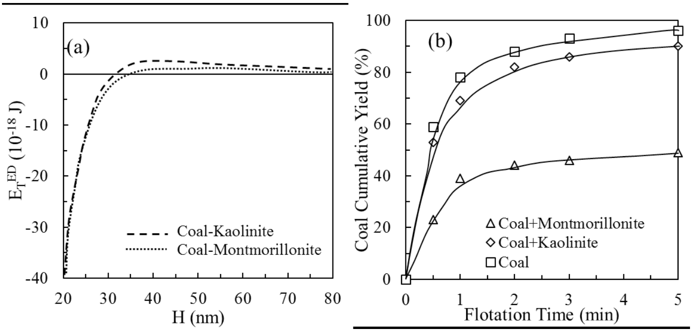

Figure 6. *(a) Total energy interaction between coal, kaolinite, and montmorillonite and (b) coarse coal cumulative yield as a function of time in the absence and presence of clay particles (adapted from Wang et al., (2018)).*

The coating of clay minerals not only depresses the mineral flotation but also reduces the concentrate grade (Chen & Peng, 2018). In addition, the coating of fine particles increases the consumption of flotation reagent and therefore increases the operational costs (Bulatovic et al., 1999; Farrokhpay et al., 2016; Oats et al., 2010; Yu et al., 2017a). Clay particles can also cover bubble surfaces and hinder the attachment of larger particles (Bulatovic et al., 1999; Yu et al., 2017a). Arnold & Aplan (1986a) stated that bentonite depresses coals by armor-coating of the bubbles, preventing coarse particle attachment, and increasing slime coatings, all because of its high surface area, charged sites, and ion-exchange-capacity.

The adverse effect of clay on coal flotation was more pronounced for a moderately floating coal than a strongly floating coal (Quast et al., 2008). This may be originated from the hydrogen bonds between hydrophilic parts at the surface of the coal and clay particles as well as the oxidation levels of the coals and the oxidation products such as humic acid (Chen & Peng, 2018).

In order to disperse clay minerals from mineral/coal surfaces, several physical and chemical treatments were carried out (Chen & Peng, 2018). One of the methods used for cleaning the surfaces of minerals from coated clay particles is using a high shear strength formed by high-intensity mechanical stirring. In this method, the conditioning process with a collector can be carried out after the clay removal process in order to prevent the desorption of collector molecules from coal particles at high stirring rates (Yu et al., 2017b).

As an alternative to high-intensity mechanical stirring, high power ultrasonic treatment can be employed (Feng & Aldrich, 2005; Mao et al., 2019a; Mao et al., 2019b; Ozkan, 2017). The ultrasonic application creates cavitation bubbles, which replace with clay particles due to surface cleaning by high energy transfer on to interfaces. Therefore, the adsorption of the collectors on coal surfaces may increase and collectors become more effective as a result of this surface cleaning effect (Ozkan, 2012; Ozkan, 2018). Therefore, the flotation recovery increased with improved bubble-coal attachment efficiency (Peng et al.,

2018) and also the collector consumption is significantly decreased with this surface cleaning effect of ultrasound (Ozkan & Kuyumcu, 2006; Ozkan & Kuyumcu, 2007).

Modifying the pH of the medium to change the zeta potentials and therefore to decrease the electrostatic attraction between coal and clay particles is another method used for preventing clay coating. Dube & Honaker (2019) reported that operating at pH values around 7.5 disperse the clay slimes and provide more surface-active dimer complexes produced from a carboxyl collector resulted in excellent flotation recovery values for hard-to-float coal. However, dispersing the ultrafine-sized clay minerals may increase the clay entrainment. In addition, changing the pulp pH may result in higher electrostatic repulsive energies between the bubbles and particles, therefore, cause a decrease in the flotation recovery.

It was reported in the literature that the presence of some specific ions in coal suspensions have a considerable effect on slime coatings (Chen & Peng, 2018). Xing et al. (2016) and Xing et al. (2017) investigated the effect of Ca^{2+} ion on coal flotation in the presence of clay minerals. The results of these studies indicated that although the combustible recovery increased in the presence of Ca^{2+} ions, the ash content of the concentrate also increased with Ca^{2+} concentration related to the mechanical entrainment. Similarly, Wang and Peng (2013) and Wang et al. (2014) used saline water for improving the flotation of clayey coals and obtained an increased combustible. However, the mineral matter recovery was also increased in the presence of saline water. They attributed these consequences to the increasing of the froth stability, promoted the aggregation of fine coal particles, and the entrapment of fine gangue particles. Furthermore, Wang and Peng (2014) reported that clay minerals promote the formation of a rigid film at the water/coal interface and therefore the stability of the flotation froth was higher in the presence of clay minerals at low concentrations, which increased combustible recovery and ash recovery.

Dispersants can also be used to create electrostatic and/or steric repulsion between clays and valuable mineral particles. These dispersants are mostly anionic polymers and adsorb on mineral surfaces, making them more negative (Huynh et al., 2000; Oats et al., 2010; Wei et al., 2013). For instance, Liu & Peng (2015) obtained an enhanced coal flotation in deionized water with dispersing clay coatings using a small amount of anionic dispersant (lignosulfonate D748) which enhances the electrostatic repulsion between coal and clay particles.

In addition to the abovementioned techniques, it is seen in the literature that there are several different methods such as sieving (Quast et al., 2008), cycloning (Boylu et al., 2010; Greet & Smart, 1997; Oats et al., 2010; Quast et al., 2008), sedimentation/decantation (Greet & Smart, 1997), selective flocculation (Zou et al., 2019), and reverse-and-direct flotation (Zhu et al., 2019) used for the removal of clay coatings.

3. INCREASING THE PULP VISCOSITY

The rheology of a suspension is a complex function of the physical properties of the presenting particles and the processes that occur at the scale of the suspended particles (Mueller et al., 2010). Clay minerals are considered as colloidal materials with an upper particle size between 1 μm and 4 μm. In their suspensions, the clay minerals can be present as randomly orientated, constantly moving individual layers in a dispersed mode. However, depending on the concentration and properties of clay minerals, van der Waals attraction, electrostatic forces, shear stress, and the solution chemistry, clay minerals also can be present as aggregates in three different modes (network structures) which are face-to-face (F–F), edge-to-face (E–F), and edge-to-edge (E–E) as seen in Fig. 7. The formation of the clay aggregates is governed by the van der Waals attraction and electrostatic forces between the double layers and clay platelets which can be attractive or repulsive depending on the charge of the surfaces (Chen & Peng, 2018).

In the dispersed phase and F-F structure, the viscosity of the suspension is lower than that of the viscosity in the presence of E-F and E-E network structures (Bulatovic et al., 1999; Chen & Peng, 2018; Luckham & Rossi, 1999).

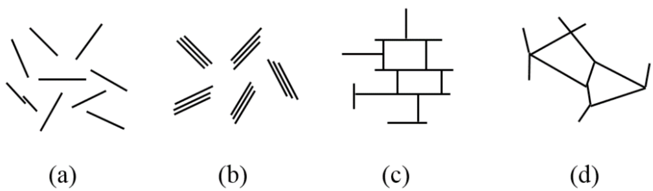

Figure 7. *Network structures of particle associations in clay suspensions (a) dispersed, (b) F-F, (c) E-F (house-of-cards network), and (d) E-E (Luckham & Rossi, 1999).*

The dispersion/aggregation state of clay minerals has a significant effect on pulp rheology which considerably affects the success of the flotation process via changing gas dispersion and gas hold-up, mobility of particles and bubbles as well as bubble-particle collision and attachment processes (Chen & Peng, 2018).

The viscosity of the flotation pulp increased significantly with its fibrous and/or phyllosilicate mineral content such as clays. An increase in the pulp viscosity affects the hydrodynamics of the flotation cell, bubble/particle dispersion, and therefore contributes to poor flotation recovery and rates (Bakker et al., 2010; Ndlovu et al., 2011; Patra et al., 2012). Furthermore, the rheology of the froth may affect froth mobility and stability (Farrokhpay, 2011; Farrokhpay, 2012).

However, an increase in the pulp viscosity may also cause some beneficial effects for flotation. For instance, the mobility of the bubbles and particles is limited at high viscosities which decreases the entrainment of the gangue minerals (Wang & Peng, 2014). Moreover, it causes the reduction of the three-phase contact line, which increases the dynamic contact angle of particles. This resulting in more stable bubble-particle aggregates and therefore a decrease in the detachment probability (Xu et al., 2011).

The slurry viscosity increases exponentially with solids concentration. At high solids concentrations, both bubble size and gas holdup decrease significantly. This is attributed to the generation of small bubbles in the impeller zone, but poor dispersion of these bubbles throughout the cell, resulting in low gas hold-ups by Shabalala et al. (2011).

The effect of clays on pulp rheology is also dependent upon their surface charge, morphology, and type. For instance, swelling clays (smectite), have a dramatic effect on the viscosity of mineral slurries, meanwhile, non-swelling clays including chlorite and talc have a lesser effect (Farrokhpay, 2012). Cruz et al. (2013) reported that bentonite has a stronger effect on the viscosity of suspensions than kaolinite. They also stated that the flotation reagents such as pH modifiers, collectors, and frothers have the potential to alter the rheological behaviors of kaolinite and bentonite suspensions and the effect of the pH modifiers is more pronounced. Zhang & Peng (2015) reported that bentonite increased pulp viscosity more than kaolinite. It is measured by Ndlovu et al. (2014) that talc and kaolinite suspensions are characterized by higher yield stresses than illite.

The high pulp viscosity, which is generally detrimental for flotation was tried to decrease by several researchers by flocculating clay particles (Farrow et al., 2000; Mpofu et al., 2004; Tao et al., 2007). Furthermore, inorganic or polymetric dispersants can be also preferred (Chen & Peng, 2018) such as sodium tripolyphosphate, sodium polyphosphate (Papo et al., 2002), alkylammonium, and a negatively charged grafted block copolymer (CTP) (Konan et al., 2008) as well as polycarboxylate ether (Zhang et al., 2012).

4. ENTRAINMENT OF CLAY MINERALS

Entrainment is transferring the hydrophilic suspended mineral particles from the pulp region to the flotation froth. Therefore, entrainment process decrease the selectivity of the flotation process and the grade of the concentrate, considerably. Particle size is the most important parameter that influencing the entrainment process where the effects of impeller speed and pulp density were lesser (Akdemir & Sonmez, 2003). The recovery of hydrophilic particles by entrainment increases with a decrease in their size (Zheng et al., 2006). Fine particles are easily suspended in the flotation pulp and in the water film surrounding the bubbles. Therefore, they can easily move to the froth zone (Wang et al., 2015a). The coarse particles drain more readily from the voids between the bubbles than the fine particles. Therefore, coarse particles are less entrained to the concentrate. Mineral particles generally under the size of 50 µm are known to be recovered by entrainment more easily (Li et al., 2020; Wang et al., 2015a).

Since clays are very fine particles with a low mass, in the flotation process they can be recovered by entrainment easily and increase the ash content of the clean coal (Li et al., 2020). Kaolinite and illite, which do not significantly depress coal flotation, contaminate the floated clean coal largely by carry-over with the froth, though electrostatic attachment to the coal contributes in a lesser way to the ash content of the froth (Arnold & Aplan, 1986a).

The type of clays also plays a significant role in the entrainment process. While illite has a lower degree of entrainment, kaolinite and bentonite can entrain easier. The entrainment of clay particles was also dependent upon the network structures of the aggregates. Loose network structures facilitate the entrainment process. The adjusting of the ambient pH can change the network structures of the clay aggregates and therefore change the viscosity of the flotation pulp (Chen & Peng, 2018). Furthermore, dissolved ions were used to provide the adsorption of cations on clay (kaolinite) surface and therefore the compression of the electrical double layer. This helps the formation of cross-linked network structures instead of dispersed clay platelets and exacerbating the entrainment process (Zhang et al., 2015). Flocculating of clay minerals using high molecular weight polymers is another method used for the reducing of clay entrainment (Liu & Peng, 2014). Li et al. (2020) used polyamonium chloride to flocculate the clay particles which entrained in the presence of nano-bubbles.

5. CONCLUSIONS

Coal is the most abundant and widely used fossil fuel in the world. Most of the world reserve consisted of low-rank coals with high ash content. Therefore, they need to be cleaned before using for technical and environmental reasons. Flotation, which is a physicochemical mineral separation method, is widely used in the cleaning of low-rank coals. Clays are one of the important ash-forming minerals accompanied by the low-rank coals. They create several deleterious effects for the recovery and selectivity of coal flotation depending on the clay type. It is reported in literature that while illite has the worst effect on coal flotation, chlorite has an intermediate and kaolinite has the least effect. This study contributed to the understanding of the effect of clays on the flotation of coal.

The first detrimental effect of clays on the flotation of coal is the coating of coal surfaces. Electrostatic attraction is one of the theories that explain this coating effect. A clay mineral can carry different charges on its faces and edges at the same time because of its anisotropic structure and depending on the pH of the medium. Clay particles can coat the coal surface, hinders the collector adsorption and keep them hydrophilic. It is seen in literature that high-intensity mechanical stirring, high power ultrasonic treatment, sieving, cycloning, using of pH modifying agents, dispersants, and flocculants are the most preferred methods for the removal of clay particles from coal surfaces.

In flotation, the existence of clay minerals can also change the rheology of the flotation pulp depending on their concentration and network structures of their aggregates. An increase in the pulp viscosity may affect the flotation success in a negative way by changing bubble/particle dispersion. However, it may also cause some beneficial effects for flotation such as increasing the dynamic contact angle.

Furthermore, according to their very small size, clay minerals have a high potential of entrainment. The entrainment of hydrophilic particles decreases the selectivity of flotation and the grade of the concentrate significantly. The sizes and network structures of clays have an important effect on their entrainment behaviors. In order to alleviate the entrainment of clay minerals, flocculants can be used for increasing the size of the clays and, the pH of the medium can be adjusted to manage the network structures of clay platelets.

In order to increase the success of coal flotation in the presence of clay minerals, the future research should be focused on the negative effects of clays on the floatability of coal, on the understanding of clay/coal interactions, and on the development of more effective clay managing methods in the flotation process.

REFERENCES

Akdemir, U., & Sonmez, I. (2003). Investigation of coal and ash recovery and entrainment in flotation. *Fuel Processing Technology, 82*(1), 1-9. doi:10.1016/s0378-3820(02)00248-5

Aplan, F. F., & Arnold, B. J. (1991). *Flotation. Part 2: Wet fine particle concentration. Section 3: Flotation. Coal Preparation*. Hardinge, Littleton, Colorado: SME.

Arnold, B. J., & Aplan, F. F. (1986a). The effect of clay slimes on coal flotation, Part I: The nature of the clay. *International Journal of Mineral Processing, 17*, 225-242.

Arnold, B. J., & Aplan, F. F. (1986b). The effect of clay slimes on coal flotation, Part II: The role of water quality. *International Journal of Mineral Processing, 17*, 243-260.

Bakker, C. W., Meyer, C. J., & Deglon, D. A. (2010). The development of a cavern model for mechanical flotation cells. *Minerals Engineering, 23*(11-13), 968-972. doi:10.1016/j.mineng.2010.03.016

Boshoff, E. T., Morkel, J., Vermaak, M. K. G., & Pistorius, P. C. (2007). Kimberlite degradation: The role of cation type. *Minerals Engineering, 20*(15), 1351-1359. doi:10.1016/j.mineng.2007.08.008

Boylu, F., Cinku, K., Esenli, F., & Celik, M. S. (2010). The separation efficiency of Na-bentonite by hydrocyclone and characterization of hydrocyclone products. *International Journal of Mineral Processing, 94*(3-4), 196-202. doi:10.1016/j.minpro.2009.12.004

Bulatovic, S. M., Wyslouzil, D. M., & Kant, C. (1998). Operating practices in the beneficiation of major porphyry copper/molybdenum plants from Chile: Innovated technology and opportunities, a review. *Minerals Engineering, 11*(4), 313-331.

Bulatovic, S. M., Wyslouzil, D. M., & Kant, C. (1999). Effect of clay slimes on copper, molybdenum flotation from porphyry ores. *Mineral Processing/Environment, Health and Safety, 2*, 95-111.

Chen, X., & Peng, Y. (2018). Managing clay minerals in froth flotation—A critical review. *Mineral Processing and Extractive Metallurgy Review, 39*(5), 289-307. doi:10.1080/08827508.2018.1433175

Cruz, N., Peng, Y., Farrokhpay, S., & Bradshaw, D. (2013). Interactions of clay minerals in copper–gold flotation: Part 1 – Rheological properties of clay mineral suspensions in the presence of flotation reagents. *Minerals Engineering, 50-51*, 30-37. doi:10.1016/j.mineng.2013.06.003

Cruz, N., Peng, Y., Wightman, E., & Xu, N. (2015). The interaction of pH modifiers with kaolinite in copper–gold flotation. *Minerals Engineering, 84*, 27-33. doi:10.1016/j.mineng.2015.09.019

Demirbas, M. F. (2007). Progress of fossil fuel science. *Energy Sources, Part B: Economics, Planning, and Policy, 2*(3), 243-257. doi:10.1080/15567240500402909

Dube, R., & Honaker, R. (2019). Improving the flotation performance of an oxidized bituminous coal source. *Minerals Engineering, 142*, 105937. doi:10.1016/j.mineng.2019.105937

Farrokhpay, S. (2011). The significance of froth stability in mineral flotation - A review. *Adv Colloid Interface Sci, 166*(1-2), 1-7. doi:10.1016/j.cis.2011.03.001

Farrokhpay, S. (2012). The importance of rheology in mineral flotation: A review. *Minerals Engineering, 36-38*, 272-278. doi:10.1016/j.mineng.2012.05.009

Farrokhpay, S., Ndlovu, B., & Bradshaw, D. (2016). Behaviour of swelling clays versus non-swelling clays in flotation. *Minerals Engineering, 96-97*, 59-66. doi:10.1016/j.mineng.2016.04.011

Farrow, J. B., Johnson, R. R. M., Simic, K., & Swift, J. D. (2000). Consolidation and aggregate densification during gravity thickening. *Chemical Engineering Journal, 80*, 141-148.

Feng, D., & Aldrich, C. (2005). Effect of Preconditioning on the flotation of coal. *Chemical Engineering Communications, 192*(7), 972-983. doi:10.1080/009864490521534

Forbes, E., Davey, K. J., & Smith, L. (2014). Decoupling rheology and slime coatings effect on the natural flotability of chalcopyrite in a clay-rich flotation pulp. *Minerals Engineering, 56*, 136-144. doi:10.1016/j.mineng.2013.11.012

Greet, C. J., & Smart, R. S. C. (1997). The effect of size separation by cyclosizing and sedimentation/decantation on mineral surfaces. *Mineral Engineering, 10*(9), 995-1011.

Gungoren, C., Guven, O., Cinar, M., & Ozdemir, O. (2019). An investigation of the effect of clay type on coal flotation along with DLVO theoretical analyses. *International Journal of Coal Preparation and Utilization*, 1-13. doi:10.1080/19392699.2019.1603146

Honaker, R. Q., Yoon, R. H., & Luttrell, G. H. (2005). Ultrafine coal cleaning using selective hydrophobic coagulation. *Coal Preparation, 25*(2), 81-97. doi:10.1080/07349340590927413

Hussain, S. A., Demirci, S., & Ozbayoglu, G. (1996). Zeta potential measurements on three clays from Turkey and effects of clays on coal flotation. *Journal of Colloid and Interface Science, 184*, 535-541.

Huynh, L., Feiler, A., Michelmore, A., Ralston, J., & Jenkins, P. (2000). Control of slime coatings by the use of anionic phosphates: A fundamental study. *Minerals Engineering, 13*(10-11), 1059-1069.

Kelebek, S., Demir, U., Sahbaz, O., Ucar, A., Cinar, M., Karaguzel, C., & Oteyaka, B. (2008). The effects of dodecylamine, kerosene and pH on batch flotation of Turkey's Tuncbilek coal. *International Journal of*

Mineral Processing, 88(3-4), 65-71. doi:10.1016/j.minpro.2008.06.004

Konan, K. L., Peyratout, C., Carbelaud, M., Smith, A., Bonnet, J. P., & Alain, J. (2008). Influence of two dispersants on the rheological behavior of kaolin and illite in concentrated calcium hydroxide dispersions. *Applied Clay Science, 42*, 252-257. doi:10.1016/j.clay.2008.01.001

Li, C., Xu, M., & Zhang, H. (2020). Efficient separation of high-ash fine coal by the collaboration of nanobubbles and polyaluminum chloride. *Fuel, 260*, 116325. doi:10.1016/j.fuel.2019.116325

Liu, D., & Peng, Y. (2014). Reducing the entrainment of clay minerals in flotation using tap and saline water. *Powder Technology, 253*, 216-222. doi:10.1016/j.powtec.2013.11.019

Liu, D., & Peng, Y. (2015). Understanding different roles of lignosulfonate in dispersing clay minerals in coal flotation using deionised water and saline water. *Fuel, 142*, 235-242. doi:10.1016/j.fuel.2014.10.082

Luckham, P. F., & Rossi, S. (1999). The colloidal and rheological properties of bentonite suspensions. *Advances in Colloid and Interface Science, 82*, 43-92.

Mao, Y., Xia, W., Peng, Y., & Xie, G. (2019a). Ultrasonic-assisted flotation of fine coal: A review. *Fuel Processing Technology, 195*, 106150. doi:10.1016/j.fuproc.2019.106150

Mao, Y., Xie, G., Liang, L., Xia, W., & Peng, Y. (2019b). Effects of ultrasonic treatment on the particle size, shape and ash content of fine coal. *Physicochemical Problems of Mineral Processing, 55*(3), 679-688. doi:10.5277/ppmp18182

Mpofu, P., Addai-Mensah, J., & Ralston, J. (2004). Flocculation and dewatering behaviour of smectite dispersions: effect of polymer structure type. *Minerals Engineering, 17*(3), 411-423. doi:10.1016/j.mineng.2003.11.010

Mueller, S., LleWellin, E. W., & Mader, H. M. (2010). The rheology of suspensions of solid particles. *Proceedings of the Royal Society, 466*, 1201-1288.

Ndlovu, B., Backer, M., Forbes, E., Deglon, D. A., & Franzidis, J. P. (2011). The influence of phyllosilicate mineralogy on the rheology of mineral slurries. *Minerals Engineering, 24*, 1314–1322. doi:10.1016/j.mineng.2011.05.008

Ndlovu, B., Farrokhpay, S., & Bradshaw, D. (2013). The effect of phyllosilicate minerals on mineral processing industry. *International Journal of Mineral Processing, 125*, 149-156. doi:10.1016/j.minpro.2013.09.011

Ndlovu, B., Forbes, E., Farrokhpay, S., Becker, M., Bradshaw, D., & Deglon, D. (2014). A preliminary rheological classification of phyllosilicate group minerals. *Minerals Engineering, 55*, 190-200. doi:10.1016/j.mineng.2013.06.004

Oats, W. J., Ozdemir, O., & Nguyen, A. V. (2010). Effect of mechanical and chemical clay removals by hydrocyclone and dispersants on coal flotation. *Minerals Engineering, 23*(5), 413-419. doi:10.1016/j.mineng.2009.12.002

Ozkan, S. G. (2012). Effects of simultaneous ultrasonic treatment on flotation of hard coal slimes. *Fuel, 93*, 576-580. doi:10.1016/j.fuel.2011.10.032

Ozkan, S. G. (2017). Further investigations on simultaneous ultrasonic coal flotation. *Minerals, 7*(10), 1-9. doi:10.3390/min7100177

Ozkan, S. G. (2018). A review of simultaneous ultrasound-assisted coal flotation. *Journal of Mining and Environment*. doi:10.22044/jme.2018.6784.1502

Ozkan, S. G., & Kuyumcu, H. Z. (2006). Investigation of mechanism of ultrasound on coal flotation. *International Journal of Mineral Processing, 81*(3), 201-203. doi:10.1016/j.minpro.2006.07.011

Ozkan, S. G., & Kuyumcu, H. Z. (2007). Design of a flotation cell equipped with ultrasound transducers to enhance coal flotation. *Ultrason Sonochem, 14*(5), 639-645. doi:10.1016/j.ultsonch.2006.10.001

Papo, A., Piani, L., & Ricceri, R. (2002). Sodium tripolyphosphate and polyphosphate as dispersing agents for kaolin suspensions: rheological characterization. *Colloids and Surfaces A: Physicochemical and Engineering Aspects, 201*, 219-230.

Patra, P., Bhambhani, T., Nagaraj, D. R., & Somasundaran, P. (2012). Impact of pulp rheological behavior on selective separation of Ni minerals from fibrous serpentine ores. *Colloids and Surfaces A: Physicochemical and Engineering Aspects, 411*, 24-26. doi:10.1016/j.colsurfa.2012.06.037

Peng, Y., Mao, Y., Xia, W., & Li, Y. (2018). Ultrasonic flotation cleaning of high-ash lignite and its mechanism. *Fuel, 220*, 558-566. doi:10.1016/j.fuel.2018.02.049

Quast, K., Ding, L., Fornasiero, D., & Ralston, J. (2008, 28 September - 1 October). *Effect of slime clay particles on coal flotation.* Paper presented at the Chemeca 2008 Conference, Newcastle City Hall, New South Wales, Australia.

Shabalala, N. Z. P., Harris, M., Leal Filho, L. S., & Deglon, D. A. (2011). Effect of slurry rheology on gas dispersion in a pilot-scale mechanical flotation cell. *Minerals Engineering, 24*(13), 1448-1453. doi:10.1016/j.mineng.2011.07.004

Sivrikaya, O. (2014). Cleaning study of a low-rank lignite with DMS, Reichert spiral and flotation. *Fuel, 119*, 252-258. doi:10.1016/j.fuel.2013.11.061

Tao, D., Zhou, X. H., Zhao, C., Fan, M. M., Chen, G. L., Aron, A., & Wright, J. (2007). Coal and potash flotation enhancement using a clay binder. *Canadian Metallurgical Quarterly, 46*(3), 243-250. doi:10.1179/cmq.2007.46.3.243

Wang, B., & Peng, Y. (2014). The interaction of clay minerals and saline water in coarse coal flotation. *Fuel, 134*, 326-332. doi:10.1016/j.fuel.2014.05.085

Wang, B., Peng, Y., & Vink, S. (2014). Effect of saline water on the flotation of fine and coarse coal particles in the presence of clay minerals. *Minerals Engineering, 66-68*, 145-151. doi:10.1016/j.mineng.2014.03.016

Wang, H., Zhu, H., Zhu, J., Xu, W., Li, M., & Fei, Z. (2018). Flotation of coal in the presence of quartz and clay minerals. *International Journal of Coal Preparation and Utilization*, 1-11. doi:10.1080/19392699.2018.1487408

Wang, L., Peng, Y., Runge, K., & Bradshaw, D. (2015a). A review of entrainment: Mechanisms, contributing factors and modelling in flotation. *Minerals Engineering, 70*, 77-91. doi:10.1016/j.mineng.2014.09.003

Wang, Y., Peng, Y., Nicholson, T., & Lauten, R. A. (2015b). The different effects of bentonite and kaolin on copper flotation. *Applied Clay Science, 114*, 48-52. doi:10.1016/j.clay.2015.05.008

Wei, R., Peng, Y., & Seaman, D. (2013). The interaction of lignosulfonate dispersants and grinding media in copper–gold flotation from a high clay ore. *Minerals Engineering, 50-51*, 93-98. doi:10.1016/j.mineng.2013.06.012

Xia, Y., Zhang, R., Cao, Y., Xing, Y., & Gui, X. (2020). Role of molecular simulation in understanding the mechanism of low-rank coal flotation: A review. *Fuel, 262*, 116535. doi:10.1016/j.fuel.2019.116535

Xing, Y., Gui, X., & Cao, Y. (2016). Effect of calcium ion on coal flotation in the presence of kaolinite clay. *Energy & Fuels*. doi:10.1021/acs.energyfuels.5b02474

Xing, Y., Xu, M., Guo, F., Luo, J., Zhang, Y., Cao, Y., & Gui, X. (2019). Role of different types of clay in the floatability of coal: Induction time and bubble-particle attachment kinetics analysis. *Powder Technology, 344*, 814-818. doi:10.1016/j.powtec.2018.12.074

Xing, Y., Xu, X., Gui, X., Cao, Y., & Xu, M. (2017). Effect of kaolinite and montmorillonite on fine coal flotation. *Fuel, 195*, 284-289. doi:10.1016/j.fuel.2017.01.058

Xu, D., Ametov, I., & Grano, S. R. (2011). Detachment of coarse particles from oscillating bubbles—The effect of particle contact angle, shape and medium viscosity. *International Journal of Mineral Processing, 101*(1-4), 50-57. doi:10.1016/j.minpro.2011.07.003

Xu, Z., Liu, J., Choung, J. W., & Zho, Z. (2003). Electrokinetic study of clay interactions with coal in flotation. *International Journal of Mineral Processing, 68*, 183-196.

Yu, J., Tahmasebi, A., Han, Y., Yin, F., & Li, X. (2013). A review on water in low rank coals: The existence, interaction with coal structure and effects on coal utilization. *Fuel Processing Technology, 106*, 9-20. doi:10.1016/j.fuproc.2012.09.051

Yu, Y., Ma, L., Cao, M., & Liu, Q. (2017a). Slime coatings in froth flotation: A review. *Minerals Engineering, 114*, 26-36. doi:10.1016/j.mineng.2017.09.002

Yu, Y., Ma, L., Wu, L., Ye, G., & Sun, X. (2017b). The role of surface cleaning in high intensity conditioning. *Powder Technology, 319*, 26-33. doi:10.1016/j.powtec.2017.06.048

Zhang, L. Z., Lu, Q., Xu, Z., Liu, Q., & Zeng, H. (2012). Effect of polycarboxylate ether comb-type polymer on viscosity and interfacial properties of kaolinite clay suspensions. *Journal of Colloid and Interface Science, 378*, 222-231. doi:10.1016/j.jcis.2012.04.029

Zhang, M., & Peng, Y. (2015). Effect of clay minerals on pulp rheology and the flotation of copper and gold minerals. *Minerals Engineering, 70*, 8-13. doi:10.1016/j.mineng.2014.08.014

Zhang, M., Xu, N., & Peng, Y. (2015). The entrainment of kaolinite particles in copper and gold flotation using fresh water and sea water. *Powder Technology, 286*, 431-437. doi:10.1016/j.powtec.2015.08.042

Zheng, X., Johnson, N. W., & Franzidis, J. P. (2006). Modelling of entrainment in industrial flotation cells: Water recovery and degree of entrainment. *Minerals Engineering, 19*, 1191–1203. doi:10.1016/j.mineng.2005.11.005

Zhu, Z., Yin, W., Yang, B., Fu, Y., & Xue, J. (2019). Reduction of the slime contamination on fine coking coal by using the reverse-and-direct flotation process. *Colloids and Surfaces A: Physicochemical and Engineering Aspects, 579*, 123681. doi:10.1016/j.colsurfa.2019.123681

Zou, W., Gong, L., Huang, J., Zhang, Z., Sun, C., & Zeng, H. (2019). Adsorption of hydrophobically modified polyacrylamide P(AM-NaAA-C16DMAAC) on model coal and clay surfaces and the effect on selective flocculation of fine coal. *Minerals Engineering, 142*, 105887. doi:10.1016/j.mineng.2019.105887

Chapter 5

MEASUREMENT AND ANALYSIS WITH LABVIEW SOFTWARE

Ahmet ÖZMEN[1], Aykut COŞKUN[2], Mehmet ERTUĞRUL[3]

1 Department of Electronics and Automation, Vocational School, Ağrı İbrahim Çeçen University, Ağrı, Turkey, 0000-0002-3631-4883, ahmet25440@gmail.com
2 Department of Electronics and Automation, Vocational School of Technical Sciences, Bayburt University, Bayburt, Turkey, 0000-0002-7240-6865
3 Department of Electrical and Electronics, Engineering Faculty, Atatürk University, Erzurum, Turkey, 0000-0003-1921-7704

INTRODUCTION TO LABVIEW PROGRAM

The LabVIEW program consists of two screens. These screens are Block diagram and Front panels. The block diagram section is the part where the programmer works. That is, this is the part where the programmer creates the operations to be performed depending on the algorithm. The front panel is the screen that will appear to the user when the algorithm runs. Block diagram can be considered as coding part. Programming by combining blocks without writing code is the convenience of LabVIEW program. This section contains the content that the programmer needs such as mathematical operations, control structures, textual operations, file reading, writing and recording, network operations, database operations, libraries of loaded devices. The front panel is the part of the program to be shown to the user.

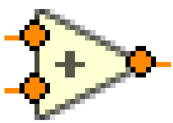

In the **Block Diagram**, there are icons corresponding to the operation we want to do. These icons are encoded and made available to us by LabVIEW programmers. These icons are basically composed of two parts: input and output. Using these parts, the desired operation is performed depending on our algorithm. For example, let's create a program, which shows the sum with a fixed value of a number entered externally. To do this, right-click on the block diagram and select "**Add"** from the "**Numeric**" section as shown in Figure 1. As shown in the collection process icon, there are connection points around the icon. These points will be used to determine our flowchart that will form our algorithm. Right-click on the part you want to connect to and click "**Create**". Here, 3 parts will be observed as shown in Figure 2. These are "**Constant, Control, Indicator**" sections. Selecting

Constant allows us to enter a constant value in the Blog diagram. When **Control** is selected, it creates an icon on the Front panel and allows the user to intervene in this section. These two operations can be applied to the input part of the icon. **Indicator** is applied to the output part of the icon. This will display the result of the action on the icon in the Front panel. These three sections are the most commonly used parts of the LabVIEW program. In addition, the output of one icon may be the input of another icon. To do this, left-click one of the parts to be connected. Operation is performed by moving the mouse and right-clicking on the port of the other icon again.

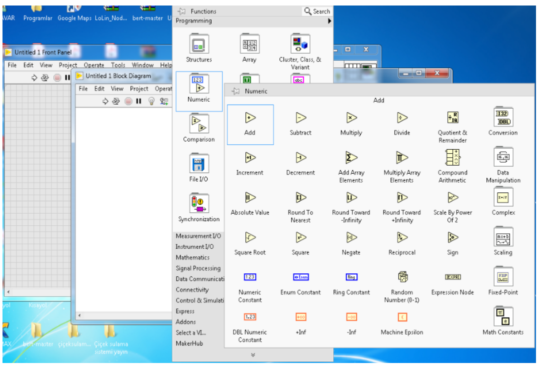

Figure 1. *LabVIEW Program Collection Process*

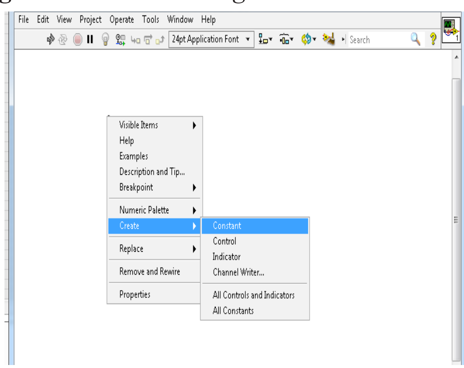

Figure 2. *Create Process*

CONTROL THE KEITLEY DEVICE WITH THE LABVIEW PROGRAM

Many devices communicate easily with LabVIEW (Academy, Sciences, & Academy, 2013; Akgül, 2017; Ballesteros, Fernández Palop, Hernández, Crespo, & del Pino, 2004; Bohórquez, Enrique Gómez, & Andújar Márquez, 2009; Boutana, Mellit, Haddad, Rabhi, & Pavan, 2017; Chouder, Silvestre, Taghezouit, & Karatepe, 2013; Demirbaş & Bayhan, 2009; Forero, Hernández, & Gordillo, 2006; Hamel & Mohellebi, 2020; Hu et al., 2020; Kobayashi, Takano, & Sawada, 2006; ŞAHİN, BAYRAKTAR, KAVUR, & EVREN ŞAHİN, 2017; Sziki, Sarvajcz, Szántó, & Mankovits, 2019; Technology, 2010; Zhang et al., 2020). Especially the KEITLEY device used in laboratories will be controlled with LabVIEW. Other devices are controlled in a similar way to this device. In this process, we need to install LabVIEW drivers of our device. This can be done in several different ways. First, the device name is added from the NI LabVIEW website by typing and searching. Similarly, the program is loaded from the device manufacturer's website or on the CD supplied with the device. In another method, "**Help / Find Instrument Drivers...**" is selected from the LabVIEW software.

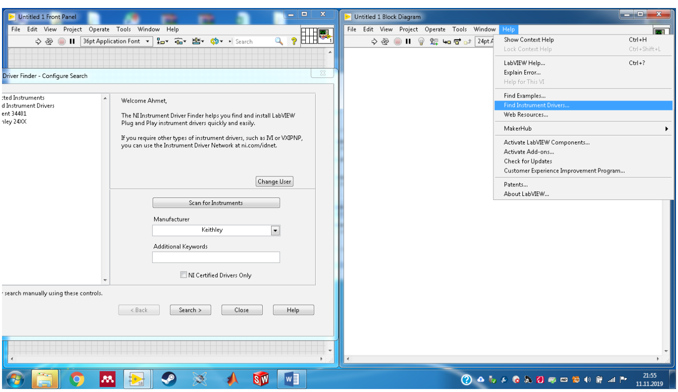

Figure 3. *Adding Drivers*

The "**NI Instrument Driver Finder - Configure Search**" window will open as shown in Figure 3. In this section, if you want a user name and password, you can register for free on the **NI Instrument** home page. **Keithley** is selected from **Manufacturer** in this window. In this section, the name of the device we want to use or the name of the company is selected. The model of the device is selected from Additional Keywords. Then click on "Search" to find the drivers from the database. Found drivers are installed by selecting and clicking "**Install**".

Installed device VIs are located in **Instrument Drivers** section of **Instrument I / O** section by right clicking on **Block Diagram** as shown in Figure 4. In this section, we have VIs for all the devices we have installed.

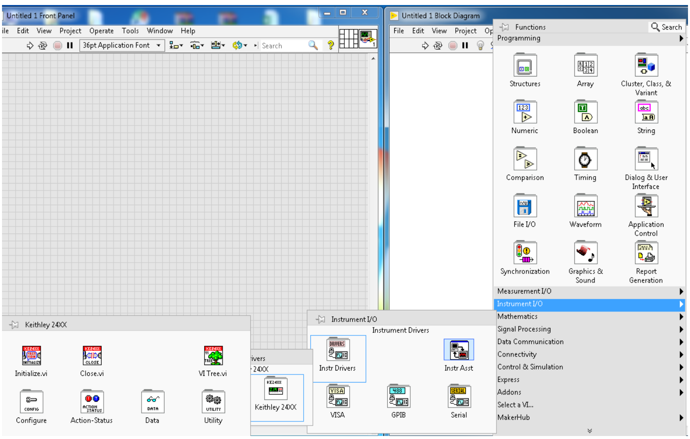

Figure 4. *Installed Drivers*

Now that all this is complete, we can now create our application. To control a device, basically our computer and software need to speak the same language as this device. Now that we've installed this plug-ins, let's look at the first VI, **Initialize.vi**. As shown in Figure 5, this VI will allow us to select the way in which the devices communicate and to make the settings of this communication protocol. These communication paths are a protocol such as **VISA, BPIB and Serial** and are determined according to the device we have. The device is connected to our computer with the connection cable according to this protocol. After seeing the device on the computer, it will appear in the **VISA** resource name of Initialize.vi. First of all, we should right-click the VISA resource name and select **Create / Control** so that we can see the link in the Front Panel. After seeing the port to which our device is connected, we need to set the other connection settings to match the connection settings of the device. If these settings are not known, we will need to learn from the device user manual or the connection information section of the device's own menus.

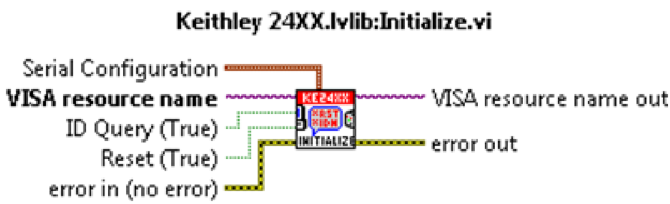

Figure 5. *Initialize.vi*

Let us not forget that in this way we can communicate with all devices with LabVIEW drivers. Now, we can make measurements, we can change the device parameters, we can check the input and output ports of the device, we can perform mathematical operations, we can analyze, we can draw graphs, we can save our data to our computer. The LabVIEW program allows a large number of analyzes similar to these procedures. As an example, let's measure voltage from our Keithley device. To do this, open the screen in Figure 4 and select **Read.vi** from the **Data** section. As shown in Figure 6, the outputs at the top right and bottom of **Initialize.vi** are connected to the inputs at the top left and bottom of Read.vi, and the outputs are terminated by connecting to **Close.vi**. This process is basically done in this way in such applications. Generally, the connections at the bottom are used to identify and show the errors that occur in the system. The connections on the upper side are generally used to transfer the information to the next VI. In addition, **While Loop** is used as shown in Figure 6. This is to repeat the measurement for one cycle. **While Loop** is selected as shown in Figure 7, the part of the loop to be created by holding down the left mouse button is selected and released. A delay is added for the cycle repeat time, and finally a button is added the red dot on the bottom left cause the loop to end by clicking.

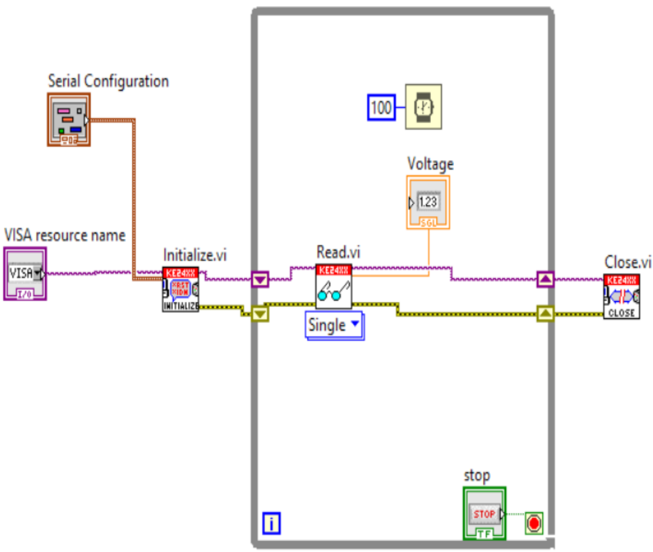

Figure 6. *Voltage Reading*

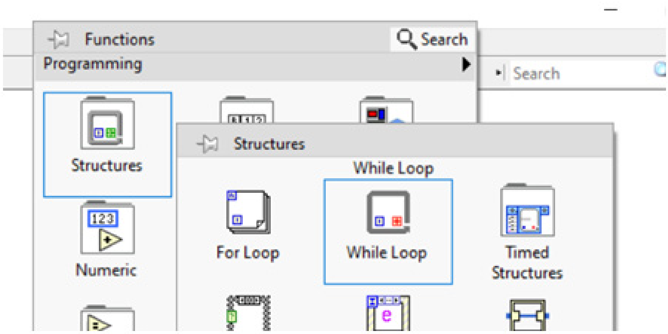

Figure 7. *While Loop*

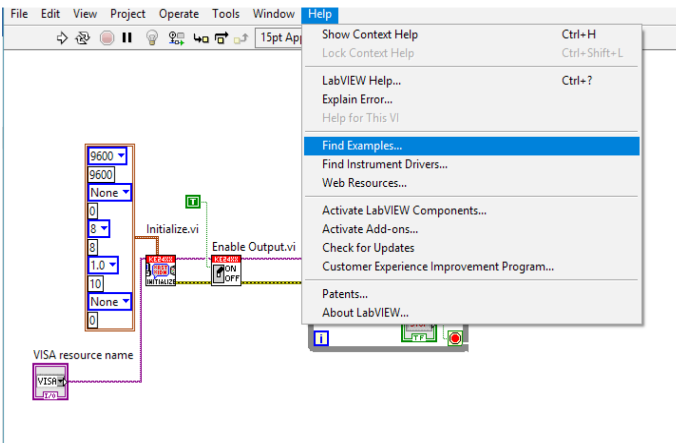

Figure 8. *Example applications*

The sample applications of many devices that we will use are available in the LabVIEW program. We can use these sample applications or develop our own application by examining them. Sample applications can be accessed the “Find Examples…” section of the “Help Menu” in Figure 8.

RESULT

As can be seen, it can be controlled from a device in a very short time by using LabVIEW software without the need of any code information. In this way, both we can easily create our own systems and we can save by analyzing our data in computer environment. In addition, a complex system of several devices and sensors can run synchronously with each other in a single software environment. In this way, if the operation of one device depends on the result produced by another device, we can do it in a very short time in a single software environment.

REFERENCES

Academy, T. N., Sciences, N., & Academy, T. N. (2013). Labview Based Target Recognition And Tracking System. *Deniz Bilimleri ve Mühendisliği Dergisi*, *9*(2), 66–71.

Akgül, A. (2017). Elektronik devrelerin gerçek zamanlı bode diyagramlarının LabVIEW ile elde edilmesi. *SAÜ Fen Bilimleri Enstitüsü Dergisi*, 1–1. https://doi.org/10.16984/saufenbilder.310655

Ballesteros, J., Fernández Palop, J. I., Hernández, M. A., Crespo, R. M., & del Pino, S. B. (2004). LabView virtual instrument for automatic plasma diagnostic. *Review of Scientific Instruments*, *75*(1), 90–93. https://doi.org/10.1063/1.1634356

Bohórquez, M. A. M., Enrique Gómez, J. M., & Andújar Márquez, J. M. (2009). A new and inexpensive temperature-measuring system: Application to photovoltaic solar facilities. *Solar Energy*, *83*(6), 883–890. https://doi.org/10.1016/J.SOLENER.2008.12.007

Boutana, N., Mellit, A., Haddad, S., Rabhi, A., & Pavan, A. M. (2017). An explicit I-V model for photovoltaic module technologies. *Energy Conversion and Management*, *138*, 400–412. https://doi.org/10.1016/J.ENCONMAN.2017.02.016

Chouder, A., Silvestre, S., Taghezouit, B., & Karatepe, E. (2013). Monitoring, modelling and simulation of PV systems using LabVIEW. *Solar Energy*, *91*, 337–349. https://doi.org/10.1016/J.SOLENER.2012.09.016

Demirbaş, Ş., & Bayhan, S. (2009). Güç sistemlerinde harmoniklerin gerçek zamanli ölçüm ve analizi. *Journal of the Faculty of Engineering and Architecture of Gazi University*, *24*(3), 461–468.

Forero, N., Hernández, J., & Gordillo, G. (2006). Development of a monitoring system for a PV solar plant. *Energy*

Conversion and Management, *47*(15–16), 2329–2336. https://doi.org/10.1016/J.ENCONMAN.2005.11.012

Hamel, M., & Mohellebi, H. (2020). A LabVIEW-based real-time acquisition system for crack detection in conductive materials. *Mathematics and Computers in Simulation*, *167*, 381–388. https://doi.org/10.1016/J.MATCOM.2018.02.004

Hu, Y., Wang, T., Chen, T., Song, N., Yao, K., & Luo, Y. (2020). Design and implementation of testing system of LED driver power based on LabVIEW. *Optik*, *200*, 163411. https://doi.org/10.1016/J.IJLEO.2019.163411

Kobayashi, K., Takano, I., & Sawada, Y. (2006). A study of a two stage maximum power point tracking control of a photovoltaic system under partially shaded insolation conditions. *Solar Energy Materials and Solar Cells*, *90*(18–19), 2975–2988. https://doi.org/10.1016/J.SOLMAT.2006.06.050

ŞAHİN, S., BAYRAKTAR, M., KAVUR, A. E., & EVREN ŞAHİN, K. (2017). Arduino ve LabVIEW Kullanarak EMG Verilerinden Eşik Seviye Belirleme ile Motor Kontrol Düzeneği Tasarımı. *Süleyman Demirel Üniversitesi Fen Bilimleri Enstitüsü Dergisi*, *22*(2), 736. https://doi.org/10.19113/sdufbed.06905

Sziki, G. Á., Sarvajcz, K., Szántó, A., & Mankovits, T. (2019). Series Wound DC Motor Simulation Applying MATLAB SIMULINK and LabVIEW Control Design and Simulation Module. *Periodica Polytechnica Transportation Engineering*, *48*(1), 65–69. https://doi.org/10.3311/pptr.12908

Technology, C. (2010). *ELEKTRONİK DENEY MODÜLLERİNİN LabVIEW İLE KONTROLÜ*. *2*(3), 1–8.

Zhang, Y., Li, Y., Gu, X., Liu, H., Zhang, Y., & Hu, W. (2020). Research on measurement of laser beam M2 factor based on LabVIEW. *Optik*, *203*, 163759. https://doi.org/10.1016/J.IJLEO.2019.163759

Chapter 6

REMOVAL OF LEAD (II) AND COPPER (II) FROM WASTEWATER WITH ACTIVE CARBON OBTAINED FROM THE ELEAGNUS SEEDS

Bahdişen GEZER[1]

1 Engineering Faculty, Usak University, Usak, Turkey E-Mail:bahdisen.gezer@usak.edu.tr

1. INTRODUCTION

Increasing vital needs due to the rapid growth of the world's population brought about industrial developments. As a result of industrial activities carried out in order to raise the living standards of human beings, it causes the formation of pollutions which causes significant harm to environmental health [1]. Water is essential for the sustainability of natural life and is the most important element for every stage of human life. Contrary to popular belief, water is a limited resource. Today, the effective use of water resources is one of the most important issues. Because water use directly affects water resources. Effective use requires optimal management of water resources, more precisely, the simultaneous management of water quality and quantity. The efficient and sustainable use of water resources has not yet been achieved in the world. Turkey is also facing similar problems. Sustainable management of water resources plays an important role in long-term economic development. From this point of view, water resources in terms of pollution. In addition to revealing the current situation, it is also important for identifying and solving the problems related to the provision of sustainable water use.

According to the "Regulation on Water Pollution Control water pollution is observed as a negative change in the physical, chemical, bacteriological, radioactive and ecological characteristics of the water source and directly or indirectly prevented in biological resources, human health, fishing, water quality and the use of water for other purposes. the disintegration of materials and energy wastes.

One of the most important problems related to water pollution is the pollution of receiving environments such as lakes, inland seas, rivers and gulfs by industrial and domestic wastewater. The most important effect of phosphate in these wastewaters in the receiving water environment is eutrophication. Eutrophication causes a deterioration of the ecological balance in the receiving water environment [2]. For these reasons, wastewater should be discharged to receiving environments after treatment.

The mixing of toxic heavy metals with surface water and groundwater has become an important issue in recent years due to the potential risk of living things. The main sources for the introduction of heavy metals to surface waters are the use of sewage sludge in agriculture, the discharging of untreated or poorly treated effluents into surface waters, and the use of fertilizers and pesticides in agriculture.Land sludge can contain significant amounts of Pb, Cu, Zn, Cd and Ni, and as a result can be dangerous on products as well as on animals and humans [3].

The introduction of used water containing one or more of the heavy metals or other toxic substances into the receiving waters has a toxic effect on the organisms in this aquatic environment and endangers the living life in the environment. Mass fish deaths often occur as a result of the introduction of toxic substances into the water beds. High-grade intoxications may occur at low concentrations of substances with high toxicity or high concentrations of substances with low toxicity.Its toxic effect also depends on the contact time of pollutants and living organisms. The primary effect of metals is on aquatic plants and animal organisms. However, the secondary effects that result in bioaccumulation and bioconcentration in food are also common nowadays, resulting in toxic effects on non-aquatic species [4].

An overdose of lead and copper, a widely used substance, can cause mucosal irritation in individuals, damage to the central nervous system, tissue changes in the liver and lungs, and many other conditions.For this reason, research to improve various techniques for recovery and removal of metallic species from wastewater is increasing day by day. In particular, techniques such as chemical precipitation, electroporation, ion exchange, reverse osmosis and adsorptionIt is used. In the adsorption process, small sludge formation and ease of operation are an important advantage.

The adsorption process is a process that occurs in the presence of an adsorbent known as a solid that effectively binds molecules by physical withdrawal, ion exchange, and chemical bonds. The adsorbent can be found in a large amount and easy, low cost andis readily available [5-6-7]. For this reason, it is often important to discover such materials and test their surface properties.

Activated carbon is a highly effective adsorbent widely used in the treatment of water and gas emissions due to its large surface area and pore volume, as well as the presence of surface functional groups, particularly oxygen groups [8].Activation can generally be carried out by passing water vapor or carbon dioxide during the carbonization, or by carbonization after saturating the materials to be used in the production of activated carbon with $ZnCl_2$, H_3PO_4, H_2SO_4, KOH and K_2S solutions [9].

In recent years, research on the production of low-cost carbohydrate adsorbents, particularly from industrial or agricultural by-products, has aroused increasing interest. Polymers [10], waste tires [11] and wood [12],numerous agricultural by-products, including almond shells [13], apple pulp [14], sugar cane bag [15], carob powder [16-17], sugar beet pulp [18] and nutshells, successfully activated carbon under laboratory conditions. can be made into.

In this study, activated carbon is obtained by the carbonation process of spindle cores which is an agricultural waste. Using this obtained activated carbon, lead (II) and copper (II) of aqueous solutions adsorption were investigated. On lead (II) and copper (II) adsorption; The effect of pH, initial solution concentration, contact time, temperature and adsorbent dose were investigated. The mechanism of adsorption is explained with the help of adsorption isotherms, adsorption kinetics, and thermodynamic parameters.

2. HEAVY METAL POLLUTİON AND ITS EFFECTS

The importance of metals in environmental engineering stems from the fact that most of them are toxic to humans, aquatic organisms and other organisms. Although some of them are “micronutrients biologic, which are required in small amounts for the development of all living things because biological enzymes are present in their active sites, they want to protect natural water life in metals drinking water because they can show toxic effects from very low concentrations quality components that need to be meticulously monitored in places and biological treatment plants [19-20].

Due to the toxic properties of heavy metals, the effects of polluting ecosystems endanger human health. However, these elements are used in the industry and a certain amount of industrial waste enters the food chain. Therefore, heavy metal contents of wastewater from pollution sources should be treated before being released to the environment and reduced to below the permissible values according to various water standards [21-22].

Treatment of wastewater containing heavy metal ions generally depends on the capacity of the plant, the flow rate and characteristics of the wastewater, the treatment plant and the method and material used in the plant, but is mainly based on the chemical precipitation of the metal ion. These economic and impractical methods are used to reduce excess metal pollution in wastewater to acceptable levels. However, the economic recovery of metals contained in industrial wastewater may constitute a secondary source for these metals in use [23].

Many industrial wastewaters are aluminum (Al), chromium (Cr), iron (Fe), zinc (Zn), arsenic (As), cadmium (Cd), mercury (Al), which are very toxic and dangerous for living organisms living in the environment where they are discharged. Hg), lead (Pb), nickel (Ni) and copper (Cu) [18-21]. In addition to the restrictions on heavy metal concentrations introduced for continental water resources and industrial wastewater in the Turkish Water Pollution Control Regulation (SKKY), the limitations imposed by many organizations in the world and by environmental organizations in the world about the presence of heavy metals, concentration values are allowed.

3. MATERIALS AND METHODS

3.1. Materials

3.1.1. Supply and preparation of eleagnus seeds

Eleagnus seeds used in the experiments were obtained from the Dikili district of İzmir province (Figure 1). Fleshy parts were removed and the seeds were removed.The nuclei were first broken into small pieces. Powdered in ball mill. It was then milled and sieved to obtain a particle size material in the range of 6-20 mesh (2.7-0.81 mm). These materials were then washed 5 times with distilled water and allowed to dry. The dried core powders were then stored in sealed containers for use in carbonization and activation processes.

Figure 1. *Eleagnus seed samples.*

3.1.2. Preparation of solutions

The Pb (II) and Cu (II) solutions used in the experiments were prepared from the standard solution prepared from electrolytically obtained lead and copper wire of 99.99% purity. The wires were washed first with sodium hydroxide to remove any possible oxide film on the surface. It was then cut into small pieces. This5 ± 0.005 g of the fractions were dissolved in dilute sodium hydroxide and washed with distilled water to 500 ml. 10000 mg/L standard Pb (II) and Cu (II) solution prepared in this manner are suitable in the experiments.

3.1.3. Carbonization and activation of eleagnus seeds

The spindle core was ground in the mill and washed 3 times with distilled water and dried in a 100 °C oven for 32 hours. $ZnCl_2$ solutions of 10%, 20%, 30% were added to the samples prepared by weighing 10 grams of each.

The resulting mixture was heated at 90 °C for one hour. After cooling, it was homogenously taken into a petri dish and kept in the oven at 90 °C for 32 hours.At the end of this period, the porcelain crucibles were taken into the ash furnace at 450 °C for 1.5 hours and carbonization was performed.The resulting activated carbons were cooled to room temperature in the desiccator. 0.1M HCl.The distillate was washed extensively with water until acidity and dried in the oven at 100 °C.Samples were stored in closed containers for use in adsorption experiments.Using these activated carbons, lead (II) andThe effect of pH, temperature, contact time, initial solution concentrations and adsorbent dose on copper (II) adsorption were investigated.

3.1.4. Adsorption experiments

Firstly, the effect of initial pH, adsorbent dose, contact time, temperature and initial phosphate concentration on lead removal using active spindle core activated carbon was investigated. Lead (II) solutions were prepared from the standard lead solution at an initial concentration of 25 mg/L and pH ranging from 3 to 10 in order to examine the effect of the initial pH. 5 g/L adsorbent was added to each solution and treated at 25 °C for 130 min. In order to investigate the effect of adsorbent dose on copper (II) adsorption, copper (II) solutions were prepared at 40 mg/L initial concentration and optimum pH. Experiments with these solutions with adsorbents in amounts ranging from 2-9 g/Ldone. All adsorption experiments were performed in an ultrasonic bath. The solutions obtained after adsorption experiments were filtered with wattman brand filter paper and final pH measurements and copper (II) and lead (II) analyzes were performed.

4. RESULTS AND DİSCUSSİON

4.1. Characterization of Activated Carbon

In the adsorption studies of lead (II) and copper (II), activated carbon which has the largest surface area (≈1591.134 m^2/g) obtained by carbonizing the spindle core at 500 °C was used.The properties of the produced activated carbon are shown in Table 1.Here, the sample represents the activated carbon obtained before activation and after activation with $ZnCl_2$ solution at a concentration of 10%, 20% and 30% at 500 °C (Table 1).In order to reduce the carbonization cost, the most suitable activation conditions were determined as $ZnCl_2$ at 500 °C.

Table 1. *Properties of activated carbon prepared with* $ZnCl_2$

Actived carbon		BET Surface Area (m^2/g)	Pore volume (cm^3/g)	Average pore diameter (nm)
Eleagnus seeds		783.820	0.421	1.823
Eleagnus seeds – ZnCl2-500°C	activated with $ZnCl_2$10%	1097.190	0.623	2.0348
	activated with $ZnCl_2$20%	1591.134	0.956	2.371
	activated with $ZnCl_2$30%	1457.463	0.978	2.596

4.2. Effect of adsorption contact time

The effect of contact time on lead removal is shown in Figure 2. Time-dependentexperiments with lead solutions of initial concentration 25 mg/L, temperature 25 °C and pH 2-11 It is made. Accordingly, in the first minutes of the adsorption lead is increased by 46.65% of the adsorption time, the lead removal percentage increases and reaches 82.6% after a contact time of 200 minutes (Figure 2).

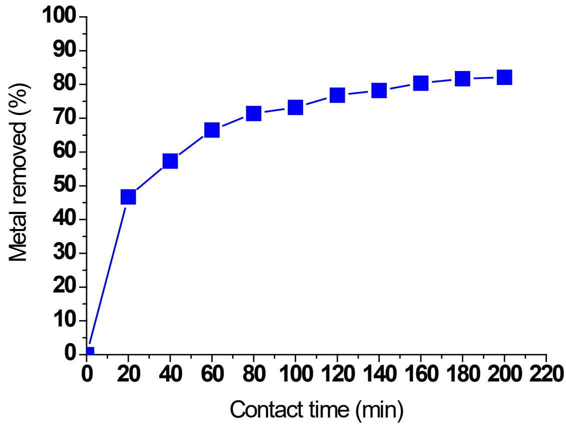

Figure 2. *Effect of contact time with Eleagnus seed activated carbon on lead (II) adsorption (temperature 25°C)*

The effect of the adsorbent dose on copper (II) removal was investigated with copper solutions with an initial concentration of 25 mg/L and in the presence of 25mg/L activated carbon dose, depending on the contact time.In Figure 3, copper removal efficiencies are given in parallel with the increase in adsorbent dose and contact time. Accordingly, the adsorbent dose of 25 mg/L at the contact time of 40-90 minutes at the end of copper removal efficiency from 55.27% to 94.4% (Figure 3).

Table 3.*Freundlich and Langmuir constants for copper (II) adsorption with eleagnus seed activated carbon*

Temperature (°C)	Freundlich Isotherm			Langmuir isotherm	
	k_f	n	1/n	b (1/mg)	Q (mg/g)
25	9.931	0.2821	3.5448	0.488	25.18
35	5.873	0.3906	2.5602	0.257	22.96
45	3.086	0.3386	2.9533	0.107	12.42

CONCLUSION

In order to produce activated carbon from low-cost wastes, considering the criteria such as storage life, footprint, practical usability and yield, and surface area, which must be considered in raw material selection, spindle It was concluded that it is a suitable material for carbon production and in this study active carbon was obtained from eleagnus seed and used in adsorption of lead (II) and copper (II) ions in aqueous solutions.

The BET surface area of the activated carbons obtained by carbonization of the eleagnus seed with a solution of $ZnCl_2$ concentration of 10%, 20% and 30% at a temperature of 500 °C is 1097.190 m^2/g, 1591.134 m^2/g and 1457.463 m_2/g. In addition, the surface area of the activated carbon obtained without eleagnus seed activation and carbonization with $ZnCl_2$ was found to be 783.820 m^2/g. Accordingly, it has been found that the optimal temperature for obtaining the eleagnus seed activated carbon is 500 °C. The yields of the samples without carbonization were approximately 43%, while the yield values of the activated carbons obtained by carbonization were 82 to 94%.

Adsorbent dose and contact time were found to be important parameters in the adsorption of lead (II) and copper (II) ions. Although a significant portion of the adsorption took place in the first minutes of the adsorption process, maximum contact lead (II) and copper (II) ions were found in the presence of a dose of 25 g/L adsorbent and a contact time of approximately 70 minutes.The suitability of the data obtained from temperature and concentration to Freundlich and Langmuir adsorption isotherms was investigated. Accordingly, it is seen that the removal of activated carbon from copper spindle (II) obtained from the eleagnus seed at 25-45 °C temperature and concentration range of 10-300 mg/L is more applicable to Langmuir isotherm than Freundlich isotherm. On the other hand, lead (II) removal of activated carbon with the eleagnus seed at 25-45 °C and a concentration range of 10-30 mg/L was found to be applicable to Freundlich isotherm rather than Langmuir isotherm.

As a result, the active carbons obtained from the eleagunus seed can be effectively used for the removal of both lead (II) and copper (II) from aqueous solutions. Thus, a more economical evaluation of the spindle speed is made in our country and in the world.

REFERENCES

[1] Shannon, M.A.,Bohn, P.W., Elimelech, M., Georgiadis, J.G., Marinas, B.J.& Mayes,A.M. (2008). Science and technology for water purification in the coming decades. *Nature,* 452, 301–310.

[2] Fu, F. & Wang, Q. (2011). Removal of heavy metal ions from wastewaters: a review.*J. Environ. Manage.,* 92, 407–418.

[3] Atanassova, I. (1999). Competitive Effect of Copper, Zinc, Cadmium and Nickel on Ion Adsorption and Desorption by Soil Clays.*Water, Air and Soil Pollution* 113, 115-125.

[4] Bolisetty, S.,Peydayesh, M. & Mezzenga, R.(2019). Sustainable technologies for water purificationfrom heavy metals: review and analysis.*Chem. Soc. Rev.,* 48, 463–487.

[5] Subramani, A. & Jacangelo, J.G. (2015). Emerging desalination technologies for water treatment:a critical review.*Water Res,.* 75, 164–187.

[6] Arris, S., Bencheikh,M.L., Meniai, A.H., Morcellet, M., Bacquet, M., Martel, B.& Mansri, A. (2003). Study and Identification of Retention Process of Heavy Metals by Adsorption on Agricultural By-Products.*Chemical Engineering & Technology. Eng. Life Sci.*, 3.

[7] Gherbi, N., Meniai, A.H., Bencheikh, M. Mansri, A., Morcellet, M., Bellir, K., Bacquet, M. & Martel, M. (2004). Study of The Retention Phenomena of Copper II by Calcinated Wheat Byproducts. *Desalination,* 166, 363–369.

[8] Chen, Y.,He, M., Wang, C. & Wei, Y. (2014). A novel polyvinyltetrazole-grafted resin with highcapacity for adsorption of Pb(II), Cu(II) and Cr(III) ions from aqueous solutions.*J. Mater. Chem. A*, 2,10444–10453.

[9] Ihsanullah, A., Abbas, A.M., Al-Amer, T., Laoui, M.J., Al-Marri, M.S., Nasser,M.& Khraisheh, M.A. (2016). Atieh, Heavy metal removal from aqueous solution by advancedcarbon nanotubes: critical review of adsorption applications.*Sep. Purif. Technol.,*157, 141–161.

[10] Yue, Z., Mangun, C.L.& Economy, J. (2002). Preparation of fibrous porous materials by chemical activation: 1. ZnCl2 activation of polymer-coated fibers. Carbon, 40, 1181–1191.

[11] San Miguel, G., Fowler, G.D.& Sollars, C.J. (2003). A study of the characteristics of activated carbons produced by steam and carbon dioxide activation of waste tyre rubber. Carbon, 41, 1009–1016.

[12] Tseng, R.L., Wu, F.C. & Juang, R.-S. (2003). Liquid-phase adsorption of dyes and phenols using pinewood-based activated carbons. Carbon, 41, 487–495.

[13] Toles, C.A., Marshall, W.E., Wartelle, L.H.& McAloon, A. (2000). Steam or carbon dioxideactivated carbons from almond shells: physical, chemical and adsorptive properties and estimated cost of production. Biores. Technol., 75, 197–203.

[14] Suarez-Garcia, F., Martinez-Alonso, A.& Tascon, J.M.D. (2001). Porous texture of activated carbons prepared by phosphoric acid activation of apple pulp. Carbon, 39, 1103–1116.

[15] Huang, L.,Chai, X., Chen, G. & Logan, B.E. (2011). Effect of set potential on hexavalentchromium reduction and electricity generation from biocathode microbial fuelcells.Environ. Sci. Technol.,45, 5025–5031.

[16] Gezer, B.,Köse, U., Zubov D., Deperlioglu, O. & Vasan, P. (2019). Determining optimum carob powder adsorbtion for cleaningwastewater: intelligent optimization with electro-search algorithm. *Wireless Networks,* 1-15, Doi: https://doi.org/10.1007/s11276-019- 02035.

[17] Gezer, B. & Ersoy, Y. (2018). Adsorption Behavior of Methylene Blue Dye Using Carob powder as Eco-Friendly New Adsorbent For Cleaning Wastewater: Optimization By Response Surface Methodology. *Erzincan Üniversitesi Fen Bilimleri Enstitüsü Dergisi,* 11(2), 306-320.

[18] Gezer, B. (2019). Removal of Pb (II) from aqueous solution with Reactive Red 198 and carbonization of sugar beet

pulp with citric acid. *International Journal of Agriculture Environment and Food Sciences,* 4, 250-256.

[19] Chuah, T.G., Jumasiah, A., Azni, I., Katayon, S.& Thomas Choong, S.Y. (2005). Rice husk as apotentially low-cost biosorbent for heavy metal and dye removal: an overview. Desalination, 175, 305-316.

[20] Ferro-Garcia, M. A., Rivera-Ultra, J., Rodriguez-Gordillo, J. & Baustita-Toledo, I. (1988).Adsorption of Zinc, Cadmium and Copper on Activated CArbons Obtained FromAgricultural by-Products.Carbon, 26 (3), 363-373.

[21] Gherbi, N., Meniai, A.H., Bencheikh M.Lehocine, Mansri, A., Morcellet, M., Bellir, K.,Bacquet, M. & Martel, M. (2004). Study of The Retention Phenomena of Copper IIby Calcinated Wheat Byproducts. Desalination, 166, 363–369.

[22] Wang, W., Tian, H., Shu, G., Huo, D., Zhang, F. Zhu, X. (2019). A bimetallic thermally regenerativeammonia-based battery for high power density and efficiently harvestinglow-grade thermal energy.J. Mater. Chem. A, 7, 5991–6000.

[23] Kobya, M., Demirbaş, E., Şentürk, E. & İnce, M. (2005). Adsorption of heavy metal ions fromaqueous solutions by activated carbon prepared from apricot Stone. Bioresource Technology, 96, 1518-1521.

[24] Krishnan,K.A.,Sreejalekshmi, K.G., Vimexen, V. & Dev, V.V. (2016). Evaluation of adsorptionproperties of sulphurised activated carbon for the effective and economically viableremoval of Zn(II) from aqueous solutions.Ecotoxicol. Environ. Saf., 124, 418–425.

[25] Mohan, D.& Singh, K.P. (2002). Single- and multi-component adsorption of cadmium and zincusing activated carbon derived from bagassean agricultural waste. Wat. Res., 36,2304–2318.

[26] Chen, X.,Ren, P., Li, T., Trembly, J.P. & Liu, X. (2018). Zinc removal from model wastewater byelectrocoagulation: processing, kinetics and mechanism.Chem. Eng. J., 349, 358–367.

Chapter 7

APPLICATION OF GEOMETRIC FORMS USED IN LANDSCAPE DESIGN

Hüseyin İNCE[1], Nuri ERDEM[2], İ. Murat OZULU[1], F. Engin TOMBUŞ[1]

1 High School of Mapping and Land Survey, Hitit University, Çorum, Turkey, huseyinince@hitit.edu.tr, imuratozulu@hitit.edu.tr, fengintombus@hitit.edu.tr

2 Engineering Faculty, Department of Geomatic Engineering, Osmaniye Korkut Ata University, Osmaniye, Turkey, **nurierdem@osmaniye.edu.tr**

1. INTRODUCTION

Nowadays, various shapes are used as pattern in the arrangement of ornamental plants and green areas in parks and gardens in landscape architecture (Bell, 2005; Booth, 1990; Eralp, 2019; Hansen, 2010; Tejszerska, 2009; Ždímalová & Vavríková, 2017). In practice, it was seen that circle springs were used in surface decorations in some parks (Figure 1-3), however, it was observed that circular arcs did not pass between the base points of the series triangles and squares in the park areas.

In this study, it was designed to pass and apply the circle arc between the equilateral triangle, the base points in the equilateral triangle and the diagonals in a square, in a park or garden area, in a sequence on a straight line. In this case, the angle or the length of the square and the angle of the circular arc are calculated according to the radius of the circular arc to be passed. The angle of the center of this arc or the radius of the circular arc to be passed is determined by taking the triangles and squares formed in a series.

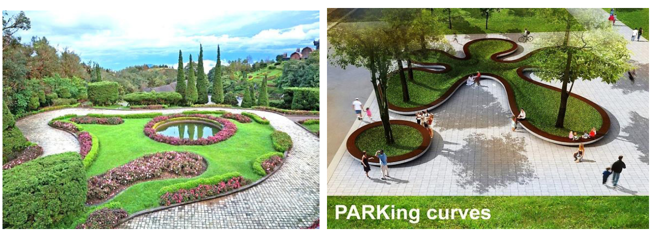

a) b)

Figure 1. *a) and b) Examples of a circular landscape in the parks*

Figure 2. *Examples of a circular landscape in the park of Gardens of Versailles*

Figure 3. *Circular arc-shaped landscape examples in a park near the Istanbul ring road*

In practice, circular arc formed between the base points in triangular series or square diagonally in a parking area; simple measurement tools and electronic tachometer is explained how to apply. The findings and conclusions of the related applications were explained.

2. Circle Arc Application between the Base Points of an Equilateral Triangle

The angles (α) at each corner of equilateral triangle ABC are equal to each other (Figure 4).

$$\alpha=60^{o}=66^{g}.6667 \quad (1)$$

If A and C points in Figure 4 are considered tangent points of the circle arc to be passed, Δ angle of direction of the circle arc at point B is expressed as (Wilfred 2001; Wolf & Ghilani 2008):

$\Delta=2\alpha=120^{o}=133^{g}.3334$ (2)

AB=BC = t tangent length

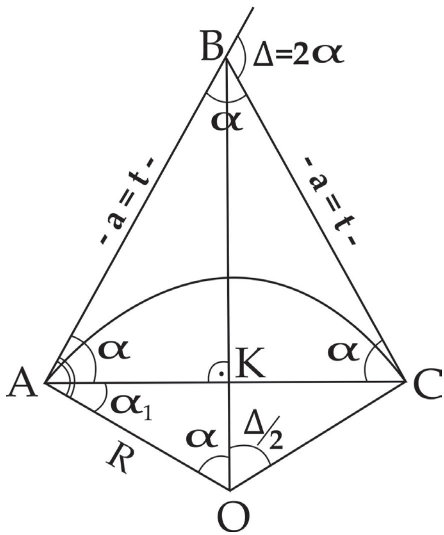

Figure 4. *Application of circle arc between base points of equilateral triangle*

$t=a=R\tan(\Delta/2)=R\tan\alpha$ (3)

R from this equality

$R=\dfrac{a}{\tan 66.6667}$ (4)

It is obtained from the connection.

The angle α_1 in Figure 4 is obtained from the following connection because of the circle arc to be passed through tangent points A and C.

$\alpha_1=100-\alpha=33^{g}.3333$ (5)

In Fig. 4, if the radius R of the circumference circle to be passed is given, the Δ angle deviation angle of the circle arc is obtained from equation (2), the edge edge a of the triangle to be formed is obtained from equation (3).

3. Circle Arc Application between the Base Points in an Isosceles Triangle

In a ABC isosceles triangle whose base is a=AC, the base angle α, AB=BC is obtained from the following correlation (Figure 5).

$$AB=\frac{a}{2cos\alpha} \tag{6}$$

If the base of the isosceles triangle a is given from the base and the height of the base AK (Figure 5), with the base angle α, the AB edge is derived from the following equation:

$$\alpha=\arctan\left(\frac{2KB}{a}\right) \tag{7}$$

$$AB=\sqrt{(KB^2)+\left(\frac{a}{2}\right)^2} \tag{8}$$

In FIG. 5, the AB and BC lines are tangent at points A and C to be formed, in this case; Δ, t and R are obtained from the following relations (Kavanagh, F.B., 2009; Wilfred 2001, Wolf & Ghilani 2008).

$$\Delta=2\alpha \tag{9}$$

$$t=AB=BC=\frac{a}{2cos\alpha} \tag{10}$$

t= R tanα(11)

$$R=\frac{a}{2sin\alpha} \tag{12}$$

In Fig. 5, if the radius R of the circumferential circle being passed and the base angle α of the isosceles triangle are given, the Δ angle of deviation of the circle spring is from the equation (9), the edge length a of the triangle to be formed is obtained by using the equation (12).

$$a=2R\sin\alpha \tag{13}$$

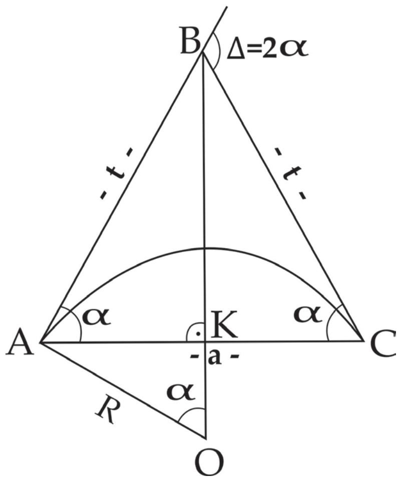

Figure 5. *Application of circle arc between base points of triangular triangle*

4. Circle Arc Application between Diameters in One Frame

An infinite number of circle arcs can be passed through the A and D corners of the ABCD-shaped, a-edge square (Figure 6).

However, as shown in Figure 6; If the point of point E where the diameters of the circle to be passed through the corner points A and D are intersected by the diagonals of the square and the lengths of the EA and ED are considered as the tangent lines of the circle arc, only one circle arc passes from the indicated points A and D.

In this case, the Δ deflection angle at the center of the circle to be passed, t tangent length and radius R are obtained from the following relations (Bannister et al., 1998).

$$\Delta=2\alpha=100^{g} \tag{14}$$

$$t=EA=ED=\frac{a}{2cos50} \tag{15}$$

$$R=\frac{a}{2sin50}=t \tag{16}$$

When the radius of the circle passing through the interior of the square and the corner points is given the radius R; the edge of the square is obtained by using (16).

$$a=2R\,sin50^{g} \tag{17}$$

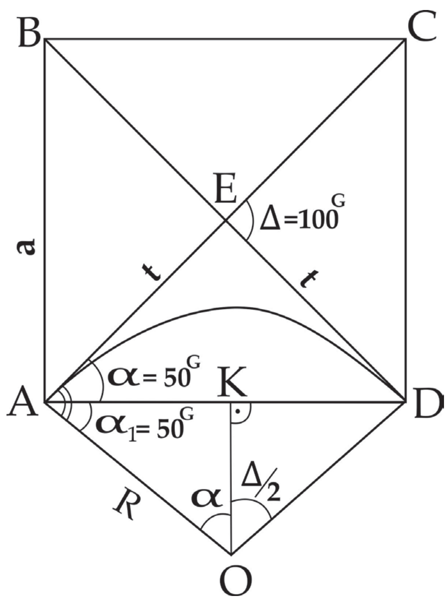

Figure 6- *Application of the circle arc between the diagonals of the square*

5. Formation of Triangles and Squares in Series and Application of Circle Springs between Their Bases

5.1. Equilateral Triangle Sequences

In Figure 7, if the equilaterals triangles are aligned so that their sides are parallel to one another, their bases are parallel to each other; the points A, C, E and G forming the lower bases of the triangles are located on the line in the same direction. The points B, D and F, which form the upper bases of the triangles, are located along the direction parallel to the line passing through the A-G points. The heights of the triangles created in series are obtained from the following correlation.

$$BK=DJ=FH=a\sin 66.6667=\frac{a}{2}\tan 66.6667 \qquad (18)$$

While an equilateral triangle sequence is applied; on a specified direction, from a designated starting point A, lengths and lengths thereof are measured by measuring the length. Thus, points A, C, E and G are made visible. The center points of the sub-bases of the specified triangles are then measured at points a / 2 from the corresponding corner points and the points K, J, H are marked. The a length taken from point A, BK lengths taken from point K are intersected or or up to BK on the upright direction exiting from point K the point B is marked. Similar operation is applied at points C, J and E, H and points D and F are marked. The base center points of the triangles L and I formed at the top of the base are marked with a / 2 in the base direction from the B and D points.

In Figure 7, in passing the circular spring between the base points of the array equilateral triangles having two points common and the bases of which are arranged parallel to each other;

AK, KO_1, AO_1 application elements for the application of circle spring between points A and C from O1 point. And for the application of the circle spring between points B and D from the O_2 point, BL, LO_2, BO_2 application elements are required. Base angles of ABC and BDC equilateral triangles are $\alpha=66^g.6667$ and α_1 is expressed as follows:

$$\alpha_1=100^g-\alpha=33.3333 \tag{19}$$

If a side of the equilateral triangles is known, the above-mentioned application elements are obtained from the following relations.

$$AK=\frac{a}{2} \tag{20}$$

$$AO_1=\frac{a}{2cos\alpha_1} \tag{21}$$

$$KO_1=AK*\tan\alpha_1 \tag{22}$$

BDC in equilateral triangle; BD // AC and BC edge are the common edge of the two triangles, so BL = AK, BO2 = AO1 LO2 = KO1 (Figure 7).

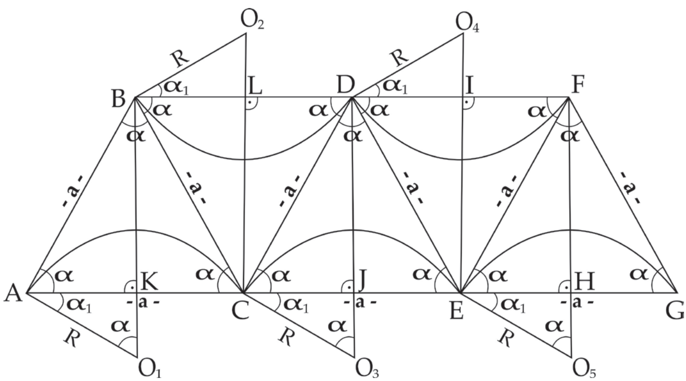

Figure 7. *Formation of equilateral triangles in series and application of circle arcs between their base points*

5.1.2. In Twin Triangle Sequences

In Figure 8, if one side is shared, and the base is parallel to each other, then the triangle becomes a series of equilateral triangles. The points a, C, E, and G, which form the base of the triangle A, are on the right side of the line in the same direction. These triangles that make up a top of the base B, points D and F, and G at the position directly parallel to the direction passing through the point A is located on. The height of the triangles formed in series and AB=BC length, a base length and α base angle are obtained from the following relations taking into account.

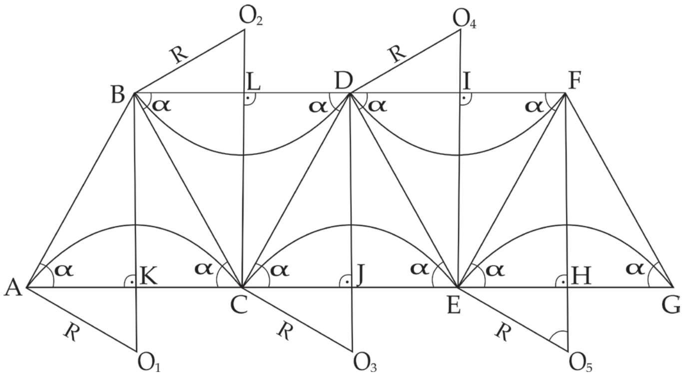

Figure 8- *Formation of isosceles triangles in series and application of circle arcs between their base points*

$$BK=DJ=FH=a\sin\alpha=\frac{a}{2}\tan\alpha \tag{23}$$

$$AB=BC=\frac{a}{2\cos\alpha} \tag{24}$$

When applying a twin triangle sequence;

On a specified direction, from A designated starting point, length A and multiple lengths are measured and marked, and points A, C, E and I are made visible. Then, the middle points of the identified sub-bases are measured up to a/2 from the related corner points and K, J, h points are marked. The length taken from point A to Point AB is cut from point K to point B, or the length taken from point K is cut from point B to point B.

Similar operation is applied at points C, J and E, H and points D and F are marked. The base of the triangles formed on the upper side is marked as L, I, midpoints, a/2 in the direction of the base starting from B and D points. In Figure 8, in the application of the circle arc between the base points of the array isosceles triangles, which have two points in common and their bases are parallel to each other;

For the application of the flat between the points A and C from point O_1 to the application elements AK, KO_1, AO_1. And for the application of the circle spring between points B and D from the O_2 point, BL, LO_2, BO_2 application elements are required. The base angles of ABC and BDC are expressed as follows if α is given.

$$\alpha_1 = 100^g - \alpha \qquad (25)$$

If the base angle of A and A are known, then the above-mentioned application elements are obtained from AK (20), AO_1 (21), and KO_1 (22), respectively. BDC isosceles triangle; BD//AC and BC, since Common Edge is the edge of two triangles, BL=AK, BO2 =LO2 AO1= KO1.

5.2. In Square Sequences

In Figure 9, if the Square is converted into a series with the common side and the base parallel to each other;

A, D, and e points forming the bottom edges of squares are on the same line. The points B, C and F, which form the upper edges of these squares, are located on the line parallel to the point A through the point E. The height of the squares created in series is AB=CD=EF.

When applying a square array, the lengths of a length and its multiple times are measured and marked on a specified direction, so that points a, D and E is made visible. Then, on the vertical direction from points a, D and E, B, C and F points are marked by taking the length of the given edge of the square.

In Figure 9, in the application of the circle arc between the corner points of the squared squares arranged with two points in common and their bases parallel to each other;

AK, KO_1, AO_1 application elements for the application of circle spring between points A and C from O_1 point. And for the application of the circle spring between points B and D from the O_2 point, BL, LO_2, BO_2 application elements are required. In Figure 9, the ABCD and dcfe frames are given on one side of the square (a) and α is obtained as follows:

$$\alpha=\alpha_1=50^g \tag{26}$$

If a is known, the above-mentioned application elements are obtained from AK (20), AO_1 (21) and KO_1 (22), respectively. Since the generated frames are name=BC and DF=CE, BL=AK, $BO_2 = AO_1$, $LO_2 = KO_1$.

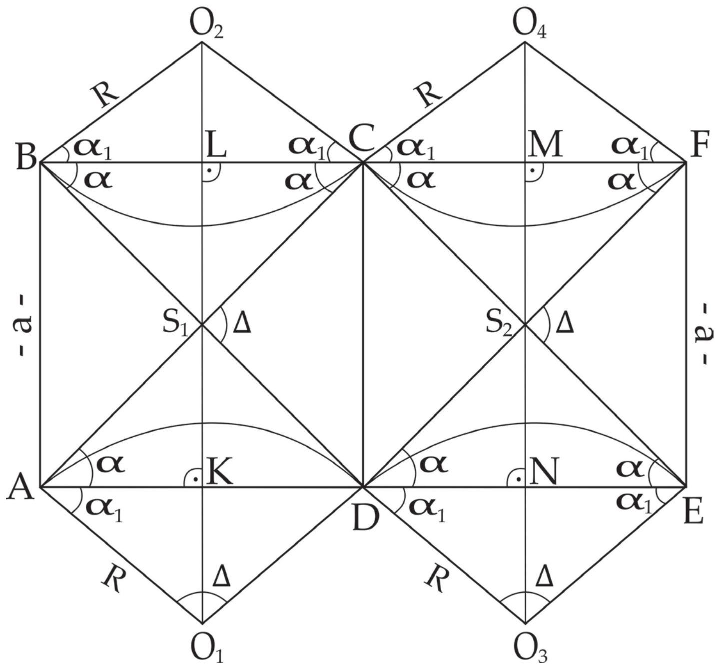

Figure 9- *Creating squares in series and application of circle arcs between their diagonals*

6. Arrangement of Circle Arcs between Triangles and Squares in the Parks and Gardens

The application of circular arcs between corner points in a square triangle, between the base points in the twin edge triangle and in a frame can be made with simple measuring instruments and with an electronic takeometer. The radiuses of circular arcs formed in parks or gardens are generally small in size compared to the radii of curves on highways, as can be seen in Figure 10 and Figure 11.

Figure 10- *Circular designs in a park*

Figure 11- *Circular designs in a park*

It is sufficient to apply circular arcs in parks or gardens with a precision of ± 1 cm. Circular springs to be formed in parks can be applied with simple measuring instruments, radius up to 10 meters on sloping terrain, and radius of up to 20 meters on flat terrain. If the radius of the circular arc is more than 10 meters from the slope, it is difficult to mark the circular arc in the field by keeping the steel tape measure horizontal and taut. If the radius of the circular arc exceeds 10 meters in sloping terrain, the intermediate points of the circular arc can be applied with polar coordinate method at equal arc intervals in order to increase the position accuracy of the points to be applied.

6.1. Between the Base Points of the Equilateral Triangles and Isosceles of Triangles in Sequence

6.1.1. Application with simple measurement tools

The equilateral triangle and isosceles triangles are applied in a park or garden area; In a direction determined from a starting point A in Figure 7 and Figure 8, the length a and the lengths thereof are measured and measured by the length measuring device. Points A, C, E and G are made clear. Then, the midpoints of the sub-bases of the specified triangles are measured from the respective corner points a / 2 and the points K, J, H are marked. With the length taken from point A, point B is taken by intersecting the lengths taken from point K to BK, or by taking BK on the upright direction exiting from point K. Similar operations are applied at points C, J and E, H, and points D and F are marked.

The base center points of the triangles L, I which are formed on the upper side of the triangles are marked up to a / 2 in the base direction from the B and D points. In Figure 7 and Figure 8; From the K point to the right side of the AC base and from the L point to the left side of the BD base, the vertical length of the KO1 length calculated on the perpendicular direction is applied with simple measurement tools. The center of O2, which will be passed through points A and C, and B and D points, is marked O2 center. For the circular spring application, the knot to be placed in the center of the circular arc is connected.

In the equilateral triangle (4), the other end of the rope length, calculated from the correlation in the isosceles triangle (12), is connected to a 40-50 cm bar with a tip 20 mm in diameter or a nail of 20 cm. The tied rope is held taut, and the circular springs are drawn between the corner points of the triangles by pressing on the bar or nail at the other end of the rope. Powder paint or powdered lime is carefully discarded on the circular arc seen on the floor and the circular springs are made visible.

6.1.2. Application with Polar Coordinate Method

The equilateral triangle and isosceles triangles are applied in a park or garden area; An electronic takeometer is installed at an A starting point set in Figure 7 and Figure 8.

The distances of the corner points (C, E, G) of the triangles to be formed from A point are calculated and applied on a direction determined from point A, a pile of wood pile to each of these points so that the points are made clear. The electronic takeometer installed at point A is directed to point C, from this direction to the left side, the angle of angle α of the equilateral triangle or isosceles triangle is applied. In line with the applied angle; in the equilateral triangle, the distance AB is calculated with the correlation between the isosceles triangle (24) and the point B is marked with the help of the reflector. D and F points are marked by applying similar operation at points C and E. In Figure 7 and Figure 8, the length of the AC circle arc is calculated from the following correlation.

$$AC=\frac{2\pi R\Delta}{400} \tag{27}$$

While the intermediate points are marked in a circular arc, R=approximate arc length between two intermediate points at curves up to 300 meters (*l'*);

$$l' = R/10 \tag{28}$$

taken as; the difference between the beam and the spring part of this circle is minimum (İnce, 2010).

AC apartment is on air;

n’: approximate number of waypoints, n: the exact number of waypoints (obtained by rounding of n’), *l*: the exact arc length between the two intermediate points, the angle seen from the center of the ε: *l* arc, S: the beam between point A and the arc intermediate point is the length.

n’, *l*, ε and S are obtained from following relations.

$$n' = \frac{AC}{l'} - 1 \tag{29}$$

$$l = \frac{AC}{n+1} \tag{30}$$

$$\varepsilon = \frac{l}{R}\rho \tag{31}$$

$$S = 2R\sin\frac{\epsilon}{2} \tag{32}$$

Point A is taken with electronic takeometer point B, The polar application elements of the intermediate points of the AC spring are calculated as specified in Table 1 at equal arc intervals from the AB direction.

If the elements calculated in Table 1 are applied by considering the tangent directions determined at the points C, E, B and D, the circle springs between the bases points of the triangles are marked on the floor.

Table 1. *Application elements to be applied by polar method from A station point*

Station Point	Point of	Horizontal Angle	Horizontal Distance
A	B	0.0000	
	1	$\varepsilon_1 = \frac{\epsilon}{2}$	A1=2Rsin ε_1
	2	$\varepsilon_2 = \frac{2\epsilon}{2}$	A2=2Rsin ε_2
	..	...	….
	n	$\varepsilon_n = \frac{n*\epsilon}{2}$	An=2Rsin ε_n

6.2. Between Diagonals of Frames in Sequence

6.2.1. With simple measuring tools

When the frame sequence is applied (as shown in Figure 9); from a designated starting point A, length a and lengths of it are measured and the points A, D and E are marked. Then points B, C and F are taken over the vertical direction exited from the points A, D and E by taking the length of the given edge of the frame.

In Figure 9, the right length from the K point to the right of the AD base, and from the L point to the left side of the BD base, is calculated as perpendicular to the length of the KO1 length. With simple measurement tools, the center of O2 to be passed through the points A and D and the center of O2 to be passed through points B and C are marked. For the circular spring application, the knot to be placed in the center of the circular arc is connected. The other end of the rope length calculated from the relation (16) at the square is connected to a 40-50 cm bar with a tip of 20 mm diameter or a nail of 20 cm.

The tied rope is held taut, and the circular springs are drawn between the corner points of the triangles by pressing on the bar or nail at the other end of the rope.

Powder paint or powdered lime is carefully discarded on the circular arc seen on the floor and the circular springs are made visible.

6.2.2. With polar coordinate method

In a park or garden area; as shown in Figure 9, an electronic startometer is installed at a designated starting point A.

From the point A, the length A and the lengths thereof are measured on a determined direction, and the points A, D and E are machined with a wooden pile. Then the angle of α=50g from the AD direction is applied and in this direction the AS1 horizontal distance calculated by the correlation with (15) is applied. Then the point of S1 is marked and in this direction, the horizontal distance of 2 * AS1 is applied and point C is marked. From the AS1 direction, 50 g angle is applied, in this direction the edge of the square is applied, point B is marked. S2 and F points are marked by applying a similar operation at point C.

In Figure 9, the length of the AD circle arc is calculated from the correlation (27). After the AD arc length is found, the process specified in section 5.1.2 is performed; the elements required for the polarization of the intermediate points of the AD arc are calculated in equal arc intervals. The waypoints are marked on the floor.

7. Application

As a field of application, it has been selected as a parking area in centre of Corum Province. In the park area, an array of equilateral triangles is formed in a square and square position apart from each other in a 5-meter series. The calculations of the elements mentioned in Figure 6 in relation to the square array are shown below.

$\Delta=2\alpha=100^g$

$t=EA=ED=\frac{a}{2\cos 50}=3.536$

$R=\frac{a}{2\sin 50}=t$

In the park area, it was decided to apply the circular arc between the diagonals of the square by polar coordinate method. For this purpose, before the square corners are applied as indicated in section 5.2, the intersection point (E) of the diagonals shown in Figure 6 is applied. For polar application; the length of the circular arc, the number of the intermediate points created (n), the exact arc length (l) between the two intermediate points, and the angle (ε) that sees this exact arc length from the center is calculated below and is shown in Table 2.

Length of AD arc in Figure 6 $AD=\frac{2\pi R\Delta}{400}=5.554\text{m}$

$l'\approx\frac{R}{10}=0.354\text{m}$, $n'=\frac{5.554}{0.354}-1=14.689$, n=15,

$l=\frac{5.554}{16}=0.347m$, $\varepsilon=\frac{0.347}{3.536}63.6620=6^g.2474$

Table 2. *A station point to be implemented by the polar method application elements*

Station Point	Point of	Horizontal Angle	Horizontal Distance
A	E	0.0000	
	1	3.1237	0.347
	2	6.2474	0.693
	3	9.3711	1.037
	4	12.4947	1.379
	5	15.6184	1.718
	..	……	…….
	15	46.8553	4.748

As indicated in section 5.1, first the 5m rhombic triangular triangles are applied and the corner points of the triangles are marked on the ground. The calculations of the elements mentioned in Figure 4 in relation to the equilateral triangle sequence are shown below and in Table 3.

$\Delta=2\alpha=120^{o}=133^{g}.3334$

$R=\frac{a}{\tan 66.6667}\ 2.887\ m.$, AC arc length $=\frac{2\pi*2.887*133.3334}{400}$ $=6.046$m, $l'\approx\frac{2.887}{10}=0.289$ m.

AC arc length $=\frac{2\pi*2.887*133.3334}{400}=6.046$ m.

$n'=\frac{6.046}{0.289}-1=19.92$, $n=20$, $l=\frac{6.046}{21}=0.288$ m,

$\varepsilon=\frac{0.288}{2.887}63.6620=6^{g}.3508$

Table 3- *Application elements to be applied by polar method from A station point*

Station Point	Point of	Horizontal Angle	Horizontal Distance
A	B	0.0000	
	1	3.1724	0.287
	2	6.3508	0.574
	3	9.5262	0.860
	4	12.7016	1.143
	5	158770	1.424
	..	.....	....
	20	46.8553	4.848

The above-mentioned application elements have been applied from other determined corner points of the squares in series and from other base points determined in equilateral triangles and the circle arcs were formed in series on the ground (Figure 12 and Figure 13).

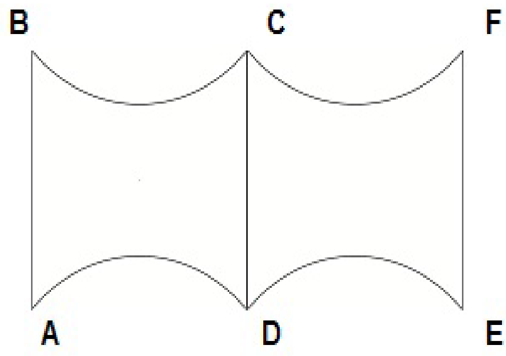

Figure 12. *The shape of the circle arcs between the diagonals in the square series created in a park area*

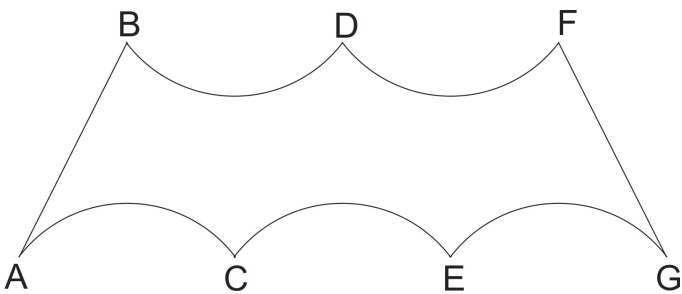

Figure 13. *In the equilateral triangle series created in a park area, the shape of the circle arcs between the base points of the triangles*

8. Conclusion and Suggestions

- In the equilateral triangle formed in series on a parking space, the application of the circle arcs between the corner points in the twin edge triangle and between the corner points in one frame can be made by simple measuring instruments and with electronic takeometer.
- With simple measurement tools, up to 10 meters radius on steep slopes, flat areas up to 20 meters radius radius can be appliqued.

- With the help of simple measurement tools, the application of the circle arcs formed in a park area; the center of the circle arcs in the park area must be marked on the field.
- In the application of intermediate points of circle arc in equal arc spacing with electronic takeometer and polar coordinate method; it does not need to be marked on the terrain. The tool is installed in one of the corner points on the base of the triangle or square formed in the park area, after the connection to the point determined as some point, the application of the intermediate points is started.
- In the application of intermediate points belonging to circle arc in equal arc intervals by polarity method with electronic takeometer; if the tool cannot be installed on the triangles or square corners of the parking area, the center of the hub is applied, the polar application is made from the center point of the blade.
- In a park or garden area; between the corners points of the triangle or square, the circle springs to be passed under the above-mentioned conditions are quickly applied with simple measurement tools. However, it is recommended to apply the polar coordinate method to increase the position accuracy of the points to be applied at equal arc intervals.

REFERENCES

Bannister, A., Raymond, S. and Baker, R., (1998). Surveying. 7th ed. Harlow, UK: Addison Wesley Longman Limited Edinburg Gate, pp.81–82.

Bell, S., (2005). Elements of Visual Design in the Landscape, Second Edition by Spon Press, ISBN 0-203-35814-7, Taylor & Francis e-Library.

Booth, N.K., (1990). Basic Elements of Landscape Architecture Design, Ohio Üniversity, Newyork

Eralp, A., (2019). Modern Peyzaj ve Ötesi. www:arkitera.com/gorus/499/modern peyzaj ve ötesi

Hansen, G., (2010). Basic Principles of Landscape Design, Reviewed September 2016, http://edis.ifas.ufl.edu, UF/IFAS Extension, Gainesville, Florida, USA.

İnce, H., (2010). A New Relation Developed in Aplication of Vertical Intervals in Vertical Coordinate System, TMMOB HKMO, 5. Ulusal Mühendislik Ölçmeleri Sempozyumu, 20-22 Ekim, ZKÜ Zonguldak, Bildiriler Kitabı, s.547-553, (in Turkish)

Kavanagh, F.B., (2009). Surveying principles and application, 8th ed. Columbus: Pearson Education Inc., pp.525–526.

Kavanagh, F. B., (2003). Geomatics. Pearson Education ˙Inc. Prentice Hall, Upper Saddle River, NJ pp. 159–160.

Tejszerska, A., (2009). Geometry and Graphics in Landscape Architecture, The Journal of Polish Society for Geometry and Engineering Graphics, ISSN 1644-9363, Volume 19 (2009), pp.45–48.

Wilfred S., (2001). Engineering Surveying. Fifth Edition, Butterworth Heinemann, pp. 395-397

Wolf, P. R. & Ghilani, C. D., (2008). Elementary Surveying an Introduction to Geomatics. 12th Edition, Upper Saddle River, New Jersey: Pearson Prentice-Hall. pp. 754-755

Ždímalová, M. & Vavríková, L., (2017). Mathematics, Garden and Landscape Architecture, 16th Conference on Applied Mathematics, APLIMAT 2017.

Chapter 8

EXHIBITION OF IMMOVABLE ARTICLES TO BE EXHIBITED IN ARCHAEOLOGICAL MUSEUMS ON PLATFORMS ON THE SAME CENTER WITH DIFFERENT RADIUS AND DIFFERENT HEIGHT CIRCULAR SPRINGS

Hüseyin İNCE[1], Nuri ERDEM[2],

Selma YILMAZ[1], F. Engin TOMBUŞ[1]

1 Vocational School of Technical Sciences, Hitit University, Çorum, Turkey, hince2017@gmail.com, selmayilmaz@hitit.edu.tr, fengintombus@hitit.edu.tr

2 Engineering Faculty, Department of Geomatic Engineering, OsmaniyeKorkut Ata University, Osmaniye, Turkey, nurierdem@osmaniye.edu.tr

1. INTRODUCTION

In the museums affiliated to the Ministry of Culture and Tourism in our country, there are regulations regarding the protection of movable cultural assets that are required to be protected within the scope of the Law on the Protection of Cultural and Natural Assets No. 2663. In this context, in accordance with the provisions of many laws on the subject, the Law on the Protection of Cultural and Natural Heritage No. 2863, which must be protected, movable cultural and natural assets for inventory and inventory transactions, and museums, ruins of the movable and immovable cultural and natural assets, all kinds of in order to ensure protection against danger and to take necessary measures, the Museum Guide has been put into force.

The historical artifacts of archeology excavations in our country are exhibited in archeology museums. In classical museums, hand-held historical artifacts are exhibited in glass-enclosed enclosures created in front of the wall, and historical artifacts in large sizes are displayed on an appropriately sized stand in the open area (Ames, 1986). In the halls where historical artifacts are exhibited, the area outside the stands and showcases in the hallway is the visitors' promenade (Ivan and Steven, 1991).

In order to use the museum exhibition halls more profitably, a new settlement model was proposed for the historical artifacts to be exhibited in the exhibition hall (Michalek, and Papalambros, 2002; Yildiz, 2007; Jin and Wang, 2011; Jin and Wang, 2015). Proposed new settlement model; and immovable historical artifacts to be exhibited in the exhibition hall on the same center of different radius and different height of the circle springs are placed on the stands created in a certain size.

In this study, in respect of the subject, as mentioned earlier, an exhibition hall with a certain size and area of rectangular shape was taken into account. After a certain width of a walkway is left in front of the walls of this exhibition hall, information is given on the calculation of the radius of the circle arc, the angle of deflection and the length of the arc to be passed to the diagonal in the hall at the marked corner points. Next, it is explained how the aperture points to be marked on the circular arcs of the circular arcs, the arc lengths, and the circular arcs to be passed in parallel with the fixed passage of the first circle passed to the first circle are explained. The numerical application was made, and the findings and opinions obtained were stated.

2. Calculating the Elements of the Circular Curve Tangled to the Diagonal Lines Passed from the Points Determined in the Exhibition Hall

The diagonal lengths of the hall are measured with a steel tape measure before circular curves are created in the exhibition hall. If the hall is a rectangular shape, the diagonal lengths are equal to each other. The midpoint of a diagonal determined by measuring with a steel tape measure is taken as the intersection point (F point) of the diagonal (Figure 1).

From point F, the lengths specified in FA = FB = FC = FE are applied, with points A, B, C, and E respectively, so that there is some clearance in front of the walls in the diagonal directions in front of the walls. Thus, a complete rectangular shape is created in the hall. This process is done very precisely and easily using the dot laser tool (Yavuz & Ersoy, 2007). In Figure 1, it is accepted that the first circular curve to be formed in the hall is to be tangent to the AC and EB diagonal points, considering that the shape formed after the space left for navigation is rectangular.

In Figure 1; The deflection angle (Δ_0) with the radius R_0 of the first circular curve passing through points A and E is obtained from the following relations, a = AE, b = CE.

$$\alpha = \arctan\left(\frac{b}{a}\right) \tag{1}$$

$$R_0 = \frac{a}{2 * \sin \alpha} \tag{2}$$

$$\Delta_0 = 2\alpha \tag{3}$$

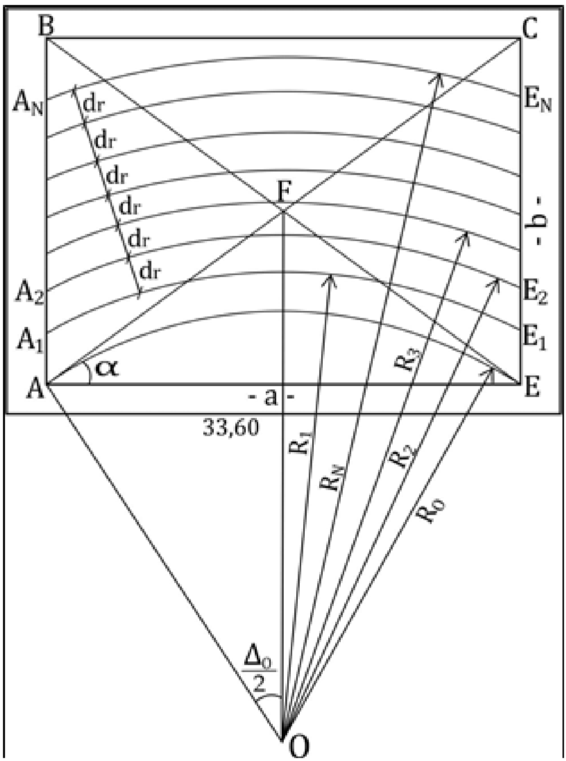

Figure 1. *The intersection point (F point) of the diagonal*

3. Obtaining Radius, Deviation Angles and Spring Lengths of the Circles of the Same Center Created in Hall

After the R_o is obtained, a fixed interval (dr) is left between the circular arcs, which will take place in the second and subsequent rows. The radii of the circular curves (R_1, R_2, .. R_N) in the second and subsequent rows are obtained from the following relations.

$$R_1=R_0+dr \tag{4}$$

$$R_2=R_1+dr \tag{5}$$

…………

…………

$$R_N=R_{N-1}+dr \tag{6}$$

In Figure 2; It is seen that all the beam lengths of the circular curves A_1E_1, A_2E_2, … .A_NE_N are equal to each other.

$$AE=A_1E_1=A_2E_2=A_3E_3=……….=A_NE_N \tag{7}$$

$$A_1E_1=2R_1\sin\left(\frac{\Delta_1}{2}\right) \tag{8}$$

Δ_1 from equation (8), similarly Δ_2, Δ_3, …Δ_N is obtained from the following equations.

$$\Delta_1=2*\arcsin\left(\frac{AE}{2R_1}\right) \tag{9}$$

$$\Delta_2=2*\arcsin\left(\frac{AE}{2R_2}\right) \tag{10}$$

…………………

$$\Delta_N=2*\arcsin\left(\frac{AE}{2R_N}\right) \tag{11}$$

In Figure 1: α_1, α_2, α_3,… α_N are obtained from the following equations.

$$\alpha_1=\frac{\Delta_o-\Delta_1}{2} \tag{12}$$

$$\alpha_2=\frac{\Delta_o-\Delta_2}{2} \tag{13}$$

…………

$$\alpha_N=\frac{\Delta_o-\Delta_N}{2} \tag{14}$$

In Figure 2: AA_1, AA_2,.. AA_N are obtained from the following relations in the triangles to which they are related, taking into account the radii of the circular curves (Ro, R_1, R_2, .. R_N) and α_1, α_2, .. α_N.

$$AA_1=\sqrt{(R_o^2+R_1^2-2R_oR_1\cos\alpha_1)} \tag{15}$$

$$AA_2=\sqrt{(R_o^2+R_2^2-2R_oR_2\cos\alpha_2)} \tag{16}$$

………………………………………..

$$AA_N=\sqrt{(R_o^2+R_N^2-2R_oR_N\cos\alpha_N)} \tag{17}$$

Considering that the exhibition hall is rectangular, the distances of the intersection points of the circular curves with line AB and EC up to A and E are expressed as follows:

$EE_1=AA_1$

$EE_2=AA_2$

$EE_3=AA_3$

…………..

$EE_N=AA_N$

In the exhibition hall, the length of each circular curve (D_O, D_1, D_2, ……D_N) is obtained from the following relations (Schofield and Breach, 2007; Kavanagh, 2009; McCormac, 1991; Cuomo, 1998; Ghilani and Wolf 2012):

$$D_0=\frac{2\pi R_O}{400}\Delta_O \tag{18}$$

$$D_1=\frac{2\pi R_1}{400}\Delta_1 \tag{19}$$

$$D_2=\frac{2\pi R_2}{400}\Delta_2 \tag{20}$$

…………

$$D_N=\frac{2\pi R_N}{400}\Delta_N \tag{21}$$

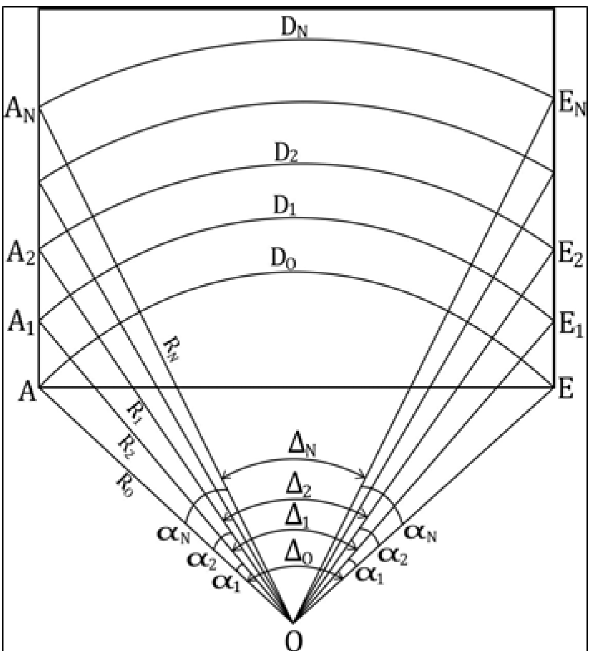

Figure 2. *The beam lengths of the circular curves*

4. Calculation of the Exact Curve Length, the Number Of İntermediate Points and the Angle That Sees the Exact Curve Length from the Center in the Circular Curves in the Hall

According to the basic principle in the application of circular arcs in cartography, the difference between the arc length between the intermediate points to be formed in equal spacing on the circular arcs and the beam length of this spring should not exceed 0.01m.

$$l'=\frac{R}{10} \tag{22}$$

Equally spaced with this principle, while the intermediate points are determined, the approximate curve length (l') between two intermediate points on a circular curve is determined according to the following relation in curves with radius up to 250 m (İnce, 2010).

When the average length of the stands to be placed at the intermediate points to be formed in the circular curves in the exhibition hall is 1.0 m. The curve length to be determined by the correlation (22) is greater than the specified size.

The determined stand length (d) is assumed to be the exact curve length, taking into account the length (D) of the curve and the radius R, the number of intermediate points (n) to be formed and the angle (ε), which views the exact curve length from the center, is obtained from the following relations.

$$n'=\frac{D}{d}-1 \tag{23}$$

n is obtained by converting the n' fractional number to an integer

$$\varepsilon=\frac{d}{R}\rho \tag{24}$$

5. Calculation of the number of intermediate points and polar application elements in the case of separation of path share between circular curves in the middle of the hall

5.1. Calculation of Number of Intermediate Point and the Angle of the Exact Curve Length from the Center of the Curve on Circular Curves in the Hall

In the middle part of the hall, if the road share (y) is divided between the circular curves. The circular curves in each row are divided into two equal parts, and the lengths of the segments in each circular curve (Figure 3) are obtained from the following equations.

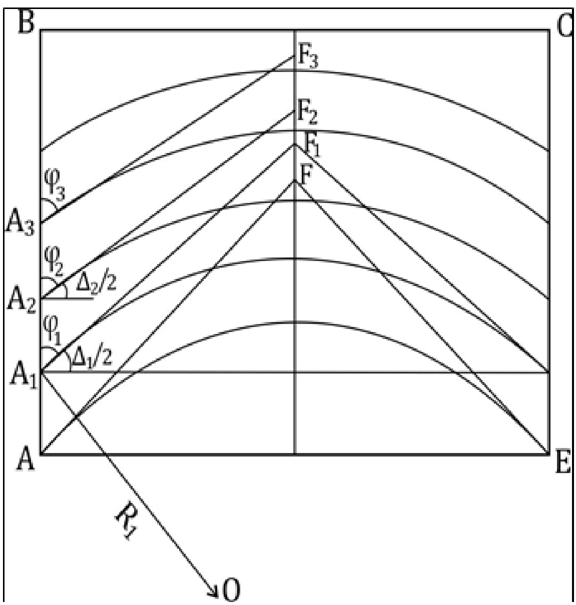

Figure 3. *The lengths of the segments in each circular curve*

$$D_{O1}=D_{O2}=D_{O}-y \tag{25}$$

$$D_{11}=D_{12}=D_{1}-y \tag{26}$$

$D_{21}=D_{22}=D_2\text{-}y$ (27)

....

$D_{N1}=D_{N2}=D_N\text{-}y$ (28)

In the first order, circular parts in accordance with the basic principle specified in section 3. In all circular curves in the hall, the stand length (d) is accepted and the number of points (n_o) to be formed in the circular curve part, and the angle (d) that are seen from the center of the curve is obtained from the following relations.

$n_o'=\frac{D_{01}}{d}-1$ (29)

n_o = Total number of intermediate points

$\varepsilon_0=\frac{d}{R_0}\rho$ (30)

n_0 when calculating; If the fraction of n_0' is greater than 5, the integer part of the number is taken as n_0.

$D_{01}<(n_0+1) * d$ in this case

The difference between the values of D_{01} to $(n_0+1) *$ d (t_{01}) occurs as a space to leave.

$t_{01}=D_{01}-(n_0+1)*d$ (31)

Before the waypoints are applied from the point determined as the station point, the space required for t is left.

For this, the angle (ε_{0t}), which sees the t_{01} curve part from the center, is calculated by the following correlation.

$\varepsilon_{0t}=\frac{t_{01}}{R_0}\rho$ (32)

The above elements obtained for D_{01} also apply to D_{02}.

In the second and the other row of segmented circular curves, the operations as mentioned above are carried out similarly.

5.2. Calculation of Application Elements by Polar Coordinate Method of Intermediate Points

In the hall, according to the polar coordinate method of the equal range intermediate points belonging to the spring of the circle with radius R0. Considering the ε_{0t} angle for the space at the station point side of the circular curve, A is used as the point of connection, the point F as the connection point and the relations in Table 1 (Kavanagh, 2009) are used for intermediate points to be applied in this circular curve.

Table 1. *Polar application elements from point A of intermediate points in a radius of radius R_0*

Radius It's number	Station Point	Point of View	Horizontal Angle	Horizontal Distance
R_O	A	F	$0^g.0000$	
		1	$\varepsilon_{01}=\frac{\varepsilon_0+\varepsilon_{0t}}{2}$	$A\text{-}1=2R_1 \sin \varepsilon_{01}$
		2	$\varepsilon_{02}=\frac{2\varepsilon_0+\varepsilon_{0t}}{2}$	$A\text{-}2=2R_o \sin \varepsilon_{02}$
		…..	………….	……………….
		n	$\varepsilon_{0n}=\frac{n\varepsilon_0+\varepsilon_{0t}}{2}$	$A\text{-}n=2R_o \sin \varepsilon_{0n}$

In the hall, with the R_1 radius circular curve in the application of equally spaced intermediate points; If point B is selected as the point of departure, point B is selected as the port. The angle between the tangent direction passing through point A_1 and the A_1D_1 direction of the circular curve at radius R_1 is equal to $(\frac{\Delta_1}{2})$ taking into account the deviation angle Δ_1

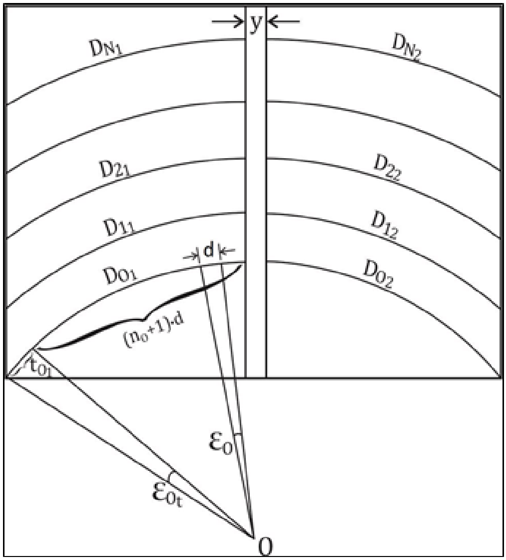

Figure 4. *The ε_{0t} angle for the space at the station point side of the circular curve*

The φ_1 angle between the direction A_1B and the tangent direction passing through A_1 is obtained from the following correlation.

$$\varphi_1 = 100^g - \frac{\Delta_1}{2} \tag{33}$$

Considering the ε1t angle calculated for the radius at the station point side of the circular curve in the circular curve with radius R1. It is used the relations in Table 2 (Kavanagh, 2009) for intermediate points to be applied on this circular curve, accepted as the A_1 station point and connection B.

Table 2. *Polar application elements from point A_1 of intermediate points in circular curve of with radius R_1*

Radius It's number	Station Number	Point of View	Horizontal Angle	Horizontal Distance
R_1	A_1	B	$0^g.0000$	
		1	$\varepsilon_{11} = \frac{\epsilon_1+\epsilon_{1t}}{2} + \varphi_1$	$A_1 - 1 = 2R_1 \sin\left(\frac{\epsilon_1+\epsilon_{1t}}{2}\right)$
		2	$\varepsilon_{12} = \frac{2\epsilon_1+\epsilon_{1t}}{2} + \varphi_1$	$A_1 - 2 = 2R_1 \sin\left(\frac{2\epsilon_1+\epsilon_{1t}}{2}\right)$
		…..	…………..	…………………..
		n	$\varepsilon_{1n} = \frac{n\epsilon_1+\epsilon_{1t}}{2} + \varphi_1$	$A_1 - n = 2R_1 \sin\left(\frac{n\epsilon_1+\epsilon_{1t}}{2}\right)$

Similar operations are also applied for circular curves in other rows.

5.3. Calculating Application Elements of Different Height Stands Placed on Circular Curves

Taking into consideration the physical size of the historical artifacts to be exhibited, it must be at a certain height from the ground so that it rises from the front row to the rear row.

According to this, the difference between the stand length H_0 and the successive stand heights (dh), which will be placed at the intermediate points in the R_0 circular curve in the exhibition hall, shall be considered as constant and the heights of the other stands from the ground according to the radii are expressed as follows (Figure 5).

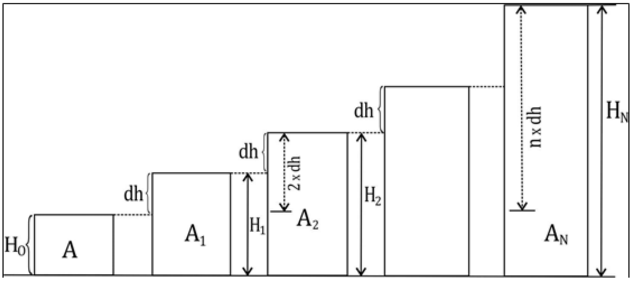

Fig. 5. *Platforms should be placed at the height of the front row at the height of the rear row in the exhibition hall.*

Stand height H_1=H_0+dh in the circular curve in radius R_1 (34)

Stand height H_2 = H_0 +2* dh in the circular curve in radius R_2 (35)

……………………………………………………..

Stand height H_N = H_0 +n* dh in the circular curve in radius R_N (36)

6. Application

As can be seen in the Çorum Archeology Museum, there are various rectangular halls (6m * 8m, 4m * 6m, 8m * 12m, 10m * 15m) in the museums. In museums, valuable archaeological artifacts that are legally portable and which can be stolen by visitors are exhibited indoors in enclosed enclosed cabinets. Archaeological artifacts that are heavily stolen and carried by the visitors are exhibited in the garden of the museum in the open area or indoors. Accordingly, an exhibition hall with a surface area of 8m * 12m = 96 m2 was chosen in order to exhibit the archaeological artifacts which are heavy to carry. The procedures to be followed in the application are listed as follows.

1-At the beginning of the application, the intersection F of the diagonals F in the hall is marked as indicated in section 1.

Diagonal diameters of 14.422 m and 14.20m were measured in the exhibition hall mentioned in Figure 1.

Subsequently, the lengths of FA = FB = FC = FE = 6.50m were determined, and points A, B, C, and E were applied so that a suitable width was left in front of the walls parallel to the hall walls.

2-In Figure 1, after clearing the road shares in front of the walls in the exhibition hall, the size of the rectangle was 10.816m*7.21m.

The radius (R_0) and the deflection angle (Δ_0) of a circular curve to be passed tangent to the diagonals formed in the hall at points A and E were obtained from the relations (1), (2) and (3).

$\Delta_0 = 74.8668 \quad R_0 = 9.75$m

3-In the hall between the circle curves, two people to walk around the 2.50m walkway and R_0 from two circular curves have been adopted to create.

Accordingly, the radii of the circular curves in other rows are formed as follows.

$R_1 = R_0 + 2.5 = 12.25$m, $R_2 = R_1 + 2.5 = 14.75$m,

4-AE = BC edge in the hall is the common beam of all the springs of each circular curve deviation angles (9) and (10) were obtained by using the number of relations.

$\Delta_1 = 58^g.2208$, $\Delta_2 = 47.8003$

5- The angles α_1 and α_2 are derived from the relations (12) and (13) by using the deviation angles obtained above.

$\alpha_1 = 8^g.3230$, $\alpha_2 = 13.5332$

6-The distances of the intersection points of the circular curves with the EU line to A are obtained from the correlations (15) and (16).

AA_1=2.879m, AA_2=5.610m

The distances calculated here also applies to the distances of the intersection points of the circular curves with the EC line to E.

That is, $EE_1 = AA_1$, $EE_2 = AA_2$.

The points A_1, A_2, E_1, E_2 are marked on the AB and EC lines taking into consideration the distances as mentioned above.

7-The length of each circular curve (D_0, D_1, D_2) in the exhibition hall was obtained from the equations (18), (19) and (20).

D_0=11.466m, D_1=11.203m, D_2=11.075m

8-It is designed to pass 1m wide path for visitors to navigate from the middle of the curves, divide the circular curves in each row in two in the exhibition hall.

After passing through the middle of the circular curves, the part lengths (25), (26) and (27) of each circular curve were obtained from the equations.

D_{01}=5.233m, D_{11}=5.101m, D_{21}=5.038m

9- According to (22); When the approximate curve length between two intermediate points is calculated in a circular curve, the values of *l'* ride remain between 0.975 m and 1.475m.

The stands to be placed on each circular curve are assumed to be square.

Considering the physical size of the historical artifacts to be exhibited on the stand, the side length of the stand was 1. 00 m, and the space between the stands was taken as 1.00 m to move between the stands.

This value is considered to be the exact curve length between the intermediate points.

10- Considering the specified stand length, the approximate number of intermediate points to be formed in the circular curve parts in each row is obtained by the correlation (29).

n_{01}'=4.233, n_{11}'=4.101, n_{21}'=4.037

When the numbers obtained are rounded according to the specified rule, n_{01}= n_{11}=n21= 4

In this case, three stands will be placed in all circular curves in the hall, taking into account the gaps formed at the end of each row.

Accordingly, the length and number of the stand in the hall were determined to be fixed; the gaps remaining from the stand placement during each circular curve were obtained by the correlation (31).

t_{01}=0.233m, t_{11}=0.103m, t_{21}=0.038m

11- The calculated gaps are applied in the circular curves in the hall on the side of the station points (A, A_1, A_2, E, E_1, E_2) the left and right of the hall.

12-The application elements, which are calculated by taking into account the precise curve length (1.00m) and the gap t_{01}, are shown in Table 3 for the intermediate points in the circular curve with radius R_0 to be applied from point A.

Table 3. *Polar application elements from point A of intermediate points in a circular curve with radius R_0*

Radius It's number	Station Number	Point of View	Horizontal Angle	Horizontal Distance
R_0	A	F	0.0000	
		1	4.0254	1.232
		2	7.2901	2.228
		…	………	……
		5	17.0843	5.170

13- φ_1 angle between the tangent direction passing through the A_1 and A_1B direction at the A_1 point in the circular curve with radius R_1 is calculated as $\varphi_1 = 70^g.8896$ from correlation (33).

The circular curve with R_1 radius in the hall, point A, station point B point is taken the connection point.

The angle φ_1 calculated in the application to be made by looking at the B point from the A_1 station point is taken into consideration.

Application elements of the circular curve 1, 2, …5 points were calculated as indicated in Table 2, and the results are shown in Table 4.

Table 4. *Polar application elements from point A_1 of intermediate points in circular curve with radius R_1*

Radius It's Number	Station Point	Point of View	Horizontal Angle	Horizontal Distance
R_1	A_1	B	0.0000	7.21
		1	73.7557	1.103
		2	76.3541	2.100
		…….	………	……
		5	84.1495	5.066

14- The intermediate points of the circular curves to the left of the road in the center of the hall have been applied from the station points on the left. Similarly, the ones to the right of the middle road are applicated from the station points on the right.

15- In determining the height of the stands to be placed at intermediate points in the circular curves in the exhibition hall, the physical sizes of the historical artifacts to be exhibited were taken into consideration.

Stand height, R_0 from the ground during the H_0 = 0.50m, and the difference between the successive stand heights dh = 0.20m is considered constant, and the height of the other stands according to the radius of the exhibition is expressed as follows.

Stand height H_1 = 0.70m in the circular curve in radius R_1

Stand height H_2 = 0.90m in the circular curve in radius R_2

The stands, as calculated above, are located at the points applied with the application elements in Table 3 and Table 4 in the circle curves of which they are related.

7. Results

- At the height of the front row of the exhibition hall in the exhibition hall, the placement of the stands on the circular curves ensured that both the exhibition hall and the rantabıl were used and all the historical artifacts to be exhibited were displayed better.
- Passing through the middle of the exhibition hall, the access between the circular springs is easier in the hall.
- The intermediate points to be applied on the circular springs divided into two parts bypassing

the intermediate road from the middle of the hall are symmetrical with respect to the path. According to this, the application elements of the intermediate points to be applied from a station point on the right side of a circular curve part also apply to the intermediate points to be applied on the left-hand circular curve from the station point at the left end of the respective circular arc.

- Due to the calculation of application elements for the intermediate points on the left side of the middle road in the hall, there is also no need for calculation due to the symmetrical position of the intermediate road on the right-hand side, but it requires to establish tooling at the beginning and endpoints of the circular curves on the left and right sides of the hall.
- In the hall from the second row of circular arcs on a span of a designated station point application points, as the connection point, there is no need to apply the tangent direction passing through the station point in the hall by taking the endpoint of the line on which the station point is.
- Since the existing archaeological museums exhibit historical artifacts according to the criteria determined by the Ministry of Culture and Tourism, it will be possible to exhibit immovable cultural and natural assets in the archeology museums to be constructed in the indoor or outdoor spaces as proposed.

REFERENCES

Ames, M.M., 1986. Museums, the public and anthropology. L.P. Vidayathi (Ed). Vancouver: University of British Columbia Press.

Cuomo, P. A., PLS, 1998. Surveying Principles for Civil Engineers, Proffesional Publication Inc. Belmont California, USA, p. 62-63

Ghilani, C.D. and Wolf, P.R., 2012. Elementary Surveying an Introduction to Geomatics, Thirteenth Edition, Pearson Prentice Hall, New Jersey, USA, p.716-717, pp. 938, ISBN-13: 978-0-13-255434-3

İnce, H., 2010. A New Relation Developing on Application of Curve Intermediate Points by Method of Sequential Tangents, (Turkish) TMMOB Chamber of Surveying and Cadastre Engineers, 5. Engineering Measures Symposium, 20-22 October, Zonguldak-Turkey, Manuscript Book, p. 547-554

Ivan, K. and Steven, D.L., 1991. Exhibiting Cultures: The Poetics and Politics of Museum Display, Washington D.C. Smithsonian Institution Press.

Jin, J. and Wang, Q., 2015. Analysis and Psychological Thinking on Visual Forms of interface of Exhibition Halls--Taking the Exhibition Halls of World Expo as an Example. International Conference on Engineering Management, Engineering Education and Information Technology (EMEEIT 2015), p. 114-117.

Jin, J. and Wang, Q., 2011. Design of Exhibition Hall Space. Shanghai People’s Publishing House.

Kavanagh, B., 2009. Surveying Principles and Applications, Eighth Edition, Person International Edition, p. 506, 510-511

McCormac, J. C., 1991. Surveying Fundamentals, Second Edition, Prentice-Hall İnc. New Jersey USA, p.472

Michalek, J.J. and Papalambros, P.Y., 2002. Interactive Design Optimization of Architectural Layouts, Eng. Opt., Vol. 34(5), pp. 485–501.

Schofield, W., & Breach, M., 2007. Engineering Surveying, Sixth Edition, www.elsevier.com, P.372-375

Yavuz, E. & Ersoy, N. 2007, 'Modern Geodetic Tools Used in Construction Sites', (Turkish) TMMOB Chamber of Surveying and Cadastre Engineers, 3. Engineering Measurements Symposium, 24-26 October, Selcuk University, Proceedings, p.224-229 Konya.

Yildiz, P., 2007. The Interactive Approaches of Exhibition Halls by Computational Facilities, International Journal of Education and Information Technologies, Issue 1, Volume 1, p. 17-22.

Chapter 9

USE OF WASTE WATER AS IRRIGATION WATER

İsmail TAŞ[1]

1 Assoc. Prof. Dr. İsmail Taş. Çanakkale Onsekiz Mart University, Agriculture Faculty, Department of Agricultural Structures and Irrigation, 17020 Terzioglu Campus Canakkale / TURKEY e-mail address: tas_ismail@yahoo.com

1. INTRODUCTION

There are several scientific and magazinal scenarios created for water worldwide. The recent scenarios focus on water resources as a potential reason of prospective world wars. When the previous cases were evaluated meticulously, it could clearly be seen that similar cases repeated several times for ages. Water resources are continuously polluted and become insufficient day by day. Such cases then bring those prospective wars earlier. Prevention/retardation of prospective scenarios will only be possible through efficient use of water resources and creation of alternative irrigation water supplies. Recent researches are mostly focused on maximum gain per unit of water and reuse of water resources. When the insufficient and low quality waters are used in irrigations, it is evident to have distorted quantity and quality. To meet ever increasing demands of every increasing populations, unit area yields should also be increased beside maximum benefit per unit water.

Water scarcity is an obvious problem in several parts of the world, especially in arid and semi-arid sections of the world. The problem will get bigger in near future. Fresh water demands of increasing population and developing industry are also increasing. To meet these increasing demands, initially the amount used in the greatest water-consuming sector, agricultural sector, should be reduced. However, such reductions in agricultural production activities will also reduce both the quantity and quality of the agricultural products. Then, already existing food scarcity will get larger in this case. Considering all these interdependent variables, it is only possible with increasing yields in agricultural productions to reduce the hunger in the world. Irrigation is the most significant input to increase yields in agricultural production and product diversity. Waste waters of all industries can be treated through various treatment processes and reused in irrigations. Polluted waters are reused in various parts of the world as irrigation water and they will even be used more in near future. Throughout the world, more than 20 million hectare land area is irrigated with partially treated or raw waste waters in 50 countries [1].

Water needed for irrigation in some places accounts for 3/4 of total demand. Regulations and guidelines vary widely about reuse in the world. Benefits of agricultural reuse could be suggested as high concentrations of nutrients may reduce the demand for fertilizers, long-term soil enrichment, decreases demand of potable water supply, additional treatment in soil, and water being not discharged to receiving waters. Thus, water pollution would be prevented. There are also some disadvantages of agricultural reuse such as health risk from associated pathogens, health risk from other contaminants (e.g., heavy metals, chemicals, and pharmaceuticals), decrease in soil quality from accumulation of salts and soil acidification, and infiltration of pollutants into groundwater [2; 3].

Irrigation water quality is first issue to be considered in irrigated fields of arid and semi-arid regions. Water quantity and quality are the greatest reasons of soil salinity in irrigated fields. Unconscious fertilizer uses are also contribute to soil salinization. Either in proper quality or in low quality, unconscious irrigations may result in serious problems in plants and soils. Irrigation water salinity negative influences plant osmatic pressure and plant nutrient uptake. Such irrigations also results in ion toxicity through ion accumulation in soils [4]. While toxic impact is considered as the primary salt damage, the other impacts are considered as secondary salt damage on plants. Salinity has negative impacts on plant growth and development. It also increases osmotic pressure and ion stress and disturb hormonal balance of the plants [5]. Increasing salt densities destroy soil structure, hinder plant water uptake and reduce plant growth and development

[6]. Parallel to increasing salt concentrations in growth ambient of the plants, production quantities and plant resistance levels are also reduced.

Wastewater is a valuable resource, however without a properly developed framework policy, safe and efficient management of this resource cannot be achieved. The major objectives of wastewater irrigation are that it provides a reliable source of water supply to agriculture and has the beneficial aspects of adding valuable plant nutrients and organic matter to soil [7; 8]. With careful planning and management, the positive aspects of wastewater irrigation can be achieved [9]. Sustainable agriculture can only be provided with appropriate land and water conservation practices. The idea of using wastewater in agricultural production is critical to the conservation and use of water resources during periods of water scarcity. However, plant nutrients, heavy metals and trace elements in wastewaters are important pollutants for plants and soils. In particular, heavy metals and trace elements are important threats to environment and plant health as well as human and animal health.

The term “waste water (including residential, nonresidential, agricultural, even industrial)” was coined by those who pioneered the technology. For them, the term seemed appropriate because it was generic and could be used in the context of the wide variety of materials under consideration. Now, the concern of many is that the word waste implies that the material is only suitable for disposal and as such, detracts from proper utilization. Even though another word or term might better convey the beneficial aspects, waste is so entrenched in the literature it would now be difficult to change.

According to the Cambridge Dictionary, waste is “things that are not wanted, especially what remains after you have used something”. According to the Oxford

Dictionary, waste is "unwanted or unusable material, substances, or by-products". On the other hand, in these two dictionaries, the meaning of waste water is given as "water that has been used in the home, in a business, or as part of an industrial process." Dictionary meaning of waste water is "used water". There is nothing to imply as waste. There is pollution because of utilization. It is a natural process already existing in nature. However, human-induced pollution is always greater than the pollution created through natural processes.

With the currently available knowledge and technology, it is impossible to call several materials created after various processes as "waste". Wastes and waste waters actually are not things to be considered as headache or as something totally useless. Such so called waste materials and waste waters can practically be utilized as raw material for other activities. Varied from one community to another, polluted waters usually contain organic matters, nutrients (nitrogen, phosphorus, potassium), inorganic materials (dissolved minerals), toxic substances and pathogens.

The waters so called as waste waters are polluted or low quality waters through utilization in different processes. It is quite a false concept to call them as "waste". These waters could either directly be used or be used after passing through some kind of treatment processes. Then they can provide significant savings in various inputs. In this way, it will be possible to preserve, development and utilization of water resources, to reduce treatment and disposal costs, reduce or totally eliminate chemical fertilizer needs. The waters so called as fresh waters are on the other hand drainage waters of a basin. In other words, they are somehow polluted with dissolved ions. Ground waters are also the same quality waters. İn this case, fresh waters are the waste waters of a watershed.

However, such waters are classified as fresh or clean waters.

Domestic wastewater has been used for irrigation by prehistoric civilizations (e.g., Mesopotamian, Indus valley, and Minoan) since the Bronze Age (ca. 3200–1100 BC) [10]. Thereafter, wastewater was used for disposal, irrigation, and fertilization purposes by Hellenic civilizations and later by Romans in areas surrounding cities (e.g., Athens and Rome) [11]. In more recent history, the "sewage farms" (i.e., wastewater application to the land for disposal and agricultural use) were operated in Bunzlau (Silesia) in 1531 and in Edinburgh (Scotland) in 1650, where wastewater was used for beneficial crop production [12]. In the following centuries in many rapidly growing cities of Europe and the United States, "sewage farms" were increasingly seen as a solution for the disposal of large volumes of the wastewater, some of which are still in operation today. Paris was a typical example with the first sewage farms established at Gennevilliers in 1872, eventually processing wastewater of the entire town. At the beginning of the last century, the sewage farms in France supplied with raw wastewater by the Colombes pumping station in Paris reached their maximum implementation, having been established in four different areas; in Gennevilliers (900 ha) and Achères (Achères plain, 1400 ha, Pierrelaye, 2010 ha and Triel, 950 ha) [13]. A large "sewage farm" was also established in Melbourne, Australia in 1897 [12;13;14]. The use of the land treatment systems continued into the twentieth century in central Europe, USA, and other locations all over the world, but not without causing serious public health concerns and negative environmental impacts. However, by the end of the first half of the current century, these systems were not easily accepted, due to drawbacks such as large area requirements, field operation problems, and the inability to achieve the higher hygiene criteria requirements required [12].

Today, planning of projects for the wastewater treatment and reuse of effluents is significantly increasing in several countries. The main (re)uses of treated wastewater are: irrigation (both agricultural and landscape), recharge of aquifers, seawater barriers, industrial applications, dual-distribution systems for toilet flushing, and other urban uses. International organizations, such as the World Bank, the Food and Agriculture Organization (FAO) of the United Nations, and the World Health Organization (WHO) estimate that the average annual increase in the reused volume of such water in the USA, China, Japan, Spain, Israel and Australia ranges from up to 25. For example, in California only 860 Mm^3/year of treated wastewater effluent (4300 Mm^3/year) was reused in 2010, whereas, over 80% (3440 Mm^3/year) of treated wastewater effluent was discharged to the ocean. In 2030, 2470 Mm^3/year is planned to be reused [7]. In Spain more than 500 Mm3/year of treated wastewater is currently reused and is expected to reach 1000 Mm^3/year [15]. In Israel over 80% of treated wastewater effluent is reused, mainly for agricultural irrigation. In Singapore NEWater meets up to 30% of the nation's current water needs [16], which may increase to 55% by 2060 [17]. Large-scale droughts in California and Texas in the USA have led to greater exploration and implementation of direct potable reuse. In California, the governor announced in 2013 that guidelines for potable reuse, including direct, needed to be established by 2016. Texas already has moved forward with direct potable reuse with full-scale projects in operation in Big Spring and Wichita Falls.

Recent scientific knowledge and technological developments pointed out reuse of polluted or low quality waters by taking ion concentrations and pollution loads into the consideration. Previous definitions and ambiguous concepts should be revised and waste waters should be redefined. Relevant social and scientific consciousness should be raised about reuse of polluted waters.

Irrigation water quality is one of the main factors limiting plant growth. Recycled wastewater effluent is an important source of irrigation water in arid and semiarid regions. Wastewater effluents generally contain high concentrations of suspended and dissolved solids, both organic and inorganic. Conventional sewage treatment (seconder or tertiary) can remove inorganic dissolved solids from effluent wastewater. Actually most of the salts added during domestic and industrial usage remain in the irrigation water. This salt in water reach the soil by irrigation. A number of researchers have reported that dissolved salts reduced hydraulic conductivity of soils to which treated wastewater has been applied. The use of wastewater in irrigation depends on a series of factors, such as community size, fresh water resources, socio-economic aspects, soil and plant requirements, relative location to other communities, education of framer and land availability for effluent reuse [18].

The major objectives of wastewater irrigation are that it provides a reliable source of water supply to farmers and has the beneficial aspects of adding valuable plant nutrients and organic matter to soil [7; 8]. With careful planning and management, the positive aspects of wastewater irrigation can be achieved [9]. Treatment of wastewater, as a segment of water management, usually produces a liquid effluent of suitable quality that can be used for irrigation purposes with minimum impacts on human health or the environment [19; 20; 21].

Wastewater may be used directly or after mixing with sewage channeled into natural drainage systems, from where the polluted water is used for farming [22]. Most commonly, a year-round vegetable production is practiced, for which farmers have a good market. In many places in the world, this form of production has great importance as a source of income and livelihood for many people [23].

Oxygen concentration is even more significant when the wastewaters are used for irrigation. As it was well-known that wastewaters have low oxygen concentrations. In other words, both biological and chemical oxygen demands are tried to be met during the entire processes of wastewater treatment. Such treatments may also prevent biofilm formation and dripper clogging especially in surface and sub-surface drip irrigation implementations [24].

In present study, potential use of polluted waters as irrigation water supply was discussed. Utilization conditions, issues to be taken into consideration and sustainable use of such sources were also pointed out.

2. Could the water be considered as a "waste"?

The water, the essential element of the life is a quite valuable item not be considered as "waste". Instead of waste water, such waters should be considered as polluted waters. It a more accurate and realistic approach. In all of the natural waters, some ions more or less exist in dissolved forms. These ions, whether occur naturally or exist as a result of some activities, then are considered as pollutants. The indicative parameter is the purpose of use of water resource. For instance, it is quite misleading to consider the waters used for domestic purposes and for some activities of a livestock facility and polluted then as waste water. The waters discharged from homes and livestock facilities are quite rich in plant nutrients, thus they are quite valuable as not to consider them as waste. Based on dissolved ion concentrations, these discharged waters can either be used as irrigation water directly or be used after a couple simple treatment processes. Only the heavy industry (including radioactive) effluents may create some problems when they were used as irrigation water. The other effluents can reliably be used as irrigation water just after some kind of treatment processes. Therefore, the water considered as waste are not actually the waste. They should be called as polluted waters and a social perception should be creates along this direction. Water resources should be classified in accordance with the purpose of use. Then, different standard and classification systems were developed. Availability of a water resource for a relevant purpose is assessed through relevant standard and classification systems, samples are analyzed and decisions are made accordingly.

2.1. Classification of polluted (waste) waters

The effective management of any wastewater flow requires a reasonably accurate knowledge of its characteristics. This is particularly true for wastewater flows from rural residential dwellings, commercial facilities and other facilities where individual water- using activities create an intermittent flow of wastewater that can vary widely in volume and degree of pollution. Detailed characterization data regarding these flows are necessary not only to facilitate the effective design of wastewater treatment and disposal systems, but also to enable the development and application of water conservation and waste load reduction strategies. For existing developments, characterization of the actual wastewaters to be encountered may often times be accomplished. However, for many existing developments, and for almost any new development, wastewater characteristics must be predicted [25].

Residential Poor (Waste) Water Characteristics: Residential dwellings exist in a variety of forms, including single- and multi- family households, condominium homes, apartment houses and cottages or resort residences. In all cases, occupancy can occur on a seasonal or year- round basis. The wastewater discharged from these dwellings is comprised of a number of individual wastewaters, generated through water-using activities employing a variety of plumbing fixtures and appliances.

Nonresidential Poor (Waste) Water Characteristics: The rural population, as well as the transient population moving through the rural areas, is served by a wide variety of isolated commercial establishments and facilities. For many establishments, the wastewater- generating sources are sufficiently similar to those in a residential dwelling that residential wastewater characteristics can be applied. For other establishments, however, the wastewater characteristics can be considerably different from those of a typical residence.

Industrial Poor (Waste) Water Characteristics: Wastewater discharges from industrial and commercial sources may contain pollutants at levels that could affect the quality of receiving waters or interfere with publicly owned treatment works (POTWs) that receive those discharges. The NPDES permitting program establishes discharge limits and conditions for industrial and commercial sources with specific limitations based on the type of facility/activity generating the discharge.

Agricultural Poor (Waste) Water Characteristics: Agricultural wastewater is produced in the course of agricultural activities. Agriculture is a highly intensified industry in many parts of the world, producing a range of wastewaters requiring a variety of treatment technologies and management practices. Agriculture-induced water pollution is basically divided into two groups as of point-source (animal wastes, treatment, piggery waste, silage liquor, milking parlor, dairy farming wastes, slaughtering waste, vegetable washing water, firewater ect.) and non-point source (drainage water, sediment runoff, nutrient runoff, pesticides ect.) pollution.

There are several standards and classification systems used to assess the availability of a water resource as irrigation water. The FAO classification system and limit values used for basic parameters are provided in Table 1 [26].

Table 1 *Guidelines For Interpretations Of Water Quality For Irrigation*[2]

Potential Irrigation Problem				Units	Degree of Restriction on Use		
					None	Slight to Moderate	Severe
Salinity *(affects crop water availability)*[3]							
	EC_w			dS/m	< 0.7	0.7 – 3.0	> 3.0
	TDS			mg/l	< 450	450 – 2000	> 2000
Infiltration *(affects infiltration rate of water into the soil. Evaluate using EC_w and SAR together)*[4]							
SAR	= 0 – 3	and EC_w	=		> 0.7	0.7 – 0.2	< 0.2
	= 3 – 6		=		> 1.2	1.2 – 0.3	< 0.3
	= 6 – 12		=		> 1.9	1.9 – 0.5	< 0.5
	= 12 – 20		=		> 2.9	2.9 – 1.3	< 1.3
	= 20 – 40		=		> 5.0	5.0 – 2.9	< 2.9
Specific Ion Toxicity *(affects sensitive crops)*							

2 Adapted from University of California Committee of Consultants 1974.

3 ECw means electrical conductivity, a measure of the water salinity, reported in deciSiemens per metre at 25°C (dS/m) or in units millimhos per centimetre (mmho/cm). Both are equiva-lent. TDS means total dissolved solids, reported in milligrams per litre (mg/l).

4 SAR means sodium adsorption ratio. SAR is sometimes reported by the symbol RNa. See Figure1 for the SAR calculation procedure. At a given SAR, infiltration rate increases as watersalinity increases. Evaluate the potential infiltration problem by SAR as modified by ECw.Adapted from Rhoades 1977, and Oster and Schroer 1979.

	Sodium (Na)[4]				
	surface irrigation	SAR	< 3	3 – 9	> 9
	sprinkler irrigation	me/l	< 3	> 3	
	Chloride (Cl)[5]				
	surface irrigation	me/l	< 4	4 – 10	> 10
	sprinkler irrigation	me/l	< 3	> 3	
	Boron (B)[6]	mg/l	< 0.7	0.7 – 3.0	> 3.0
	Trace Elements (following Table 2[7])				
Miscellaneous Effects *(affects susceptible crops)*					
	Nitrogen (NO_3 - N)[8]	mg/l	< 5	5 – 30	> 30
	Bicarbonate (HCO_3)				
	(overhead sprinkling only)	me/l	< 1.5	1.5 – 8.5	> 8.5
	pH		Normal Range 6.5 – 8.4		

In this table, the waters polluted through various utilizations are not considered and mostly the naturally existing waters apart from drinking and domestic waters were considered and classification was made accordingly. EC is the primary parameter used to evaluate the water quality for irrigation. It was followed by TDS and SAR. For specific ion toxicity, then comes the parameters of pH, sodium, chlorine, boron, NO_3–N and bicarbonate. There are several other parameters to be considered for the use of polluted waters as irrigation water. But these parameters were not considered in Table 1. The parameters provided in Table 2 are used for the assessment of polluted waters.

5 For surface irrigation, most tree crops and woody plants are sensitive to sodium and chlor-ide; use the values shown. Most annual crops are not sensitive; use the salinity tolerance tables (Tables 4 and 5). For chloride tolerance of selected fruit crops, see Table 14. With overhead sprinkler irrigation and low humidity (< 30 percent), sodium and chloride may be absorbed through the leaves of sensitive crops. For crop sensitivity to absorption, see Tables 18, 19 and 20.

6 For boron tolerances, see Tables 16 and 17.

7 NO_3 -N means nitrate nitrogen reported in terms of elemental nitrogen (NH_4 -N and Organic-N should be included when wastewater is being tested).

8 Updated values of Ayers and Westgot (1994) by USA-EPA (2004)

Sustainable agricultural production is only possible through taking all these parameters into consideration. Organic matter, nitrogenous, phosphorus and potassium compounds are the most abundant substances in domestic waste waters. All these parameters are common nutrients needed in agricultural production activities. Use of these waste waters to meet plant needs will reduce treatment costs and fertilizer needs. Right at this point, heavy metal loads may be concern. It was indicated in a study [27] that waste water-induced heavy metal pollution did not exerted a threat both in soils and plants.

The limit values recommended for the use of treated waters as irrigation water are provided in Table 2 [28]. The limit values and corresponding explanations are possible with sustainable use of polluted waters through proper operation, irrigation management and methods.

The recommended maximum concentrations for "long term continuous use on all soils" are set conservatively to include sandy soils that have low capacity to leach (and so to sequester or remove) the element in question. These maxima are below the concentrations that produce toxicity when the most sensitive plants are grown in nutrient solutions or sand cultures to which the pollutant has been added. This does not mean that if the suggested limit is exceeded that phyto-toxicity will occur. Most of the elements are readily fixed or tied up in soil and accumulate with time. Repeated applications in excess of suggested levels might induce phyto-toxicity. The criteria for short-term use (up to 20 years) are recommended for fine-textured neutral and alkaline soils with high capacities to remove the different pollutant elements.

Table 2. *Recommended Limits for Constituents in Reclaimed Water for Irrigation*

Constituent	Long Term Use (mg/l)	Short Term Use (mg/l)	Remarks
Aluminum	5.0	20	Can cause nonproductiveness in acid soils, but soils at pH 5.5 to 8.0 will precipitate the ion and eliminate toxicity.
Arsenic	0.10	2.0	Toxicity to plants varies widely, ranging from 12 mg/L for Sudan grass to less than 0.05 mg/L for rice.
Beryllium	0.10	0.5	Toxicity to plants varies widely, ranging from 5 mg/L for kale to 0.5 mg/L for bush beans.
Boron	0.75	2.0	Essential to plant growth, with optimum yields for many obtained at a few- tenths mg/L in nutrient solutions. Toxic to many sensitive plants (e.g., citrus) at 1 mg/L. Usually sufficient quantities in reclaimed water to correct soil deficiencies. Most grasses are relatively tolerant at 2.0 to 10 mg/L.
Cadmium	0.01	0.05	Toxic to beans, beets, and turnips at concentrations as low as 0.1 mg/L in nutrient solution. Conservative limits recommended.
Chromium	0.1	1.0	Not generally recognized as an essential growth element. Conservative limits recommended due to lack of knowledge on toxicity to plants.
Cobalt	0.05	5.0	Toxic to tomato plants at 0.1 mg/L in nutrient solution. Tends to be inactivated by neutral and alkaline soils.
Copper	0.2	5.0	Toxic to a number of plants at 0.1 to 1.0 mg/L in nutrient solution.
Fluoride	1.0	15.0	Inactivated by neutral and alkaline soils.
Iron	5.0	20.0	Not toxic to plants in aerated soils, but can contribute to soil acidification and loss of essential phosphorus and molybdenum.
Lead	5.0	10.0	Can inhibit plant cell growth at very high concentrations.

Lithium	2.5	2.5	Tolerated by most crops at concentrations up to 5 mg/L; mobile in soil. Toxic to citrus at low doses - recommended limit is 0.075 mg/L.
Manganese	0.2	10.0	Toxic to a number of crops at a few-tenths to a few mg/L in acidic soils.
Molybdenum	0.01	0.05	Nontoxic to plants at normal concentrations in soil and water. Can be toxic to livestock if forage is grown in soils with high levels of available molybdenum.
Nickel	0.2	2.0	Toxic to a number of plants at 0.5 to 1.0 mg/L; reduced toxicity at neutral or alkaline pH.
Selenium	0.02	0.02	Toxic to plants at low concentrations and to livestock if forage is grown in soils with low levels of selenium.
Tin, Tungsten, & Titanium	-	-	Effectively excluded by plants; specific tolerance levels unknown
Vanadium	0.1	1.0	Toxic to many plants at relatively low concentrations.
Zinc	2.0	10.0	Toxic to many plants at widely varying concentrations; reduced toxicity at increased pH (6 or above) and in fine-textured or organic soils.
Constituent	**Recommended Limit**		**Remarks**
pH	6.0		Most effects of pH on plant growth are indirect (e.g., pH effects on heavy metals' toxicity described above).
TDS	500 - 2,000 mg/l		Below 500 mg/L, no detrimental effects are usually noticed. Between 500 and 1,000 mg/L, TDS in irrigation water can affect sensitive plants. At 1,000 to 2,000 mg/L, TDS levels can affect many crops and careful management practices should be followed. Above 2,000 mg/L, water can be used regularly only for tolerant plants on permeable soils.
Free Chlorine Residual	<1 mg/l		Concentrations greater than 5 mg/l causes severe damage to most plants. Some sensitive plants may be damaged at levels as low as 0.05 mg/l.

Source: Adapted from [29]

2.2 Effects of polluted waters on soils

Plant root zone salinity is the significant problem in arid and semi-arid regions. Salinity distribution has long been investigated by several researchers throughout the world. Allowable salinity thresholds and the measures to be taken to prevent high salinity levels are the greatest issues to be considered in salinity management. The salts transferred to and accumulated within the plant root zone increase osmotic pressure of the solution. Increased osmotic pressure then makes water uptake of the plants difficult and even hinders water uptake in some cases. Reduced water uptake ultimately slows down plant growth and development. Increasing salinity levels within root zone also alter leaf moisture potentials and leaf areas. Depending of type of crop cultivated, yield losses are also evident under saline conditions [30]. Increasing dissolved salt levels in root zones also hinder plant nutrient uptake from the soils. Such cases can only be balanced through reduced osmatic potential.

Long-term use of low quality irrigation waters ultimately ends up with soil salinization, heavy metal accumulation, nutrient imbalances, inefficient microorganism activities, eutrophication in water resources and nutrient accumulation in soils. It also ends up with indirect environmental problems like release of nitrogenous and sulphurous gases.

Together with increasing pollution levels of irrigation waters, available agricultural techniques are also limited. The salts accumulated within root zones should be removed from there after certain period of time. In other words, in places where saline irrigation waters are used, accumulated salts should be leached out and removed from the fields with winter precipitations. Otherwise, salts should be leached out by using sufficient leaching water throughout the growing season. When these practices are not performed, salinity will ultimately reduce both the yield levels and soil fertility. Saline groundwater can be mixed with surface waters and reused in irrigations. It is a method of groundwater control and management. However for such irrigations, type of plant, salinity level of irrigation water, sensitive periods of the plants, climate parameters, salinity level of groundwater and type of salts in groundwater should all be determined ahead [31; 32].

In places where polluted irrigation waters are used, salt accumulation in soil should definitely be monitored. Throughout the monitoring period, sampling methods, sampling depths, timely analysis of samples, proper sampling methods, proper assessment of analysis results, proper leaching, operation and management strategies should all be taken into consideration. It was pointed out that either treated or untreated effluents were used in irrigations. However, proper operation, management, monitoring and assessment strategies should sufficiently be practices when such effluents are used in irrigations. Traditional soil sampling may be difficult in undulated topographies. In such cases, number of samples should be increased. Then soil sampling become costly and time-consuming. To overcome such problems, technological equipment (EM38) are used. EM38 allow rapid ECa readings in saline soils. In this way, ion distribution maps are created at low-costs.

Irrigation systems, irrigation programs md water management plans should be developed and implemented by expert personnel to mitigate the negative impacts of polluted waters on groundwater quality. The following issues should also be considered to reduce such negative impacts:

i) Besides the water resource, soil types over which these waters are to be used and plant characteristics should be reported and updated.

ii) Realistic water use, soil storage and plant yield projections should be developed.

iii) Plant nutrients of fertilizers or treatment sludge and of soils over which these substances are to be applied should be analyzed and assessed.

iv) Other potential nutrient sources (for instance, peas, beans, trefoil, peanut, alfalfa and etc.) should be identified.

v) Besides erodibility of the soils, surficial aquifers and sub-surface drainage characteristics should be determined.

vi) Precise agricultural techniques may provide great aids in places where polluted waters are used in irrigations.

Soil permeability should be proper when the irrigation waters with low SAR and high EC were used in irrigations. Soils should also have quite low exchange capacity and should not be influenced from chemical composition of the water as much as possible. Leaching water should be applied together with irrigation water. Low SAR values may not create a problem at the beginning, but improper cultural practices may destroy soil ion balance and reduce soil permeability, thus make leaching insufficient. Depending on types of salts in irrigation water, some kind of balance reactions are formed and characteristics of soil-water solution are altered.

It is desired that soils should have water-air balance and an aggregate structure. Such an aggregate structure facilitates water movement and allows a well water-air balance. Divalent and trivalent cations are the greatest factors influencing aggregate stability of the soils. These cations, especially Ca, result in loose aggregation of soil grains. Such aggregates then become stronger with the effect of organic substances. On the other hand, monovalent cations like Na, contrary to divalent and trivalent cations, result in singular soil structure. Organic and clay fractions of the soils are negatively charged, thus they absorb positively charged cations. In case the soils had sufficient Ca ions, soil physical structure is available for plant growth and development. Soil infiltration rate, air and water permeability and porosity are also available for plant development. However, if the Na quantities exceed 10 and 15% of total cations, clay complexes are dispersed and consequently infiltration rates, air and water permeability values decrease. Under low clay contents in plant root region, an exchangeable sodium percentage of 15 is allowed. But, such a value should be lower than 6 in soils with high clay contents. Therefore in saline irrigation waters, EC, SAR, ESP and CEC values should continuously be monitored.

Chlorine (Cl), SO_4, boron and HCO_3 are essentials elements to be existed in soils for both soil chemical characteristics and plant requirements. Chlorine is needed for photosynthesis and leaf turgor creation. SO_4 constitute the primary structure for amino acids, protein and chlorophyll. Boron is required for calcium uptake cell wall formation and cell membrane integrity. Iron compounds are not dissolved in lime soils with high pH values. High pH, lime and clay levels and low organic matter contents limit zinc uptake of the plants [33]. The bicarbonate ions resulted from dissolved lime in soils are the most significant indicator of iron deficiency. Excessive bicarbonate ions in root zone slow down iron mobility and result in iron deficiency. For a sustainable agricultural production, anions and cations should be balanced within the root zone. Boron is the primary trace element needed by the plants. It is required not only for yield, but also for the quality. Boron deficiency has anatomic, physiological and biochemical impacts on plants. Abundance on the other hand toxic impacts on plants and it is quite hard to reduce boron levels of the soils [34].

Excessive quantities of an element may reduce the availability of the other elements in soils. In other words, elements have synergic and antagonistic interactions. For instance, excessive calcium quantities may result in potassium, magnesium and iron deficiencies. Similarly, excessive phosphorus may result in zinc deficiency. Such cases are valid more or less for every ions. Reverse of these cases is also valid. In other words, excessive quantities of an element may increase the availability of other elements. Such an impact is defined as synergic impacts. For instance, high calcium quantities may promote nitrogen uptakes of the plants.

2.3 Effects of polluted waters on plants

For healthy plant growth and development, the nutrients required should be well-balanced in water, soil and air and they should reach to toxic levels. Plant nutrients have long been investigated by researchers. Plants uptake about 90 nutrients from the water, soil and air. Of these elements, 20 are essential ones and the rest promotes plant growth and development, high yields and quality. Each element has a special function and play a special role in plant growth. Therefore, a classification is made based on element quantities. The ones required by the plants the most and existed in plant structures are called macro elements (carbon, hydrogen, oxygen, nitrogen, potassium calcium, phosphorus, magnesium and sulphur). The rest are called micro elements (iron, chlorine, copper, manganese, zinc, molybdenum, boron and nickel).

Salt accumulation in root zone significantly limits plant growth and development. Accumulated salts have physical, chemical and indirect impacts on plants.

Physical impacts; increased osmotic pressure reduce or totally inhibit plant water uptake and nutrition. Chemical impacts; some salts make plant nutrient uptake difficult and distracts plant metabolism. Indirect impacts; salinity and alkalinity alters soil structure and plants are then influenced accordingly [35].

According to [36], two criteria are considered for plant nutrient requirements. The first one; whether or not the plant nutrients constitute a primary portion of plant metabolism or structure. The second one; anomalies in plant growth and development are resulted from nutrient deficiency, while regular growth and development is resulted from existence of nutrients [37].

Plants mostly need 17 nutrients. The first three are hydrogen, oxygen and carbon [38; 39;40]. Since these elements are taken mostly from water and air, they are classified as non-mineral elements. Although they constitute about 955 of plant biomass, they were not considered in plant nutrition since the sufficient sources are always available [41; 40; 39; 37]. Chlorine play a great role in photosynthesis and ATP activation. It is also effective in stomal conductance and cell division [43; 44; 45; 42; 37]. Chlorine also retards nitrification, coverts Mn^{+3} and Mn^{+4} oxides into available Mn^{+2} forms. It retards various diseases in plants [39; 42; 37].

As it was stated earlier, the waters polluted through domestic uses contain significant quantities of nutrients. Such nutrients may exist at quantities toxic to plants in some cases. Abundance of nitrogen prolongs plant vegetative periods, retards flowering and reduce sugar synthesis. Late ripening is observed under excessive nitrogen conditions. High nitrogen levels reduce plant resistance to some diseases [46; 44; 47; 48]. It also retards harvests in various crops [42; 37]. Contrary to nitrogen and phosphorus, excessive potassium levels do not have negative impacts on plants. However, excessive potassium negative influences manganese uptake of the plants [44]. Excessive phosphorus levels have indirect negative impacts on plants. Since phosphate ions are tightly held by soil particles, plants spend greater efforts to take phosphorus. Therefore, excessive phosphorus is not a common case in plants. Excess phosphorus levels result in zinc and iron deficiency. Under excessive phosphorus levels calcium, boron, copper and manganese deficiencies are also observed [46; 49; 37; 47]. Excessive iron levels reduce copper, zinc, magnesium and manganese absorption [44; 37]. High chlorine concentrations in soil solution increase soil osmotic potential. Then, plants are not able to get sufficient water from the soils and chlorine-induced drought is evident [50; 42; 37].

Excessive copper levels may have toxic impacts on plants. It also makes iron uptake difficult and choloris similar to iron deficiency is observed. Excess copper negatively influences availability of molybdenum [44;50; 42; 37]. Excessive manganese levels result in MnO_2 accumulation in soils and brown spots and chlorisis around these spots. Manganese toxicity reduce growth-regulation auxin hormone formation and plant growth accordingly [44; 42; 37]. Excessive zinc levels may result in zinc toxicity. But this is not a common case and only observed in fields around ore quarries. Under high zinc conditions, root and leaf development is significantly slowed down, phosphorus and iron uptake is reduced [44; 42; 37]. High molybdenum levels may have toxic impacts on animals grazing animals. In other words, do not have toxic impacts on plants [50; 39; 37]. Toxic impacts can be seen in plants grown over the soils with high nickel levels. Potassium and calcium fertilization may prevent toxic impacts of nickel. On the other hand, phosphate fertilizers increase toxic impacts of nickel [51; 42; 37].

Chlorine in irrigation waters directly influence plant nutrient uptake. While it promoted nutrient uptake at low concentrations, it may have toxic impacts and destruct nutrient uptake at high concentrations. Plant chlorine concentration should be lower than 400 mg/kg [52; 53]. Plant chlorine requirements are so low that chlorine deficiency is not a common case. Chlorine in rain drops can easily meet chlorine requirement of the plants. Chlorine concentrations of coastal zones may be quite high, well above plant requirements. Beside irrigation waters, fertilizers, plant growth regulators, hormones and pesticides may also contain significant quantities of chlorine.

2.4 Points to be considered while using polluted waters in agricultural irrigations

When the polluted waters are to be used in irrigations, human health should be considered at the first instance. Such waters may exert serious health risks. The microbiological guidelines to be used in cases where treated polluted waters are used are provided in Table 3. These criteria should be taken into consideration before, while and after using such waters. The waters polluted through domestic and agricultural uses contain serious quantities of pathogens. Ion composition of these waters should also be well-assessed. Accumulations in soils and plants should not be allowed. Conscious and controlled use are significant issues to be considered in use of polluted waters as irrigation water. Every individual in contact with such waters should have sufficient knowledge and experience. The points to be considered while using these waters in irrigations are summarized below [56; 57; 18];

- Comprehensive realization of the importance of wastewater use in agriculture is still on the peripheral edges of public awareness, and is not always clear to many policy-makers and donors;

- There is insufficient understanding of the social and economic factors that drive farmers to use wastewater, and thus inadequate consideration of these in policy formulation;

Table 3 *Recommended revised microbiological guidelines for treated wastewater use in agriculture**[a]

Category	Reuse conditions	Exposed group	Irrigation technique	Intestinal nematodes[b] (arithmetic mean no of eggs per litre[c])	Faecal coliforms (geometric mean no per 100 ml[d])	Wastewater treatment expected to achieve required microbiological quality
A	**Unrestricted irrigation** A1 Vegetable and salad crops eaten uncooked, sports fields, public parks[e]	Workers, consumers, public	Any	≤ 0.1 [≤ 1][f]	$\leq 10^3$	Well designed series of waste stabilization ponds (WSP), sequential batch-fed wastewater storage and treatment reservoirs (WSTR) or equivalent treatment (e.g. conventional secondary treatment supplemented by either polishing ponds or filtration and disinfection)

B	**Restricted irrigation** Cereal crops, industrial crops, fodder crops, pasture and trees[g]	B1 Workers (but no children ≤15 years), nearby communities	(a) Spray/ sprinkler	≤ 1	≤ 10^5 [no standard]	Retention in WSP series inc. one maturation pond or in sequential WSTR or equivalent treatment (e.g. conventional secondary treatment supplemented by either polishing ponds or filtration)
		B2 As B1	(b) Flood/ furrow	1	≤ 10^3 [no standard]	As for Category A
		B3 Workers including children 15 years, nearby communities	Any	0.1 [≤ 1]	≤ 10^3 [no standard]	As for Category A
C	Localised irrigation of crops in category B if exposure of workers and the public does not occur	None	Trickle, drip or bubbler	Not applicable	Not applicable	Pretreatment as required by the irrigation technology, but not less than primary sedimentation.

Sources: Adapted from [20; 54; 55]

* Values in brackets are the 1989 guideline values.

[a] In specific cases, local epidemiological, sociocultural and environmental factors should be taken into account and the guidelines modified accordingly.

[b] Ascaris and Trichuris species and hookworms; the guideline is also intended to protect against risks from parasitic protozoa.

[c] During the irrigation season (if the wastewater is treated in WSP or WSTR which have been designed to achieve these egg numbers, then routine effluent quality monitoring is not required).

[d] During the irrigation season (faecal coliform counts should preferably be done weekly, but at least monthly).

[e] A more stringent guideline (≤ 200 faecal coliforms per 100 ml) is appropriate for public lawns, such as hotel lawns, with which the public may come into direct contact.

[f] This guideline can be increased to ≤1 egg per litre if (i) conditions are hot and dry and surface irrigation is not used, or (ii) if wastewater treatment is supplemented with anthelmintic chemotherapy campaigns in areas of wastewater re-use.

[g] In the case of fruit trees, irrigation should cease two weeks before fruit is picked and no fruit should be picked off the ground. Spray/sprinkler irrigation should not be used.

- The protection of public health and the alleviation of poverty are not mutually exclusive outcomes when it comes to wastewater use, however, one may have to be given greater emphasis than the other in different contexts;
- Effective measures do exist to protect health and environmental quality, particularly when these are included in integrated, multi-barrier approaches to wastewater management;
- Rigid wastewater use guidelines tend to become targets rather than norms;

- Effective, lower-cost, decentralized treatment systems exist; conventional, northern treatment technologies tend to be unsustainable, in part because of high capital and recurring costs;
- Many forms of wastewater use are practiced in various contexts for different reasons, and individual socioeconomic contexts contribute to varying levels of acceptability of wastewater use;
- Increasing year-round demand for fresh fruits and vegetables in developed countries, and increasing tourism in a globalize world, make wastewater use an issue for more than just developing countries;
- Sound legal and regulatory frameworks require sustained application and enforcement;
- Insecure land tenure mitigates against farmer investment in safer and more efficient wastewater irrigation technologies;
- The informal nature of wastewater irrigation tends to leave it in institutional no-man's land; and
- A lack of coordination among institutions within and outside of government, and the tendency towards isolated, uni-disciplinary research on wastewater, has inhibited the testing and design of integrated, workable solutions.

Conscious and controlled use are significant issues to be considered in use of polluted waters as irrigation water. Every individual in contact with such waters should have sufficient knowledge and experience. The points to be considered while using these waters in irrigations

It is known that wastewater has the potential to increase yields while saving on fertilizer and irrigation costs. However, under these conditions, it can be possible that is important to choose groves that are well designed without low spots to facilitate maximum drainage. The potential negative effects of wastewater irrigation are considered to be the following: (i) health risks; (ii) contamination of groundwater (iii) Soil pollution (iv) creation of habitats for disease vectors (v) excessive growth of algae and vegetation in canals carrying wastewater (eutrophication) (vi) some problems on pressurized irrigation system.

In general, the main problem that can create significant obstacles in the safe reuse of the treated wastewater in agriculture is the lack of information of all the involved actors, namely [58]:

Governmental authorities: lack of legislation and guidelines on the reuse of treated wastewater

Local authorities and authorities responsible in wastewater treatment: (i) lack of information on innovative cost effective technologies for wastewater treatment, (ii) difficulties in the development of technical specifications for the construction and operation of appropriate wastewater treatment systems (in terms of technology, size, quality of the outflow), (iii) difficulties in the development of specifications for the proper use of the final outflow, (iv) difficulties in finding the appropriate funds for the improvement of the wastewater treatment system

Operators: lack of knowledge for the efficient operation, control and monitoring of the wastewater treatment system

Farmers: lack of information on the health risks related to the use of treated wastewater and the appropriate management procedures

3. Conclusion

When the polluted waters are to be used in irrigation, besides soil and crops, surrounding public health, groundwater resources, property values, ecological impacts and social impacts should be assessed in detail by expert personnel. Each parameters should be assessed with regard to allowable limits, use/implementation type and conditions, monitoring and assessment. Then a decision should be made by considering all these parameters. In case of possible changes, reassessments should be made and new decisions should be made. Otherwise, undesired outcomes are evident and it may be timely and costly to recover the cases.

Heavy metals in polluted waters may exert serious risks on soils and plants. Therefore, heavy metals should be removed from these waters before to reuse them. The heavy metals and trace elements may accumulate in plants and soils and may reach to toxic levels for living organisms. Effects of heavy metal stress on plants vary based on element type and concentration and also type of plant and plant genetics [59]. Thus, plant response and adaptation mechanisms should be determined. Researchers indicated that some plants were endemic to soils rich in heavy metals and were able to tolerate quite high levels of toxic substances [60; 61].

Economic analyses should also be performed definitely while using polluted waters. In this sense, Approach to date and its limitations, A suggested framework for valuing impacts, Public Health, Crops, Soil Resources, Groundwater Resources, Property Values, Ecological Impacts, Social Impacts, Indirect Impacts should be assessed in detail.

According to [27], polluted waters did not create a significant increase in heavy metal pollution both in soils and plants as compared to chemical fertilizers. Also, oxygen concentration is even more significant when the wastewaters are used for irrigation. As it was well-known that waste waters have low oxygen concentrations. In other words, both biological and chemical oxygen demands are tried to be met during the entire processes of waste water treatment. Such treatments may also prevent biofilm formation and dripper clogging especially in surface and sub-surface drip irrigation implementations [24].

Irrigation methods should be selected carefully when polluted waters are to be used in irrigations. Drainage volumes should be reduced and a uniform water distribution should be supplied in soil profile and sufficient leaching should also be practiced. In case of false selection of irrigation method, soil salinity may increase, drainage problems and groundwater pollution may increase. Besides the requirements of irrigation method and systems, water and salt distribution in soil, plant resistance to wet conditions, effects of polluted waters on yield and quality should also be taken into consideration. Also, irrigation schedules (including irrigation water quantity, irrigation intervals, timing, leaching fractions) should be properly arranged.

Malpractices in irrigation and other implementations may result in various problems in long run. Irrigation water quality is a basic component of sustainable agricultural production. Irrigation water pollution directly influences yield and quality, also destructs production environment in long run. Reclamation of destructed environments takes long time and require quite much investments. For instance, salinity-induced production loss of Australia sums about 130 million dollars and such a value is still increasing. Also, annually 100 million dollars are spend for infrastructures like roads and bridges [62]. Salinity is the greatest factor limiting yields in agricultural productions. The annual cost of salinity to the USA agriculture is about 12 billion dollars [63]. Besides increasing production costs, salinity also significant impacts on infrastructure, water resources, social life and stability [64]. The saline waters carried by Catrina storm resulted in about 1 billion dollars lost in Louisiana agriculture [65]. The water pollution-induced lost worldwide is estimated about 11 billion dollars [66; 67; 68]. According to [69], one ppm increase in water salinity create a damage or loss of 230 000 dollars in agricultural, urban and industrial uses.

Soil permeability should be proper when the irrigation waters with low SAR and high EC were used in irrigations. Soils should also have quite low exchange capacity and should not be influenced from chemical composition of the water as much as possible. Leaching water should be applied together with irrigation water. Low SAR values may not create a problem at the beginning, but improper cultural practices may destroy soil ion balance and reduce soil permeability, thus make leaching insufficient. Depending on types of salts in irrigation water, some kind of balance reactions are formed and characteristics of soil-water solution are altered.

It is desired that soils should have water-air balance and an aggregate structure. Such an aggregate structure facilitates water movement and allows a well water-air balance. Divalent and trivalent cations are the greatest factors influencing aggregate stability of the soils. These cations, especially Ca, result in loose aggregation of soil grains. Such aggregates then become stronger with the effect of organic substances. On the other hand, monovalent cations like Na, contrary to divalent and trivalent cations, result in singular soil structure.

Organic and clay fractions of the soils are negatively charged, thus they absorb positively charged cations. In case the soils had sufficient Ca ions, soil physical structure is available for plant growth and development. Soil infiltration rate, air and water permeability and porosity are also available for plant development. However, if the Na quantities exceed 10 and 15% of total cations, clay complexes are dispersed and consequently infiltration rates, air and water permeability values decrease.

Under low clay contents in plant root region, an exchangeable sodium percentage of 15 is allowed. But, such a value should be lower than 6 in soils with high clay contents. Therefore in saline irrigation waters, EC, SAR, ESP and CEC values should continuously be monitored [34].

Whether treated waters or raw polluted waters are used as irrigation water, synergic and antagonistic effects should be considered for both soils and plants. Seepage to groundwater should also be taken into consideration when such waters are used in irrigations. Soils should be analyzed regularly and a well-operating drainage system should be established.

Long-term use of low quality irrigation waters ultimately ends up with soil salinization, heavy metal accumulation, nutrient imbalances, inefficient microorganism activities, eutrophication in water resources and nutrient accumulation in soils. It also ends up with indirect environmental problems like release of nitrogenous and sulphurous gases. It also ends up with indirect environmental problems like release of nitrogenous and sulphurous gases. Elimination of such problems requires serious economic investments. Therefore, previously mentioned issues should be taken into consideration when such waters are used for irrigation.

Acknowledgments

The author is grateful to Assoc. Prof. Dr. Zeki Gokalp (a Certified English Translator and an expert in Biosystems Engineering) for his critical reading and through syntactic corrections of the manuscript.

REFERENCES

[1] Scott CA, Faruquie NI, Reschid-Sally L. Wastewater use in irrigated agriculture: management challenges in developing countries. In: Scott CA, Faruquie NI, Reschid-Sally L (ed) Waste water use in irrigated agriculture: confronting the livelihood and environmental realities. CABI Publishing, 2004 p. 1-10. DOI: 10.1079/9780851998237. 0001

[2] Lund E. Health Problems Associated with the Reuse of Sewerage, WHO Seminar on Health Aspects of Treated Sewage Reuse, Regional Office for Europe. World Health Organization, 1980. ISBN 92 890 120S 0.

[3] Pair CH, Hinz WH, Frost KR, Sneed RE, Schiltz TJ. Irrigation, 5th edition. The Irrigation Association. Silver Spring. 1980. Maryland. USA

[4] Lewitt J. Responses of Plants to Environmental Stresses, Vol.II, (2nd ed.) Academic Press, New York. 1980.

[5] Ashraf M, Foolad MR. 2007. Improving plant abiotic-stress resistance by exogenous application of osmoprotectants glycine betaine and proline. Environ. Exp. Bot., 2007., 59: 206-216.

[6] Kanber R, Ünlü M. Tarımda Su ve Toprak Tuzluluğu. Çukurova Üniversitesi Ziraat Fakültesi Genel Yayın No: 281. Adana. 2010. 307p.

[7] Liu WH, Zhao JZ, Ouyang ZY, Solderland L, Liu GH. Impacts of sewage irrigation on heavy metal distribution and contamination in Beijing, China. Environmental International, 2005;32:805–812.

[8] Horswell J, Speir TW, van Schaik AP. Bioindicators to assess impacts of heavy metals in the landapplied sewage sludge. Soil Biology & Biochemistry, 2003;35:1501–1505.

[9] WHO (World Health Organization). Guidelines for the safe use of wastewater, excreta and greywater: Wastewater use in agriculture (Volume II). Retrieved from persistent

URL: http://www.who.int/water_ sanitation_ health/ wastewater/gsuweg2/en/index.html. 2006.

[10] Angelakis AN, Snyder SA. Wastewater Treatment and Reuse: Past, Present, and Future. Water 2015;7:4887-4895.

[11] Tzanakakis VE, Paranychianakis NV, Angelakis AN. Soil as a wastewater treatment system: Historical development. Water Sci. Technol.: Water Supply 2007;7:67–76.

[12] Tzanakakis VE, Koo-Oshima S, Haddad M, Apostolidis N, Angelakis AN. The history of land application and hydroponic systems for wastewater treatment and reuse. In Evolution of Sanitation and Wastewater Management through the Centuries. Angelakis, A.N., Rose, J.B., Eds.; IWA Publishing: London, UK, 2014; Chapter 24, 2014. p. 459–482.

[13] Kamizoulis G, Bahri A, Brissaud F, Angelakis AN. Wastewater Recycling and Reuse Practices in Mediterranean Region: Recommended Guidelines 2002. Available online: http://www.aangelakis.gr/files/pubrep/recycling_med.pdf. 2015.

[14] Reed SC, Crites RW, Middlebrooks EJ. Natural Systems for Waste Management and Treatment, 2nd ed.; McGraw Hill Co.: New York, NY, USA, 1995. p. 433.

[15] Mudgal S, van Long L, Saidi N, Haines R, McNeil D, Jeffrey P, Smith H, Knox J. Optimization Water Reuse in EU: Final Report; BIO by Deloitte: Brussels, Belgium 2015. p. 199.

[16] Angelakis AN, Gikas P. Water Reuse: Overview of current practices and trends in the World with emphasis in EU. Water Utility J. 2014; 6:67–78.

[17] PUB (Singapore's National Water Agency). NEWater History, Singapore, 2015. Available online: http://www.pub.gov.sg/water/newater/Pages/default.aspx (accessed on 14 June 2015).

[18] Tas I. Yildirim YE. Ozkay F. The Potentiality of Wastewater Use for Irrigation in Turkey. Plants, Pollutants and

Remediation. Eds. Münir Öztürk, Muhammad Ashraf, Ahmet Aksoy, M.S.A. Ahmad, Khalid Rehman Hakeem. Springer Science+Business Media Dordrecht. Springer Dordrecht Heidelberg New York London. 2015. p. 137-155

[19] Hussain I, Raschid L, Hanjra MA, Marikar F, Van der Hoek W. A framework for analyzing socioeconomic, health and environmental impacts of wastewater use in agriculture in developing countries. Working Paper 26. Colombo: International Water Management Institute (IWMI). 2001.

[20] Blumenthal U, Peasey A, Ruiz-Palacios G, Mara DD. Guidelines for wastewater reuse in agriculture and aquaculture: recommended revisions based on new research evidence. Task No. 68, Part 1. Retrieved from persistent URL: http://www.lboro.ac.uk/well/resources/well-studies/full-reports-pdf. 2000.

[21] Qishlaqi A, Moore F, Forghani G. Impact of untreated wastewater irrigation on soils and crops in Shiraz suburban area, SW Iran. Environ Monit Assess 2008;141:257–273

[22] Qadir M, Wichlns D, Raschid-Sally L, McCornick PG, Dreschsel P, Bahri A, Minhas PS. The Challenges of Wastewater irrigation in developing countries. Agricultural Water Management 2010;97: 561-568.

[23] Huibers FP, Raschid-Sally L. Design in Domestic Wastewater Irrigation. Irrigation and Drainage 2005;54:113-118.

[24] Tas I, Yıldırım YE, Özkay F, Yeter T, Görgüşen C. Morphological Characteristics of Tomato Irrigated With Wastewaters With Different Oxygen Concentrations. Current Trends in Natural Sciences 2016; Vol. 5, Issue 9, p. 187-193.

[25] EPA (Environmental Protection Agency). Design Manual. Onsite Wastewater Treatment And Disposal Systems. U.S. Environmental Protection Agency. Ofifice of Water Program Operations Office of Research and

Development Municipal Environmental Research Laboratory. EPA 625/1-80-012. 1980.

[26] Ayers RS, Westcot DW. Water Quality for Agriculture. FAO Irrig. And Drain. Paper No.29. Rome, 1994.

[27] Hussain GA, Al-Saati J. Wastewater quality and its reuse in agriculture in Saudi Arabia. Desalination, 1999; 123 (2-3) p. 241-251

[28] EPA (Environmental Protection Agency). Guidelines for Water Reuse. U.S. Environmental Protection Agency. EPA/625/R-04/108 September 2004.

[29] Rowe DR, Abdel-Magid IM. Handbook of Wastewater Reclamation and Reuse. CRC Press. Boca Raton, FL. 1995.

[30] Maas EV, Hoffman GJ. Crop salt tolerance - current assessment. J. Irrig. and Drainage Div., ASCE 1977;103 (IR2): 115-134.

[31] Yurtseven E. Ülkemiz Nehir Su Kaynaklarının Kalite Değerlendirmesi. VI. Ulusal Kültürteknik Kongresi Bildirileri, 5-8 Haziran 1997, Kirazlıyayla, Bursa, p. 453-459

[32] Kara T, Apan M. Tuzlu Taban Suyunun Sulamada Tekrar Kullanımı İçin Bir Hesaplama Yöntemi, OMÜ Ziraat Fakültesi Dergisi, 2000; 15(3): 62-67.

[33] Marschner H. Mineral Nutrition of Higher Plants. Secon Edition. Academic Press Limited, 24-28. Oval Road, Londan, NW1 7DX. 1995.

[34] Tas I, Coskun Y, Yeter T, Yıldırım YE, Gorgusen C, Ozkay F. Düşük SAR'a ve Yüksek Elektriksel İletkenliğe Sahip Sulama Sularının Toprak İyon İçeriğine Etkisi. V. Uluslararası Katılımlı Toprak ve Su Kaynakları Kongresi. 12-15 Eylül 2017, Kırklareli.

[35] Ekmekçi E, Apan M, Kara T. Tuzluluğun bitki gelişimine etkisi. OMÜ Zir. Fak. Dergisi, 2005; 20(3):118-125.

[36] Epstein E, Bloom A. Mineral Nutrition of Plants: Principles and Perspectives. 2nd Edition, Sunderland, Mass: Sinauer Associates, USA. 2005.

[37] Bolat I. Kara O. Bitki Besin Elementleri: Kaynakları, İşlevleri, Eksik ve Fazlalıkları. Bartın Orman Fakültesi Dergisi, 2017;19(1): 218-228.

[38] White RE. Principles and Practice of Soil Science: The Soil as a Natural Resource. 4th Edition, Wiley-Blackwell Scientific Publication, London, United Kingdom. 2006.

[39] Gardiner DT, Miller RW. Soils in Our Environment. 11th Edition, Pearson/Prentice Hall, Upper Saddle Hill, Ne Jersey, USA. 2008.

[40] Fageria NK. The Use of Nutrients in Crop Plants. CRC Pres, Boca Raton, Florida, New York. 2009.

[41] Jones C, Jacobsen J. Plant Nutrition and Soil Fertility. Nutrient management module 2. Montana State University Extension Service. Publication, 4449–2. 2001.

[42] Kacar B, Katkat V. Bitki Besleme. 5. Baskı, Nobel Yayın Dağıtım Tic. Ltd. Şti, Kızılay-Ankara. 2010.

[43] Plaster EJ. Soil Science and Management. 2nd Edition, Delmar Publishers Inc., Albany, New York, USA. 1992.

[44] Bosgelmez A, Bosgelmez I, Savasci S, Pasli N. Ekoloji – II (Toprak). Başkent Klişe Matbaacılık, Kızılay-Ankara. 2001.

[45] Mccauley A, Jones C, Jacobsen J. Nutrient Management. Nutrient management module 9 Montana State University Extension Service. Publication, 2009; 4449(9):1-16.

[46] Aktas M, Ates A. Bitkilerde Beslenme Bozuklukları Nedenleri Tanınmaları. Nurol Matbaacılık A.Ş. Ostim-Ankara. 1998. p. 212.

[47] Tas I, Coskun Y, Yeter T, Yildirim YE, Gorgusen C, Ozkay F. Yüksek Klor İçeren Sulama Sularının Buğday Türlerinde Bitki İyon İçeriğine Etkisi. V. Uluslararası

Katılımlı Toprak ve Su Kaynakları Kongresi. 12-15 Eylül 2017, Kırklareli.

[48] Fageria NK, Baligar VC, Jones CA. Growth and Mineral Nutrition of Field Crops. 3rd Edition, CRC Pres, Boca Raton, FL, USA. 2010. p.586. ISBN 9781439816950

[49] Aktas M., Ates A. Bitkilerde Beslenme Bozuklukları Nedenleri Tanınmaları. 2. BasımNurol Matbaacılık A.Ş. Ostim-Ankara. 2005. p. 248.

[50] Guzel N, Gulut KY, Buyuk G. Toprak Verimliliği ve Gubreler. Ç.Ü. Ziraat Fakültesi Genel Yayın No: 246, Ders Kitapları Yayın No: A-80, Adana. 2004.

[51] Kantarcı MD. Toprak Ilmi. Istanbul Universitesi Orman Fakultesi Yayınları İ.Ü. Yayın No: 4261 O.F.Yayın No: 462. 2000. p.296.

[52] Chen W, He Zl, Yang Xe, Mıshra S, Stoffella Pj. Chlorıne nutrition of higher plants: progress and perspectives. Journal of Plant Nutrition, 2010; 33:943-952.

[53] Wang DQ, Guo PC, Dong XY. Study on the toxicity of chlorine to the crops. Chinese Journal of Soil Science 1990;21:258-261.

[54] WHO (World Health Organization). Health guidelines for the use of wastewater in agriculture and aquaculture. Technical Report No. 778. WHO, Geneva. 1989.

[55] Carr RM, Blumenthal UJ, Mara DD. Health Guidelines for the Use of Wastewater in Agriculture: Developing Realistic Guidelines. Waste Water Use In: Scott CA, Faruquie NI, Reschid-Sally L (ed) Waste water use in irrigated agriculture: confronting the livelihood and environmental realities. CABI Publishing, 2004 p. 41-58. DOI: 10.1079/9780851998237. 0001

[56] Faruquie NI, Scott CA, Reschid-Sally L (2004) Confronting the realities of wastewater use in agriculture: lesson learned and recommendations. In: Scott CA, Faruquie NI, Reschid-Sally L (eds) Waste water use in irrigated agriculture: confronting the livelihood and

environmental realities. CABI Publishing. 2004 p. 173-186. DOI: 10.1079/9780851998237. 0001

[57] Gokalp Z, Tas I, Ozkay F, Akgul S. Wastewater use in irrigation - Ankara case study. African Journal of Agricultural Research 2011; 6(7), pp. 1807-1812.

[58] Fatta D, Alaton IA, Gokcay C, Rusan MM, Assobhei O, Mountadar M, Papadopoulos A. Wastewater reuse: problems and challenges in cyprus, Turkey, Jordan and Morocco. Eur Water 2005;11(12):63–69

[59] Haktanır K, Arcak S. Çevre Kirliliği. Ankara Üniversitesi Yayın No: 1503, Ders Kitabı: 457, Ankara. 1998.p.323.

[60] Raskin I, Ensley BD. Phytoremediation of Toxic Metals: Using Plants to Clean Up tthe Enviroment. John Wiley and Sons, NewYork, 2000. p.304.

[61] Dahmani-Muller H, Oort F, Gelie B, Blabene M. Strategies of heavy metal uptake by three plants species growing near a metal smelter. Environ. Pollut. 2000;109: 231-238.

[62] Anonim. Web Sayfası. Adres: https://www.qld.gov.au/environment/land/soil/ salinity/impacts Erişim Tarihi: 20.09.2016.

[63] Ghassemi F, Jakeman AJ, Nix HA. Salinization of Land and Water Resources. Univ. of New South Wales Press, Ltd., Canberra, Australia. 1995. p. 526

[64] Pitman MG, Läuchli A. Global Impact of Salinity And Agricultural Ecosystems. A. Läuchli and U. Lüttge (eds.), Salinity: Environment - Plants - Molecules, 3–20. 2002 Kluwer Academic Publishers. Printed in the Netherlands. 2002. p.3-20.

[65] Williams WJ. Identifying the Economic Effects of Salt Water Intrusion after Hurricane Katrina. Journal of Sustainable Development 2010; 3(1):29-37.

[66] Palaniappan M, Gleick PH, Allen L, Cohen MJ, Christian-Smith J, Smith C. Clearing the Waters. A focus on water quality solutions. Ed. Nancy Ross. United Nations

Environment Programme Pacific Institute. 654 13th Street, Preservation Park, Oakland, CA 94612. 2010. p.88.

[67] Revenga C, Brunner J, Henninger N, Kassem K, Payne R. Pilot Analysis of Global Ecosystems: Freshwater Systems. World Resources Institute: Washington D.C. Retrieved January 28, 2010 from at http://www.wri.org/wr2000. 2000. p. 65.

[68] Postel S. Pillar of Sand: Can the Irrigation Miracle Last? New York: W.W. Norton & Company. 1999. p.320.

[69] Koteen J, Alexander SJ, Loomis JB. Evaluating Benefits and Costs of Changes in Water Quality. United States Department of Agriculture Forest Service. Pacific Northwest Research Station, General Technical Report PNW-GTR-548 July 2002. p. 33.

Chapter 10

OPTIMIZATION STUDY FOR IMPROVED PERFORMANCE OF ORGANIC COATINGS BY NOVEL EXTERNAL ADDITIVES

Nil ACARALI[1]

1 Yıldız Technical University, Davutpasa Campus, Faculty of Chemical-Metallurgical, Department of Chemical Engineering, Esenler/Istanbul

1. INTRODUCTION

The problems of ecological and environmental pollution are increasing by developing of industrial applications in the world. Some approaches about environment are being developed with solutions to these problems. Nowadays, energy resources, economics etc. are related between each other. The usage of low-cost, sustainable resources is one of the approaches that increase productivity. Therefore, high quality materials and low-cost budget are required in the construction sector (Azemati et al., 2013). With the developing market, the variety of products produced and the choice of consumers increases. Accordingly, consumer products are preferred depending on the need, quality and cost. Consumer preferences are important in every sector as well as in coatings sector. In addition to its decorative appearance, coatings used in various sectors for protection purposes is a material that has been going on for centuries and takes place in human life. The selection of the parameters in this sector are the long life products, the durability of the products and the cost. In addition, it is requested not to harm human health and not to disturb the different surface on which it is applied (Altun, 2017). Particular attention is paid to any element that may adversely affect human health in construction coatings without separating them as interior or exterior. Today, in coatings sector, these factors are taken into consideration and production is made depending on the climatic conditions. Minerals and natural substances are encouraged to use these additives to ensure these properties. On the other hand, general factors such as ease of access, economy, and the least possible harm to human health are effective in additives. With the mentioned additives, physical and chemical properties of coatings are changed and improved (Mahmoodi et al. 2018; Mukherjee et al. 2019; Taheri et al. 2017; Uzoma et al. 2019). For instance, as thermal insulation is provided with improved coatings, it provides energy saving and long-lasting economic recovery (Panyakaew and Fotios, 2011).

The importance of optimization has increased for alternative solutions due to the problems with the development of technology. As the problems increase, it becomes more difficult to decide or find solutions. It is possible to define optimization as the best evaluation of conditions for any system and situation. In other words, the efficient use of resources is to keep the system at an optimum level. The main purpose in optimization is to increase productivity, reduce costs and the use of excess raw materials. In mathematical applications, it is termed as maximizing-minimizing to provide the optimum point in problems. There are basically two components in optimization, modeling and analysis. Modeling is the mathematical expression of problems. Analysis is the most appropriate solution method to the model applied. In research, scientists have directed the priority to modeling in general. The optimization models are used generally in economics, production systems and problems have been realized, but research is developed with theoretical knowledge. The optimization technology provides to solve problems and facilitates the right decision in sector (Winston, 2003). This technology increases economically and produces alternative process methods for the manufacturer. Modeling in the process can be defined as a small specification in engineering and basic sciences, and the results can be evaluated as linearly and nonlinearly (Hillier and Lieberman, 2005). In the past, Box and Wilson avoided mathematical modeling and improved Response Surface Method as a method (Gacuka and Singh, 1984). This method was used to obtain the optimum process parameters. A research had been made in different years and it was concluded that this method can be used in different applications (Myers et al., 1989).

In response surface method, a model for regression is formed by using regression coefficient and different level/factors. It is possible to create different levels for different levels. Two-level models are called a 2k factorial layout. In this model, the main effects and the first order equation are examined and expressed as in the equation (Mead and Pike, 1975). Three-factor (3k) levels are expressed as Central Composite and Box-Behnken levels. In the methods, the optimum point, variables, equation of the required model are evaluated together (Walker and Parkhust, 1984).

In this study, in addition to decorative appearance, it was aimed to develop physical and chemical properties by adding various components to the coating which has protective effect. High fiber material is generally used for the production of antioxidants in some areas (medicine, food industry). Organic materials wastes such as calcium source, high fiber material, increasing the effectiveness of minerals such as nanotubular clay and chitosan were added to coatings as additives. Instrumental devices were used to determine the content analysis of the coatings, the grain formation and the homogenization of the coatings. The nanotubular clay had been selected for coating and had been considered to have flame retardant properties due to its constituents. Chitosan has been used as a biopolymer in various fields and can be preferred as corrosion inhibitor in coating industry. The additives had a certain interaction with chitosan.

2. EXPERIMENTAL

Grinders and sieves were used for pretreatment. In order to bring the high fiber material into small pieces, it was made into small pieces in grinding device and then the current size was reduced as much as possible. Then, 355 µm particles were passed through the sieve and the quality part was obtained. It was then passed through 150 µm and 90 µm sieves to bring the grain size to the desired amount of coating. The calcium source material was broken into small pieces (Figure 1).

The Box-Behnken method of the Design Expert optimization program was used for the preparation of the coatings. In this method, 4 parameters consist of 29 sets of experiments were determined. The specified additives were selected in the range of 0-6% by weight (Table 1).

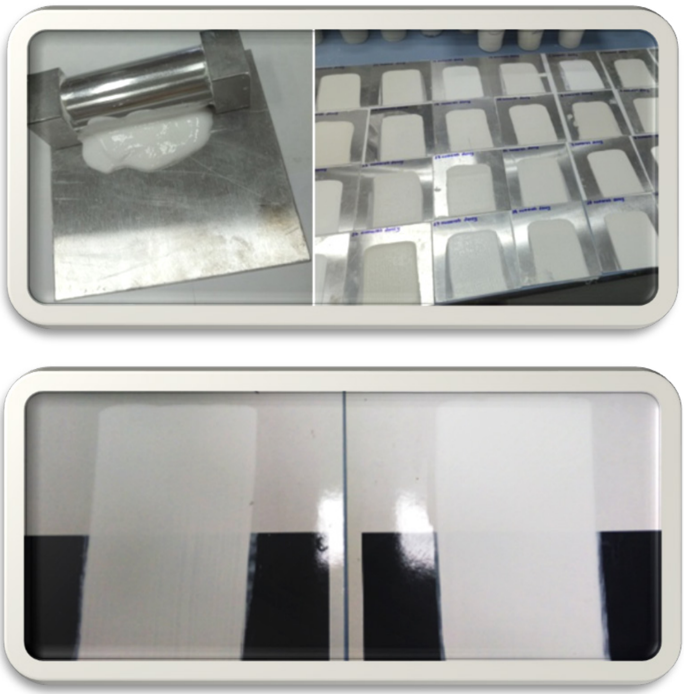

Figure 1. *Applications of organic coatings*

Table 1. *Design Expert Method*

No	Factor-1	Factor-2	Factor-3	Factor-4
1	-1,00	-1,00	0,00	0,00
2	1,00	0,00	0,00	-1,00
3	-1,00	0,00	1,00	0,00
4	1,00	0,00	0,00	1,00
5	1,00	1,00	0,00	0,00
6	1,00	0,00	1,00	0,00
7	0,00	-1,00	0,00	-1,00
8	0,00	1,00	0,00	1,00
9	0,00	0,00	1,00	-1,00
10	0,00	0,00	0,00	0,00
11	1,00	-1,00	0,00	0,00
12	0,00	-1,00	1,00	0,00
13	0,00	0,00	-1,00	-1,00
14	0,00	0,00	0,00	0,00
15	-1,00	1,00	0,00	0,00
16	0,00	1,00	1,00	0,00
17	0,00	1,00	-1,00	0,00
18	0,00	0,00	0,00	0,00
19	0,00	-1,00	-1,00	0,00
20	0,00	-1,00	0,00	1,00
21	-1,00	0,00	-1,00	0,00
22	0,00	0,00	1,00	1,00
23	0,00	0,00	0,00	0,00
24	0,00	0,00	0,00	0,00
25	-1,00	0,00	0,00	-1,00
26	1,00	0,00	-1,00	0,00
27	-1,00	0,00	0,00	1,00
28	0,00	1,00	0,00	-1,00
29	0,00	0,00	-1,00	1,00

Prepared coatings were applied to aluminum plates with applicator and kept under laboratory conditions for

24 hours and subjected to various tests. The applicator was 150 µm and the plates were aluminum.

Thermogravimetric and Differential Thermal Analysis (TG-DTA) was used to specify the heat resistance of the materials to be tested, the temperature at which the combustion process taken place, the reaction rate, mass loss and energy transitions. With the analysis it was understood whether the additives had an effect on the flame retardancy of the coating. Scanning Electron Microscope (SEM) was used to determine the morphological structure of substances, particle size and composition of the substance.

3. RESULTS AND DISCUSSION

3.1. Results of Design Expert Method

The viscosity values measured were between 2400 and 4600 mPa.s values. A linear model had been proposed to describe the effects of independent variables with high fiber material, nanotubular clay, chitosan and calcium source material on viscosity. The model had the smallest p value, R^2 with the largest expected value and the sum of the smallest residual error squares. The p value of the model was calculated as <0.0001 and it was determined that at least one of the independent variables had a statistically significant effect on the viscosity of the coatings ($p < 0.05$).

It was seen that the amount of A (high fiber material), C (chitosan) and D (material of calcium source) of these parameters were significant on viscosity results ($p < 0.05$), but nanotubular clay amount was not significant on viscosity results ($p > 0.05$). p value of 0.0001 in the lack of fit test indicated that the lack of fit was significant ($p < 0.05$). R^2 value of the model was found to be 90.06% of the variability in the experimental data that this model could be explained. The corrected R^2 value was found to be 0.8840, indicating a high concordance between the experimental values. The expected R^2 value of 0.8464 indicated that it could explain 84.64% of the variability in the estimation of these observations. Since the difference between expected and corrected R^2 was small, they showed an acceptable degree of compatibility. Adequate precision value which was desired to be greater than 4 was calculated as 16,894 and the variation coefficient which should be below 10% was calculated as 5.70%. This proposed model was found sufficient to predict new observations.

When the coefficients of the variables in the regression model for the viscosity values of the coatings and the response surface graphs were examined, viscosity increased with the increase of A (high fiber material), C (chitosan) and D (material of calcium source) amounts due to their positive effects. However, it was concluded that the increase in B (nanotubular clay) amount did not cause any change in viscosity. On the other hand, although there was no change in the interactions containing B (nanotubular clay), the interaction increased as the other additives increase (Figure 2).

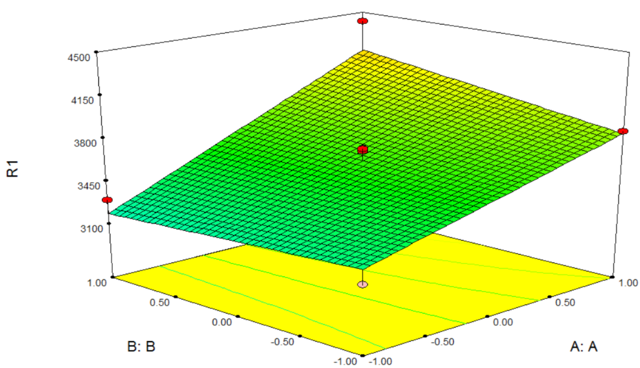

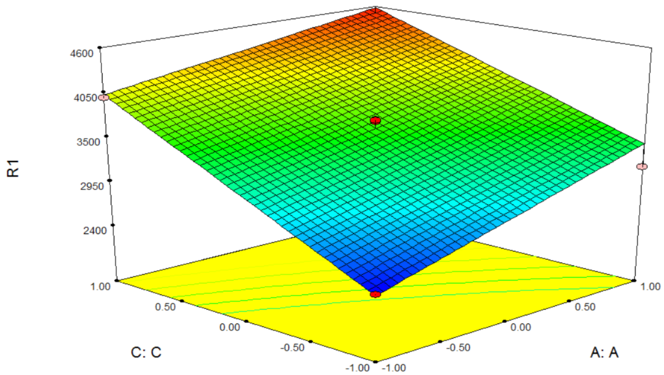
4600
4050
3500
2950
2400
R1
1.00
0.50
0.00
-0.50
-1.00
C: C
-1.00
-0.50
0.00
0.50
1.00
A: A

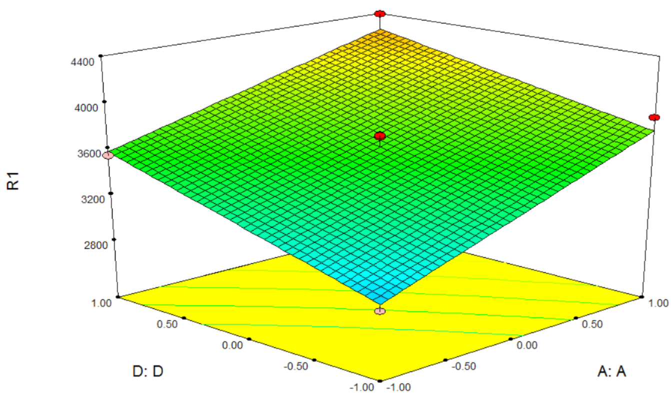
4400
4000
3600
3200
2800
R1
1.00
0.50
0.00
-0.50
-1.00
D: D
-1.00
-0.50
0.00
0.50
1.00
A: A

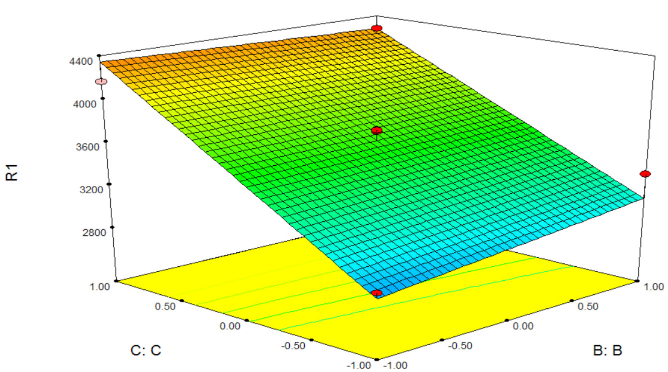
4400
4000
3600
3200
2800
R1
1.00
0.50
0.00
-0.50
-1.00
C: C
-1.00
-0.50
0.00
0.50
1.00
B: B

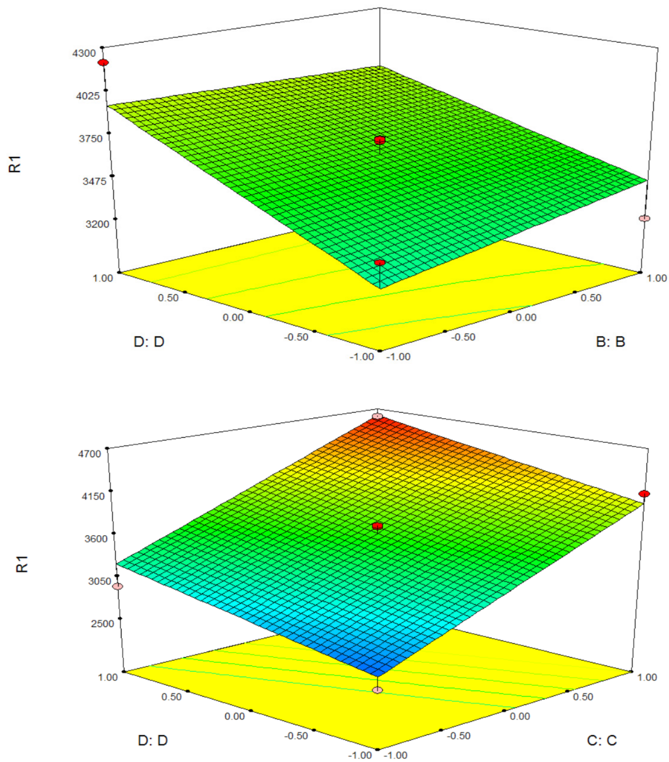

Figure 2. *3D response surface graphs for viscosity*

3.2. Results of TG-DTA

As a result of the analysis, the results of the experiment 22 and the reference coating were compared. In the temperature range of 250-560°C, 16% of the material was lost. This was caused by hydrosilation. In the temperature range of 560-740°C, 25.76% perceptible material loss was observed. A total loss of 45.75% was observed. An endothermic curve occurred in the temperature range of 680-740°C. The decomposition temperature was 743°C. In the reference coating, a significant material loss of 32.3% occurred in the range of 300-500°C An endothermic curve was formed at 400°C. The decomposition temperature of the reference coating was 430°C. It was thought that the high amount of organic substances could decrease the decomposition temperature of additive (Kadi et al., 2012). The decomposition temperature of chitosan was found to be 550°C (Anitha et al., 2011). The decomposition temperature of the high fiber material was found to be 458°C (Lopes et al., 2016). Based on the samples, it had been found that organic substances affected nanotubular clay. It was concluded that the decomposition temperature increased when the reference coating was compared with the experiment 22 (Figure 3, Figure 4).

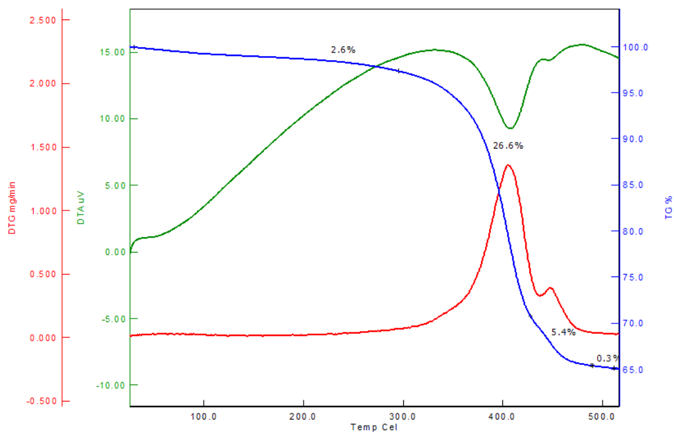

Figure 3. *TG-DTA of reference coating*

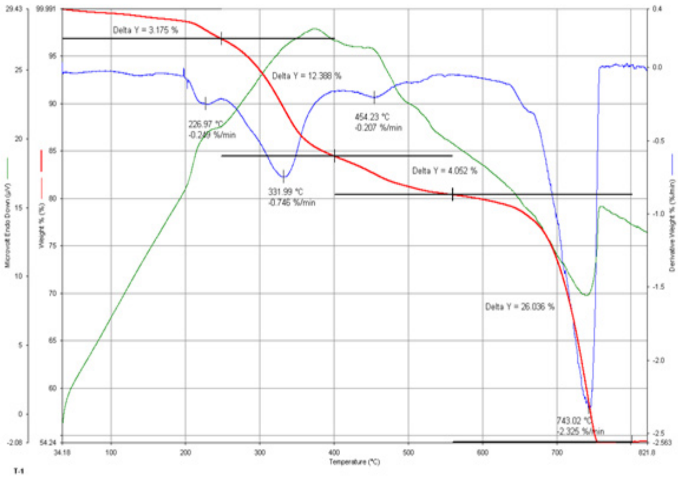

Figure 4. *TG-DTA of experiment 22*

3.3. Results of SEM analysis

For SEM analysis, the coatings were removed from the surface in powder form. As a result of 10000 amplification analysis (Figure 5), it was observed that the substances added to the content of the experiment 22 were distributed homogeneously regularly. Material of calcium source, nanotubular clay, high fiber material and chitosan provided the coating evenly granular structure which was meaningful in itself. The particle size of this granular structure varied between 0.066-0.866µm. In fact, it was seen that all substances provided homogeneity when used in certain proportions. The lack of calcium source in the coating affected the interaction of a certain substance and the specific substance did not interact with others and caused the layer appearance.

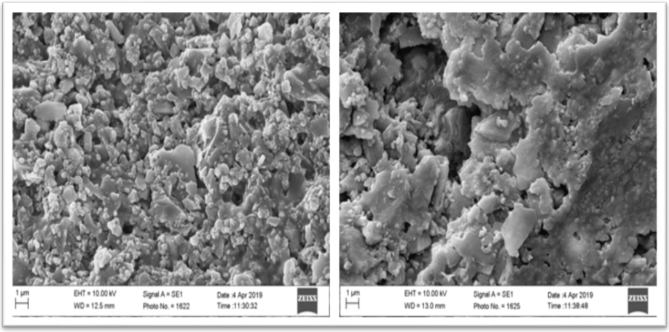

Figure 5. *SEM analysis of experiment 22 (x10000)*

Figure 6 shows the experiment 22 with 20000 magnification. As a result of the magnifications, it was seen that a layered image was formed and this was caused by the absence of calcium source. The granular structure varied between 0.2-0.93 µm for experiment 22. Since chitosan interacted with the calcium source, chitosan was exposed in the coating and disrupted the homogeneous appearance.

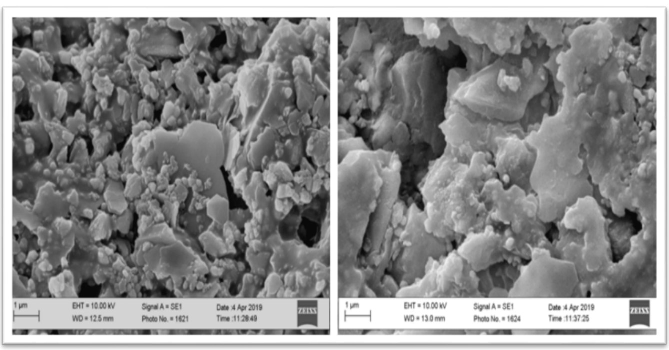

Figure 6. *SEM analysis of experiment 22 (x20000)*

4. CONCLUSION

As a result, the effects of the parameters on the coatings were measured by tests and analyzes. Viscosity was determined for all samples and optimum content was selected by Design Expert optimization program. Then, TG-DTA analysis with SEM was applied to optimum sample. As a result of the studies, performance of coating properties for various surfaces were improved by using novel external additives. In the light of this study, organic coatings on surfaces for future activities and a feasibility study could be carried out in Turkey for increasing the production of coating materials. In future studies, it is recommended that the parameters for organic coatings can be varied within the scope of the development of water/solvent-based coatings applied to surfaces.

REFERENCES

Altun, O. (2017). *Paint Marketing and Paint Industry Employees Preference Reasons for Paint*. Master Thesis. Istanbul Medeniyet University. Social Sciences Institute. Department of Business Administration, Istanbul.

Anitha, A., Deepa, N., Chennazhi, K.P., Nair, S.V., Tamura, H., Jayakumar, R. (2011). Development of Mucoadhesive Thiolated Chitosan Nanoparticles for Biomedical Applications. *Carbohydrate Polymers*, 66-73.

Azemati, A.A., Hadavand, B.S., Hosseini, H., Tajarrod, A.S. (2013). Thermal Modeling of Mineral Insulator in Coatings for Energy Saving. *Energy and Buildings*, 56:109-114.

Gacuka, M.G., Singh, J. (1984). Response Surface Designs and Analysis. *Statistical Methods in Food and Consumer Resarch*, 214-275.

Hillier, F.S., Lieberman, G.J. (2005). *Introduction to Operations Research*, 8. press, McGraw Hill, New York, USA.

Kadi, S., Lellou, S., Marouf-Khelifa, K., Schott, J., Gener-Batonneau, I., Khelifa, A. (2012). Preparation, Characterisation and Application of Thermally Treated Algerian Halloysite. *Microporous and Mesoporous Materials*, 47-54.

Lopes, B.D.M., Demiate, I.M., Ito, V.C., Oliveira, C.S., Filho, M.A.S.C., Schnitzler, E., Lacerda, L.G. (2016). Effects of Partial in Vitro Digestion on Properties of European Chestnut(Castanea Sativa Mill) Flour. *Thermochimica Acta*, 36-41.

Mahmoodi, A., Ebrahimi, M., Khosravi, A. (2018). Epoxy/Nanopigment Coatings: Preparation and Evaluation of Physical-Mechanical Properties. *Progress in Organic Coatings*, 164-170.

Mead, R., Pike, D.J.A. (1995). Biometrics Invited Paper. A Review of Reponse Surface Methdology from a Biometric Viewpoint. *Biometric*, Vol 31, 4, 803-851.

Mukherjee, A., Joshi, M., Misra, S.C., Ramesh, U.S. (2019). Antifouling Coating Schemes for Green SHIPS. *Ocean Engineering*, 227-234.

Myers, R.H., Khuri, A.I., Canter, W.H. (1989). Response Surface Methodology. *Technometrics*, 3,137-157.

Panyakaew, S., Fotios, S. (2011). New Thermal Insulation Boards Made from Coconut Husk and Bagasse. *Energy and Buildings*, 43:1732-1739.

Taheri, M., Jahanfar, M., Ogino, K. (2017). Self-Cleaning Traffic Marking Coating. *Surfaces and Interfaces*, 13-20.

Uzoma, P.C., Liu, F., Xu, L., Zhang, Z., Han, E.H., Ke, W., Arukalam, I.O. (2019). Superhydrophobicity, Conductivity and Anticorrosion of Robust Siloxane-Acrylic Coatings Modified with Graphene Nanosheets. *Progress in Organic Coatings*, 239-251.

Walker, C.E., Parkhust, A.M. (1984). Response Surface Analysis of Bake-lab Data with a Personel Computer. *Creal Foods World*, 29, 10, 662.

Winston, W.L. (2003). *Operations Research: Applicatios and Algorithms*, 4. press, International Thomson Publishing, Belmont, CA.

Chapter 11

EDGE DETECTION ANALYSIS USING EGM08 BOUGUER GRAVITY ANOMALIES IN VAN LAKE AND ITS SURROUNDINGS, EASTERN, TURKEY

Eren PAMUK[1*]

1 Dr. Eren Pamuk. Department of Geophysical Research, General Directorate of the Mineral Research & Exploration of Turkey, 06800, Ankara, Turkey

* Corresponding Author, E-mail: eren.pamuk@mta.gov.tr

1. INTRODUCTION

Determining the boundaries of buried structures is very important for modeling and interpreting anomalies in gravity technique, a potential field technique. Some commonly used boundary analysis techniques are as such: Analytic signal, total horizontal derivative (THDR), 3D Euler deconvolution, theta angle (TM), tilt angle (TA), hyperbolic of tilt angle (HTA), normalized total horizontal gradient (TDX) and normalized horizontal derivative (NTHD). For example; Pamuk (2018) applied Tilt angle (TA), total horizontal derivative (THDR) and tilt angle of the horizontal gradient (TAHG) methods to obtain the structural edges in the Bornova Plain. Oruç (2011) applied an edge detection technique based on a TA map derivated from the first vertical gradient to gravity data in the Kozaklı Region, Central Anatolia, Turkey. Altınoğlu et al. (2015) used horizontal gradient, analytic signal, and TA methods to detect the edges of the Denizli Basin and surroundings on the Bouguer gravity map. Elmas (2018) used total horizontal derivative and tilt angle techniques to the vertical first derivative to determine the structural discontinuities of the Cyprus Island. Pamuk (2019) used TA, TM, THDR and 3D Euler deconvolution method for edge detection analysis in the northern Part of Eastern Anatolia using EGM08 Bouguer gravity data.

In this study, AS, THDR, TA, TM and HTA techniques were applied to determine the boundaries of the buried geological structures in Lake Van and its surroundings. This work consists of 2 stages. First, a theoretical gravity anomaly was obtained using prisms of different depth and density. The results were discussed by applying five different boundary analysis methods to the obtained gravity anomaly. In the second phase of the study, regional gravity data of the study area was obtained from EGM08 bouguer gravity data. Then, the possible structure boundaries were estimated by applying these methods to regional gravity data.

2. Edge Detection Techniques

Detecting the edges of the buried structures in the gravity technique, plays an important role in the modeling phase. Some of the techniques commonly used are the techniques of the total horizontal derivative (THDR), the analytic signal (AS), 3D Euler deconvolution, tilt angle (TA), Theta map (TM), hyperbolic tangent (HTA), normalized horizontal derivative (NTHD) and normalized total horizontal gradient (TDX). The AS, TA, THDR, HTA and TM methods were applied to EGM08 Bouguer data to reveal the edges of the buried geological structures. The total horizontal derivative (THDR) is a widely used edge detection filter given by (Cordell and Grauch, 1985; Blakely, 1995):

$$THDR = \sqrt{\left(\frac{\partial G}{\partial x}\right)^2 + \left(\frac{\partial G}{\partial y}\right)^2} \qquad (1)$$

where G is the gravity anomaly ∂G/∂x and ∂G/∂y are the horizontal derivatives of the gravity anomaly. Tilt angle method was developed by Miller and Singh (1994). This method is the ratio of the vertical derivative to the absolute value of the horizontal derivative of the potential field data:

$$\text{TA} = tan^{-1}\left(\frac{\frac{dG}{dz}}{THDR}\right) \qquad (2)$$

Theta map (TM, θ) method was developed Wijns et al (2005):

$$TM = \frac{\sqrt{\left(\frac{\partial G}{\partial x}\right)^2+\left(\frac{\partial G}{\partial y}\right)^2}}{\sqrt{\left(\frac{\partial G}{\partial x}\right)^2+\left(\frac{\partial G}{\partial y}\right)^2+\left(\frac{\partial G}{\partial z}\right)^2}} \qquad (3)$$

Analytic Signal (AS) method was developed by Roest et. al (1992). The analytic signal is defined as the square root of the sum of the two horizontal derivatives and the vertical derivative of the gravity anomaly:

$$|AS| = \sqrt{\left(\frac{\partial G}{\partial x}\right)^2+\left(\frac{\partial G}{\partial y}\right)^2+\left(\frac{\partial G}{\partial z}\right)^2} \qquad (4)$$

Hyperbolic tangent function was defined by Cooper and Cowan (2006) below as;

$$HTA = \frac{\frac{\partial G}{\partial z}}{\sqrt{\left(\frac{\partial G}{\partial x}\right)^2+\left(\frac{\partial G}{\partial y}\right)^2}} \qquad (5)$$

where $\partial G/\partial x$, $\partial G/\partial y$, $\partial G/\partial z$ are the x-direction derivative, y-direction derivative and vertical derivative of the gravity anomaly, respectively.

3. Theoretical Studies

In this study, gravity anomalies of prisms created by using Potensoft program which was developed by Arısoy and Dikmen (2011) were calculated to determine the effect of the techniques used in the study field (Figure 1a, 1b). Two prisms of different density and depth were used in the synthetic model. Table-1 shows the properties of these prismatic structures. The obtained synthetic gravity anomaly ranges from 0 to 329 mGal.

Table 1. *The paramaters of prism models used for the synthetic examples*

Theoretical Model	X_1 (km)	X_2 (km)	Y_1 (km)	Y_2 (km)	Top Depth of Block (km)	Bottom Depth of Block (km)	Density Contrast (g/cm^3)
Prism-1	20	60	50	90	2	4	3
Prism-2	16	80	20	30	3	4	2

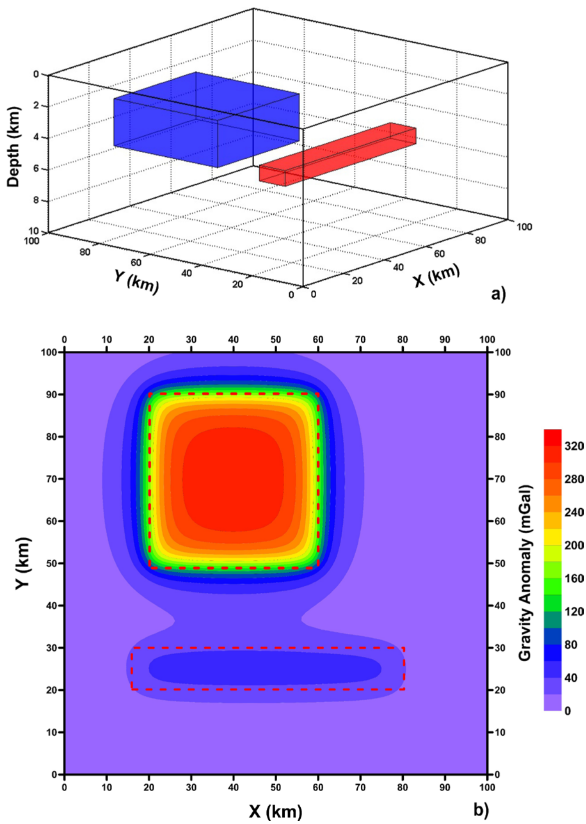

Figure 1. *Representation of b) the plan of the vertical prism models as 3D b) theoretical gravity anomaly maps (dashed red line shows edge of prisms)*

The results of boundary analysis techniques applied to calculated gravity data are given in Figure 2 (a-e). When the results of AS and THDR techniques in Figure 2a and 2b were examined, the boundaries of Prism-1, which are shallower than Prism-2, were distinctly obtained. The horizontal boundaries of prism-2, which has an upper depth of 3 km, were proportionally obtained. AS and THDR techniques were determined to be more susceptible to shallow discontinuities (Figure 2a, b). The results obtained by using TA, TM, and HTA techniques were given in Figure 2c-e. The values in the map obtained in the TA technique differ from $-\pi/2$ (-1.570) to $\pi/2$ (1.570). All these three methods have been concluded with successful results. The zero contour in the TA map directly gives the structure boundaries (Figure 2c). Although the TM and HTA technique give successful results as for TA, the HTA technique has a very small amount of deviations from the structure boundary. TA, TM, and HTA methods can be said to reliably achieve boundaries regardless of the structure depth (Figure 2c, d, e).

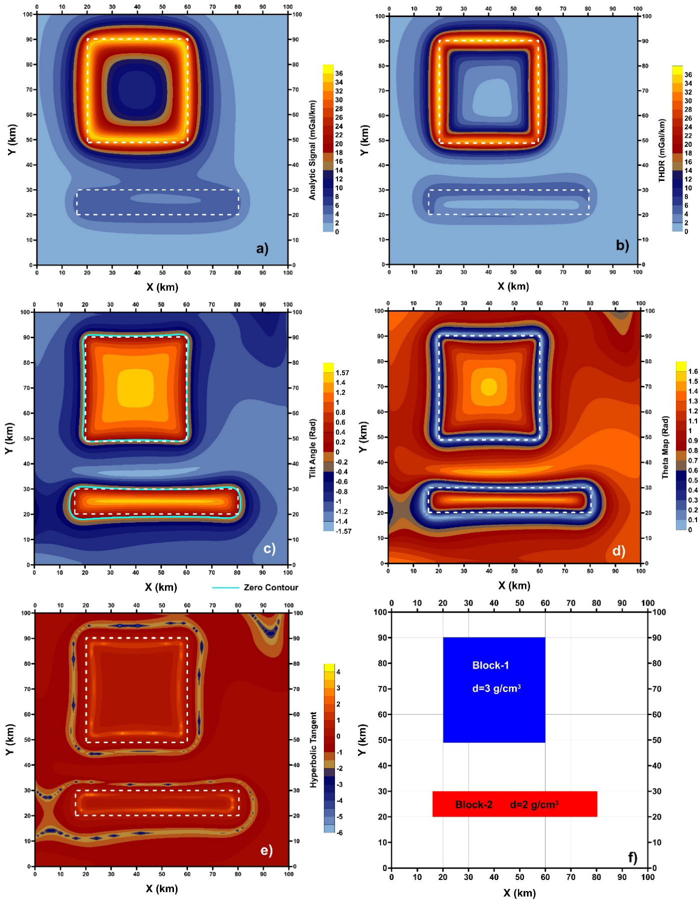

Figure 3. *a) AS map b) THDR map c) TA map d) TM map e) HTA map of the gravity anomaly for theoretical model f) location of the prisms*

4. Field Studies

Turkey is located in the Alpine-Himalayan seismic belt, with a highly tectonically active structure. In the eastern Anatolia region, normal and oblique slip faults dominate in general. The study area covers Bitlis, Ağrı and Van provinces in and around Lake Van (Figure 4). The study area is very active in terms of seismicity and numerous moderate and large scale earthquakes have occurred in the region (Utkucu, 2013; Özer, 2019). Figure 4 shows the tectonic and seismicity map of the Van Lake and its surroundings. The earthquakes in the seismicity map are between 1900 and 2019 and include earthquake data with magnitude greater than 3.5. This data was provided from Disaster and Emergency Management (AFAD). The study area and its surroundings have been exposed to numerous destructive earthquakes since the historical period. The closest one to the present day is the earthquake which occurred on 23 October 2011 as Mw 7.2. In this earthquake, 600 people died and approximate 2500 structures were damaged (Utkucu, 2013; Özer, 2019).

In this study, EGM08 bouguer gravity data -obtained within the context of the WGM (World Gravity Map) project organized in early 2008 in cooperation with UNESCO and the Commission for the Geological Map of the World (CGMW)- were used. As part of this project, archives of bouguer and free air gravity data, land, air and sea measurements, and global and regional measurements of recent years have been compiled. A Bouguer anomaly grid with spherical harmonics was determined with a sensitivity of 1 mGal by benefiting from the topography and bathymetry database of the earth, which was in 5’x5’ ranges (Pavlis et al., 2008; Pavlis et al., 2012). Low pass filter was used to obtain regional gravity anomaly of the study area from EGM08 bouguer gravity anomaly map. The regional gravity map is given in figure 5. In the examination of the regional gravity map, it is seen that the gravity values range from -210 to -130 mGal. The eastern part of the study area has relatively lower gravity values, while the highest gravity values are seen in Bitlis city and its surrounds (Figure 5).

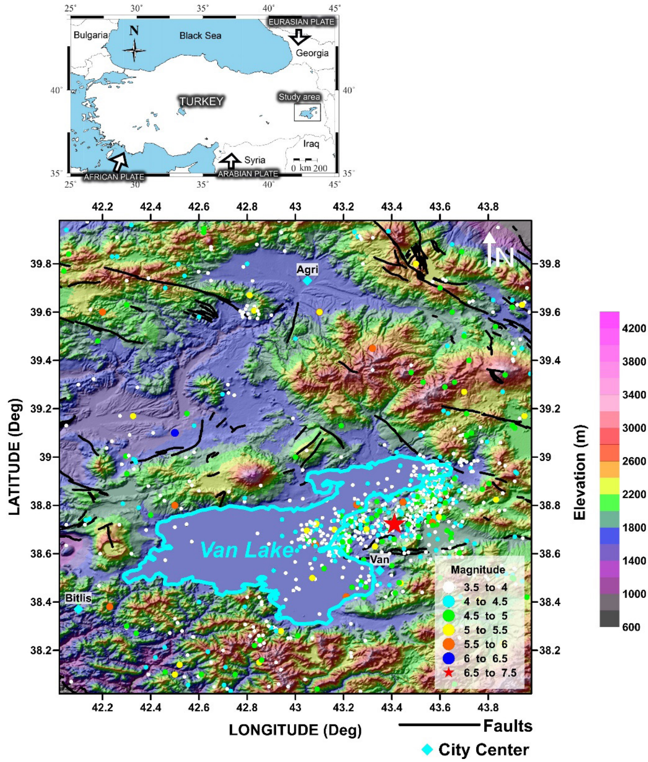

Figure 4. *Representation of the study area together with general morphology and tectonic structures (The fault lines (Emre et al.,2018) in this study are represented by black line)*

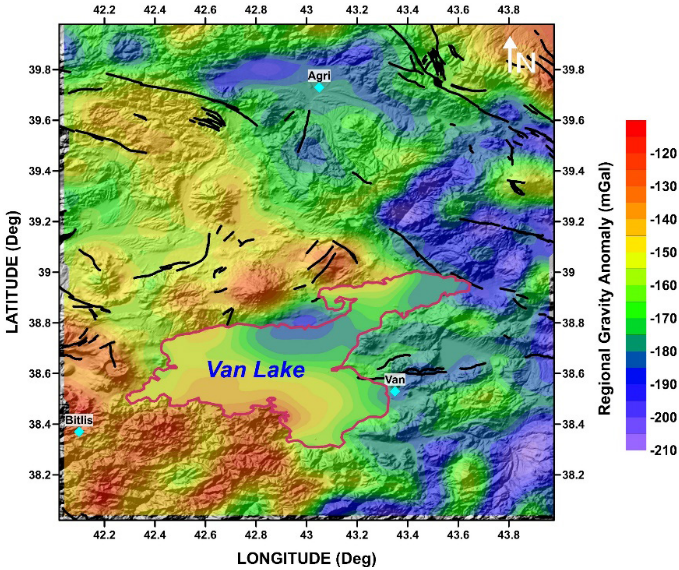

Figure 5. *Regional Gravity anomaly map of the study area*

The boundaries of the buried geological structures, obtained by five different boundary analysis techniques (AS, THDR, TA, TM and HTA), were determined (Figure 6a-e). AS and THDR techniques have given similar results. The NE-SW directed structure located in the north of Lake Van and the E-W directed structure located in the south of Lake Van raise a concern (Figure 6a, b). The boundaries of the structures obtained by the techniques of TA, TM and HTA have shown extents in different directions (Figure 6c, d, e). When the results obtained by the TA technique were examined, the structure boundaries were clearly obtained with the zero counters on the map. In the TA map, the NW-SE directional structure was seen in the north of the lake, while the NE-SW-directional structure was obtained in the east of this structure. The E-W directional structure in the lake draws attention (Figure 6c). Some of the structures that show linearity in the maps obtained correspond to the buried and out-crop faults. Similar results were obtained with TM and HTA techniques. It can be said that the boundaries of deeper structures were determined by the TA, TM and HTA techniques.

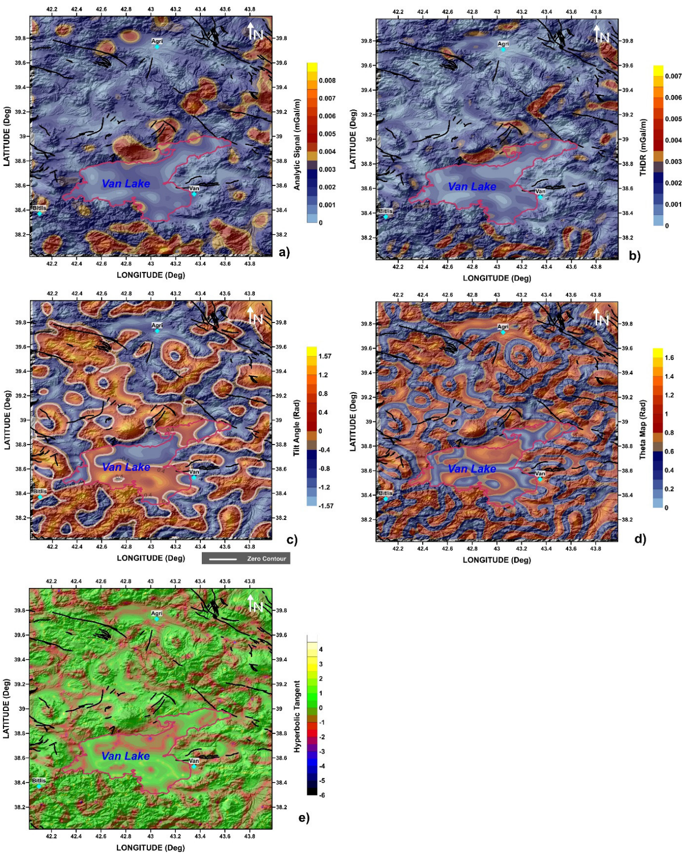

Figure 6. *a) AS map b) THDR map c) TA map d) TM map e) HTA map of the regional gravity anomaly in the study area*

5. Conclusions

In this study, the techniques of AS, THDR, TA, TM, and THA were implemented to both synthetic and EGM08 gravity data and the structure boundaries were estimated.

While the AS and THDR techniques are more successful in shallow structure boundaries, it is difficult to determine the boundaries of deep structures by using these methods, even though they outline the boundaries of deep structures.

The boundaries of both shallow and deep structures have been achieved more successfully with the techniques of TA, TM and THA. The zero contours in the TA map directly gave the structure limits.

As a result of this study, the boundaries of the previously un-obtained geological structures in and around Lake Van were revealed. In the AS and THDR maps, NE-SW directional lineaments in the north of Lake Van and E-W directional lineaments in the south of the study area have been obtained. In the NE part of Van Lake, the N-S directional structure attracts attention. The TA, TM and HTA maps generally have the same directional linearity as the existing faults. The faults in the north of the study area are generally with the extent of NW-SE. The boundaries obtained by these faults are compatible.

As seen in this study, there are advantages and disadvantages of the techniques used in determining studies of buried structure boundary. It is seen that the success of the applied techniques varies depending on the depth of the examined structure and density contrast. Therefore, more than one method to be used in such studies will allow more accurate results to be obtained.

REFERENCES

Altınoğlu FF, Sarı M, Aydın A (2015) Detection of lineaments in Denizli basin of western Anatolia region using Bouguer gravity data. Pure and Applied Geophysics 1722: 415-425.

Arısoy, M. Ö., Dikmen, Ü. 2011. Potensoft: MATLAB based software for potential field data processing, modeling and mapping, Computers and Geosciences, 37, 7, pp. 935 – 942.

Blakely RJ 1995. Potential theory in gravity and magnetic applications. Cambridge: Cambridge University Press.

Cooper, G. R. J., Cowan, D. R. 2006. Enhancing potential field data using filters based on the local phase, Computers and Geosciences, 32 (10), 1585-1591.

Cordell L, Grauch VJS (1985) Mapping basement magnetization zones from aeromagnetic data in the San Juan basin, New Mexico, in W. J. Hinze, ed., The utility of regional gravity and magnetic anomaly maps: SEG, 181-197.

Elmas, A. (2018). Kıbrıs Adası Yapısal Süreksizliklerinin EGM08 Gravite Verileri Kullanılarak Belirlenmesi. Jeoloji Mühendisliği Dergisi, 42(1), 17-32.

Emre, Ö., Duman, T. Y., Özalp, S., Şaroğlu, F., Olgun, Ş., Elmacı, H., & Can, T. (2018). Active fault database of Turkey. *Bulletin of Earthquake Engineering*, *16*(8), 3229-3275.

Miller, H.G. and Singh, V., 1994. Potential Field Tilt a New Concept for Location of Potential Field Sources, Journal of Applied Geophysics, 32, 213- 217.

Oruç B (2011) Edge detection and depth estimation using a tilt angle map from gravity gradient data of the Kozaklı-Central Anatolia Region, Turkey. Pure and Applied Geophysics, 168(10): 1769-1780.

Özer Ç., (2019) Investigation of Soil Amplification in Lake Van Basin. in: Research Reviews In Engineering, Gece Kitaplığı, Ankara, pp.63-76, 2019

Pamuk, E. (2018). Edge Detection in Microgravity Data: An Example of Bornova Plain and Its Surroundings, Western Anatolia, Turkey. Dokuz Eylül Üniversitesi Mühendislik Fakültesi Fen ve Mühendislik Dergisi, 20(60), 1026-1035.

Pamuk, E. (2019). Investigating edge detection, Curie point depth, and heat flow using EMAG2 magnetic and EGM08 gravity data in the northern part of Eastern Anatolia, Turkey. *Turkish Journal of Earth Sciences*, *28*(6), 805-821.

Pavlis NK, Holmes SA, Kenyon SC, Factor JK (2008) An earth gravitational model to degree 2160: EGM2008. EGU General Assembly, Vienna, Austria, April 13-18.

Pavlis NK, Holmes, S A, Kenyon SC, Factor JK (2012) The development and evaluation of the Earth Gravitational Model 2008 (EGM2008). Journal of Geophysical Research: Solid Earth, 117(B4).

Roest W. R., J. Verhoef, and M. Pilkington, 1992. Magnetic interpretation using the 3-D analytic signal. Geophysics, 57, 116–125.

Utkucu, M. (2013). 23 October 2011 Van, Eastern Anatolia, earthquake (M w 7.1) and seismotectonics of Lake Van area. *Journal of seismology*, *17*(2), 783-805.

Wijns, C., Perez, C. and Kowalczyk, P., 2005. Theta map: Edge detection in magnetic data. Geophysics, 70, 39-43.

Chapter 12

COMPUTER AIDED DIGITAL GAME DESIGN AND PROGRAMMING: AN EXAMPLE APPLICATION

Ahmet AYAN[1], Şakir TAŞDEMİR[2]

1 Mersin University, Vocational School of Technical Sciences, Department of Computer Technologies, Mersin Turkey
2 Selcuk University, Department of Computer Engineering, Konya Turkey ayan@mersin.edu.tr, stasdemir@selcuk.edu.tr

INTRODUCTION

In line with the rapid change in technology, the use of technology has become widespread. There have been some changes in our life with the widespread technology. With these changes, the expectations of the society from individuals have also changed. When it comes to technology, the first technology that comes to our mind is computers. With the developing technology, computers are now available in every field. Computers can be used effectively in every field and place that comes to our mind at home, at school, at work, at the market. Since the boundaries between programming and video technology are lost today, the concepts of computer games, digital games, television games, video games are seen synonymously (Mitchel & Smith, 2004). In this study, the concept of digital game is used.

There are many studies on the concept of game and digital game in the literature. Some of these studies are:

İncekara and Taşdemir designed a snake game by using C # programming language in their game. The game was played to 123 students from the 3rd and 4th grade students in the basic education level. The study aims to combine the four operations topics in mathematics with the snake game to make the education fun (İncekara & Taşdemir, 2019).

In the game named "Symmetry", Navruz and Taşdemir aimed to strengthen the learning achievements of the subject "Transformation Geometry" in the 8th grade math curriculum. The basic structure of the game; it is based on the process of automatically generating the image after the correct clicking of the corners of the image which will result from the reflection of the polygons drawn on the squared paper, dot paper and the coordinate plane with respect to the determined axis of symmetry (Navruz & Taşdemir, 2019).

Klabbers predicted that science of play will meet the needs of individuals across government institutions, industry and institutions (Klabbers, 2018).

Ullman investigated the hypothesis that many intuitive physical inference is based on a mental physics engine, which is in many respects similar to machine physics engines used in the production of interactive video games (Ulman et al., 2017).

In his article entitled “Digital educational game development”, Aslan and Balcı said that; They said that it consists of a series of complex processes that require versatile knowledge in many disciplines such as digital graphic design, education, game design, instructional design, modeling and simulation, psychology, software engineering, visual arts and learning (Aslan & Balci, 2015).

In the book by Melissons and O’Rourke, The Art of Video Games: From Pac-Man to Mass Effect, Jesse Schell said, “Digital games are a tool that includes others. Digital games will eventually be an uber-environment. You can include everything in a movie or a book” (Melissons & O’Rourke, 2012).

According to Mitchell et al., The question that designers should always ask themselves from concept design to the end stage in a game development process is: Are the visual designs developed compatible with the look and feel of the game? In this sense, visual designs are the whole of the characters, places and interfaces made for the game. Concept designs of characters, spaces, objects and interfaces are one of the first important steps in the beginning of game design. The first drawings made at this stage help shape the appearance of the game and determine how and in which world the user will interact with the characters and interfaces (Mitchell et al., 2012).

Game and Digital Game Concept

The game is generally entertaining and sometimes instructive activity for leisure time (Suits, 1967). The game is the adaptation of the stimuli taken from the outside world and the adaptation to the person's own life (Piaget, 1962). Digital game is by definition; the result of the interaction of the player with an electronic system or computer is shown through the display or similar display system (Binark et al., 2009). Digital games offer entertainment, which is a natural part of the learning process in individual development. Entertainment is a tool that motivates players (Bisson & Luckner, 1996). Computer games are simply software that can be used on computers and played for entertainment purposes. Many technical definitions can be made for computer games. The basis of these definitions is the definition that the computer game is an electronic interaction process in which the player sends electronic commands through the user interface to get a visual response on a screen (Smed & Hakonen, 2003). We can list computer game types as action, adventure, online, puzzle, RPG, simulation, sports, strategy, racing and war games.

Action Games

We can say that it is similar to action movies. There is plenty of movement and speed. It is a type of game where the excitement is continuous, there are firearms, and violent elements. For example, Half Life, Serios Sam games can be given.

Adventure Games

They are games with a specific story. In these games, there are some basic elements such as research, discovery, invention and invention. Most of them are story driven. An example is the Tomb Rider.

Online Games

These are games that can be played online over the internet. Users can play the game collectively by connecting to a specific server. For example, World of Warcraft, Leage of Legend, Knight Online.

Puzzle Games

They are puzzle style games. Improves users' visual literacy. An example is portal 2 game.

RPG Games

They are called role-playing games. There is a character in the game and the events that happen to this character are tried to be resolved. Examples include Skyrim, Dragon Age.

War Games

It is a type of game with a certain scenario where action scenes are abundant, usually a military unit is played. War games are intertwined with other game types. Examples include Call of Duty, Medal of Honor.

Simulation Games

Simulation games are games that contain the element of reality. In these games, sometimes the driving characteristics of an airplane and sometimes a car is revived. It is generally used in the training of aircraft pilots. Examples are Flight Simulator, Bus Simulator.

Sports Games

It is a type of game that is adapted by imitating a sports branch. Many sports branches have games. It is one of the most popular game types. For example, PES 2015, FIFA 2016 can be given.

Strategy Games

They are usually games in which a country is ruled. The aim of these games is to develop the country's economy, agriculture and army. Examples include Age of Empires, Total War.

Racing Games

It is a type of game where many vehicles are played by driving, usually cars and motorcycles. Some vehicles are similar to real models and are available in vehicles with different characteristics. Examples are Need for Speed, Test Drive.

Game Engines

Game engines are the general name given to software that contains libraries in many different subjects such as graphics, sound, physics engine, networking, etc. to develop video games and simulation software quickly and effectively. The development of the computer game industry has pushed users to new quests. Many companies who want to get a share from this big sector have launched products on different platforms. Every game and simulation software made in the 1980s was developed by writing code from scratch. While some games are produced only for computers, some games are produced only for solon gaming platforms. With the developing technology, many games can now be played on different platforms. In the 1990s, developers combined the libraries that were used again and again under a framework and formed the basis of today's game and simulation engines. Screenshots of various game development environments can be seen in Figure 1.

Figure 1. *Various Game Development Environments*

MATERIAL AND METHOD

This game is designed in two dimensions using the Unity 3D game engine.

Unity is preferred because of its powerful engine and physical features; it offers many advantages to users. As a result of the analyzes made after examining the game engines in the market, it was decided to use the Unity 3D game engine in order to provide a visual environment to the students and to access the modules and components to be used in the game quickly and easily. Also, the other main reason for choosing this game engine is the ease of working integrated with many programs on the market ("Unity documentation", 2020). With the Unity 3d program, which has its own online component and module store, many paid and free modules can be accessed very easily. The 2018.4 version of the Unity 3D game engine was used in the study. In addition, Visual Studio Community 2019 editor, which works in harmony with the Unity game engine, was used to encode the game scripts in the program.

Unity Game Engine

Unity is a cross-platform game engine released in June 2005 by Unity Technologies to develop video games and simulations for pc, console, mobile devices. Unity enables the development of both 2D and 3D video game and simulation thanks to the libraries and tools it contains. It is used in many game and simulation projects thanks to its easy use and cross platform (Gruszkiewicz & Baumgart, 2012; Yang & Jie, 2011; Biurrun et al., 2017). It uses the high-level Microsoft 'C # language as the Unity script language. As the graphics engine, it uses the DirectX library developed by Microsoft for Windows and Xbox platforms and OpenGL open source graphics library for mobile devices. Nvidia Physx uses it as a physics engine. Unity can be downloaded for free from its internet address for individual game developers and can be used with Windows, MacOS and Linux operating systems. The visual of the Unity 3D game engine used in our project is shown in Figure 2.

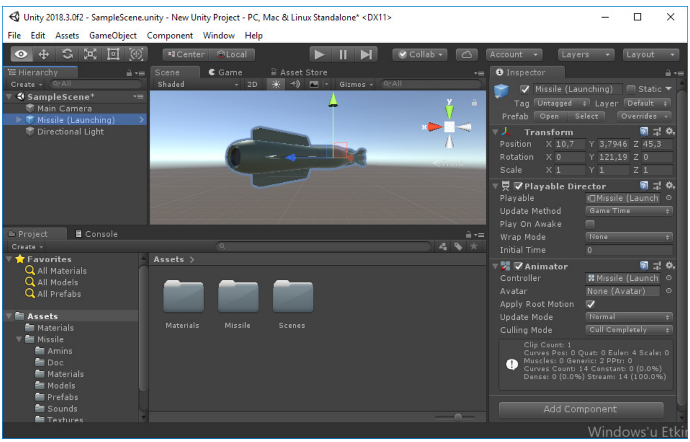

Figure 2. *Unity 3D Game Engine Screenshot (Ciesla, 2017)*

Visual Studio IDE

Visual Studio is an IDE or integrated development environment that works in harmony with Unity, where you can make programs, applications or websites using many programming languages. It is used to develop computer programs, websites, web applications, web services and mobile applications for Microsoft Windows ("Visual Studio IDE", 2019).

Visual Studio essentially does not support any programming language, solution or tool, but instead provides functionality coded as a VSPackage. Once installed, functionality can be used as a Service. IDE provides three services; SVsSolution provides the ability to enumerate projects and solutions; SVsUIShell provides windowing and UI functionality (including tabs, toolbars and tool windows); and SVsShell deals with VSPackages registration. Support for programming languages has been added using a specific VSPackage called Language Services. A language service defines various interfaces so that VSPackage applications can add support to various functions. Functions that can be added this way include syntax coloring, statement completion, bracket matching, parameter information, member lists, and background compilation as error signs. The screenshot of the editor is given in Figure 3.

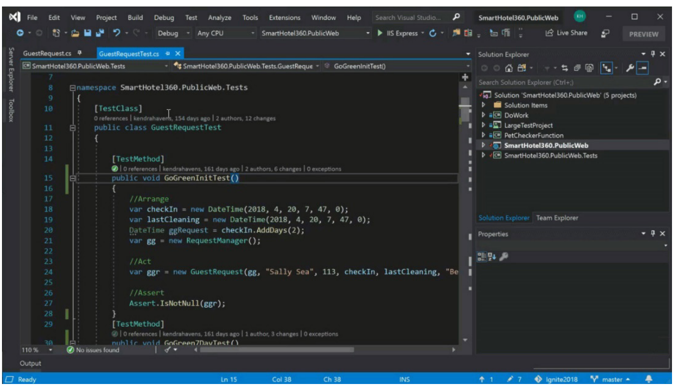

Figure 3. Microsoft Visual Studio Editor Screenshot ("Visual Studio IDE", 2019).

GAME DEVELOPMENT PROCESS

During the development process of the game, the game was developed by following the steps below.

- Determining the type and purpose of the game,
- Creating the story and script of the game,
- Determination of game characters, game objects and backgroundsoundsaccordingtothedeterminedstory,
- Game mapping,
- Determination of the game stages,
- Design and coding,
- Test phase

Unity Asset Store

Unity Asset Store is a shopping platform where paid or free multimedia content is shared using the Unity game engine (Satman, 2015). Features such as model, texture, sound downloaded from Asset Store are imported to the project. Drag and drop method is included in the project. With the Inspector, the properties of objects can be changed. To add scprit, C # code is added as a file with the add component from the Inspector section. In this way, the object is qualified.

Determining the Type and Purpose of the Game

The game genre includes fun, strategy and adventure. In addition, a game that will appeal to all age groups is designed as a leisure activity.

Creating the Story and Scenario of the Game

Before making a game with the Unity game engine, determining the scenario and design provides an easy choice for the object to be used. The scenario of the game is as follows; The character named Falconum is held in a house by prisoners. The player's aim is to save My Falcon from the house where he was captured. However, it has to overcome the obstacles on its way. The player will successfully complete the game when the obstacles pass and reach the house at the end of the map. If the player is stuck on obstacles or falls into the space on the map, the game will end, the player will not be able to save my Falcon and will have to start the game all over again.

Game Map

A free template on Asset Store, which is suitable for the scenario, was used as a game map. This template has been reshaped with visuals such as buildings, trees, clouds according to the game purpose. Attention has been paid to ensure that the scenery is visually compatible with the game. The map used in the game is shown in Figure 4.

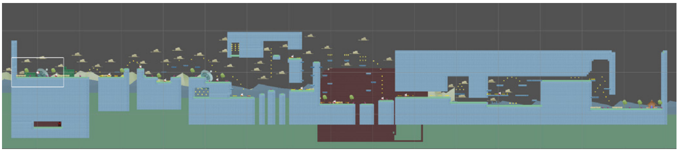

Figure 4. *Game Map*

Game Characters, Objects and Sounds

Object Oriented logic is used in game programming with Unity. This method makes the code more readable and understandable. Before starting the coding part, analysis and design are done. Whichever character we want to move or if we want to add any event, we need to add a script file to the components of that character. The object behaves according to the added script. The writing of script codes is important. Conditional structures (if, switch) and loops (for, while) are often used in the script. A script code can be used for several objects. For example, a script code written for an object to walk can be added to another object. It is important to keep the codes organized as well as correct. In this project, objects and characters are used free of charge through Asset Store. Each Unity project consists of at least one scene (Scene) and all the objects of the simulation are included in these scenes. Everything in the scene is called an object. There is at least one camera object in each scene. The user sees the inside of the simulation through the camera object. In other words, the camera is the window to the simulation world of the user. (Figure 5)

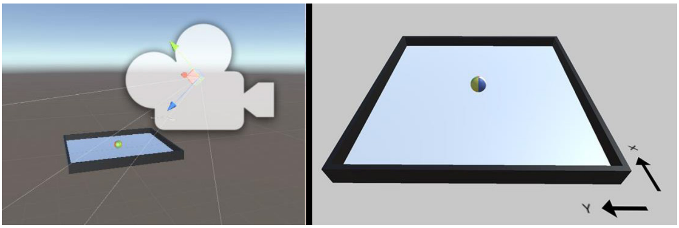

Figure 5. *Camera object and viewing angle on the left, the area seen in the simulation ("Unity documentation", 2020).*

Player: The player is the main character of the game. The player's speed and visually can be changed. The player is moving towards the goal within the game. When we create the characters, we need to add a camera in addition to the character so that we can add a behavior and take images. The player object is shown in Figure 6.

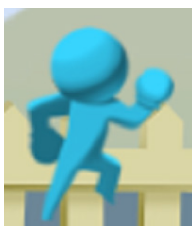

Figure 6. *Player Character*

Enemy: Enemy characters are objects that confront the player during the game. The enemy can be defined as moving or fixed. The player can get rid of him by jumping over the enemy or by crushing and killing him. Enemies are randomly positioned within the game. When the enemy attacks the character, a C # code will be written into the project where the character will burn, and the game will end. The enemy object is shown in Figure 7.

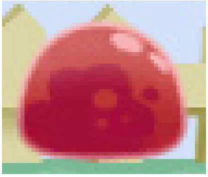

Figure 7. *Enemy Character*

Diamonds: Diamonds are objects randomly positioned so that the player can reach certain points of the game track during the game. The player can hover over the diamonds to collect them. Each of these diamonds will be reflected as +10 points in the game and will return to the player as a life in every 10 diamonds, i.e. 100 points. The diamond object is shown in Figure 8.

Figure 8. *Diamond Object*

Landscape objects: These are the objects that visually enrich the game in the landscape within the game. These can be seen as clouds, playground, trees, sky, buildings and mountains. Landscape objects are positioned constantly in the visual. The house where my Falcon is imprisoned is placed at the end of the game. The landscape objects used in the game are shown in Figure 9.

Figure 9. *Landscape objects*

Sounds: These are the background sounds while playing the game. The music to be played in the background is determined. Also, the sound during interaction with the enemy or similar sounds can be determined in the game. In this game, music compatible with the game has been determined in the background. These determined music and sounds were put into the "Audio" folder on the Unity platform within the game.

Falconum Character: It is the character that will be saved in the game. My Falcon character is positioned in the hidden pane on the game map. The character's visually can be changed. The character is shown in Figure 10.

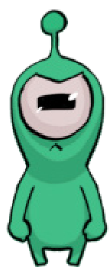

Figure 10. *Falconum Character*

Game Controls

At the beginning of the game, the character starts the game in the position determined as the starting point of the map. Then, A / D keys or "right" and "left" routing keys are used for routing in computer environment. The space key is used as the jump button.

Coding and Design

In Unity, the coding of the game is divided into four main functional layers. These layers are; basic definitions are the layers of events, models and visuals.

Basic Definitions (Mechanical)

This section contains all the codes required to identify events occurring in the game. Event definitions can be changed by updating the codes. In addition, events can be defined without writing code by using the opportunities provided by Unity.

In Unity, C # scripts are written to program the game. The following operations are defined with scripts written in the game.

• Player movement, game control keys, player moving towards the target,

• What will happen in case of error and success in the game,

• What happens when the player meets the enemy,

• Score collection events,

• Game coordinates

Events

Includes triggered events in basic codes. Here, you should avoid using Unity-specific statements, just change the model or define new events. The exact part of the events defined in the basic definitions section of this layer in the game is written here. In other words, it is the section where the game rules are written.

Model

The model folder contains the classes that hold the data required for the game. Both definition and events layers can access and edit the model. The model generally does not contain any code other than data manipulation or query methods. Points and health data are also kept in the model in the game.

Visuals

It is the layer with visual effects or animations. Game design is done in this layer. The definitions of files such as graphics, sound, and picture are made in this layer. In other words, it is the layer that contains all the processes related to game visualization.

Test Stage

The final stage in the game's development process is testing. After all the processes related to the script and coding of the game are completed, the test phase of the game is started. Posttests and debugging phase is done in this process. If there is no problem in these sections, the game is ready to publish.

Necessary tests were provided in this section in the written game and the errors that occurred in the game were corrected. Visuals related to the completed game are given below. The image of the starting moment of the game is given in Figure 11. The player character will be directed towards the target. It will try to reach the target without getting stuck on the obstacles.

Figure 11. *Game Start*

In Figure 12, the visual of the player while collecting diamonds is given. Each diamond is reflected in the player's score chamber plus 10 points and every 100 points.

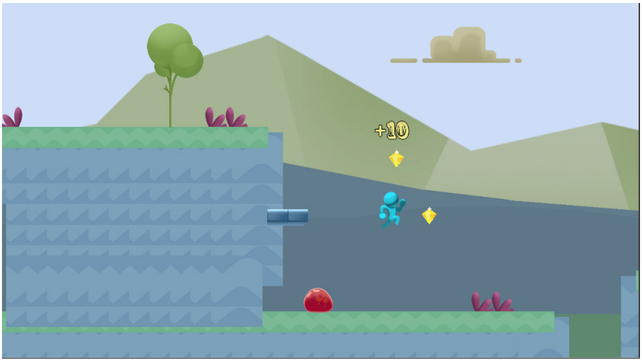

Figure 12. *Diamond Pick-up*

The player's burning moment is shown in Figure 13 and Figure 14. If the player catches the enemy, the game ends as shown in Figure 13, or if it falls into the space within the boundaries of the map, as shown in Figure 14. The player is given a "GAME OVER" message indicating that the game has failed.

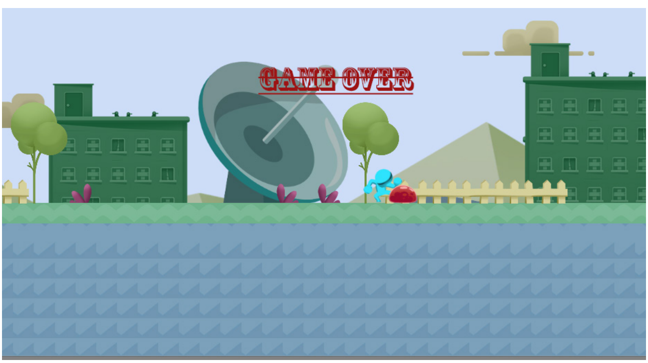

Figure 13. *Burning in Game*

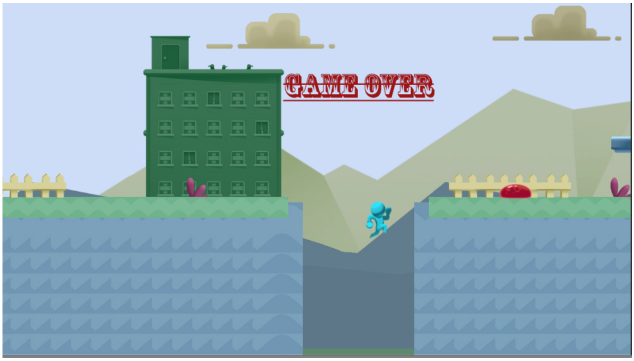

Figure 14. *Burning in Game*

Finally, when the player finishes the game track successfully and reaches the house where the "Falconum" character is held captive, a message is displayed on the screen saying that the game is completed successfully. The visual in the game finale is shown in Figure 15.

Figure 15. *Game Final*

DISCUSSION AND CONCLUSION

The information offered by digital game worlds creates an intriguing experience and constant attention. Thanks to digital games, research shows that digital games can be a useful tool to support learning. In short, digital games can increase learners' satisfaction, motivation and participation; can help recall and access information, support the development of various social and cognitive skills.

In this study, firstly, the algorithm logic of Unity and similar game engines has been investigated and it has been determined how to solve a problem step by step. These researches helped to implement the application effectively. When our imagination and talent are combined, the quality of the games we create will also increase.

REFERENCES

Mitchell, A., & Savill-Smith, C. (2004). The use of computer and video games for learning. A review of the literature.

İncekara, H., & Taşdemir, Ş. The Design Of A Digital Game For Developing Four Operations Skills In Mathematics And Its Effects On Student Success. *Gazi Mühendislik Bilimleri Dergisi (GMBD)*, *5*(3), 227-236.

Navruz, M., & Taşdemir, Ş. DESIGN AND DEVELOPMENT OF AN EDUCATIONAL DIGITAL GAME BASED ON MATHEMATICS COURSE TRANSFORMATION GEOMETRY. *International Journal of Applied Mathematics Electronics and Computers*, *7*(4), 88-95.

Klabbers, J. H. (2018). On the architecture of game science. *Simulation & Gaming*, *49*(3), 207-245.

Ullman, T. D., Spelke, E., Battaglia, P., & Tenenbaum, J. B. (2017). Mind games: Game engines as an architecture for intuitive physics. *Trends in cognitive sciences*, *21*(9), 649-665.

Aslan, S., & Balci, O. (2015). GAMED: digital educational game development methodology. *Simulation*, *91*(4), 307-319.

Melissinos, C. ve O'Rourke, P. (2012). The Art of Video Games: From Pac-Man to Mass Effect. New York: Welcome Books.

Mitchell, B. L. (2012). *Game design essentials*. John Wiley & Sons.

Suits, B. (1967). What is a Game?. *Philosophy of science*, *34*(2), 148-156.

Piaget, J. (1962). Play, dreams and imitation in childhood. New York: Norton. (Originally published in French in 1945).

Binark, M., Bayraktutan-Sütçü, G., & Fidaner, I. B. (2009). Dijital Oyun Rehberi: Oyun Tasarımı, Türler ve Oyuncu. *İstanbul: Kalkedon Yayınları*.

Bisson, C., & Luckner, J. (1996). Fun in learning: The pedagogical role of fun in adventure education. Journal of Experiential Education, 19(2), 108-112.

Smed, J., & Hakonen, H. (2003). *Towards a definition of a computer game* (pp. 1-3). Turku, Finland: Turku Centre for Computer Science.

Unity documentation. (2020). Erişim adresi: https://docs.unity3d.com/Manual/index.html

Gruszkiewicz, S. P. & Baumgart, E. (2012). Three-Dimensional Engine Simulators with Unity3D Game Software, *The 13th Annual General Assembly of the JAMU*, Newfoundland, Labrador, Canada : October 15-17.

Yang, K & Jie, J. (2011). The Designing of Training Simulation System Based on Unity3D (Ed.), *Fourth International Conference on Intelligent Computation Technology and Automation*, (pp.976-978). Shenzhen, Guangdong, China : March 28-29.

Biurrun, Carlos, Serrano, Luis & Olaverri Monreal, C. (2017). Microscopic Driver-Centric Simulator: Linking Unity3D and SUMO, *Advances in Intelligent Systems and Computing,* Vol. 1, 851-860

Ciesla, R. (2017). Mostly codeless game development. Berkeley, CA: Apress.

Visual Studio IDE documentation. (2019). Erişim adresi: https://docs.microsoft.com/bs-cyrl-ba/visualstudio/ide/?view=vs-2019

G. Satman, "Yeni Başlayanlar İçin UNITY3D, Kodlab," Temmuz 2015

Chapter 13

USING FOURIER-TRANSFORM INFRARED SPECTROSCOPY TO DETERMINE MOLECULAR HETEROGENEITY IN *ACHNANTHES* SP. AND *NITZSCHIA PALEA*

İlkay Açıkgöz ERKAYA[1], Dilek YALÇIN[2], Tülay ÖZER[3]

1 Faculty of Architecture and Engineering, Department of Environmental Engineering, Kırşehir Ahi Evran University, Kırşehir/Turkey

2 Faculty of Education, Department of Biology Education, Gazi University, Ankara/Turkey

3 Kaman High School, Food Processing Department, Kırşehir Ahi Evran University, Kırşehir/Turkey

Introduction

Fourier-transform-infrared spectroscopy (FT-IR) is a molecular vibrational method used to obtain an IR spectrum of absorption or emission of a chemical or molecule and that can determine and analyze chemical functional groups within different regions of this absorbance and detects the various elements within a compound. The peak area and intensity observed in the FT-IR spectrum of a chemical reveals the abundance of a particular functional group and the concentration percentage of a given element (Swann and Patwardhan 2011). FT-IR spectroscopy has been proved and accepted as a fast, inexpensive, and powerful tool for examining biological samples and identifying various microorganisms (Dumas and Miller 2003; Helm et al. 1991). The various biochemical components of a cell, such as lipids, proteins, and carbohydrates, have unique molecular vibrational modes (vibrational "fingerprints") and characteristic absorbance within different frequency regions of the mid-IR spectrum (Griffiths and de Haseth 1986). The composition and structure of molecular functional groups can be determined by analyzing the position, width, and intensity of IR light absorption (Yee et al. 2004). This absorbance then results in a fingerprint-like spectrum from which its components can be identified by comparing them to reference spectra. After a comprehensive and well-designed database of reference spectra has been generated, reliable identification results can be gathered from a single colony within 25 h (Oberreuter et al. 2002). FT-IR spectroscopy is used in many fields. Its investigations of bioactive surfaces, such as red blood cells, white blood cells, bacteria, cell membranes, viruses, and algae, have revealed the presence of many surface functional groups that assist in binding biomolecules and minerals (Benning et al. 2004a). In addition, different FT-IR spectroscopy techniques can be used to identify specific polysaccharides within the complex network of a plant cell wall (Copikova et al. 2001).

The analysis of phytoplankton biodiversity in aquatic ecosystems is based on examining and counting the identified species under a microscope. This process is often expensive and time consuming, and because of possible errors in diagnosis/counting, extensive analyses become difficult (Domenighini and Giordano 2009). Phytoplankton biodiversity is also used as an indicator of sudden and acute changes in water quality. Pigments are analyzed using various devices and methods to obtain information about changes in the phytoplankton composition of an aquatic environment; however, in addition to technical difficulties with these methods, they can provide only a general idea of the species or genus composition from a narrow point of view (Van Leeuwe et al. 2006). For both the detection of phytoplankton diversity and individual species, new methods should be developed that enable us to rapidly, simply, and inexpensively determine the taxonomic complexity of phytoplankton (Domenighini and Giordano 2009). FT-IR spectroscopy has traditionally been used to analyze pure compounds or simple mixtures; therefore, its application to cells is relatively new; however, this technique can provide a snapshot of a cell's biochemical composition without having to conduct complex extraction procedures and thus provides an attractive new option for phytoplankton analysis (Giordano et al. 2001; Sigee et al. 2002). The FT-IR technique and its properties have emerged as a new method by which to monitor microalgal biochemical compounds and have the potential to be an effective tool (Meng et al. 2014). This method is based on the distinct absorption bands of carbohydrates (C–O–C bonds at 1200–900 cm^{-1}), lipids (C = O of esters at 1740 cm^{-1}), proteins (C = O of amides at 1650 cm^{-1}; N–H of amides at 1540 cm^{-1}), and silica (Si–O of silica at 1075 cm^{-1}) (Giordano et al. 2001).

In the study by Hirschmugl et al. (2006) in which synchrotron-based FT-IR spectroscopy was used to follow and identify changes in the main macromolecular pools of *Euglena gracilis*, the results were shown to be applicable for both ecological and ecophysiological studies. In another study conducted on the marine microalgae *Isochrysis zhangjiangensis*, the lipid, carbohydrate, and protein contents determined by conventional methods confirmed the accuracy of the FT-IR method (Meng et al. 2014). This suggests that the FT-IR method can be used as a tool for the simultaneously measuring the lipid, carbohydrate, and protein levels in the cell. Dean et al. (2010) have produced cultures of the freshwater microalgae *Chlamydomonas reinhardtii* and *Scenedesmus subspicatus* in a nitrogen-restricted medium and used the FT-IR method to determine the lipid and carbohydrate levels of the cultures over time. The results of the study revealed that FT-IR is an effective and reliable method by which to determine lipid induction (Dean et al. 2010). D'Souza et al. (2008) have used the FT-IR method to detect structural changes in algae in the presence of cadmium, a metal pollutant, in the marine brown algae *Padina tetrastromatica* (Hauck). These researchers have demonstrated that FT-IR is an effective tool for detecting possible binding sites of cadmium in *P. tetrastromatica*.

Diatoms are an important class of microalgae (Bacillariophyceae) both in terms of their abundance in nature and their functions. They are single-celled phototrophs that developed ~180 Ma and are estimated to comprise more than 100,000 species (Drum and Gordon 2003; Kroth 2007). Diatoms have been the leading oxygen synthesizers and biomass producers in aquatic ecosystems for millions of years (Field et al. 1998; Potapova et al. 2004). They contribute ~50% to the primary productivity of phytoplankton and they are responsible for 30% of the primary carbon production in the oceans (Raven and Waite 2004). Because of these properties, they are known as organisms that hold carbon from the atmosphere, but they also have an ecologically important role in the biological reproduction of phosphate and silicon (Bidle et al. 2002; Falciatore and Bowler 2002; Lopez et al. 2005).

The structures of diatoms are extremely robust, which allows these algae to live in nearly all climates from the equator to the Polar Regions (Janech et al. 2006). Diatoms are divided into two groups according to their structure—central diatoms showing radial symmetry and pennate diatoms showing bilateral symmetry (Fuhrmann et al. 1997). Diatoms are defined by their amorphous silica cell walls that differ from each other at the nanometer scale by the morphology specific to their species (Lopez et al. 2005). It is the only phytoplankton group that needs Si directly in the growth environment. Because of their siliceous frustules, diatoms can accumulate Si up to 30% of their dry weight (Jungandreas et al. 2012). Frustules are transparent to allow light to reach the chloroplast in the cell and have holes to allow the transport of gases and solutes into the cell (Round et al. 1990). The structure of the frustule cell wall consists of two halves called the epitheca and hypotheca and is similar to the form of a petri dish. The ends of the theca structures contain valves that give morphological specificity to the species (Çinar et al. 2019). In addition to carbohydrates and proteins, unsaturated fatty acids, such as eicosapentaenoic acid, arachidonic acid, docosahexaenoic acid, and other omega-3 fatty acids, are the most important biomolecules that the diatoms produce (Kroth 2007; Bozarth et al. 2009).

The use of diatoms has been rarely considered and was limited to academic research. The recent development of biological and molecular applications for diatom cells has inspired a new perspective for diatom biotechnology (Lopez et al. 2005). Because of their great economic potential, studies have begun on diatom use in commercial and industrial applications. In particular, diatoms are used in the synthesis of carbon neutral fuels, naturally healthy food ingredients, biomolecules, antibiotics and pharmaceutically active substances, cosmetics, nanotechnology materials, and nitrogen-stabilizing biofertilizer and as bioremediators of contaminated water. In addition, their unusual cell walls are prospectively applicable in nanotechnology or use in computer chips (Bozarth et al. 2009).

Diatom identification can be misleading in morphological determinations because of the complex structures of their siliceous shells. In addition, various difficulties are encountered because of the long and cumbersome preparation procedure. Recently, FT-IR has been successfully used for diatom identification at the molecular level and detection of their biochemical structure. As a result of using FT-IR to investigate diatom surfaces, these phytoplankton have been determined to exhibit sharp peaks at ~1049–1060 cm^{-1}, which is characteristic for a Si–O bond. The interaction of inorganic and organic substances with the diatom surface causes a change in the absorption band (e.g., Si–O, Si–OH, and Si–O–Si) (Losic et al. 2009); therefore, FT-IR bands for such bonds, the intensities of their various types, and their effect on the peak areas can be a useful tool for comparing the biomineralization compatibility of different diatoms. Various diatom species have organic contents of different types and concentrations; therefore, FT-IR spectra can also provide very useful information about the lipids produced by a wide range of diatoms (Kumar et al. 2018). Jungandreas et al. (2012) have developed an FT-IR spectroscopy-based method by which to simultaneously measure the elemental compositions of two diatoms—*Cyclotella meneghiniana* and *Skeletonema costatum*—and the physiological properties of their cells. They have shown that it is possible to simultaneously monitor phytoplankton properties, such as C allocation, Si content, and the Si:C ratio using FT-IR spectroscopy. Stehfest et al. (2005) have used micro-FT-IR spectroscopy to examine the changes in the spectral properties of three cyanobacteria (*Microcystis aeruginosa*, *Chroococcus minutus*, and *Nostoc* sp.) and two Bacillariophyceae (*Cyclotella meneghiniana* and *Phaeodactylum tricornutum*) under nutritional stress. Their results have shown that the FT-IR method has the potential for use in determining single cell–biomass composition from natural phytoplankton communities.

The goal of this study was to use FT-IR analysis to identify and classify macromolecules into different diatom species *Achnanthes* sp. and *Nitzschia palea* (Kützing) W. Smith obtained from different freshwater sources and cultured in media containing the same nutrients. In addition, we aimed to demonstrate the molecular differences between the two species using statistical analyses, such as correlation analysis, principal component analysis (PCA), and hierarchical cluster analysis (HCA).

Materials and Methods

Diatom culture and growth conditions

Samples of diatoms were collected from natural freshwaters in Ankara (Turkey). *Achnanthes* sp. and *Nitzschia palea* (Kützing) W. Smith species were then isolated from these samples, transported to the laboratory, and transferred into the liquid medium prepared for enrichment of the cultures. The pre-enrichment liquid medium comprised 2.50 g $MgSO_4 \cdot 7H_2O$, 5.0 g KNO_3, 1.25 g KH_2PO_4, 0.009 g $FeSO_4 \cdot 7H_2O$, and 1000 mL distilled water (Andersen and Kawachi 2005; Nichols 1973). The micromanipulation technique was used to isolate the diatoms. Using this technique, the target cells, as determined under the microscope, were removed using a micropipette and transferred onto a sterile agar plate. The cells that amplified in the resulting colonies were transferred to culture tubes containing liquid medium. The culture tubes were first incubated under the appropriate low-temperature conditions (19–20°C). Cell growth was determined by microscopic examination approximately 2–3 weeks after the cultures were transferred to the medium (Perumal et al. 2012). Diatom species were identified using species-identification keys (Krammer and Lange-Bertalot 1999). Diatom strain are preserved in the Kırşehir Ahi Evran University (AEU-CCA) catalog of culture collections under code numbers CCA04Ach01 and CCA04Nitz01.

The appearance of living cells under the light microscope of *N. palea* and *Achnanthes* sp. is shown in Figs. 1(A) and 2(A), respectively, and FTIR images are shown in Figs. 1(B) and 2(B), respectively. The IR absorption spectra were obtained from a central region of cells, as indicated in Figs. 1(B) and 2(B).

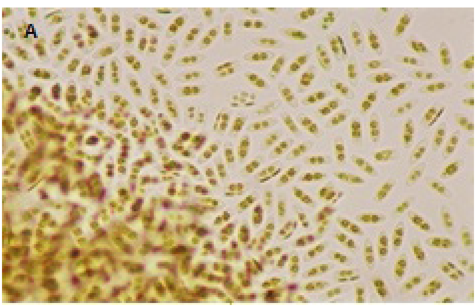

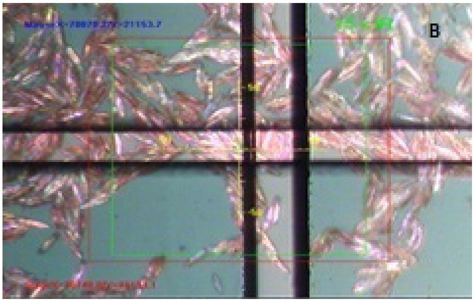

Fig. 1 (A) *Light microscope image of living cells from N. palea (CCA04Nitz01) culture (400X).* **(B)** *The region of analysis of air-dried sample position taken with light microscope attached to FT-IR.*

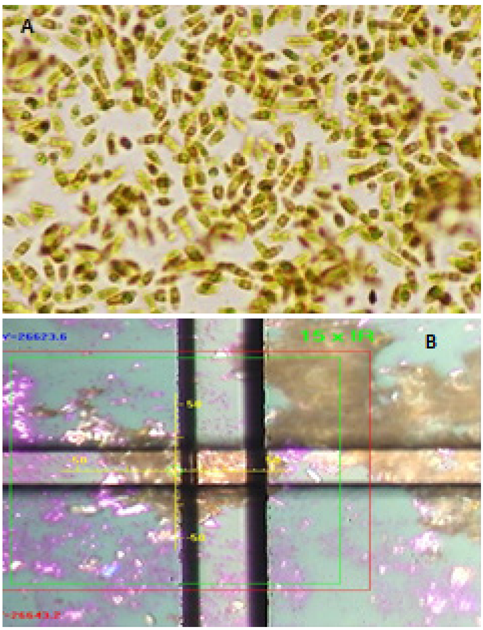

Fig. 2 (A) *Light microscope image of living cells from Achnanthes sp. (CCA04Ach01) culture (400X).* **(B)** *The region of analysis of air-dried sample position taken with light microscope attached to FT-IR.*

Allen medium was used to grow the diatom cultures. The medium contained 1.5 g/L $NaNO_3$, 1 mL/L P-IV metal solution (5 mL/L K_2HPO_4 in 1.5 g/200 mL dH_2O, 5 mL/L $MgSO_4 \cdot 7H_2O$ in 1.5 g/200 mL dH_2O, 5 mL/L Na_2CO_3 in 0.8 g/200 mL dH_2O, 10 mL/L $CaCl_2 \cdot 2H_2O$ in 0.5 g/200 mL dH_2O, 10 mL/L $Na_2SiO_3 \cdot 9H_2O$ in 1.16 g/200 mL dH_2O, and 1 mL/L citric acid$\cdot H_2O$ in 1.2 g/200 mL dH_2O). Distilled water was added to a final volume of 1000 mL (UTEX 2018). All chemicals were obtained from Merck KGaA (Darmstadt, Germany). The cultures were cultivated in 30 mL nutrient media using 50-mL Erlenmeyer flasks. The medium was adjusted to pH 6.8 with 1 N NaOH (Czerpak et al. 2003). All cultures were illuminated at 20–25°C in a 16-h light/8-h-dark cycle with a photon flux density of 50 µmol photons m^{-2} s^{-1} using fluorescent tubes (Guillard 2005). All equipment and nutrient media were sterilized using microbiological methods so as to not cause any contamination. The materials were sterilized using an autoclave at 15 lb in-2 pressure and 121°C for 15–30 mins. The glass materials were sterilized for 1 h at 170°C (World Health Organization (WHO) 2016).

Fourier-Transform Infrared Analysis

IR analysis was conducted at the Bilkent University Institute of Materials Science and Nanotechnology (UNAM), Ankara, Turkey, using a Vertex 70 Hyperion Scanning Microscope fitted with a Bruker Tensor Model 37 FT-IR spectrophotometer. A view on the microscope was chosen from the transmission region at a wave number between 4000 and 900 cm^{-1}, resolution of 4 cm^{-1}, and a 20- by 20-µm square aperture; 128 scans were taken as the spectra. The IR absorption spectra were collected from a clear field (background) and from diatom cells, and a ratio was obtained of the sample-to-background spectrum. The specimens were examined and analyzed in the dry state without a mounting medium or coverslip.

For spectral analyses and all other measurements, the samples were prepared during their exponential phases and 0.5 mL aliquots from these were resuspended in deionized water. Droplets of the culture suspension were spread over low-e reflectance microscope slides (Kevley Technologies, Chesterland, OH, USA) for monolayer preparations. Samples were subsequently air dried in a laminar flow at room temperature and stored in a desiccator until analyses (Sigee et al. 2002; Duygu et al. 2012). Each preparate of the Achnantes and Nitzschia strains was initially examined using brightfield microscopy with no coverslip, and 30 individual colonies of each sample were selected from the monolayer populations for analyses (one spectrum per colony).

Spectral analyses

The spectra were manipulated using Bruker OPUS 6.5 (https://www.bruker.com/products/infrared-near-infrared-and-raman-spectroscopy/opus-spectroscopy-software.html). The spectra were baseline corrected using an automatic baseline-correction algorithm and normalized to the silica band at 1072 cm^{-1}.

Qualitative analyses

Spectral absorption bands (e.g., proteins, nucleic acids, fatty acids, and carbohydrates) were identified in relation to published information. In addition, supporting information on band assignments was provided from the analysis of a range of pure biochemical standards, as detailed in Sigee et al. (2002).

Quantitative analyses

In quantitative analyses, first, the intensities of 10 bands (wave number) that could be distinguished were recorded for each spectrum. Because there were not more than 30 spectral data analyzed, nonparametric analysis methods were used. Statistical values, such as the mean (X), standard deviation (SD), and coefficient of variation (CV) were used to compare band positions (wave number) and band intensities. The data were analyzed using SPSS 25 (IBM Corp., Waltham, NY, USA) at the 99% confidence level. The Mann–Whitney test was used to compare normalized band intensities for both species, Spearman correlation test to determine the relationship of band intensities within species, and PCA to investigate intergroup differences in band intensity.

Second, multivariate analysis methods were used to compare the band intensities of all spectra within the wave number range of 1750–900 cm^{-1}, which is the region containing the majority of molecular information and 442 data points per spectrum (Figs. 6 and 7). PCA was conducted using score plots to visualize the data sets within the specified reference range for spectra from each species. In addition, HCA was used to determine the cluster structure. Score plots and dendrogram graphs were created and used for detailed analyses of the results.

Results and Discussion

The absorption spectra from each diatom strain is shown in Figs. 3 and 4 and exhibits 10 clear bands >4000–900 cm^{-1}. The tentative assignment of the bands obtained from the two diatom species (Table 1) are provided by considering the specific molecular groups of the previous FT-IR studies on algae. FT-IR can determine the chemical bond information in the organic compounds; however, elements or molecules cannot be detected. Overlapping spectral regions of the different components may lead to a misinterpretation of the results; therefore, because a number of molecular groups representing different macromolecular components may contribute to individual bands, correlation and PCA analyses were used to assign the bands. Bands are attributed to various vibrational states in lipids, proteins, nucleic acids, and carbohydrates (Dean et al. 2007). Band contributions were postulated from residual water (band 1), proteins (bands 1, 4, 5, 6), lipids (bands 2, 3, 6, 7), cellulose (band 3), nucleic acids (bands 8, 9), Si (band 9), and carbohydrates (band 10). In FT-IR analysis, peaks at 1063 cm^{-1} and 1068 cm^{-1} wavelengths show diatom-specific Si-O-Si stretching, peaks at 1206 and 1210 cm^{-1} wavelength, P=O bond, peak at 1441 and 1452 cm^{-1} wavelength, respectively, the peak NH_2 group at 1536 and 1541 cm^{-1} wavelength, C=O stretching at peak amides at 1641 and 1609 cm^{-1}, peak CH bond at 2915 and 2924 cm^{-1}. The large peak around the wavelength of 3300 cm^{-1} shows the O-H bond due to moisture in the sample.

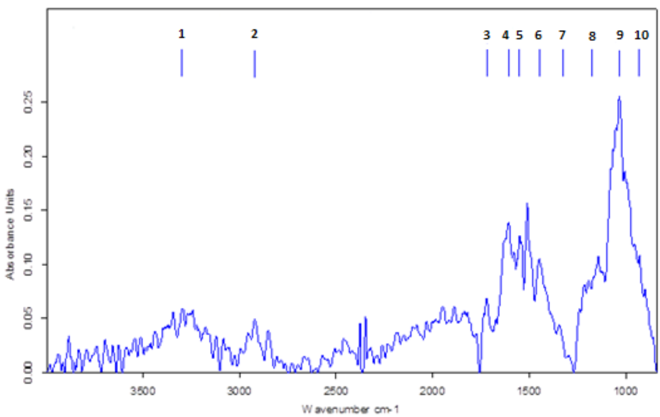

Fig. 3 *Infrared absorption spectra from Achnanthes sp. (CCA04Ach01)*

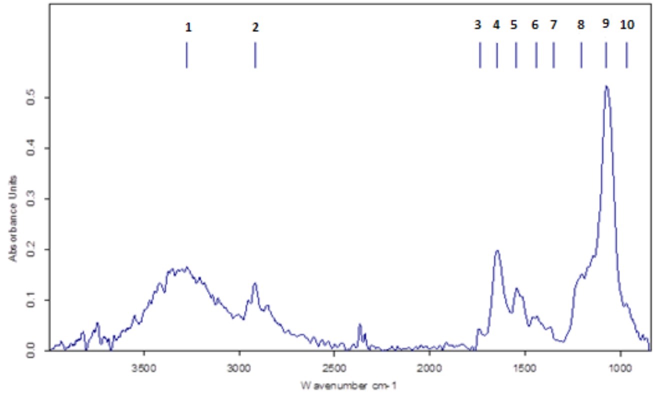

Fig. 4 *Infrared absorption spectra from N. palea (CCA-04Nitz01)*

Table 1. *Tentative assignment of bands found in the Fourier-transform infrared spectra of Achnanthes sp. (CCA04Ach01) and N. palea (CCA04Nitz01)**

Band no	Band wave number (cm^{-1})		Wavenumber range (cm^{-1})	Tentative assignment of bands
	CCA04Ach01	CCA04Nitz01		
1	3292	3274	3029–3639	**Water** v(O–H) **Protein** v(N–H) stretching (amide A)
2	2924	2915	2809–3012	**Lipid** Mainly $v_{as}(CH_2)$ and $v_s(CH_2)$ stretching of methyl (2850 v_s(C-H) from methylene (-CH_2) groups, primarily from lipids; 2920 v_{as}(C–H) from methylene (CH_2) groups, primarily from lipids; 2960 v_{as}(C–H) from methyl (CH_3) groups, primarily from proteins)
3	1729	1736	1763–1712	**Cellulose** **Fatty Acids** v(C=O) stretching of esters (from lipids and fatty acids)
4	1609	1641	1583–1709	**Protein** amide I band, v(C=O) of amides associated with proteins

5	1541	1536	1481–1585	**Protein** amide II band, δ(N–H) of amides associated with proteins
6	1452	1441	1425–1477	**Protein** $\delta_{as}(CH_2)$ and $\delta_{as}(CH_3)$ bending of methyl **Lipid** $\delta_{as}(CH_2)$ bending of methyl
7	1385	1380	1357–1423	**Protein** $\delta_s(CH_2)$ and $\delta_s(CH_3)$ bending of methyl **Carboxylic Acid** v_s(C–O) of COO^- groups of carboxylates **Lipid** $\delta_s(N(CH_3)_3)$ bending of methyl
8	1210	1206	1191–1356	**Nucleic Acid** v_{as}(>P=O); stretching of phosphodiester backbone of nucleic acid (DNA and RNA)
9	1068	1063	1060, 1072, 1086	**For silica several bands Si-O-Si** stretching **Carbohydrate** v(C–O–C) of polysaccharides **Nucleic Acid** (and other phosphate-containing compounds) v_s(>P=O) stretching of phosphodiesters
10	966	962	1072–980	**Carbohydrate** v(C–O–C) of polysaccharides

Notes: v_{as}, asymmetric stretch; v_s, symmetric stretch; δ_{as}, asymmetric deformation (bend); δ_s, symmetric deformation (bend).

[*]Band assignments based on Kumar et al. (2018), Dean et al. (2007), Sigee et al. (2002), Giordano et al. (2001), Naumann et al. (1996).

Intraspecific heterogeneity

Intraspecific variations in band intensities for *Achnantes* sp. and *N. palea* were studied to determine how intracellular concentrations of the species' macromolecular components varied in population heterogeneity. Table 2 shows the mean band intensities for each species, together with CV. In *Achnanthes* sp., bands 4 and 10 showed the smallest CV (38%), bands 1 and 7 showed the highest CVs (78 and 66%, respectively), and other bands had

CVs between 40 and 62%. In *N. Palea*, band 8 showed the smallest CV (8%), bands 2 and 3 showed the highest CVs (42 and 44%, respectively), and other bands had CVs of <36%.

Table 2. *Comparison of band intensities*

Band	CCA04Ach01		CCA04Nitz01		Significance
	Mean	CV	Mean	CV	
1	0.25	78	0.26	34	**0.261**
2	0.32	62	0.19	43	**0.002***
3	0.32	48	0.09	44	**0.000***
4	0.52	38	0.35	25	**0.000***
5	0.55	46	0.22	30	**0.000***
6	0.35	50	0.11	36	**0.000***
7	0.26	66	0.08	35	**0.000***
8	0.34	40	0.28	8	**0.012**
9					
10	0.53	38	0.20	24	**0.000***

Notes: CV, coefficient of variation.

For each diatom species, the mean band intensities are shown as normalized data referenced to band 9 (n = 30).

**p < 0.01 significant difference, p > 0.01 no significant difference (Mann–Whitney test).*

Comparison of species

Statistical comparisons between the two species were made according to individual band intensities, band positions, and PCA of the band sequence.

Comparison of band intensities using the Mann-Whitney test

Significant differences were found between the two diatom species in relation to the relative densities of bands 2, 3, 4, 5, 6, 7, and 10 at a 99% significance level (Table 2). Only bands 1 and 8 did not show any significance difference. In addition, because band 9 was kept constant, it was not included in the analysis (band 9 = 1).

Table 3. *Nonparametric correlations between band intensities in CCA04Ach01 and CCA04Nitz01*

	1	2	3	4	5	6	7	8	10
1	-	**.769****							
2	.831**	-						**.525****	
3	.495**	.711**	-	**.469****	**.625****		**.466****	**.534****	
4	.701**	.867**	.881**	-	**.541****	**.599****	**.472****		
5	.616**	.819**	.849**	.943**	-	**.735****	**.648****	**.503****	
6		.732**	.852**	.843**	.864**	-	**.858****	**.552****	
7		.700**	.685**	.742**	.843**	.805**	-		
8								-	
9									
10					.509**	.571**	.490**		-

*Notes: **p < 0.01, significant correlation; CCA04Ach01, right top thick; CCA04Nitz01, left bottom normal; 0 < r < 0.299, weak; 0.300 < r < 0.599; moderate, 0.600 < r < 0.799 strong; 0.800 < r < 0.999 very strong (Spearman correlation).*

Nonparametric (Spearman) correlations

Table 3 reveals the correlations levels between and among certain band intensities (99% probability level). In *Achnanthes* sp., bands 1 and 2 showed a strong correlation (r = 0.769). Bands 3, 5, and 8 showed positive correlations (r = 0.625 and r = 0.534) with each other, as did bands 5, 6, and 7 (r = 0.735 and r = 0.648). In *N. palea*, bands 2, 3, 4, 5, 6, and 7 showed positive correlations (r = 0.711, 0.867, 0.819, 0.732, and 0.700, respectively) with each other, as did bands 3, 4, 5, 6, and 7 (r = 0.881, 0.849, 0.852, and 0.685, respectively). In addition, bands 4, 5, and 6 showed positive correlations (r = 0.943 and r = 0.843) with each other, as did bands 5 and 6 (r = 0.864) with bands 6 and 7 (r = 0.805). Apart from a strong correlation between bands 5 and 6, the pattern of correlations was very different between the two diatoms.

Table 4. *Comparison of band positions of Achnanthes sp. (CCA04Ach01) and N. palea (CCA04Nitz01) (n= 30)*

Band	CCA04Ach01		CCA04Nitz01		Significance
	Mean	SD	Mean	SD	
1	3291,81	6,54	3274,26	8,20	**0,000***
2	2924,24	5,74	2915,37	4,24	**0,000***
3	1729,41	9,64	1736,93	3,52	**0,004***
4	1609,65	7,90	1641,60	3,23	**0,000***
5	1541,38	2,63	1536,82	3,22	**0,000***
6	1452,09	3,87	1441,42	6,73	**0,000***
7	1385,56	7,18	1380,27	7,41	**0,022**
8	1210,19	5,86	1206,09	9,11	**0,018**
9	1038,43	18,41	1063,11	8,64	**0,000***
10	966,95	6,84	962,18	6,60	**0,005***

*Notes: *p < 0.01, significant difference; p > 0.01 no significant difference (Mann–Whitney).*

Although the two phytoplankton species had a similar band patterns, individual band positions showed interspecific differences (Table 4). The average position of the bands, except bands 5 and 6 in *Achnanthes* sp., and again excluding bands 3, 4, and 5 in *N. palea*, differed by >4 cm^{-1} resolution of the instrument; however, a variation was seen between spectra, and whole bands, except bands 7 and 8, were significantly different at the 99% probability level.

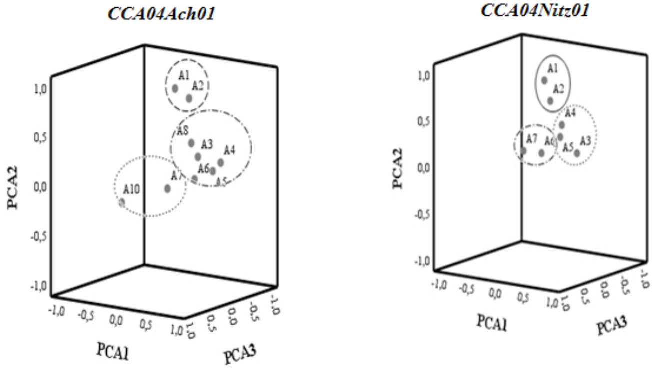

Fig. 5 *Principal component analysis (PCA) plot of peak intensities for CCA04Ach01 and CCA04Nitz01.*

Principal component analysis

PCA of the sequence of band intensities exhibited distinctive three-dimensional plots for the two diatom strains (Fig. 5). In both strains, three factors were derived. For *Achnanthes* sp., PC1 (36%) consisted of bands 3, 4, 5, 6, and 8, PC2 (24%) of bands 1 and 2, and PC3 (18%) of bands 7 and 10. For *Nitzschia* sp., PC 1 (34%) consisted of bands 3, 4, and 5, PC2 (31%) of bands 1 and 2, and PC3 (30%) of bands 7 and 6.

Multivariate analysis of spectral region (1750–900 cm^{-1})

PCA and HCA were conducted for the combined set of spectra (n = 30 for both diatoms) at a wave number region >1750–900 cm^{-1}. Two statistical factors—principal component 1 (PC1, 57% of variability) and principal component 2 (PC2, 26% of variability)—accounted for the variations within this data set.

PCA showed a clear distinction between PC1 and PC2 on the score plots between species, decreasing the dimensionality of the multidimensional spectral data within the 1750–900 cm^{-1} region of the two species while preserving most of the variance. The PC score plot shown in Fig. 6 displays the two distinct clusters belonging to *Achnanthes* and *Nitzschia* strains.

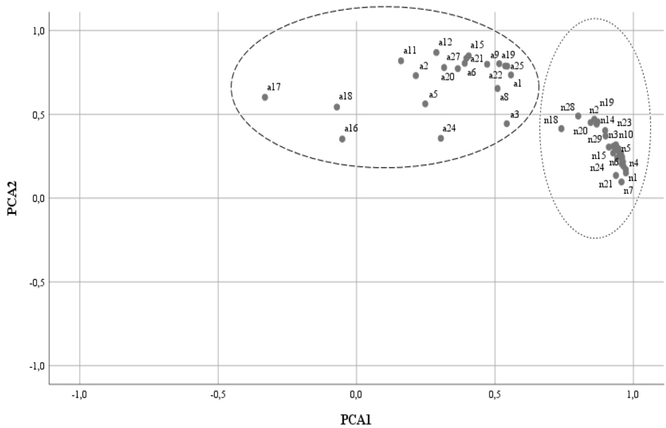

Fig. 6 *Score plot for CCA04Ach01 (a1…ax) and CCA04Nitz01 (n1…nx). Each point on the plot represents band intensities of the spectral region at 1750–900 cm^{-1} of an individual spectrum. Thirty spectra were analyzed for each species.*

Fig. 7 shows the results from the HCA (Ward's method) using Euclidian distance squared as the measure of similarity. When the dendogram was examined, we observed that the spectra were sharply collected from each in two clusters. In addition, the spectra of *Nitzschia* are represented in the aggregated cluster with fewer groups, while that of *Achnanthes* had more groups.

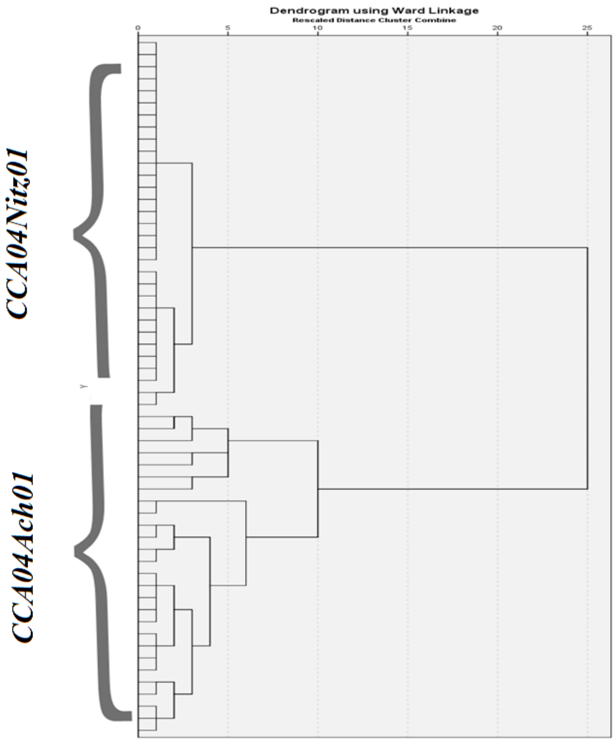

Fig. 7 *Results of the hierarchical cluster analysis of CCA04Ach01 and CCA04Nitz01. The dendrogram was constructed using spectra normalized to the Si band within the wavelength of 1750–900 cm*$^{-1}$.

The spatial resolution achievable with FTIR microspectroscopy allows for the analysis of macromolecular pools (e.g., proteins, lipids, and carbohydrates) in individual cells and for species-specific measurements within the microscopic culture (Murdock and Wetzel 2009; Giordano et al. 2009). FTIR analyses were conducted on living diatoms *Achnanthes* sp. and *N. palea*. The differences between the spectra obtained from both cultured diatom species are visually noticeable (Figs.

3 and 4). In typical spectra, it is inevitable that individual molecular groups contribute to different bands, and most of the individual bands observed are derived from several molecular sources (Naumann et al. 1996; Dean and Sigee 2006). In typical FTIR spectra for algae, wavelengths of 1200–900 cm^{-1} contain more carbohydrate bands; however, in diatoms, there is a distinct Si band at both 1060 and 1035 cm^{-1} covered by this area (Murdock and Wetzel 2009; Gendron-Badou et al. 2003). FTIR spectra of individual cells of *N. palea* and *Achnanthes* sp. were characterized by a very strong band at 1063 and 1068 cm^{1}, respectively, which was attributed to the Si–O stretching vibration of the silica frustules, as observed in previous studies on diatoms (Wagner et al. 2010; Dean and Sigee 2006; Stehfest et al. 2005; Vardy and Uwins 2002; Giordano et al. 2001). In addition, because this region also covers the P–O–C ring vibrations of polysaccharides and perhaps the Si–O–C stretch of the cell wall bonded to proteins (a theorized structure for diatoms), the region within wavelengths 1100–1000 cm^{-1} will contain a combination of these bands (Vardy and Uwins 2002). Clearly, the intense and broad Si stretch reduced the number of noticeable compounds by obscuring some of the bands from nucleic acids and carbohydrates. Because Si absorption bands overlap with carbohydrate absorption bands (Wagner et al. 2010; Stehfest et al. 2005; Gendron-Badou et al. 2003), lipid:protein and carbohydrate:protein ratios were not used to analyze the levels of carbon allocation within the cells.

Information about band assignments can be obtained from correlation and factor analyses of the principal bands because the bands obtained from a common source should show a relationship (Dean et al. 2007). In this study, the v(C–O–C) stretching of polysaccharides, sometimes as v_s(>P=O) stretching of phosphodiesters, which was attributed to band 9 in some nondiatom organisms and was generally recorded at the band positions at 1150, 1078, 1066, 1050, and 1030 cm^{-1} (Wong et al. 1991; Brandenburg and Seydel 1996; Kansız et al. 1999; Benning et al. 2004 (b); Dean et al. 2007), could not be read. In any case, the band values could be saved incorrectly because they were close to those for Si in diatoms. In this case, only band 10 can be defined distinctly as a carbohydrate band in both phytoplankton. If nucleic acids were present at the band 10 position, band 10 would then be expected to correlate with band 8; however, no correlation was observed. This suggests that carbohydrate is a distinct major contributor to ban 10. *Achnanthes* and *Nitzschia* species showed different vibrational modes according to the results of band correlation and factor analysis.

According to band densities, in both types, bands 1 and 2 formed a group, but their characteristic modes were different. In *Achnanthes,* a strong correlation of band 2 with only band 1 indicated that band 2 is mainly from carbohydrates and that band 1 was derived from carbohydrates and not water/protein (Dean et al. 2007). Likewise, the correlation between band 3 and 7 indicated only that lipids were involved in the structure of band 7. In *Nitzschia,* the lack of a correlation between bands 1 and 2 indicated that band 1 was water/protein derived. Furthermore, the strong correlation between bands 2 and 3 (even bands 6 and 7), band 3 with bands 6 and 7, and between bands 6 and 7 showed that bands 3, 6, and 7 arose from lipids. In both species, the strong correlation between bands 4 and 5 showed that these bands resulted from ν(C=O) stretching, δ(N–H) bending, and C–N stretching modes of amides I and II. In addition, in Achnanthes, the strong correlations between bands 4 and 5 (also with band 6), and bands 6 and 7 show that the major components of these bands come from functional groups of proteins.

Factor analyses also substantially showed these groups. Band 8 (ν_{as}[>P=O]) at positions 1204 and 1210

cm^{-1} was likely to have a strong contribution from nucleic acid, but it is also likely that the band also has a contribution from the internally stored polyphosphates (Murdock et al. 2010; Dean et. al. 2008). In *Nitzschia*, band 8 was not correlated with any others, which suggests that it is the only band with a dominant v_{as}(>P=O) contribution, and that it is not included in any group in factor analysis. Unlike, in Achnanthes, band 8 did correlate with bands 6 (1452 cm^{-1}) and 7 (1385 cm^{-1}). The fact that bands 10 and 7 of *Achnanthes* species were in the same group may indicated that they were sourced from polysaccharides containing carboxyl functional groups.

In different single-cell colonies grown in the same culture medium and under the same conditions, alterations in the intracellular concentrations of macromolecular components show population heterogeneity (Murdock et al. 2010; Dean et al. 2007). The lowest variation in this study was seen at band 8 (8%) in *Nitzschia* and at band 10 (30%) in *Achnanthes*, which may have resulted from the normalization of spectra relative to band 9. A similar result was obtained in the study conducted with *Microcystis* and *Ceratium* (Dean et al. 2007) for band 5 when the bands were normalized with respect to band 4 (amide I). The highest variations were observed in *Achnanthes* (Table 2). In this species, high variations in bands 1 (78%) and 2 (62%) indicated that functional groups from carbohydrates, as mentioned above, are more likely to participate in the water/protein and lipid bands. In addition, the fact that band 7 had the highest variation (66%) indicates that the vibrational modes from lipids contribute to the protein groups. In *Nitzschia*, the highest variation coefficients were observed in bands 2 (43%), 3 (44%), 6 (36%), and 7 (35%). The high variation coefficients of bands 2 and 3, which were attributed to lipids, may be the result of intraspecific heterogeneity in the amount of intracellular phosphorus compounds stored during the logarithmic increase. The high variations in bands 6 and 7 were largely from proteins. As stated in the correlation relationships, the high correlations of bands 2 and 3 with bands 6 and 7 indicates that other functional groups, such as lipids, were associated with these bands and that their amounts may also have varied. In both species, except for bands 1 and 10, the variations of other band intensities were high. This indicates that the components of intracellular molecular concentrations of both species are different (Heraud et al. 2008).

With respect to the band positions, all bands except 7 and 8, in the spectra of both species showed significant differences at 99% probability levels. For example, high variations in the position of band 1 (3291 cm^{-1} in *Achnanthes*, 3274 cm^{-1} in *Nitzschia*) and band 9 (1068 cm^{-1} in *Achnanthes*, 1063 cm^{-1} in *Nitzschia*) may reflect the distinctness in molecular structures of carbohydrate storage products in both species. The intraspecific variations in band positions in *Achnanthes* were much higher. This was also evident from the large number of groups formed in favor of *Achnanthes* in cluster analysis.

Nitzschia and *Achnanthes* species were clearly divided into two separate clusters using PCA and HCA for their two combined spectra within wave numbers 1750–900 cm^{-1}.

Conclusion

Methods involving FTIR microscopy (and also IR microspectroscopy) for determining macromolecular components of cells and differentiating species from each other, which were previously performed on a small number of diatom species, such as *Chaetoceros muellerii* (Giordano et al. 2001), *Cyclotella meneghiniana* (Stehfest et al. 2005), *Thalassiosira weissflogii* (Giordano et al. 2009), *N. closterium* and *N. longissima* (Vardy and

Uwins, 2002), and *A. affinis* and *Fragilaria virescens* (Murdock et al. 2010), have also yielded successful results for *Achnanthes* and *Nitzschia* species; however, because carbohydrates and Si show strongly overlapping absorption bands, better spectra must be selected and a more detailed analysis must be conducted to quantitatively analyze the spectral data. Because Si shows a strong IR absorption, variations in cellular Si concentration cause clear changes in the shape of the FTIR spectra; therefore, Si content may be proportionally quantified from these spectra.

Discrete band assignments and variations in band densities between species, particularly in culture media, may be more accurately determined using FTIR analyses. FTIR is a practical and easy method that provides accurate results, thus any alterations in intracellular macromolecular composition can be revealed quickly and with frequent changes in culture environments (e.g., light and nutrients). Because of their different structural features, the reactions of the functional groups of macromolecules to FTIR under varying environmental conditions can be different among species. By identifying its spectral properties as well as the classical and molecular classifications of a species, FTIR applications can provide an improbable and up-to-date potential for revealing intra- and interspecies differences.

Acknowledgement

We thank Gazi University, Scientific Projects Research Management, for financing this research. We also thank Professor Andrew Dean for providing the preliminary skills necessary for qualitative and quantitative applications on spectral data.

Compliance with Ethical Standards: The authors declare that they have no conflict of interest.

REFERENCES

Andersen RA, Kawachi M (2005) Traditional microalgae isolation techniques. In: Andersen, R.A. (ed) Algal culturing techniques, Elsevier Press, London, pp 83-100

Benning LG, Phoenix VR, Yee N, Tobin MJ 2004 (a) Molecular characterization of cyanobacterial silicification using synchrotron infrared micro-spectroscopy. Geochim Cosmochim Acta 68: 729-741

Benning LG, Phoenix VR, Yee N, Konhauser KO 2004 (b) The dynamics of cyanobacterial silicification: An infrared micro-spectroscopic investigation. Geochim Cosmochim Acta 68: 743-757

Bidle KD, Manganelli M, Azam F (2002) Regulation of oceanic silicon and carbon preservation by temperature control on bacteria. Science 298:1980–1984

Bozarth A, Maier UG, Zauner S (2009) Diatoms in biotechnology: modern tools and applications. Appl Microbiol Biotechnol. https://doi.org/10.1007/s00253-008-1804-8

Brandenburg K, Seydel U (1996) Infrared spectroscopy of nucleic acids. In: Mantsch HH, Chapman D (ed) Infrared spectroscopy of biomolecules, Wiley, Chichester pp 159-202

Copikova J, Synytsya A, Cerna M, Kaasova J, Novotna M (2001) Application of FT-IR spectroscopy in detection of food hydrocolloids in confectionery jellies and food supplements. Czech J. Food Sci 19: 51-59

Czerpak R, Piotrowska A, Weierzbowska M (2003) Biochemical activity of biochanin a in the green alga *Chlorella vulgaris* Beijerinck (Chlorofhyceae). Polish Journal of Environmental Studies 12: 163-169

Çinar S, Özçimen D, Yılmaz M (2019) Marine diatom isolation, identification and investigation of nutrient effects on the diatom growth. Journal of the Faculty of Engineering and Architecture of Gazi University 34(3): 1143-1153

Dean AP, Sigee DC (2006) Molecular heterogeneity in *Aphanizomenon flos-aquae* and *Anabaena flos-aquae* (Cyanophyta): A synchrotron-based Fourier-transform infrared study of lake micropopulations. Eur. J. Phycol 41: 201-212

Dean AP, Martin MC, Sigee DC (2007) Resolution of codominant phytoplankton species in a eutrophic lake using synchrotron-based Fourier transform infrared spectroscopy. Phycologia 46: 151-159

Dean AP, Estrada B, Nicholson JM, Sigee DC (2008) Molecular responses of *Anabaena flos-aquae* to differing concentrations of phosphorus: A combined Fourier transform infrared and X-ray microanalytical study. Phycological Research 56: 193-201

Dean AP, Sigee DC, Estrada B, Pittman JK (2010) Using FTIR spectroscopy for rapid determination of lipid accumulation in response to nitrogen limitation in freshwater microalgae. Bioresource Technology 101: 4499-4507

Domenighini A, Giordano M (2009) Fourier transform infrared spectroscopy of microalgae as a novel tool for biodiversity studies, species identification, and the assesment of water quality. J Phycol 45: 522-531

Drum RW, Gordon R (2003) Star trek replicators and diatom nanotechnology. Trends Biotechnol 21: 325-328

Dumas P, Miller L (2003) The use of synchrotron infrared microspectroscopy in biological and biomedical investigations. Vib Spec 32: 3-21

Duygu D, Udoh AU, Özer Baykal T, Akbulut A, Erkaya Açıkgöz I, Yıldız K, Güler D (2012) Fourier Transform Infrared (FTIR) spectroscopy for identification of *Chlorella vulgaris* Beijerinck 1890 and *Scenedesmus obliquus* (Turpin) Kützing 1833. African Journal of Biotechnology 11(16): 3817-3824

D'Souza L, Devi P, Divya Shridhar MP, Chandrakant G (2008) Use of Fourier Transform Infrared (FTIR) spectroscopy to study Cadmium-induced changes in *Padina Tetrastromatica* (Hauck). Chemistry Insights 3: 135-143

Falciatore A, Bowler C (2002) Revealing the molecular secrets of marine diatoms. Annu Rev Plant Biol 53: 109-130

Field CB, Behrenfeld MJ, Randerson JT, Falkowski P (1998) Primary production of the biosphere: integrating terrestrial and oceanic components. Science 281: 237–240

Fuhrmann T, Lanwehr S, El Rharbi – Kucki M, SumperM (1997) Diatoms as living photonic crystals. Applied Physics 82: 909-965

Gendron-Badou A, Coradin T, Maquet J, François F, Livage J (2003) Spectroscopic characterization of biogenic silica. Journal of Non-Crystalline Solids 316: 331-337

Giordano M, Kansız M, Heraud P, Beardall J, Wood B, McNaughton D (2001) Fourier transform infrared spectroscopy as a novel tool to investigate changes in intracellular macromolecular pools in the marine microalgae *Chaetoceros muellerii* (Bacillariophyceae). J Phycol 37: 271-279

Giordano M, Rattia S, Domenighinia A, Vogtb F (2009) Spectroscopic classification of 14 different microalga species: first steps towards spectroscopic measurement of phytoplankton biodiversity. Plant Ecology & Diversity 2(2): 155-164

Griffiths PR, de Haseth JA (1986) Fourier Transform Infrared Spectrometry. New York, John Wiley

Guillard RRL (2005) Purification methods for microalgae. In: Andersen RA (ed), Algal culturing techniques, Elsevier Press, London, pp 117-132

Heraud P, Stojkovic S, Beardall J, McNaughton D, Wood BR (2008) Intercolonial variability in macromolecular composition in P-starved and P-replete Scenedesmus populations revealed by infrared microspectroscopy. J Phycol 44: 1335–1339

Helm D, Labischinski H, Schallehn G, Naumann D (1991) Classification and identification of bacteria by Fourier-transform infrared spectroscopy. J Gen Microbiol 137: 69-79

Hirschmugl C, Bayarri ZE, Bunta M, Holt JB, Giordano M (2006) Analysis of nutritional status of algae by Fourier transform infrared chemical imaging. Infrared Phys Techn 49: 57-63

Janech MG, Krell A, Mock T, Kang J-S, Raymond JA (2006) Ice binding proteins from sea ice diatoms (Bacillariophyceae). J Phycol 42: 410-416

Jungandreas A, Wagner H, Wilhelm C (2012) Simultaneous measurement of the silicon content and physiological parameters by ftır spectroscopy in diatoms with siliceous cell walls. Plant Cell Physiol 53(12): 2153–2162

Kansiz M, Heraud P, Wood B, Burden F, Beardall J, McNaughton D (1999) Fourier transform infrared microspectroscopy and chemometrics as a tool for the discrimination of cyanobacterial strains. Phytochemistry 52: 407–417

Krammer K, Lange–Bertalot H (1999) Süβwasserflora von Mitteleuropa, Bacillariophyceae, Band 2/2, 2. Teil: Bacillariaceae, Epithemiaceae, Surirellaceae. Gustav Fischer Verlag, Stuttgart

Kroth P (2007) Molecular biology and the biotechnological potential of diatoms. Springer, Berlin

Kumar V, Kashyap M, Gautam S, Shukla P, Joshi KB, Vinayak V (2018) Fast Fourier Infrared spectroscopy to characterize the biochemical composition in diatoms. Journal of Bioscience 43(4): 717-729.

Lopez PJ, Descles J, Allen AE, Bowler C (2005) Prospects in diatom research. Curr Opin Biotechnol 16:180–186

Losic D, Mitchell JG and Voelcker NH (2009) Diatomaceous lessons in nanotechnology and advanced materials. Adv Mater 21 2947–2958

Meng Y, Yao C, Xue S, Yang H (2014) Application of Fourier transform infrared (FT-IR) spectroscopy in determination of microalgal compositions. Bioresource Technology 151: 347-354

Murdock JN, Wetzel DL (2009) FT-IR microspectroscopy enhances biological and ecological analysis of algae. Applied Spectroscopy Reviews 44: 335-361

Murdock JN, Dodds WK, Reffner JA, Wetzel DL (2010) Measuring cellular-scale nutrient distribution in algal biofilms with synchotron confocal infrared microspectroscopy. Spectroscopy 25(10): 1-12

Naumann D, Schultz CP, Helm D (1996) What can infrared spectroscopy tell us about the structure and composition of intact bacterial cells In: Mantsch HH, Chapman D (ed) Infrared spectroscopy of biomolecules, Wiley, Chichester, pp 159-202

Nichols HW (1973) Growth Media-Freshwater. In: Stein JR (eds), Handbook of phycological methods: culture methods and growth measurements, Cambridge University Press, UK, pp 7-24

Oberreuter H, Charzinski J, Scherer S (2002) Intraspecific diversity of *Brevibacterium linens, Corynebacterium glutamicum* and *Rhodococcus erythropolis* based on partial 16S rDNA sequence analysis and Fourier-transform infrared (FT-IR) spectroscopy. Microbiology 148: 1523-1532

Perumal P, Prasath BB, Santhanam P, Ananth S, Shenbaga Devi A, Kumar DS (2012) Isolation and culture of microalgae. Workshop on Advances in Aquaculture Technology, 166-181

Potapova MG, Charles DF, Ponader KC, Winter DM (2004) Quantifying species indicator values for trophic diatom indices: a comparison of approaches. Hydrobiologia 517: 25-41

Raven JA, Waite AM (2004) The evolution of silicification in diatoms: inescapable sinking and sinking as escape, New Phytologist 162: 45-61

Round FR, Crawford RM, Mann DG (1990) The Diatoms: biology and morphology of the genera. Cambridge University Press, Cambridge

Sigee DC, Dean A, Levado E, Tobin MJ (2002) Fourier-transform infrared microscopy of *Pediastrum dublex*: characterization of a micro- population isolated from a eutrophic lake. *European Journal of Phycology* 37: 19-26

Stehfest K, Toepel J, Wilhelm C (2005) The application of micro-FTIR spectroscopy to analyze nutrient stress-related changes in biomass composition of phytoplankton algae. Plant Physiol Biochem 43: 717-726

Swann GE, Patwardhan S (2011) Application of Fourier Transform Infrared Spectroscopy (FTIR) for assessing biogenic silica sample purity in geochemical analyses and palaeoenvironmental research. Clim Past 7: 65-74

UTEX, (2018) Culture Collection of Algae at the University of Texas at Austin. (http://web.biosci.utexas.edu/utex/Media%20PDF/allen%20medium.pdf), Accessed: 23 November 2018

Wagner H, Liu Z, Langner U, Stehfest K, Wilhelm C (2010) The use of FTIR spectroscopy to asses quantitative changes in the biochemical composition of microalgae. J Biophoton 1-10

Wong PTT, Wong RK, Caputo TA, Godwin TA, Rigas B (1991) Infrared spectroscopy of exfoliated human cervical cells: evidence of extensive structural changes during carcinogenesis. Pro- ceedings of the Natural Academy of Science 88: 10988-10992

WHO (2016) Methods of Sterilization, The International Pharmacopoeia. http://apps.who.int/phint/en/p/about/ Accessed 11 June 2016

Vardy S, Uwins P (2002) Fourier transform infrared microspectroscopy as a tool to differentiate *Nitzschia closterium* and *Nitzschia longissima*. Appl Spectros 56: 1545-1548

Yee N, Benning LG, Phoenix VR, Ferris FG (2004) Characterization of metal-Cyanobacteria sorption reactions: A combined Macroscopic and infrared spectroscopic investigation. Environ Sci Technol 38:775-82

Van Leeuwe MA, Villerius LA, Roggeveld J, Visser RJW, Stefels J (2006) An optimized method for automated analysisof algal pigments by HPLC. Mar Chem 102: 267-75

ACADEMIC STUDIES IN ENGINEERING

gece kitaplığı

www.gecekitapligi.com

/gecekitapligi

/gecekitap

/gecekitapligi

9 786257 912167